Non-destructive measurement of pomegranate fruit quality

By

Ebrahiema Arendse

Dissertation presented for a Degree of Doctor of Philosophy (Food Science) in the Faculty of AgriSciences
Stellenbosch University

Supervisor: Prof. Umezuruike Linus Opara
SARChI Postharvest Technology
Department of Horticultural Science
Stellenbosch University
South Africa

Co-supervisor: Dr Olaniyi Amos Fawole
Department of Horticultural Science
Stellenbosch University
South Africa

Co-supervisor: Dr Lembe Samukelo Magwaza
Department of Crop Science
University of KwaZulu-Natal
South Africa

December 2017

Stellenbosch University https://scholar.sun.ac.za

DECLARATION

By submitting this thesis/dissertation electronically, I declare that the entirety of the work contained therein is my own, original work, that I am the sole author thereof (save to the extent explicitly otherwise stated), that reproduction and publication thereof by Stellenbosch University will not infringe any third party rights and that I have not previously in its entirety or in part submitted it for obtaining any qualification.

December 2017

Copyright © 2017 Stellenbosch University
All rights reserved

Stellenbosch University https://scholar.sun.ac.za

SUMMARY

Pomegranate (*Punica granatum* L.) is an emerging fruit within the South African horticultural industry, which has experienced dramatic growth in annual production from 350 tonnes in the 2009 season to over 8000 tonnes in 2017. Literature shows that the fruit consists of considerable amount of sugars, organic acids, vitamins, mineral elements and possess potent pharmacological activities due to an array of phytochemical compounds found in the fruit. However, the fruit is highly susceptible to pest and disease infestation, including the development of physiological rind disorders during storage and shipping. The increased growth of the pomegranate industry has coincided with consumer demand for consistent supply of safe, nutritious and traceable fruit and processed products. Hence, non-destructive assessment of fruit quality and its processed products can contribute to the implementation of suitable management strategies to predict and control desired quality attributes. This will ensure delivery of high quality fruit and its derived products without the presence of defects in international and local markets.

Therefore, the overall aim of this study was to develop non-destructive methods to predict external and internal quality attributes of pomegranate fruit. Section I of the thesis focuses on a critical review of non-destructive techniques for assessing the external and internal quality of fruit with thick rind. Thick rind fruits, such as pomegranate, have been reported to interfere with accurate measurement of internal quality using near-infrared spectroscopy. Hence, this review provides an overview of the issues related to quality measurement using non-destructive methods, including a concise summary of the current research and potential commercial applications.

In section II (chapter 3), the feasibility of X-ray micro-computed tomography (µCT) as a non-destructive technique to characterise and quantify the internal structure of pomegranate fruit was investigated. µCT in combination with image analysis successfully characterised and quantified the volumes of the internal fruit components (arils, peel, kernel, juice content, air space). The calculated volume for total arils, peel, and air space were 162.45 ±16.21, 163.87 ±21.42 and 10.89 ±2.57 mL, respectively, which accounted for 48.04, 48.46 and 3.22% of the total fruit volume (338.19 ±22.4 mL). The calculated volume of juice content and kernels were 146.07 ±16.28 and 16.38 ±1.81 mL per fruit which were equivalent to an average of 89.92 and 10.08% of the total aril volume. Destructive validation results showed no significant difference with those obtained from the µCT-based non-invasive method. This study has demonstrated the potential use

Stellenbosch University https://scholar.sun.ac.za

of µCT and associated image analysis as a promising tool for non-destructive characterization of the internal and external structure of pomegranate fruit.

In chapter 4, the prospects of Fourier-transform near-infrared (FT-NIR) spectroscopy (FT-NIRS) and associated chemometric analysis were evaluated for the prediction of external and internal quality parameters of intact pomegranate fruit. Two diffuse reflectance spectral acquisition modes were assessed, namely, direct contact between the sample with an integrating sphere (IS) using the Multi-Purpose Analyser (MPA) and a contact-less measurement (distance 17 cm) using an optic fibre coupled emission head (EH) of the MATRIX^{TM}-F analyser. Partial least squares (PLS) regression was used to construct calibration models over a spectral region of 800-2500 nm, and the results showed that optimal model performance was obtained using first derivative and second derivative spectral pre-processing methods. It was found that models obtained from the EH spectral data predicted fruit firmness, colour components (a* and C*), total soluble solids, titratable acidity, BrimA, total phenolics and vitamin C with high accuracy (RPD values ranging from 2.06 to 3.34), while the IS showed good prediction ability for h° colour component (RPD = 2.50), TSS:TA (RPD = 2.72) and total anthocyanin (RPD = 1.64). The results suggest that the contactless option of the MATRIX-F could be used to evaluate quality attributes of intact pomegranate fruit.

In chapter 5, the development of calibration models by FT-NIRS for the evaluation of pomegranate aril quality was investigated using two different FT-NIR acquisition methods (IS and EH) over 800-2500 nm spectral region. Model development was based on pre-processing methods that yielded higher values of coefficient of determination (R^2) and residual predictive deviation (RPD), lower root mean square error estimation (RMSEE) and root mean square error of prediction (RMSEP). The results showed that models based on the EH provided good prediction of TSS, pH, TA, BrimA, aril hue, total phenolic, total anthocyanin and vitamin C concentration, while those based on IS provided the best results for TSS:TA, firmness, arils redness (a*) and colour intensity (chroma). Furthermore, a follow-up study was conducted to compare near and mid infrared (MIR) spectrometers for predicting organoleptic and phytochemical quality attributes of pomegranate juice (chapter 6 (section II)). Three Fourier transform infrared (FT-IR) spectrometers (representing three different spectral acquisition modes) were assessed; namely, MPA FT-NIR spectrometer, Alpha-P FT-MIR spectrometer and WineScan FT-NIR/MIR spectrometer. Results obtained showed that spectral acquisition mode affected model ability to accurately predict various

Stellenbosch University https://scholar.sun.ac.za

pomegranate quality attributes, with the WineScan in the NIR/MIR region outperforming the Alpha-P and MPA instruments. However, statistical comparison using Bland and Altman and Passing-Bablok analytical algorithms showed no statistical differences among the three spectrometers for the prediction of selected aril quality parameters.

Section III of the thesis investigated the prospects for non-destructive detection and classification of pomegranate fruit affected by internal defects and postharvest rind scald. In chapter 7, the feasibility of µCT with a calibration function to differentiate between fruit fractions (albedo and arils) and detect the presence of false codling moth and blackheart disease in pomegranate fruit was assessed. A calibration function was implemented using different homogenous polymeric materials with a density ranging from 910 to 2150 kg m^{-3}. The estimation of fruit density was successfully accomplished within the calibration range. The density of whole fruit (1070 ±20 kg m^{-3}), arils (1120 ±40 kg m^{-3}) and albedo 1040 ±30 kg m^{-3}) were significantly higher compared to the larva of codling moth (940 ±40 kg m^{-3}) inside the fruit. Furthermore, healthy fruit had significantly higher density (1070 ±20 kg m^{-3}) compared to those with blackheart (870–1000 ±50 kg m^{-3}). An increase in the severity of blackheart infestation was characterised by a decrease in density of affected fruit. The results of this study suggested that the use of X-ray µCT, in combination with a calibration function of polymers and image analysis, could be applied to non-destructively identify and differentiate between fruit fractions, and detect the presence of larva of false codling moth and blackheart in pomegranate fruit.

The research reported in chapter 8 (section III) evaluated several biochemical markers associated with the development of husk scald (peel browning) and based on these markers, assess the feasibility of non-destructive discrimination of healthy and scalded affected fruit using Fourier transform near-infrared (FT-NIR) spectroscopy. The results suggest that enzymatic browning was the main cause of husk scald, phenolic compounds such as tannins acting as substrates for polyphenol oxidase and peroxidase activity. The severity of browning index increased with storage temperature and duration. FT-NIR reflectance spectroscopy spectral data and reference data were subjected to orthogonal partial least squares discriminant analysis (OPLS-DA) to discriminate between healthy and scalded fruit. Resulting in high classification accuracy (100%, 93% and 92.6% for healthy, severe and moderately scalded fruit, respectively). Therefore, this study has successfully demonstrated that biochemical markers associated with the development of husk scald could potentially be used to non-destructively discriminate between healthy and scalded fruit.

Stellenbosch University https://scholar.sun.ac.za

OPSOMMING

Die granaat (*Punica granatum* L.) is ‘n opkomende vrug in die Suid-Afrikaanse tuinboubedryf wat dramatiese produksie groei getoon het van 350 ton in die 2009-seisoen tot meer as 8000 ton in 2017. Literatuur dui aan dat die vrug bestaan uit aansienlike hoeveelhede suikers, organiese sure, vitamiene en minerale; asook kragtige farmakologiese aktiwiteite as gevolg van 'n verskeidenheid fitochemiese verbindings. Die vrugte is egter hoogs vatbaar vir plaag- en siektesbesmetting, insluitend die ontwikkeling van fisiologiese skil kwale tydens berging en besending. Die stygende groei van die granaatbedryf beweeg saam met verbruikersvereiste na konsekwente voorsiening van veilige, voedsame en opspoorbare vrugte en verwerkte produkte. Gevolglik kan nie-vernietigende assessering van vrugkwaliteit en verwerkte produkte bydra tot die implementering van geskikte bestuurstrategieë om gewenste kwaliteitseienskappe te voorspel en te beheer. Dit sal verseker dat vrugte en produkte van ‘n hoë gehalte, sonder kwale, in die internasionale en plaaslike markte sal voorkom.

Die oorhoofse doel van hierdie studie was dus om nie-vernietigende metodes te ontwikkel om die eksterne en interne kwaliteitseienskappe van granaatvrugte te voorspel. Afdeling I van die proefskrif fokus op 'n kritiese oorsig van nie-vernietigende tegnieke wat gebruik word om die eksterne en interne kwaliteit van vrugte met ‘n dik skil te assesseer. Volgens literatuur word die akkuraatheid van interne kwaliteitsmetings deur middel van naby infrarooi spektroskopie beïnvloed deur vrugte met ‘n dik skil, soos granate. Hierdie oorsig bespreek kwessies wat verband hou met gehaltemeting deur middel van nie-destruktiewe metodes, insluitend 'n bondige opsomming van die huidige navorsing en potensiële kommersiële toepassings.

In afdeling II (hoofstuk 3) word die lewensvatbaarheid van X-straal mikro-berekende-tomografie (µCT) as 'n nie-vernietigende tegniek ondersoek, om die interne struktuur van granaatvrugte te karakteriseer en te kwantifiseer. Die kombinasie van µCT en beeldontleding het die volumes van die interne vrug komponente (arils, skil, pitte, sap inhoud, lugruimte) suksesvol gekenmerk en gekwantifiseer. Die berekende volume vir totale arils, skil en lugruimte was onderskeidelik 162.45 ±16.21 mL, 163.87 ±21.42 mL en 10.89 ±2.57 mL, wat verantwoordelik was vir 48.04%, 48.46% en 3.22% van die totale vrugvolume (338.19 ±22.4 mL). Die berekende volume vir sap-inhoud en pitte was onderskeidelik 146.07 ±16.28 mL en 16.38 ±1.81 mL per vrug wat gelykstaande is aan 'n gemiddeld van 89.92 en 10.08% van die totale aril volume. Destruktiewe validasie resultate het geen betekenisvolle verskil getoon met dié wat verkry is uit µCT-gebaseerde

Stellenbosch University https://scholar.sun.ac.za

nie-indringende metode. Hierdie studie het die potensiële gebruik van µCT en geassosieerde beeldanalise getoon as 'n belowende instrument vir nie-vernietigende karakterisering van interne en eksterne struktuur van granaatvrugte.

In hoofstuk 4 is die vooruitsigte van Fourier-transform naby-infrarooi (FT-NIR) spektroskopie (FT-NIRS) en geassosieerde chemometriese analise geëvalueer vir die voorspelling van eksterne en interne gehalte-parameters van ongeskonde granaatvrugte. Twee diffusie weerkaatsde spektrale verkrygingsmetodes is geassesseer naamlik, direkte kontak tussen die monster met 'n integrerende sfeer (IS) met behulp van die Multi-Purpose Analyser (MPA) en 'n kontaklose meting (afstand 17 cm) met behulp van 'n optiese vesel-gekoppelde emissiekop (EH) van die MATRIXTM-F ontleder. Gedeeltelike minimum vierkantpassing (PLS) regressie is gebruik om kalibrasie modelle oor 'n spektrale gebied van 800-2500 nm te bou, en die resultate het getoon dat optimale modelprestasie verkry is deur gebruik te maak van eerste afgeleide en tweede afgeleide spektrale voorafverwerkingsmetodes. Daar is gevind dat modelle verkry uit die EH-spektrale data, die vrugte se gehalte-graad, kleurkomponente (a* en C*), totale oplosbare vastestowwe (TSS), titreerbare suurheidsgraad (TA), BrimA, totale fenolieke en vitamien C met hoë akkuraatheid (RPD waardes wat wissel tussen 2.06 en 3.34) voorspel, terwyl die IS goeie voorspellingsvermoë vir h° kleurkomponent (RPD = 2.50), TSS: TA (RPD = 2.72) en totale antosianien (RPD = 1.64) getoon het. Die resultate dui daarop dat die kontaklose opsie van die MATRIX-F, gebruik kan word om gehalte-eienskappe van ongeskonde granaatvrugte te evalueer.

In hoofstuk 5 is die ontwikkeling van kalibrasie-modelle deur FT-NIRS vir die evaluering van aril-kwaliteit ondersoek met behulp van twee verskillende FT-NIR-verkrygingsmetodes (IS en EH) oor 800-2500 nm spektrale gebied. Die model-ontwikkeling is gebaseer op voorafverwerkingsmetodes wat hoër waardes van bepalingskoëffisiënt (R^2) en residuele voorspellende afwyking (RPD), laer wortel gemiddelde vierkante foutberaming (RMSEE) en wortel gemiddelde vierkante fout van voorspelling (RMSEP) gegee het. Die resultate het getoon dat modelle wat op die EH gebaseer is, goeie voorspelling van TSS, pH, TA, BrimA, aril tint, totale fenoliese, totale anthosianien en vitamien C konsentrasie gegee het, terwyl dié wat op IS gebaseer is, die beste resultate vir TSS:TA, fermheid, aril rooiheid (a*) en kleurintensiteit (chroma) verskaf het. Verder is 'n opvolgstudie gedoen om naby- en middelinfrarooi (MIR) spektrometers te vergelyk vir die voorspelling van organoleptiese en fito-chemiese gehalte-eienskappe van granaatsap (hoofstuk 6 (afdeling II)). Drie Fourier-transform infrarooi (FT-IR) spektrometers (wat

Stellenbosch University https://scholar.sun.ac.za

drie verskillende spektrale verkrygingsmetodes verteenwoordig) is beoordeel; naamlik MPA FT-NIR spektrometer, Alpha-P FT-MIR spektrometer en WineScan FT-NIR / MIR spektrometer. Resultate het getoon dat die spektrale verkrygingsmodus die vermoë gehad het om verskeie eienskappe van granaatkwaliteit akkuraat voor te stel, met die WineScan in die NIR / MIR-streek beter as die Alpha-P en MPA-instrumente. Statistiese vergelyking met behulp van Bland en Altman, en Passing-Bablok-analitiese algoritmes het egter geen statistiese verskille tussen die drie spektrometers getoon vir die voorspelling van geselekteerde arilkwaliteit parameters nie.

Afdeling III van die proefskrif het die vooruitsigte vir nie-vernietigende ontdekking en klassifikasie van interne defekte en na-oes-skil-verbruining in granaatvrugte ondersoek. In hoofstuk 7 is die uitvoerbaarheid van μCT geassesseer om met 'n kalibrasie funksie tussen vrugte dele (albedo en arils) te onderskei, en die teenwoordigheid van valskodlingmot en swarthartbloutjie in granaatvrugte te bepaal. Die kalibreringsfunksie is geïmplementeer deur verskillende homogene polimeermateriale te gebruik met digthede wat wissel van 910 tot 2150 kg m^{-3}. Die skatting van vrugtedigtheid was suksesvol binne die kalibrasie bereik. Die digtheid van heelvrugte (1070 ±20 kg m^{-3}), arils (1120 ±40 kg m^{-3}) en albedo (1040 ±30 kg m^{-3}) was aansienlik hoër in vergelyking met die larwes van valskodlingmot (940 ±40 kg m^{-3}) binne-in die vrugte. Verder is die digtheid van gesonde vrugte aansienlik hoër (1070 ±20 kg m^{-3}) in vergelyking met dié met swarthartbloutjie (870-1000 ±50 kg m^{-3}). 'n Toename in die graad van swarthartbloutjie-besmetting is gekenmerk deur 'n afname in die digtheid van geaffekteerde vrugte. Die resultate van hierdie studie het voorgestel dat die gebruik van X-straal μCT, in kombinasie met 'n kalibreringsfunksie van polimere en beeldontleding, toegepas kan word om nie-destruktief te identifiseer en te onderskei tussen vrugte dele, sowel as om larwes van valskodlingmot en swarthartbloutjie in granaatvrugte te ontdek.

Die navorsing wat in hoofstuk 8 (afdeling III) gerapporteer is, het verskeie biochemiese merkers geëvalueer wat verband hou met die ontwikkeling van skilverbruining. Hierdie merkers is gebruik as ‘n grondslag om die uitvoerbaarheid te assesseer van nie-vernietigende diskriminasie van gesonde en verbruinde vrugte, met behulp van Fourier transform naby- Infrarooi (FT-NIR) spektroskopie. Die resultate dui daarop dat skilverbruining hoofsaaklik deur ensimatiese verbruining veroorsaak word met fenoliese verbindings, soos tanniene, wat as substrate vir polifenol-oksidase en peroksidase-aktiwiteite optree. Die graad van verbruining het toegeneem met bergingstemperatuur en –duur. FT-NIR-weerkaatsde spektroskopie spektrale data en

Stellenbosch University https://scholar.sun.ac.za

verwysingsdata is onderskei deur middel van ortogonale gedeeltelike minimale vierkante diskriminasie analise (OPLS-DA) om gesonde en verbruinde vrugte aan te dui. Dit het gelei tot hoë klassifikasie akkuraatheid (100%, 93% en 92.6% vir onderskeidelik gesonde, erge en matig verbruinde vrugte). Daarom was hierdie studie suksesvol om te wys dat die biochemiese merkers, wat geassosieer word met die ontwikkeling van verbruining, moontlik gebruik kan word om nie-vernietigend te onderskei tussen gesonde en verbruinde vrugte.

Stellenbosch University https://scholar.sun.ac.za

LIST OF PUBLICATIONS AND SUBMITTED MANUSCIPTS FROM THIS THESIS

Published articles

1. Arendse, E., Fawole, O.A., Magwaza, L.S. & Opara, U.L. (2017). Non-destructive prediction of internal and external quality attributes of fruit with thick rind: A review. *Journal of Food Engineering*. Doi: https://doi.org/10.1016/j.jfoodeng.2017.08.009.
2. Arendse, E., Fawole, O.A., Magwaza, L.S., Nieuwoudt, H.H. & Opara U.L. (2017). Development of calibration models for the evaluation of pomegranate aril quality by Fourier-transform near infrared spectroscopy combined with chemometrics. *Biosystems Engineering*, **159**, 22–32.
3. Arendse, E., Fawole, O.A., Magwaza, L.S. & Opara, U.L. (2016). Estimation of the density of pomegranate fruit and their fractions using X-ray computed tomography calibrated with polymeric materials. *Biosystems Engineering*, **148**, 148–156.
4. Arendse, E., Fawole, O.A., Magwaza, L.S. & Opara, U.L. (2016). Non-destructive characterization and volume estimation of pomegranate fruit external and internal morphological fractions using X-ray computed tomography. *Journal of Food Engineering*, **186**, 42–49.

Submitted articles

1. Arendse, E., Fawole, O.A., Magwaza, L.S., Nieuwoudt, H.H. & Opara U.L. Using Fourier transform near infrared diffuse reflectance spectroscopy and two spectral acquisition modes for the evaluation of the external and internal quality of intact pomegranate fruit. Submitted to *Postharvest Biology and Technology*.
2. Arendse, E., Fawole, O.A., Magwaza, L.S., Nieuwoudt, H.H. & Opara U.L. Comparing the analytical performance of near and mid infrared spectrometers for evaluating pomegranate juice quality. Submitted to *LWT Journal of Food Science.*
3. Arendse, E., Fawole, O.A., Magwaza, L.S., Nieuwoudt, H.H. & Opara U.L. Evaluation of biochemical markers associated with the development of husk scald and the use of diffuse reflectance NIR spectroscopy to predict husk scald in pomegranate fruit. Submitted to *Scientia Horticulturae.*

Stellenbosch University https://scholar.sun.ac.za

ACKNOWLEDGEMENTS

Unto God Almighty, most Gracious, most Beneficent, to HIM I give all praise for having favoured and given me the strength including sound health to pursue this path.

To my supervisor Prof U.L. Opara and co-supervisors Dr O.A. Fawole and Dr L.S. Magwaza, my sincere gratitude and appreciation for their guidance, advice, motivation and support throughout my research programme.

Dr Hélène Nieuwoudt, for your expert advice on NIR spectroscopy, including assisting with chemometrics and interpretation of data.

Dr Anton du Plessis and Mr Stephan Le Roux for their technical support and analysis with micro X-ray CT.

Prof M. Kidd Director of the Centre for Statistical Consultation (CSC), Stellenbosch University for his contributions to the statistical analysis.

Ms. Nazneen Ebrahim and Daleen du Preez for administrative duties and technical support.

Special thanks to my friends and postgraduate colleagues at SARChI Postharvest Technology Research Laboratory for their support, encouragement and advice as words cannot express my sincere gratitude.

I would like to thank my spouse, children, parents, brother and relatives and all those who contributed towards the success of my journey through their love, encouragement and support

I acknowledge the bursary awards by the National Research Foundation through the DST/NRF South African Research Chair Initiative (SARChI), and by Agri-Edge Ltd funded by the Department of Trade and Industry (DTI) through the Technology and Human Resources for Industry Programme (THRIP).
This work is based upon research supported by South African Research Chairs Initiative of the Department of Science and Technology and National Research Foundation.

Stellenbosch University https://scholar.sun.ac.za

This dissertation is dedicated to my spouse (Zuraida) and children (Uthman and Amir).

Stellenbosch University https://scholar.sun.ac.za

Preference

This dissertation is presented as a compilation of manuscripts where each chapter is an independent entity introduced separately. Some repetition between chapters has, therefore, been unavoidable. The chapters in this dissertation are written in accordance with the requirements of International Journal of Food Science and Technology.

Stellenbosch University https://scholar.sun.ac.za

Nomenclature

µCT	Microfocus X-ray computed tomography
NIRS	Near-infrared spectroscopy
NMR	Nuclear magnetic resonance
OCT	Optical coherence tomography
FCM	False codling moth
FD larva	False codling larva
2-D	Two dimensional Image
3-D	Three dimensional image
PUC	Production units code
UHMW PE	Ultra-high molecular weight polyethylene
PTFE	Polytetrafluoroethylene
PC	Sustanat polycarbonate
PP	Polypropylene (PP)
HDPE	High density polyethylene
PET	Polyethylene terephthalate
kg m^{-3}	Kilogram per cubic metre
mm	Millimetre
µm	Micrometre
nm	Nanometre
µA	Microampere
kV	Kilovolt
Tiff	Tagged image files
ANOVA	Analysis of variance
ROI	Region of interest
FT-NIR	Fourier transform near-infrared
FT-MIR	Fourier transform mid-infrared
FT-IR	Fourier transform infrared
IS	Integrating sphere
MPA	Multi-Purpose Analyser
EH	Emission head
PLS	Partial least squares
PCA	Principal component analysis
OPLS-DA	Orthogonal partial least squares discriminant analysis
OD	Optical density
R^2	Coefficient of determination
RMSEE	Root mean square error of estimation
RMSEP	Root mean square error of prediction
SEC	Standard error of calibration
SECV	Standard error of cross validation
SSE	Sum of squared error
RPD	Residual predictive deviation
LV	Latent variables
Corr	Correlation coefficient

Stellenbosch University https://scholar.sun.ac.za

FD	First derivative
SD	Second derivative
MSC	Multiplicative scattering correction
SNV	Vector normalisation
CV	Coefficient of variation
RSD	Relative standard derivation
SD	Standard deviation
VIP	Variable importance projection
TSS	Total soluble solids
TA	Titratable acidity
TSS:TA ratio	Total soluble solids: titratable acidity ratio
HFR	Heinrich Frederich Schaefer
C*	Chroma
h°	Hue angle
GAE	Gallic acid equivalents
PJ	Pomegranate juice
TP	Total phenolic concentration
T Ant	Total anthocyanin concentration
BI	Browning index
PPO	Polyphenol oxidase
POD	Peroxidase

Stellenbosch University https://scholar.sun.ac.za

TABLE OF CONTENTS

Stellenbosch University https://scholar.sun.ac.za

Stellenbosch University https://scholar.sun.ac.za

Section I

Chapter 1: General introduction

Chapter 2: Literature review[1]

[1.] Journal of Food Engineering. Doi: https://doi.org/10.1016/j.jfoodeng.2017.08.009.

Stellenbosch University https://scholar.sun.ac.za

DECLARATION BY THE CANDIDATE

Regarding **Chapter 1 (pp 3-9)**, the nature and scope of my contribution were as follows:

Nature of contribution	Extent of contribution (%)
Writing of chapter	75

The following co-authors have contributed to **Chapter 1 (pp 3-9)**

Name	e-mail address	Nature of contribution	Extent of contribution (%)
Prof U.L. Opara	opara@sun.ac.za	Editorial suggestion and proof reading	10
Dr O.A. Fawole	olaniyi@sun.ac.za	Editorial suggestion and proof reading	10
Dr L.S. Magwaza	Magwazal@ukzn.ac.za	Editorial suggestion	5

E Arendse **Signature of candidate**	29/08/2017 **Date**

DECLARATION BY CO-AUTHORS

The undersigned hereby confirm that:

1. the declaration above accurately reflects the nature and extent of the contributions of the candidate and the co-authors to **Chapter 1 (pp 3-9)**

2. no other authors contributed to **Chapter 1 (pp 3-9)** besides those specified above, and

3. potential conflicts of interest have been revealed to all interested parties and that the necessary arrangements have been made to use the material in **Chapter 1 (pp 3-9)** of this dissertation.

Signature	Institutional affiliation	Date
Prof U.L. Opara	Stellenbosch University	29/08/2017
Dr O.A. Fawole	Stellenbosch University	29/08/2017
Dr L.S. Magwaza	University of KwaZulu-Natal	29/08/2017

Stellenbosch University https://scholar.sun.ac.za

CHAPTER 1

GENERAL INTRODUCTION

1. Background

Pomegranate (*Punica granatum* L.) is an emerging crop in the global horticultural export industry. The fruit has a leathery exocarp and the interior is separated by membranous walls and white spongy tissue into compartments. The compartments consist of edible portion called arils which is surrounded by a translucent sac containing juice and each aril as a kernel (Holland *et al.*, 2009). The fruit has gained popularity for its high nutritional content, potent pharmacological and antioxidant properties which have been linked to improved health outcomes (Lansky & Newman, 2007; Viuda-Martos *et al.*, 2010). Scientific studies have linked potent pharmacological activities of pomegranates to several groups of phytochemicals found in the fruit (Viuda-Martos *et al.*, 2010; Fawole *et al.*, 2012). These phytochemicals, including polyphenolic compounds, have been reported to possess anti-microbial, anti-diabetic, anti-mutagenic and anti-inflammatory activities (Seeram *et al.*, 2006; Opara *et al.*, 2009). Consequently, the rising consumer interest has spurred a global growth in pomegranate fruit production, marketing, consumption and research (Arendse *et al.*, 2014). Currently, less than 10% of the global commercial production of pomegranate fruit occurs in the Southern Hemisphere, with South Africa being one of the few producers competing with Chile and Peru to fill the counter season window during spring and early summer months in Northern Hemisphere (Fawole & Opara, 2013a,b). Pomegranate cultivar Wonderful is the most widely grown and consumed pomegranate cultivar globally (Holland *et al*., 2009) and during the past ten years, South Africa has seen increase in its commercial production, with cv. Wonderful accounting for almost 70% of total production of 8000 tons (Hortgro, 2017).

Pomegranate fruit is non-climacteric and therefore requires a minimum maturity state at harvest for good postharvest performance (Elyatem & Kader, 1984). Early harvesting of pomegranate fruit may result in good external appearance with unacceptable internal characteristics quality such as poor aril colour and undesirable flavour. On the other hand, fruit harvested at late maturity are more susceptible to spoilage and short storage life (Fawole & Opara, 2013b). Therefore, harvesting fruit at optimum commercial maturity is critical followed by accurate measurement and monitoring of internal and external quality postharvest attributes. Internal attributes include soluble solids, titratable acidity, flavour (sugar/acid ratio) and phytochemical content while external attributes include fruit shape and size and skin appearance (Arendse *et al.*, 2015). However, the most common methods for measuring internal attributes involve destructive procedures, which often require specialised sample preparation, are labour intensive and use only a

Stellenbosch University https://scholar.sun.ac.za

representative sample set. Furthermore, results of tests using representative samples only reflect the properties of the specific fruit being evaluated. Hence, fruit quality determined using this approach may display significant variation in both internal and external quality due to variations in maturity, position in the canopy and other environmental factors (Magwaza *et al.,* 2013). A recent trend in agribusiness and postharvest research are moving away from subjective to objective, quantitative and non-destructive methods for quality assessment of fresh produce on colour (Pathare *et al.,* 2013); sweetness (Magwaza & Opara, 2015) and texture (Chen & Opara, 2013a,b).

Pomegranate fruit is prone to develop various types of insect infestation, physiological disorders (such as chilling injury, husk scald) and diseases and decay which contribute to preharvest and postharvest losses. Blackheart is one of the main diseases associated with pomegranate fruit and is recognised as a postharvest quality problem; however, infection begins in the orchard. The disease causing fungi include *Alternaria* spp. and *Aspergillus* spp. (Yehia, 2013; Munhuweyi *et al.,* 2016). These fungi enter the fruit during bloom and early fruit set, grow and spread as the fruit develops. The fungus *Alternaria* spp. causes blackening of arils inside the fruit, ranging from sections of the pomegranate fruit to all arils without showing any external symptoms except for slight abnormal peel colour (Zhang & McCarthy, 2012; Munhuweyi *et al.,* 2016). Therefore, the identification of affected fruit by sorters during packinghouse operations or processing is a challenge due to the lack of obvious external symptoms. Another limiting factor affecting the storability and marketability of pomegranates is the occurrence of husk scald (browning of the peel surface). This rind disorder has been proposed to be due to the enzymatic oxidation of phenolic compounds on the husk of the fruit when stored at temperatures exceeding 5 °C with no observable changes to the internal fruit quality (Defilippi *et al.*, 2006). However, the underlining mechanism remains unclear. Scalding of the husk manifests mainly during the later stages of postharvest handling and shipping this usually coincides with commercial shipping period and/or point of sale. This may be problematic as scalding may lead to increase fruit susceptibility to decay and other physiological disorders such as chilling injury which could lead to tremendous financial losses (Defilippi *et al.*, 2006; Kader, 2006). Limited knowledge of the physiological mechanisms underlying this disorder hinders the development of cost-effective solutions to minimise losses, and assure a consistent supply of quality fruit.

South African pomegranate export industry is currently plagued with quality losses due to insect infestation and occurrence of physiological disorders. Limited research has been conducted to develop technologies that can assess, predict and monitor pomegranate fruit quality during postharvest handling and storage. Therefore, for the South African pomegranate industry to maintain its competitive edge in the international market, there is a need for the development of non-destructive methods for assessing fruit quality and presence of defects. Such non-destructive methods would permit the evaluation of internal quality and morphological characteristics to ensure that minimum levels of acceptance in the market (Magwaza & Opara, 2014).

Stellenbosch University https://scholar.sun.ac.za

A wide range of non-destructive instrumentation for measuring the quality of fresh produce has been used for non-destructive quality evaluation of fresh produce. These include near-infrared spectroscopy (NIRS), Magwaza *et al.,* 2012), NIRS based systems such as multispectral and hyperspectral imaging (Khodabakhshian *et al.*, 2016), nuclear magnetic resonance imaging (NMR/MRI), Zhang & McCarthy, 2012), and X-ray computed tomography (CT), Magwaza & Opara, 2014; Arendse *et al.*, 2016a). Amongst non-destructive methods, NIRS combined with chemometric techniques is the most widely used due to its accuracy, rapidity and cost-effectiveness for quantification of chemical constituents (Magwaza *et al.,* 2016). NIRS has become one of the most used methods for the assessment of fresh fruit according to their internal quality attributes (Nicolaï *et al.,* 2007). Furthermore, the feasibility of NIRS to assess the quality attributes of fresh fruits and vegetables have been reported in many horticultural products (McGlone *et al.,* 2002; Zude, 2003; Gomez *et al.*, 2006; Nicolaï *et al.*, 2007; Bobelyn *et al.*, 2010; Magwaza *et al.,* 2012). NIRS has been extensively used as an alternative analytical tool in the food industry. Therefore, different spectral acquisition methods were considered in this dissertation.

The use of X-ray CT as a non-destructive technique for studying the external and internal morphological characteristics and defects of horticultural products is well documented (Cantre *et al.,* 2014; Donis-González *et al.,* 2014; Magwaza & Opara, 2014; Kotwaliwale *et al.,* 2014, Arendse *et al.,* 2016 a,b). X-ray CT measures variation in material density of the sample and is based on the attenuation of X-ray that depends on the density of the irradiated object. The advantage of the X-ray μCT technique is that it allows reproduction of high resolution three dimensional (3-D) visualisation and analysis of microstructures without sample preparation or chemical fixation (Léonard *et al.,* 2008; Guelpa *et al.,* 2015).

The growing pomegranate industry requires non-invasive methods that allow accurate, rapid and cost-effective analysis of fruit quality. Therefore, to fully harness the opportunity of existing and future competitive export markets, there is a need for the development and application of objective, fast and non-destructive assessment methods that can be used to accurately determine internal fruit quality and detect physiological disorders during postharvest handling and storage. Very limited studies have been conducted to assess the suitability of NIRS and X-ray CT for an assessment of internal and external quality parameters of pomegranate fruit in particular.

2. Research aim and objectives

The overall aim of this research study was to develop non-destructive methods to predict the internal and external quality of pomegranate fruit. To achieve this, the study included the following specific objectives:

1. Determine optimum conditions for NIRS measurements by evaluating the accuracy of various analytical techniques to quantify physicochemical quality attributes.
2. Identify potential biochemical markers that can be analysed non-destructively to detect the presence of external defects.

Stellenbosch University https://scholar.sun.ac.za

3. Investigate the feasibility of non-destructive methods to characterise the volume fractions of pomegranate fruit and detect internal defects.

3. Thesis structure

This dissertation was structured into four sections.

- Section I: provides a brief background, discusses the aim and objectives of the study (*General introduction*), and also provides a review of literature on non-destructive methods for the assessing quality of fruit with thick rind such as pomegranates (Chapter 1 & 2)
- Section II: evaluates non-destructive methods for the measuring physicochemical quality attributes of pomegranate fruit and its fractions (Chapters 3 to 6)
- Section III: focuses on the use of non-destructive methods for the evaluation and prediction of internal defects and husk (peel) scald disorder affecting pomegranate fruit (Chapters 7 & 8)
- Section IV: presents a general discussion which integrates the results from previous chapters. It highlights the important practical contribution of this thesis towards successful non-destructive evaluation of the external and internal quality of pomegranate fruit (Chapter 9)

References

Arendse, E., Fawole, O.A. & Opara, U.L. (2014). Effects of postharvest storage conditions on phytochemical and radical-scavenging activity of pomegranate fruit (cv. Wonderful). *Scientia Horticulturae*, **169**, 125–129.

Arendse, E., Fawole, O.A. & Opara, U.L. (2015). Effects of postharvest handling and storage on physiological attributes and quality of pomegranate fruit (*Punica granatum* L.): a review. *International Journal of Postharvest Technology and Innovation*, **5**, 13–31.

Arendse, E., Fawole, O.A., Magwaza, L.S. & Opara, U.L. (2016a). Non-destructive characterization and volume estimation of pomegranate fruit external and internal morphological fractions using X-ray computed tomography. *Journal of Food Engineering*, **186**, 42–49.

Arendse, E., Fawole, O.A., Magwaza, L.S. & Opara, U.L. (2016b). Estimation of the density of pomegranate fruit and their fractions using X-ray computed tomography calibrated with polymeric materials. *Biosystems Engineering*, **148**, 148–156.

Bobelyn, E., Serban, A., Nicu, M., Lammertyn, J., Nicolaï, B.M. & Saeys, W. (2010). Postharvest quality of apple predicted by NIR spectroscopy: Study of the effect of biological variability on spectra and model performance. *Postharvest Biology and Technology*, **55**, 133–143.

Stellenbosch University https://scholar.sun.ac.za

Cantre, D., Herremans, E., Verboven, P., Ampofo-Asiama, J. & Nicolaï, B.M. (2014). Characterization of the 3-D microstructure of mango (*Mangifera indica* L. cv. Carabao) during ripening using X-ray computed microtomography. *Innovative Food Science and Emerging Technologies*, **24**, 28–39.

Chen, L. & Opara, U.L. (2013a). Texture measurement approaches in fresh and processed foods–a review. *Food Research International*, **51**, 823–835.

Chen, L. & Opara, U.L. (2013b). Approaches to analysis and modeling texture in fresh and processed foods–a review. *Journal of Food Engineering*, **119**, 497–507.

Defilippi, B.G., Whitaker, B.D., Hess-Pierce, B.M. & Kader, A.A. (2006). Development and control of scald on 'Wonderful' pomegranates during long-term storage. *Postharvest Biology and Technology*, **41**, 234–243.

Donis-Gonzalez, I.R., Guyer, D.E., Pease, A. & Barthel, F. (2014). Internal characterisation of fresh agricultural products using traditional and ultrafast electron beam X-ray. *Biosystems Engineering*, **117**, 104-113.

Elyatem, S.M. & Kader, A.A. (1984). Post-harvest physiology and storage behaviour of pomegranate fruits. *Scientia Horticulturae*, **24**, 287–298.

Fawole, O.A., Makunga, N.P. & Opara, U.L. (2012). Antibacterial, antioxidant and tyrosine- inhibition activities of pomegranate fruit peel methonolic extract. *BMC Complementary and Alternative Medicine*, **12**, 200–225.

Fawole, O.A. & Opara, U.L. (2013a). Changes in physical properties, chemical and elemental composition and antioxidant capacity of pomegranate (cv. Ruby) fruit at five maturity stages. *Scientia Horticulturae*, **150**, 37–46.

Fawole, O.A. & Opara, U.L. (2013b). Developmental changes in maturity indices of pomegranate fruit: A descriptive review. *Scientia Horticulturae*, **159**, 152–161.

Gomez, A.H., He, Y. & Pereira A.G. (2006). Non-destructive measurement of acidity, soluble solids and firmness of Satsuma mandarin using Vis/NIR-spectroscopy techniques. *Journal of Food Engineering*, **77**, 313–319.

Guelpa, A., du Plessis, A., Kidd, M., & Manley, M. (2015). Non-destructive estimation of maize (*Zea mays* L.) kernel hardness by means of an X-ray micro-computed tomography (µ CT) density calibration. *Food Bioprocess Technology*, **8**, 1419–1429.

Holland, D., Hatib, K. & Bar-Ya'akov, I. (2009). Pomegranate: botany, horticulture, breeding. *Horticultural Reviews*, **35**, 127–191.

Hortgro, (2017). Pomegranate industry statistics. www.hortgro.co.za. Accessed on (11/11/2017)

Kader, A.A. (2006). Postharvest Biology and Technology of Pomegranates. In: Seeram, N.P. et al (eds). Pomegranates: Ancient Roots to Modern Medicine. CRC Press Taylor & Francis Group, Boca Raton, London & New York, pp. 216.

Stellenbosch University https://scholar.sun.ac.za

Kotwaliwale, N., Singh, K., Kalne, A., Jha, S.N., Seth, N. & Kar, A. (2014). X-ray imaging methods for internal quality evaluation of agricultural produce. *Journal of Food Science and Technology*, **51**, 1–15.

Khodabakhshian, R., Emadi, B., Khojastehpour, M., Golzarian, M.R., & Sazgarnia, A. (2016). Development of a multispectral imaging system for online quality assessment of pomegranate fruit. *International Journal of Food Properties*. DOI: 10.1080/10942912.2016.1144200.

Léonard, A., Blacher, S., Nimmol, C., & Devahastin, S. (2008). Effect of far-infrared radiation assisted drying on microstructure of banana slices: an illustrative use of X-ray micro tomography in microstructural evaluation of a food product. *Journal of Food Engineering*, **85**, 154–162

Lansky, E.P. & Newman, R.A. (2007). *Punica granatum* (pomegranate) and its potential for prevention and treatment of inflammation and cancer. *Journal of Ethnopharmacology*, **109**, 177–206.

Magwaza, L.S., Opara, U.L., Nieuwoudt, H. Cronje, P.J.R., Saeys, W. & Nicolai, B.M. (2012). NIR spectroscopy applications for internal and external quality analysis of Citrus Fruit-A Review. *Food and Bioprocess Technology*, **5**, 425–444.

Magwaza, L.S., Opara, U.L., Terry, L.A., Landahl, S., Cronje, P.J.R., Nieuwoudt, H.H., Hanssens, A., Saeys, W. & Nicolai, B.M. (2013). Evaluation of Fourier transform NIR-spectroscopy for integrated external and internal quality assessment of Valencia oranges. *Journal of Food Composition and Analysis*, **31**, 144–154.

Magwaza, L.S. & Opara, U.L. (2014). Investigating non-destructive quantification and characterization of pomegranate fruit internal structure using x-ray computed tomography. *Postharvest Biology and Technology*, **95**, 1–6.

Magwaza, L.S. & Opara. U.L. (2015). Analytical methods for determination of sugars and sweetness of horticultural products A–review. *Scientia Horticulturae*, **184**, 179–192.

Magwaza, L.S., Naidoo, S.I.M., Laurie, S.M., Laing, M.D. & Shimelis, H. (2016). Development of NIRS models for rapid quantification of protein content in sweetpotato [Ipomoea batatas (L.) LAM.]. *LWT-Food Science and Technology*, **72**, 63–70.

McGlone, V.A., Jordan, R.B. & Martinsen, P.J. (2002). Vis/NIR estimation at harvest of pre- and post-storage quality indices for 'Royal Gala' apple. *Postharvest Biology and Technology*, **25**, 135–144.

Munhuweyi, K., Lennox, C.L., Meitz-Hopkins, J.C., Caleb, O.J. & Opara, U.L. (2016). Major diseases of pomegranate (*Punica granatum* L.), their causes and management–A review. *Scientia Horticulturae*, **211**, 126–139.

Nicolaï, B.M., Beullens, K., Bobelyn, E., Peirs, A., Saeys, W., Theron, I.K. & Lammertyn, J. (2007). Non-destructive measurement of fruit and vegetable quality by means of NIR spectroscopy: A review. *Postharvest Biology and Technology*, **46**, 99–118.

Stellenbosch University https://scholar.sun.ac.za

Opara, L.U., Al-Ani, M.R. & Al-Shuaibi, Y.S. (2009). Physiochemical properties, vitamin C content, and antimicrobial properties of pomegranate fruit (*Punica granatum* L.). *Food and Bioprocess Technology*, **2**, 315–321.

Pathare, P.B., Opara, U.L. & Al-Said, F.A.J. (2013). Colour measurement and analysis in fresh and processed foods: A review. *Food and Bioprocess Technology,* **6**, 36–60.

Seeram, N.P., Zhang, Y., Reed, J.D., Krueger, C.G. & Vaya, J. (2006). Pomegranate phytochemicals. In: Seeram, N.P. et al (eds). Pomegranates: Ancient Roots to Modern Medicine. CRC Press Taylor & Francis Group, Boca Raton, London & New York, pp. 3–29.

Viuda-Martos, M., Fernández-López, J. & Pérez-Álvarez, J. A. (2010). Pomegranate and its many functional components as related to human health: A Review. *Comprehensive Reviews in Food Science and Food Safety*, **9**, 635–654.

Yehia, H.M. (2013). Heart rot caused by *Aspergillus niger* through splitting in leathery skin of pomegranate fruit. *African Journal of Microbiology Research*, **7**, 834–837.

Zhang, L. & McCarthy, M.J. (2012). Measurement and evaluation of tomato maturity using magnetic resonance imaging. *Postharvest Biology and Technology*, **67**, 37–43.

Zude, M. (2003). Non-destructive prediction of banana fruit quality using VIS/NIR spectroscopy. *Fruits*, **58**, 135–142.

Stellenbosch University https://scholar.sun.ac.za

DECLARATION BY THE CANDIDATE

Regarding **Chapter 2 (pp 12-48)**, the nature and scope of my contribution were as follows:

Nature of contribution	Extent of contribution (%)
Literature research, writing of chapter and final approval of the published version	75

The following co-authors have contributed to **Chapter 2 (pp 12-48)**

Name	e-mail address	Nature of contribution	Extent of contribution (%)
Prof U.L. Opara	opara@sun.ac.za	Conception of the work, proof reading and final approval of the published version	10
Dr O.A. Fawole	olaniyi@sun.ac.za	Research input, editorial suggestion, proof reading and final approval of the published version	10
Dr L.S. Magwaza	Magwazal@ukzn.ac.za	Editorial suggestion and final approval of the published version	5

Stellenbosch University https://scholar.sun.ac.za

E Arendse **Signature of candidate**	29/08/2017 **Date**

DECLARATION BY CO-AUTHORS

The undersigned hereby confirm that:

1. the declaration above accurately reflects the nature and extent of the contributions of the candidate and the co-authors to **Chapter 2 (pp 12-48)**

2. no other authors contributed to **Chapter 2 (pp 12-48)** besides those specified above, and

3. potential conflicts of interest have been revealed to all interested parties and that the necessary arrangements have been made to use the material in **Chapter 2 (pp 12-48)** of this dissertation.

Signature	Institutional affiliation	Date
Prof U.L. Opara	Stellenbosch University	29/08/2017
Dr O.A. Fawole	Stellenbosch University	29/08/2017
Dr L.S. Magwaza	University of KwaZulu-Natal	29/08/2017

Stellenbosch University https://scholar.sun.ac.za

CHAPTER 2

Non-destructive prediction of internal and external quality attributes of fruit with thick rind: A review

Abstract

Fruits with thick rind have been reported to interfere with the measurement of internal quality of non-destructive near-infrared spectroscopy. This review provides an overview of issues related to the use of near-infrared spectroscopy for measuring internal and external quality attributes of horticultural produce with thick rinds. The use of other non-destructive techniques for assessing internal and external quality thick rind fruit, such as hyperspectral and multispectral imaging systems, X-ray micro-computed tomography, nuclear magnetic resonance and Raman spectroscopy are also discussed. A concise summary of research and potential commercial application for each of the techniques is highlighted.

Keywords: Fruit quality, *Punica granatum* L, Near-infrared spectroscopy, Hyperspectral imaging, X-ray micro-computed tomography, Nuclear magnetic resonance, Raman spectroscopy.

Stellenbosch University https://scholar.sun.ac.za

1. Introduction

The main quality aspects consumers are confronted with when purchasing fruit and vegetables are based on external aspects such as appearance, colour, size, and absence of blemishes (Opara & Pathare, 2014). Subsequent, purchases are dependent upon consumers satisfaction based on internal quality parameters related to soluble solids content (SSC), titratable acidity (TA), soluble solids to acid (SSC/TA) ratio and texture (Chen & Opara, 2013a,b; Magwaza & Opara, 2015). Over the past decade, non-destructive methods have been employed to evaluate fruit quality and are preferred to destructive techniques because they allow the measurement and analysis of individual fruit, reduce waste and permit repeated measures on the same item over time (Nicolaï *et al*., 2007a). Furthermore, the use of destructive methods are known to be more labour intensive, time-consuming, requires specialised sample preparation and inapplicable to in-line grading and sorting. In addition, fruit quality determined using this approach may exhibit significant variation in both external and internal quality due to variability amongst cultivars, fruit maturity status, position in the canopy and other environmental factors (Peiris *et al*., 1999; Guthrie *et al*., 2005a,b; Magwaza *et al*., 2013a). Increasing consumer demand for both external and internal quality assurance has spurred considerable interest in the fresh produce industry to develop fast, cost-effective non-invasive instrumentation for detection and monitoring of fruit quality.

Several non-destructive techniques have been used for the assessment of internal and external quality attributes of horticultural produce. These include near-infrared spectroscopy (NIRS, Nicolaï *et al*., 2007a), NIRS-based systems such as multispectral and hyperspectral imaging (Gowen *et al*., 2007), nuclear magnetic resonance imaging (NMR/MRI, Marcone *et al*., 2013; Zhang & McCarthy, 2013), and X-ray computed tomography (µCT, Donis-González *et al*., 2014; Magwaza & Opara, 2014). NIRS has become one of the most used methods for the assessment of fresh fruit according to their internal quality attributes (Nicolaï *et al*., 2007a). Furthermore, the feasibility of NIRS to assess quality attributes of fresh fruits and commercial application have been reported by numerous authors (McGlone *et al*., 2003; Gómez *et al*., 2006; Nicolaï *et al*., 2007a,b; Bobelyn *et al*., 2010; Magwaza *et al*., 2013a). However, the successful application of NIR spectroscopy to assess the quality attributes of fresh fruits and vegetables has mainly been restricted to fruits with homogeneous pulp and thin rind (De Oliveira *et al*., 2014). Applications of NIRS technology to monitor and predict quality attributes including the detection of physiological disorders in thick rind fruit have been limited due to the inadequate penetration depth of NIR radiation within the tissue. For internal quality measurements, it is important that the NIR radiation penetrates the tissue sufficiently, an issue

Stellenbosch University https://scholar.sun.ac.za

not often discussed in the literature. This is evident in Table 1, where the comparison between different non-destructive techniques for selected thick and thin rind fruit clearly indicates low prediction accuracies in fruit with thick rind compared to high prediction accuracies in those with a thin rind.

The objective of this review was, therefore, to discuss current knowledge on non-destructive measurement of internal and external quality of fruit with thick rind (such as pomegranate, pineapple, citrus, watermelon, melon, passion fruit, avocado and banana) and their limitations and potential commercial applications.

2. Application of NIR spectroscopy for quality analysis of fruit with thick rind

2.1. *Basic concepts of NIR spectroscopy*

NIR radiation covers a range of electromagnetic spectrum between 780 nm to 2500 nm. The NIR spectrum for a biological product comprise of broad bands arising from overlapping absorptions, corresponding mainly to overtones and combinations of vibrational modes. NIR radiation interacts with molecular groups and provides information about comparative proportions of C-H, O-H and N-H chemical bonds including scattering from microstructures and hence, texture (Nicolaï *et al*., 2007a; Nicolaï *et al*., 2009). In NIR spectroscopy, the sample is irradiated with NIR radiation. When the radiation penetrates the sample, the incident radiation may be either absorbed, transmitted or reflected, and the reflected light beams are collected and directed towards the detector. The NIR spectrum of a fruit or vegetable is dominated by absorption bands and therefore advance multivariate statistical techniques are applied to extract required information from spectral data.

2.2. *Measurement of internal and external quality attributes*

Several researchers have studied the potential application of NIR spectroscopy to measure internal quality in thick rind fruit. The thick rind interferes with the non-destructive internal quality measurement. This undesirable phenomenon was observed and has since been investigated by various authors. For instance, Dull *et al*. (1989) investigated non-destructive measurement of the SSC content of intact and sliced cantaloupe. The authors observed a higher coefficient of determination (R^2) of 0.97 and lower standard error of calibration (SEC) of 0.56 (TSS; °Brix) for cantaloupe slices and when intact fruit was measured lower prediction statistics were achieved (R^2 = 0.60 and SEC = 1.67 (TSS; °Brix)). In a similar study on intact melons, Dull and Birth (1989) obtained prediction statistics with a lower R^2 (0.87) and a higher SEC of 1.6 (TSS; °Brix). The authors explained their findings as a result of distorting influence

Stellenbosch University https://scholar.sun.ac.za

of the fruit rind. Furthermore, Kawano *et al*. (1993) used NIR transmittance to predict the sugar content in whole Satsuma mandarins and achieved R^2 = 0.989 and SEC = 0.28. However, the authors observed that it would be easier to determine internal composition in fruit with thin rind than in fruit with thick rind. Guthrie and Walsh (1997) observed that irregular rind surface, thick rind and variable composition present in pineapples provided unsatisfactory results in the measurement of SSC content. De Oliveira *et al*. (2014) compared the efficiency of NIR spectroscopy for prediction of internal quality traits in three structurally different fruit species (apricot, tomatoes, and passion fruit). Their results showed that NIR spectroscopy can be used to evaluate apricot internal quality, however, it was not appropriate to evaluate internal quality in fruits with thick rind, (passion fruit), and heterogeneous internal structure (tomato).

One of the most important considerations in NIR spectral acquisition is the optical path length of fruit. The fruit optical path and optical density (OD) can differ significantly due to differences in fruit size, thickness of rind and shape (Krivoshiev *et al*., 2000; Magwaza *et al*., 2012). Since the fruit rind is part of the light path, the spectrum of flesh OD will vary depending on the changes in rind OD (Krivoshiev *et al*., 2000). Regardless, the rind spectrum is always present within the spectral data used for quality evaluation. The thickness of the optical barrier affects the penetration depth defined by Chen and Nattuvetty (1980).

The reduced accuracy of NIR spectroscopy for the measurement of internal quality on thick rind fruit may be due to limited penetration depth of NIR radiation. The effects of light penetration depth and wavelength range on the measurement of fruit quality have been studied by several researchers. Guthrie and Walsh (1997) studied the quality of intact mango using NIR spectroscopy and reported that the penetration depth is dependent on the wavelength with a conclusion that all spectral information derived was from 5 mm of the fruit surface. Light penetration depth in 'Jonagold' apple fruit tissue was studied using NIR (Lammertyn *et al*., 2000). The authors reported that penetration was wavelength dependent with up to 4 mm in the 700–900 nm range and between 2 and 3 mm in the 900–1900 nm range. On the contrary, Fraser *et al*. (2001) reported that penetration depth of NIR in apple was much larger in the 700–900 nm range than in the 1400–1600 nm range mainly due to the absorption profile of water. These authors reasoned their results were due to high concentrations of water present in fresh fruit and that it is not possible to get sufficient light penetration outside the 380–1200 nm region. Fraser *et al*. (2003) assessed the light distribution across thick rind mandarin fruit (4 mm into the fruit) using illuminated laser light with 808 nm wavelength. The authors observed a rapid reduction in light level across the thick illuminated rind and a lower light reduction as the light continued to pass into the flesh (14 mm into the fruit). Furthermore, previous authors have

Stellenbosch University https://scholar.sun.ac.za

shown that the light intensity to detect fruit quality decreases exponentially with increased distance from the source (Birth, 1978; Chen & Nattuvetty, 1980; Lammertyn *et al*., 2000; Greensill and Walsh, 2000). The limited penetration depth restricts the potential of NIR for detecting internal defects and decreases the accuracy of NIR measurements of internal quality attributes of thick rind fruit (Nicolaï *et al*., 2007a).

The NIR wavelengths for determining quality parameters of different fruits and vegetables have been well established by many researchers. As a result of variability in species of horticultural products, cultivars within the species and the influence of growing environment, there is no agreement on the best wavelength range to study each quality parameter (Peiris *et al*., 1999). According to McGlone *et al*. (2003), the NIRS region of 750–1100 nm was optimal for internal quality assessment of mandarin fruit, whereas Gómez *et al*. (2006) reported NIR measurements for soluble solid content and acidity of Satsuma mandarin in the region of 350–2500 nm, with calibration models to predict SSC being R^2 = 0.94, root mean square error of prediction (RMSEP) = 0.33 for °Brix and R^2 = 0.80, RMSEP = 0.18% for acidity. However, optimal wavelength range for internal quality assessment of watermelon was in the region of 300–1000 nm (Hai-qing *et al*., 2007). Similarly, Flores *et al*. (2008) used a wavelength in the region between 400 and 1700 nm to assess the internal qualities of intact and sliced melons and watermelon by reflectance mode. The authors developed a poor calibration model with a predictive ability of intact fruit (cantaloupe melon (standard error of cross-validation (SECV)) = 1.43 °Brix and R^2 = 0.12; Galia melon SECV = 0.92 °Brix and R^2 = 0.67), respectively, however, when seasonal variation was considered a better calibration model was achieved for whole cantaloupe melon (SECV = 1.05 °Brix and R^2 = 0.73) and for Galia melon SECV = 0.98 °Brix and R^2 = 0.76). In a study aimed at assessing the internal quality attributes such as SSC, TA and ascorbic acid content in passion fruit, Maniwara *et al*. (2014) used the wavelength range of 600 to 1090 nm. The evaluation of literature gives a clear indication that majority of the investigators used a short wavelength region (300–1100 nm) and long wavelength region (up to 2400 nm) to measure the quality of fruit with thick rinds. This wavelength range is relevant to sugar and water as it includes the second and third overtone of OH stretching and vibrations which have been mainly associated with compounds such as soluble solids and acidity. Despite the challenge of the optical thickness of some fruit rinds, NIRS has been successfully used to measure internal quality attributes of fruits with thick rind such as melons, watermelon, citrus, passion fruit, pomegranates and avocados (Table 2).

The external appearance is the primary quality aspect used to evaluate fruits and vegetables when consumers are confronted with buying food products (Nicolai *et al*., 2009).

Stellenbosch University https://scholar.sun.ac.za

The presence of slight external disorders such as scalds, splitting, and chilling injury are challenges which reduce marketability, consumers acceptance thus causing economic loses. Under fruit grading systems, fruit with slight external defects are graded and marketed with sound fruit, thereby reducing the quality of the batch. Alternatively, fruit with slight defects is graded while seriously damaged fruit is removed altogether (Blasco *et al*., 2007; Magwaza *et al*., 2012). One of the challenges regarding rind disorders is that they do not manifest during harvest but rather between 1 to 12 weeks during postharvest storage and handling. For instance, scalding in pomegranates (Matityahu *et al*., 2014) and rind breakdown disorder of 'Clementine' mandarin (Magwaza *et al*., 2014a,b). The most current non-destructive quality measurement technologies have been developed to assess fresh fruit according to their internal quality attributes (Butz *et al*., 2005). However, very limited research has been conducted to develop a technology that can assess, predict and monitor physiological disorders in thick rind fruit (Magwaza *et al*., 2012b; Magwaza *et al*., 2014a, b). Nevertheless, NIR has been successfully used to detect surface bruising in apple (Geeola *et al*., 1994), peach surface defects (Miller & Delwiche, 1991), kiwifruit disorders (chilling injury and fruit rot) during storage (Clark *et al*., 2004a) and rind breakdown in mandarins (Magwaza *et al*., 2014b).

2.3. *Commercial applications of NIR spectroscopy*

NIR spectroscopy's online assessment of fruit quality for industrial application has been used in the rapid analysis of thin rind fruit such as peaches, apples and more recently applied to thick rind fruit such as citrus and watermelons (Miller & Zude, 2002; Jie *et al*., 2014). Although NIR is a well-established non-destructive tool for the measurement of internal quality attributes, one of the disadvantages of NIR application for online sorting is that new calibrations are required for different fruit species and cultivars. A review by Walsh (2005) discussed the applications and limitations to the adoption of commercially available, low cost, miniaturised NIR spectrophotometers for the assessment of the sugar content of intact fruit. Improving the robustness of multivariate calibration models of Vis/NIR would present a high potential for in-line commercial measurements (Cozzolino, 2014, Magwaza & Opara, 2015). Furthermore, future designing of specialised NIR systems need to consider higher light intensity sources, increased integration time as well as increased spectrometer aperture/detector size for internal information acquisition (Magwaza & Opara, 2015). Through the improvement of photodetectors and measuring devices the problems in non-destructive quality evaluation and sorting are gradually being eliminated. Although the technology is available for commercial application, it has been limited due to the high cost of NIR spectroscopy, technical limitations,

Stellenbosch University https://scholar.sun.ac.za

grower resistance and supply chain limitations. Given the recent developments in NIR technology, its adoption for commercial online sorting has a huge potential in the industry.

3. Multispectral and hyperspectral imaging

3.1. *Basic concepts of hyperspectral and multispectral systems*

Multispectral imaging involves creating images using more than one spectral component of the electromagnetic energy from the same region of an object and at the same scale (Magwaza *et al*., 2012). In general, multispectral imaging is a form of imaging that involves capturing two or more waveband monochromatic images in the spectrum (Zhang *et al*., 2014). On the other hand, hyperspectral imaging also known as chemical and spectroscopic imaging integrates both spectroscopic and imaging into one system. Hyperspectral imaging uses a set of monochromatic images from hundreds of contiguous wavebands for each spatial position of a sample studied thus each pixel in an image contains the spectrum for that specific position (Gómez-Sanchis *et al*., 2008).

Since image data are considered two dimensional, by adding a new dimension of spectral information, the hyperspectral data can be perceived as three-dimensional data cube known as 'hypercubes' (Iqbal *et al*., 2014). Further information on the principles of these technologies can be found in a review by Gowen *et al*. (2007).

3.2. *Measurement of fruit internal and external quality attributes*

Recently, multispectral and hyperspectral imaging systems have been successfully used to study the internal quality of thick rind fruits. Table 3 summarises the applications of multispectral and hyperspectral imaging to assess the internal quality parameters of thick rind fruit. Sugiyama and Tsuta (2010) investigated the use of hyperspectral imaging to determine the physiological ripeness of melons by mapping sugar distribution at different maturity stages. Ma *et al*. (2012) applied hyperspectral imaging technique in the wavelength region of 400–1000 nm by comparing different spectrum correction and pre-treatment methods to predict the SSC of melons using diffuse reflectance. The authors also reported good prediction with a correlation coefficient of 0.86 and RMSEP of 0.87. Makino *et al*. (2013) applied hyperspectral imaging technique for predicting SSC of mango during storage using the visible to short wavelength region (380–1000 nm). Using artificial neural networks (ANN) chemometric tool, the authors predicted SSC of mangoes with reasonable accuracy (R^2 = 0.79; root mean square error of calibration (RMSEC) = 0.069 °Brix). In a recent study, Khodabakhshian *et al*. (2015) investigated the use of multispectral imaging to determine the quality and maturity of

Stellenbosch University https://scholar.sun.ac.za

pomegranate fruit. The authors observed high correlation coefficient and residual predictive deviation (RPD) values for TSS (R^2 = 0.97, RPD = 6.7), pH (R^2 = 0.93, RPD = 5.01), and firmness (R^2 = 0.95, RPD = 5.65).

Several spectroscopic studies have demonstrated the potential of multispectral and hyperspectral imaging to detect external defects. Table 4 presents an overview of applications of multispectral and hyperspectral imaging systems to assess the external quality attributes of different fruits. For example, Gómez-Sanchis *et al*. (2008) applied hyperspectral imaging for early detection of rottenness caused by *Penicillium digitatum* in mandarins fruit rind. The authors reported a classification rate of above 91% for the detection of rotten fruit. Blasco *et al*. (2009) developed a multispectral inspection system to detect and sort citrus fruits according to 11 different types of external defects with 86% accuracy. Furthermore, Balasundaram *et al*. (2009) investigated the use of multispectral imaging for the detection of citrus cranker on rind of grapefruit within a wavelength range of 200–2500 nm. The authors performed discriminatory data analysis on reflectance spectral data and accurately predicted 100% of fruit infected by citrus canker. These studies have collectively shown the possibility of multispectral and hyperspectral systems in the evaluation of internal and external properties of different agricultural products using spectral information.

3.3. *Commercial application of multispectral and hyperspectral imaging*

Although scientific literature is replete with studies exploring the feasibility of multispectral and hyperspectral imaging systems for non-destructive evaluation of fruit quality, on-line and real-time applications are limited. The drawback of multispectral and hyperspectral systems is the accumulation of vast amounts of data which usually involves a significant amount of time for image acquisition under laboratory conditions, and relatively complicated procedures for offline image analysis (Qin *et al*., 2013). Hence, this creates novel opportunities and applications that need to be investigated in order to reduce the processing time to allow both the acquisition and image processing software to be implemented in a real-time system.

4. X-ray computed tomography

4.1. *Basic concepts of X-ray computed tomography (µCT) scanning*

X-ray CT has become one of the well-established non-destructive techniques for the measurement of internal and external morphological characteristics as well as detection of internal defects in agricultural products (Lammertyn *et al*., 2003a,b; Herremans *et al*., 2014; Kotwaliwale *et al*., 2014). X-ray CT measures variation in material density of the sample and

Stellenbosch University https://scholar.sun.ac.za

it is based on the attenuation of X-rays depending on the mass density and mass absorption coefficient of the irradiated object and has a wavelength range of 0.01 to 10 nm (Maire *et al*., 2001; Salvo *et al*., 2003). X-ray CT number is the standard unit used for measuring X-ray absorption characteristics. CT numbers are based on linear X-ray absorption coefficients and, in general, is expressed by brightness data in an image (Arendse *et al*., 2016a). A grey scale image is based on these numbers in which as the CT number increases, the pixels approach white colour (Salmanizadeh *et al*., 2014).

4.2. *Characterization of internal structures*

X-ray µCT has been shown to be an effective technique for estimation and characterization of internal structures in fruit with thick rind. Cantre *et al*. (2014) applied X-ray µCT to investigate the changes in the 3-D microstructure of mango during ripening. Through the analysis of pore and tissue network, the study revealed differences in microstructures along the radial axis of the fruit and a decrease in porosity as the fruit ripens. The study further reported a loss of connectivity of pores with increasing ripeness. Magwaza & Opara (2014) investigated the feasibility of X-ray µCT imaging for the quantification and characterization of pomegranate fruit (cv. Shani-Yonay) internal structures. The study demonstrated the potential use of X-ray µCT and image analysis as a useful technique for the quantification of edible (arils) and non-edible (albedo) portions of pomegranate fruit. In a similar study, Salmanizadeh *et al*. (2014) used X-ray µCT for volume estimation of two Iranian cultivars (‘Rabab Malas’ and ‘Rabab Torsh’) and their components, including arils, albedo, seeds, and whole fruit. More recently, Arendse *et al*. (2016a) quantified volumes of key parts of pomegranate fruit (cv. Wonderful) relevant to the food and beverage industry. The authors were able to estimate the total amount of arils per fruit and quantify volumes of arils, kernels, albedo and juice content.

In fruit such as pomegranate, physical properties such as the volume of whole fruit and juice content relative to the albedo are important in the marketing of the fruit because they influence consumer preference (Fawole & Opara, 2013a). In pomegranate fruit, aril yield is a highly desirable property for growers, breeders, processors and consumers alike. However, the proportion of aril content (number of arils, volume and juice content) relative to the albedo fraction varies depending on the variety, maturity and growing region (Fawole & Opara, 2013b). Table 5 provides a summary of application of X-ray µCT on pomegranate. The results of these studies show the use of X-ray µCT as a promising tool for non-destructive characterization of internal structures of thick rind fruit.

Stellenbosch University https://scholar.sun.ac.za

4.3. *Detection of physical defects*

Internal defects within agricultural produce are not revealed by external visual symptoms. Internal disorders are usually the result of anatomical and physiological changes within the tissue such as moisture loss, chemical conversion, senescence, microorganism attack, cell breakdown (physiological decay) and insect injury (Donis-González *et al*., 2014). Therefore, non-destructive and non-invasive monitoring techniques are beneficial to investigate the occurrence and development of internal disorders. X-ray µCT is a non-destructive tool that has been applied for the direct structural and 3-D detection of internal defects in horticultural produce. Due to the high moisture content of fruit and vegetables, water dominates X-ray absorption. Defects that affect the density and the water content of internal tissue can, therefore, be detected and visualised by X-ray imaging (Nicolaï *et al*., 2009).

X-ray µCT has been successfully applied to study internal disorders in fruit with thick rind, such as translucency in pineapples (Haff *et al*., 2006), blackheart disease and false codling moth in pomegranate (Arendse *et al*., 2016b), granulation and endoxerosis in citrus (Van Dael *et al*., 2016b). X-ray tomography can detect materials with different densities, it also has the potential for non-destructive segregation of fruit affected by internal defects such as heart rot in pomegranate (Zhang & McCarthy, 2012).

4.4. *Commercial application of X-ray µCT*

Despite its potential as a technique for inspection of horticultural produce with capabilities of detecting internal defects that go beyond the traditional inspection of the human eye, X-ray µCT has a series of problems that must be considered before it can be used for the in-line application. For instance, X-ray µCT systems are expensive and complex compared with other technologies such as NIR and hyperspectral imaging. Additionally, health and safety issues may arise from using an open X-ray µCT system for the industrial application may result in leakage of X-ray radiation, creating a health hazard. On the other hand, the current data acquisition and lengthy processing times required for analysis do not allow them to be used for in-line or real-time inspection systems, although this gives novel research opportunities that warrant further research focused on designing a proper shield that can prevent human exposure, and reduce large data size and image analysis in order to provide rapid real-time non-destructive detection of internal defects.

Stellenbosch University https://scholar.sun.ac.za

5. Nuclear magnetic resonance (NMR) and magnetic resonance imaging (MRI)

5.1. Basic concepts of NMR nuclear magnetic resonance imaging

The basic principles of NMR spectroscopy depend on the fact that most elements have at least one isotope and therefore are magnetic (Eberle, 2005). For example, ^{1}H, ^{13}C, ^{31}P have a magnetic moment and are able to absorb resonance energy when placed in a strong magnetic field (Eberle, 2005). It orientates itself in either the same direction or the opposite direction of the field. These two directions or states have different energy levels and the difference in energy is unique for each nucleus and depends on the strength of the magnetic field. The energy difference can be measured by exposing the nucleus to electromagnetic radiation causing the nucleus to change from a lower energy level to an adjacent higher energy level (Friebolin, 2005). The radiation required to induce this nuclear magnetic radiation transition is called the radio frequency field. NMR analysis is often based on the behaviour (relaxation) of NMR active nuclei in a magnetic field. Relaxation often describes a complex process of the nuclei from excitation due to the splitting of the nuclear spin levels (Zeeman effect) applied by a magnetic field to equilibrium (Marcone *et al*., 2013). Further information on the basic concepts and principles of NMR can be found in a review by Butz *et al*. (2005).

5.2. *Measurement of internal quality attributes*

NMR has been shown to be an effective non-destructive technique for internal quality assessment in a wide variety of fruit species. For instance, Gil *et al*. (2000) studied the composition of intact mango pulp and mango juice during ripening using NMR. The authors identified the main sugars (glucose, fructose and sucrose) and approximately 40 metabolites in mango during ripening. By using NMR, Marigheto *et al*. (2005) studied the relaxation time of avocados and established a good correlation between oil content and single shot pulse sequence. Khoshroo *et al*. (2009) investigated the feasibility of magnetic resonance (MR) imaging for assessment of pomegranate fruit maturity. Using discriminant analysis, the authors reported a classification accuracy of 100%, 98.47% and 100% for semi-ripe, ripe and over-ripe fruit, respectively. Zhang and McCarthy (2013) studied the relationship between NMR spin-spin (T_2) relaxation time and pomegranate fruit (cv. Wonderful) quality attributes such as soluble solid content (SSC), titratable acidity (TA), pH and SSC/TA. The authors reported that T_2 relaxation time showed a strong correlation with soluble solid content in pomegranate fruit. However, no correlation was established between pH, TA, SSC/TA and T_2. In exploring the capability of NMR, Kraszni *et al*. (2013) studied and identified the eight aromatic singlet resonances of α- and β-punicalagin in pomegranate juice in the acidic pH range. Recently,

Stellenbosch University https://scholar.sun.ac.za

Yuan *et al*. (2017) used a high-resolution NMR to study the metabolite changes in banana during postharvest senescence. The authors identified primary and secondary metabolites in banana fruit, including organic acids, amino acids, carbohydrates and phenolics. Furthermore, several metabolites responsible for postharvest senescence were identified including valine, alanine, aspartic acid, choline, acetate, glucose, malic acid, gallic acid and dopamine.

5.3. *Detection of physical defects*

The application of NMR has been applied as a qualitative tool to study worm damage (Chen *et al*., 1989), woolly breakdown in nectarines (Sonego *et al*., 1995), bruises in apples (Zion *et al*., 1995), to detect void spaces in watermelon (Saito *et al*., 1996), detect and monitor the internal browning development in 'Fuji' apples and 'Conference' pears (Gonzalez *et al*., 2001; Hernandez-Sanchez *et al*., 2007) and internal decay in pomegranates (Khoshroo *et al*., 2009). NMR has been used to determine the effect of physiological changes induced by *Alternaria* spp. and *Aspergillus* spp. and to detect black heart (heart rot) in pomegranate fruit (Zhang & McCarthy, 2012). By means of proton NMR relaxation, the authors investigated the water T_2 relaxation distribution of infected and healthy pomegranate arils. Their results indicated that T_2 relaxation distribution of healthy arils gave three distinct relaxation peaks corresponding to different water compartments of tissue. However, in affected arils, the three relaxation components shifted to a lower relaxation time and a new relaxation component appeared, indicating that water redistribution among the cell compartments caused by the infection. The infection induced an alteration in the microstructure in arils and caused a significant change in the T_2 relaxation spectrum. The authors developed a classification model based on the region of interest (ROI) for the classification of black heart using partial least squares-discriminant analysis (PLS-DA). The developed PLS-DA model based on histogram features of MR image showed 91% accuracy for the prediction of healthy fruit and 92% accuracy in detecting the presence of black heart in pomegranate fruit. Recently, Zur *et al*. (2016) used MRI to predict fruit splitting in Nova mandarins. By subjecting the fruit trees to low and high irrigation levels and by analysing the internal tissue dimensions the authors were able to predict splitting as early as 2 months before split fruit occurs.

Stellenbosch University https://scholar.sun.ac.za

5.4. *Commercial application of NMR technology*

One of the important objectives governing non-destructive technology development research in fruit postharvest science is to explore the possibilities of a technology such as NMR for in-line assessment of quality. The potential use of NMR/MRI for non-invasive monitoring of internal and external properties has been successfully applied to horticultural produce (Hills and Clark, 2003; Hills, 2006). However, extending the application of NMR technology beyond research into in-line commercial use in fruit packing houses has been restricted to several barriers including high-cost constraints for the development of NMR spectroscopy, the expertise involved, and safety issues related to magnetic field maintenance (Marcone *et al*., 2013). Furthermore, researchers also face challenges to develop standard operational procedures of NMR analysis for specific categorised products. Although integrating low-field NMR and MRI is more likely to become feasible due to the lower cost, easy maintenance and are relatively more accessible to researchers but their applications are limited. Application of NMR and MRI for in-line and real-time detection of internal quality still needs to be investigated.

Raman spectroscopy

6.1. *Basic concepts of Raman spectroscopy*

In 1928 a physicist Chandrashekhara Venkata Raman discovered the phenomena of inelastic scattering of light known as the Raman effect (Raman & Krishnan, 1928). The mechanism for Raman scattering lies in the change of the rotational or vibrational quantum states of molecules being irradiated (Wang, 2013). In this process, an inelastic collision between the incident photon and the molecule of the sample occurs. When a sample is irradiated by a laser beam, a tiny portion of photons with a known frequency and polarization are scattered from the sample. If the molecule gains vibrational energy, scattered photons are shifted to longer wavelengths, giving rise to Stokes lines in the Raman spectrum. If the molecule loses vibration energy they are shifted to shorter wavelengths, giving rise to anti-Stokes lines in the Raman spectrum (Yang & Ying, 2011). As a result, the vibrational or rotational energy of the molecule is changed, and the scattered radiation is shifted to a different wavelength causing a change in the energy, and therefore the frequency of the scattered light. The frequency difference between scattered radiation and incident radiation is called a Raman shift (Yang & Ying, 2011). The frequency shifts of scattered light can be analysed and presented as spectral data. The spectral bands represent vibrational characteristics for chemical bonds and functional groups the chemical structure of the molecules responsible for scattering (Das & Agrawal, 2011).

Stellenbosch University https://scholar.sun.ac.za

6.2. *Measurement of internal and external quality*

Many researchers have attempted to apply Raman spectroscopic techniques in structural analysis, safety control, classification, and quantification of fruits and vegetables. Limited research work has been conducted on the analysis of internal quality attributes of intact fruit. Nevertheless, Raman spectroscopy has been successfully used to predict the internal quality attributes tomatoes (Nikbakht *et al*., 2011). The authors developed calibration models using partial least squares regression (PLSR) and principal component regression (PCR) for the prediction of sugar and colour in tomato fruit. In addition, more accurate predictions using PLS for colour (R^2 = 0.85, RMSEP = 0.33) and SSC (R^2 = 0.79, RMSEP = 0.30) compared to PCR for colour (R^2 = 0.82, RMSEP = 0.38) and SSC (R^2 = 0.78, RMSEP = 0.38) were reported (Nikbakht *et al*., 2011). Raman spectroscopy has been frequently used to determine carotenoid content in fruits and vegetables. Baranska *et al*. (2006), compared the determination of lycopene and α-carotene content in tomato fruits and its related products by means of NIR and FT-Raman spectroscopy. The authors reported that the prediction quality of FT Raman for lycopene (R^2 = 0.91, SECV = 74.34) and α-carotene (R^2 = 0.89, SECV = 0.34) was better than that of NIR for lycopene (R^2 = 0.85, SECV = 91.19) and α-carotene (R^2 = 0.80, SECV = 0.41). Similarly, Qin *et al*. (2012) studied the internal maturity of tomato using spatially offset Raman spectroscopy (SORS). This study showed that SORS was able to distinguish the difference in colour based on the appearance of carotenoids throughout all tomatoes after the mature green stage to a penetration depth of 10 mm. The authors argued that the loss of lutein and β-carotene and the accumulation of lycopene in the tomatoes during the ripening caused a shift in the Raman peak from 1525 cm^{-1} (the lutein at the mature green stage) to 1513 cm^{-1} (the lycopene at the red stage). Moreover, it was reported that spectral information divergence (SID) to evaluate the Raman peaks with pure lycopene as a reference could effectively be implemented for determining the appropriate harvest time for green surfaced tomatoes. Gonzálvez *et al*. (2013) successfully used transmission resonance Raman spectroscopy to monitor the enhancement of β-carotene content in table grapes using low doses of UV-B LED irradiation.

Limited research has been applied to study external quality in thick rind fruit. However, Raman spectroscopy has been successfully applied for external analysis of fruits and vegetables. For instance, Gao *et al*. (2003) conducted bruise identification studies on apples with Raman spectroscopy. Zhang *et al* (2006), used FT Raman spectroscopy to measure pesticide residues left on the surface of fruits. Bonora *et al*. (2009) used FT Raman spectroscopy for identification of microbial disease in Kiwifruit from elephantiasis affected plants. Liu *et al*. (2012) attempted to identify and detect sulphur-containing pesticides in apple,

Stellenbosch University https://scholar.sun.ac.za

grape, pear, mango, and peach rinds, using shell thickness dependent Raman enhancement with individual silver-coated gold nanoparticles (AuNPs) for rapid identification and detection of pesticide residues at fruit rinds. Although this study did not establish calibration models for quantification, the potential of Raman spectroscopy in on-site assessment of food safety was clearly evident. Further information on the analysis Agricultural application of Raman spectroscopy has been reviewed by Yang and Ying (2011).

6.3. *Commercial application*

Raman spectroscopy is considered a promising technique for food-safety assessment because it is rapid, sensitive and requires minimal sample preparation. By integrating Raman spectroscopy with other non-destructive techniques such as NIR, FTIR and chemometric methods show promising results for online quality and safety control of horticultural produce. Nevertheless, more research needs to be conducted to assess the feasibility of Raman spectroscopy for online grading and sorting of internal and external quality attributes of horticultural produce in particular fruits with thick rind.

7. Conclusions

Many novel non-destructive tools are available for measuring internal quality attributes of fruit and vegetables. The advantages and disadvantages of each non-destructive technique have been extensively discussed in this review. It is evident that NIR spectroscopy is well suited for measurement of internal quality attributes and can be implemented in controlled processes for on-line and inline fruit grading. Through steady improvements in light intensity sources, photo detectors, optics and integration time, future NIR systems could improve the measurement of internal quality attributes of fruit with thick rind. Furthermore, innovative technologies such as Raman spectroscopy and multispectral and hyperspectral imaging offer new prospects. NIRS and similar technological tools reviewed in this review offer a potential for non-destructive measurement and prediction of these quality problems. Consequently, grading based on internal quality attributes, rather than external appearance has become possible, and this is expected to radically change the way fresh fruit is commercialised. However, these non-destructive applications face many challenges for online application such as high cost of equipment, reducing data acquisition and processing times, potential health hazard when utilizing equipment such as X-ray µCT and NMR. In conclusion, to exploit the full potential of the above-described technologies for successful commercial implementation future research

Stellenbosch University https://scholar.sun.ac.za

focusing on the reliability of measurements as well as reduction of data acquisition and processing times is required.

References

Abebe, A.T. (2006). Total sugar and maturity evaluation of intact watermelon using near infrared spectroscopy. *Journal of Near Infrared Spectroscopy*, **14**, 67–70.

Aleixos, N., Blasco, J., Navarrón, F. & Moltó, E. (2002). Multispectral inspection of citrus in real-time using machine vision and digital signal processors. *Computers and Electronics in Agriculture*, **33**, 121–137.

Arendse, E., Fawole, O.A., Magwaza, L.S. & Opara, U.L. (2016a). Non-destructive characterization and volume estimation of pomegranate fruit external and internal morphological fractions using X-ray computed tomography. *Journal of Food Engineering*, **186**, 42–49.

Arendse, E., Fawole, O.A., Magwaza, L.S. & Opara, U.L. (2016b). Estimation of the density of pomegranate fruit and their fractions using X-ray computed tomography calibrated with polymeric materials. *Biosystems Engineering*, **148**, 148–156.

Arendse, E., Fawole, O.A., Magwaza, L.S., Nieuwoudt, H.H. & Opara U.L. (2017). Development of calibration models for the evaluation of pomegranate aril quality by Fourier-transform near infrared spectroscopy combined with chemometrics. *Biosystems Engineering*, **159**, 22–32.

Balasundaram, D., Burks, T.F., Bulanon, D.M., Schubert, T. & Lee, W.S. (2009). Spectral reflectance characteristics of citrus canker and other peel condition of grapefruit. *Postharvest Biology and Technology*, **51**, 220–226.

Baranska, M., Schultze, W. & Schulz, H. (2006). Determination of lycopene and α-carotene content in tomato fruits and related products: comparison of FT-Raman, ATR-IR and NIR spectroscopy. *Analytical Chemistry,* **78**, 8456–8461.

Birth, G.S. (1978). The light scattering properties of food. *Journal of Food Science*, **43**, 916–925.

Blanco, M. & Villarroya, I. (2002). NIR spectroscopy: a rapid-response analytical tool. *Trends in Analytical Chemistry*, **21**, 240–250.

Blasco, J., Aleixos, N. & Moltó, E. (2007). Computer vision detection of peel defects in citrus by means of a region oriented segmentation algorithm. *Journal of Food Engineering*, **81**, 535–543.

Stellenbosch University https://scholar.sun.ac.za

Blasco, J., Aleixos, N., Gómez-Sanchís, J. & Moltó, E. (2009). Recognition and classification of external skin damage in citrus fruits using multispectral data and morphological features. *Biosystems Engineering*, **10**, 137–145.

Bobelyn, E., Serban, A., Nicu, M., Lammertyn, J., Nicolaï, B.M. & Saeys, W. (2010). Postharvest quality of apple predicted by NIR spectroscopy: study of the effect of biological variability on spectra and model performance. *Postharvest Biology and Technology*, **55**, 133–143.

Bonora, S., Francioso, O., Tugnoli, V., Prodi, A., Di Foggia, M., Righi, V., Nipoti, P., Filippini, G. & Pisi, A. (2009). Structural characteristics of 'Hayward' kiwifruits from elephantiasis affected plants studied by DRIFT, FT-Raman, NMR, and SEM techniques. *Journal of Agricultural and Food Chemistry*, **57**, 4827–4832.

Butz, P., Hofmann, C. & Tauscher, B. (2005). Recent developments in non-invasive techniques for fresh fruit and vegetable internal quality analysis. *Journal of Food Science*, **70**, 131–141.

Cantre, D., Herremans, E., Verboven, P., Ampofo-Asiama, J. & Nicolaï, B.M. (2014). Characterization of the 3-D microstructure of mango (*Mangifera indica* L. cv. Carabao) during ripening using X-ray computed microtomography. *Innovative Food Science & Emerging Technologies*, **24**, 28–39.

Cayuela, J.A. (2008). Vis–NIR soluble solids prediction in intact oranges (*Citrus sinensis* L.) cv. Valencia Late by reflectance. *Postharvest Biology and Technology*, **47**, 75–80.

Cen, H., Lu, R., Mendoza, F.A. & Ariana, D.P. (2011). Peach maturity/quality assessment using hyperspectral imaging-based spatially resolved technique. Proc. SPIE 8027.

Chen, P. & Nattuvetty, V.R. (1980). Light transmittance through a region of an intact fruit. *Transactions of the American Society of Agricultural Engineers*, **23**, 519–522.

Chen, P., McCarthy, J.M. & Kauten, R. (1989). NMR for internal quality evaluation of fruits and vegetables. *Transactions of the American Society of Agricultural Engineers*, **32**, 1747–1753.

Chen, L. & Opara, U.L. (2013a). Texture measurement approaches in fresh and processed foods–a review. *Food Research International*, **51**, 823–835.

Chen, L. & Opara, U.L. (2013b). Approaches to analysis and modeling texture in fresh and processed foods–a review. *Journal of Food Engineering*, **119**, 497–507.

Clark, C.J., McGlone, V.A., DeSilva, H.N., Manning, M.A., Burdon, J. & Mowat, A.D. (2004a). Prediction of storage disorders of kiwifruit (*Actanidia cinensis*) based on

Stellenbosch University https://scholar.sun.ac.za

visible-NIR spectral characteristics at harvest. *Postharvest Biology and Technology*, **32**, 147–158.

Clark, C.J, McGlone, V.A., Requejo, C., White, A. & Woolf, A.B. (2004b). Dry matter determination in 'Hass' avocado by NIR spectroscopy. *Postharvest Biology and Technology*, **29**, 300–307.

Cozzolino, D. (2014). An overview of the use of infrared spectroscopy and chemometrics in authenticity and traceability of cereals. *Food Research International*, **60**, 262–265.

Dale, L.M., Thewis, A., Boudry, C., Rotar, I., Dardenne, P., Baeten V. & Pierna, F. (2013). Hyperspectral imaging application in agriculture and agro-food product quality and safety control: A review. *Applied Spectroscopy*, **48**, 142–159.

De Oliveira, G.A., Bureau, S., Renard, C.M.G.C., Pereira-Netto, A.B. & de Castilhos, F. (2014). Comparison of NIRS approach for prediction of internal quality traits in three fruit species. *Food Chemistry*, **143**, 223–230.

Das, R.S. & Agrawal, T.K. (2011). Raman spectroscopy: Recent advancements, techniques and applications. *Vibrational Spectroscopy*, **57**, 163–176.

Donis-González, I.R., Guyer, D.E., Fulbright, D.W. & Pease, A. (2014). Postharvest non-invasive assessment of fresh chestnut (*Castanea* spp.) internal decay using computer tomography images. *Postharvest Biology and Technology*, **94**, 14–25.

Dull, G.G. & Birth, G.S. (1989). Non-destructive evaluation of fruit quality: use of near infrared spectrophotometry to measure soluble solids in intact honeydew melons. *HortScience*, **24**, 754.

Dull, G.G., Birth, G.S., Smittle, D.A. & Leffler, R.G. (1989). Near infrared analysis of soluble solids of intact cantaloupe. *Journal of Food Science*, **54**, 393–395.

Eberle, K. (2005). Evaluation of near infrared and nuclear magnetic resonance spectroscopy for rapid quality control of South African virgin olive oils. MSc in Food Science, Thesis, University of Stellenbosch, South Africa.

Fawole, O.A. & Opara, U.L. (2013a). Developmental changes in maturity indices of pomegranate fruit: A descriptive review. *Scientia Horticulturae*, **159**, 152–161.

Fawole, O.A. & Opara, U.L. (2013b). Fruit growth dynamics, respiration rate and physico-textural properties during pomegranate development and ripening. *Scientia Horticulturae*, **157**, 90–98.

Stellenbosch University https://scholar.sun.ac.za

Flores, K., Sánchez, M.T., Pérez-Martin, D.C. López, M.D. Guerrero, J.E. & Garrido-Varo, A. (2008). Prediction of soluble solid content of intact and cut melons and watermelons using near infrared spectroscopy. *Journal of Near Infrared Spectroscopy*, **16**, 91–98.

Fraser, D.G., McGlone, V.A., Jordan, R.B. & Kunnemeyer, R. (2001). NIR (Near Infra-Red) light penetration into an apple. *Postharvest Biology and Technology*, **22**, 191–194.

Fraser, D.G., Jordan, R.B., Kűnnemeyer, R. & McGlone, V.A. (2003). Light distribution inside mandarin fruit during internal quality assessment by NIR spectroscopy. *Postharvest Biology and Technology*, **27**, 185–196.

Friebolin, H. (2005). *Basic One- and Two Dimensional NMR spectroscopy*, 4th ed. Weinheim: Wiley-VCH.

Gao, X., Heinemann, P.H. & Irudayaraj, J. (2003). Non-destructive apple bruise on-line test and classification with Raman spectroscopy, American. *Society of Agricultural and Biological Engineers*, Meeting Paper No. 033025.

Geeola, F., Geeola, F. & Peiper, U.M. (1994). A spectrophotometric method for detecting surface bruises on 'Golden Delicious' apples. *Journal of Agricultural Engineering Research*, **58**, 47–51.

Gil, A.M., Duarte, I.F., Delgadillo, I., Colquhoun, I.J., Casuscelli, F. & Humpfer, E. (2000). Study of the compositional changes of mango Turing ripening by use of nuclear magnetic resonance. *Journal of Agricultural and Food Chemistry,* **48**, 1524–1536.

Giovanelli, G., Sinelli, N., Beghi, R., Guidetti, R. & Casiraghi, E. (2014). NIR spectroscopy for the optimization of postharvest apple management. *Postharvest Biology and Technology*, **87**, 13–20.

Gómez, A.H., He, Y. & Pereira, A.G. (2006). Non-destructive measurement of acidity, soluble solids and firmness of Satsuma mandarin using Vis–NIR spectroscopy techniques. *Journal of Food Engineering*, **77**, 313–319.

Gómez-Sanchis, J., Gómez-Chova, L., Aleixos, N., Camps-Valls, G., Montesinos-Herrero, C. & Moltó, E. (2008). Hyperspectral system for early detection of rottenness caused by *Penicillium digitatum* in mandarins. *Journal of Food Engineering*, **89**, 80–86.

Gonzalez, J.J., Valle, R.C., Bobroff, S., Biasi, W.V., Mitcham, E.J. & McCarthy, M.J. (2001). Detection and monitoring of internal browning development in 'Fuji' apples using MRI. *Postharvest Biology and Technology*, **22**,179–88.

Stellenbosch University https://scholar.sun.ac.za

Gonzálvez, A.G., Martínez, N.I., Telle, H.H. & Ureña. A.G. (2013). Monitoring LED-induced carotenoid increase in grapes by transmission resonance Raman spectroscopy. *Chemical Physics Letters*, **559**, 26–29.

Gowen, A.A., O'Donnell, C.P., Cullen, P.J., Downey, G. & Frias, J.M. (2007). Hyperspectral imaging-an emerging process analytical tool for food quality and safety control. *Trends in Food Science and Technology*, **18**, 590–598.

Greensill, C.V. & Walsh, K.B. (2000). A remote acceptance probe and illumination configuration for spectral assessment of internal attributes of intact fruit. *Measurement Science and Technology*, **11**, 1674–1684.

Greensill, C.V., Wolf, P.J., Spiegelman, C.H. & Walsh, K.B. (2001). Calibration transfer between PDA-based NIR spectrometers in the NIR assessment of melon soluble solids content. *Applied Spectroscopy*, **55**, 647–653.

Guthrie, J. & Walsh, K. (1997). Non-invasive assessment of pineapple and mango fruit quality using near infrared spectroscopy. *Australian Journal of Experimental Agriculture*, **37**, 253–263.

Guthrie, J.A., Wedding, B. & Walsh, K.B. (1998). Robustness of NIR calibrations for soluble solids in intact melon and pineapple. *Journal of Near Infrared Spectroscopy*, **6**, 259–265.

Guthrie, J.A., Walsh, K.B., Reid, D.J. & Liebenberg, C.J. (2005a). Assessment of internal quality attributes of mandarin fruit. 1. NIR calibration model development. *Australian Journal of Agricultural Research*, **56**, 405–416.

Guthrie, J.A., Reid, D.J. & Walsh, K.B. (2005b). Assessment of internal quality attributes of mandarin fruit. 2. NIR calibration model robustness. *Australian Journal of Agricultural Research*, **56**, 417–426.

Guthrie, J.A., Liebenberg, C.J. & Walsh, K.B. (2006). NIR model development and robustness in prediction of melon fruit total soluble solids. *Australian Journal of Agricultural Research*, **57**, 1–8.

Haff, R.P., Slaughter, D.C., Sarig, Y. & Kader, A. (2006). X-ray assessment of translucency in pineapple. *Journal of Food Processing and Preservation*, **30**, 527–533.

Hai-qing, T., Yi-bin, Y., Hui-shan, L., Xia-ping, F. & Hai-yan, Y. (2007). Measurement of soluble solids content in watermelon by Vis/NIR diffuse transmittance technique. *Journal of Zhejiang University Science B*, **8**, 105–110.

Hernandez-Sanchez, N., Hills, B.P., Barreiro, P. & Marigheto, N. (2007). An NMR study on internal browning in pears. *Postharvest Biology and Technology*, **44**, 260–270.

Stellenbosch University https://scholar.sun.ac.za

Herremans, E., Melado-Herreros, A., Defraeye, T., Verlinden, B., Hertog, M., Verboven, P., Val, J., Fernández-Valle, M.E., Bongaers, E., Estrade, P., Wevers, M., Barreiro, P. & Nicolaï, B.M. (2014). Comparison of X-ray CT and MRI of watercore disorder of different apple cultivars. *Postharvest Biology and Technology*, **87**, 42–50.

Hills, B.P. & Clark, C.J. (2003). Quality Assessment of Horticultural Products by NMR. *Annual Reports on NMR Spectroscopy*, **50**, 75–120.

Hills, B.P. (2006). NMR Relaxation and Diffusion Studies of Horticultural Products. In: *Modern Magnetic Resonance* (edited by G.A. Webb). Pp. 1721–1727. Springer, Netherlands.

Iqbal, J., Sun, D.W. & Allen, P. (2014). An overview on principle, techniques, and applications of hyperspectral imaging with special reference to ham quality evaluation and control. *Food Control*, **46**, 242–254.

Jiang, J.A., Chang, H.Y., Wu, K.H., Ouyang, C.S., Yang, M.M., Yang, E.C., Chen, T.W. & Lin, T.T. (2008). An adaptive image segmentation algorithm for X-ray quarantine inspection of selected fruits, *Computers and Electronics in Agriculture*, **60**, 190–200.

Jie, D., Xie, L., Rao, X. & Ying, Y. (2014). Using visible and near infrared diffuse transmittance technique to predict soluble solids content of watermelon in an on-line detection system. *Postharvest Biology and Technology*, **90**, 1–6.

Jin, B.H., Wook, S.Y., Santosh, L., Soo, P.E., Kwan, C.B. & Yong, K.D. (2016). Development of non-destructive sorting technique for viability of watermelon seed by using hyperspectral image processing. *Journal of the Korean Society for Non-destructive Testing*, **36**, 35–44.

Kawano, S., Fujiwara, T. & Iwamoto, M. (1993). Non-destructive determination of sugar content in 'Satsuma' mandarins using NIRS transmittance. *Journal of the Japanese Society for Horticultural Science*, **62**, 465–470.

Khodabakhshian, R., Emadi, B., Khojastehpour, M. & Golzarian, M.R. (2015). Determining quality and maturity of pomegranates using multispectral imaging. *Journal of* the *Saudi Society of Agricultural Sciences*, http://dx.doi.org/10.1016/j.jssas.2015.10.004.

Khodabakhshian, R., Emadi, B., Khojastehpour, M., Golzarian M.R. & Sazgarnia A. (2016). Non-destructive evaluation of maturity and quality parameters of pomegranate fruit by visible/near infrared spectroscopy. *International Journal of Food Properties*, **20**, 41–52.

Stellenbosch University https://scholar.sun.ac.za

Khodabakhshian, R., Emadi, B., Khojastehpour, M., Golzarian, M.R. & Sazgarnia, A. (2017). Development of a multispectral imaging system for online quality assessment of pomegranate fruit. *International Journal of Food Properties*, **20**, 107–118.

Khoshroo, A., Keyhani, A., Zoroofi, R.A., Rafiee, S., Zamani, Z. & Alsharif, M.R. (2009). Classification of pomegranate fruit using texture analysis of MR images. *Agricultural Engineering International*, **14**, 1182.

Kotwaliwale, N., Kalne, A. & Singh, K. (2011). Radiography, CT and MRI. In: *Book chapter in non-destructive evaluation of food quality-theory and practice* (edited by S.N. Jha), Springer, Berlin.

Kotwaliwale, N., Singh, K., Kalne, A., Jha, S.N., Seth, N. & Kar, A. (2014). X-ray imaging methods for internal quality evaluation of agricultural produce. *Journal of Food Science and Technology*, **51**, 1–15.

Kraszni, M., Marosi, A. & Larive, C.K. (2013). NMR assignments and the acid–base characterization of the pomegranate ellagitannin punicalagin in the acidic pH-range. *Analytical and Bioanalytical Chemistry*, **405**, 5807–5816.

Krivoshiev, G.P., Chalucova, R.P. & Moukarev, M.I. (2000). A possibility for elimination of the interference from the peel in non-destructive determination of the internal quality of fruit and vegetables by Vis–NIR spectroscopy. *LWT - Food Science and Technology*, **33**, 344–353.

Lammertyn, J., Peirs, J., De Baerdemaeker, J. & Nicolaï, B.M. (2000). Light penetration properties of NIR radiation in fruit with respect to non-destructive quality assessment. *Postharvest Biology and Technology*, **18**, 121–132.

Lammertyn, J., Jancsok, P., Dresselaers, T., Van Hecke, P., Wevers, M., De Baerdemaeker, J. & Nicolaï, B.M. (2003a). Analysis of the time course of core breakdown in 'Conference' pears by means of MRI and X- ray CT. *Postharvest Biology and Technology*, **29**, 19–28.

Lammertyn, J., Dresselaers, T., Van Hecke, P., Jancsok, P., Wevers, M. & Nicolaï, B.M. (2003b). MRI and X-ray CT study of spatial distribution of core breakdown in "Conference" pears. *Journal of Magnetic Resonance Imaging*, **21**, 805–815.

Li, B., Hou, B., Zhang, D., Zhou, Y., Zhao, M., Hong, R. & Huang, Y. (2016). Pears characteristics (soluble solids content and firmness prediction, varieties) testing methods based on visible-near infrared hyperspectral imaging. *Optik*, **127**, 2624–2630.

Stellenbosch University https://scholar.sun.ac.za

Li, J., Rao, X. & Ying, Y. (2011). Detection of common defects on oranges using hyperspectral reflectance imaging. *Computers and Electronics in Agriculture*, **78**, 38–48.

Liu, M., Hu, S., Lin, H. & Guo, E. (2008). Hyperspectral laser-induced fluorescence imaging for non-destructive assessing soluble solids content of orange. *International Federation for Information Processing***, 258**, 51–59.

Liu, Y., Sun, X. & Ouyang, A. (2010). Non-destructive measurements of soluble solid content of navel orange fruit by visible-NIR spectrometric technique with PLS and PCA-BPNN. *LWT - Food Science and Technology*, **43**, 602–607.

Liu, B., Han, G., Zhang, Z., Liu, R. & Jiang, C. (2012). Shell thickness–dependent Raman enhancement for rapid identification and detection of pesticide residues at fruit peels. *Analytical Chemistry*, **84**, 255–261.

Long, R.L. & Walsh, K.B. (2006). Limitations to the measurement of intact melon total soluble solids using near infrared spectroscopy. *Australian Journal of Agricultural Research*, **57**, 403–410.

Ma, B.X., Xiao, W.D., Qi, X.X., He, Q.H. & Li, F.X. (2012). Non-destructive measurement of sugar content of Hami melon based on diffuse reflectance hyperspectral imaging technique, **32**, 3093–3097.

Maftoonazad, N., Karimi, Y., Ramaswamy, H. & Prasher, S. (2011). Artificial neural network modeling of hyperspectral radiometric data for quality changes associated with avocados during storage. *Journal of Food Process Press*, **35**, 432–446.

Makino, Y., Isami, A., Suhara, T., Oshita, S., Kawagoe, Y., Tsukada, M., Ishiyama, R., Serizawa, M., Purwanto, Y.A., Ahmad, U., Mardjan, S. & Kuroki, S. (2013). Non-destructive analysis of internal and external qualities of mango fruits during storage by hyperspectral imaging. *Acta Horticulturae*, **1011**, 443–450.

Magwaza, L.S., Opara, U.L, Nieuwoudt, H., Cronje, P.J.R, Saeys, W. & Nicolaï, B. (2012). NIR spectroscopy applications for internal and external quality analysis of citrus fruit-A review. *Food and Bioprocess Technology*, **5**, 425–444.

Magwaza, L.S., Opara, U.L., Terry, L.A., Landahl, S., Cronje, P.J.R., Nieuwoudt, H.H., Hanssens, A., Saeys, W. & Nicolaï, B.M. (2013a). Evaluation of Fourier transform-NIR spectroscopy for integrated external and internal quality assessment of 'Valencia' oranges. *Journal of Food Composition and Analysis*, **31**, 144–154.

Magwaza, L.S., Ford, H.D., Cronje, P.J.R., Opara, U.L., Landahl, S., Tatam, R.P. & Terry, L.A. (2013b). Application of optical coherence tomography to non-destructively

Stellenbosch University https://scholar.sun.ac.za

characterise rind breakdown disorder of 'Nules Clementine' mandarins. *Postharvest Biology and Technology*, **84**, 16–21.

Magwaza, L.S., Opara, U.L., Cronje, P.J.R., Landahl, S., Nieuwoudt, H.H., Mouazen, A.M., Nicolaï, B.M. & Terry, L.A. (2014a). Assessment of rind quality of 'Nules Clementine' mandarin fruit during postharvest storage: 1. Vis/NIRS PCA models and relationship with canopy position. *Scientia Horticulturae*, **165**, 410–420.

Magwaza, L.S., Opara, U.L., Cronje, P.J.R., Landahl, S., Nieuwoudt, H.H., Mouazen, A.M., Nicolaï, B.M. & Terry, L.A. (2014b). Assessment of rind quality of 'Nules Clementine' mandarin fruit during postharvest storage: 2. Robust Vis/NIRS PLS models for prediction of physico-chemical attributes. *Scientia Horticulturae*, **165**, 421–432.

Magwaza, L.S. & Opara, U.L. (2014). Investigating non-destructive quantification and characterization of pomegranate fruit internal structure using X-ray computed tomography. *Postharvest Biology and Technology*, **95**, 1–6.

Magwaza, L.S. & Opara. U.L. (2015). Analytical methods for determination of sugars and sweetness of horticultural products A–review. *Scientia Horticulturae*, **184**, 179–192.

Maire, E., Salvo, L., Blandin, J.J., Ludwig, W. & Létang, J.M. (2001). On the application of X-ray microtomography in the field of material science. *Advanced Engineering Materials*, **3**, 539–546.

Maniwara, P., Nakano, K., Boonyakiat, D., Ohashi, S., Hiroi, M. & Tohyama, T. (2014). The use of visible to near infrared spectroscopy for evaluating passion fruit postharvest quality. *Journal of Food Engineering*, **143**, 33–43.

Marcone, M.F., Wang, S., Albabish, W., Nie, S., Somnarain, D. & Hill. A. (2013). Diverse food-based applications of nuclear magnetic resonance (NMR) technology. *Food Research International*, **51**, 729–747.

Marigheto, N., Duarte, S. & Hills, B.P. (2005). NMR relaxation study of avocado quality. *Applied Magnetic Resonance*, **29**, 687–701.

Matityahu, I., Glazer, I., Holland, D., Bar-Ya'akov, I., Ben-Arie, R. & Amir, R. (2014). Total antioxidative capacity and total phenolic levels in pomegranate husks correlate to several postharvest fruit quality parameters. *Food and Bioprocess Technology*, **7**, 1938–1949.

McGlone, V.A., Fraser, D.G., Jordan, R.B. & Kunnemeyer, R. (2003). Internal quality assessment of mandarin fruit by vis–NIR spectroscopy. *Journal of Near Infrared Spectroscopy*, **11**, 323–332.

Stellenbosch University https://scholar.sun.ac.za

Marcone, M.F., Wang, S., Albabish, W., Nie, S., Somnarain, D. & Hill. A. (2013). Diverse food-based applications of nuclear magnetic resonance (NMR) technology. *Food Research International*, **51**, 729–747.

Mendoza, F., Lu, R., Ariana, D., Cen, H. & Bailey, B. (2011). Integrated spectral and image analysis of hyperspectral scattering data for prediction of apple fruit firmness and soluble solids content. *Postharvest Biology and Technology*, **62**, 149–160.

Miller, B.K. & Delwiche, M.J. (1991). Spectral analysis of peach surface defects. *Transactions of the American Society of Agricultural Engineers*, **34**, 2509–2515.

Miller, W.M. & Zude, M. (2002). NIR-based sensing coupled with physical/color features to identify Brix level of Florida citrus. *American Society of Agricultural and Biological Engineers*, Meeting Paper No: 026037.

Møller, S.M., Travers, S., Bertram, H.C. & Bertelsen, M.G. (2013). Prediction of postharvest dry matter, soluble solids content, firmness and acidity in apples (cv. Elshof) using NMR and NIR spectroscopy: a comparative study. *European Food Research* and *Technology*, **237**, 1021–1024.

Nicolaï, B.M., Beullens, K., Bobelyn, E., Peirs, A., Saeys, W. & Theron, I.K. (2007a). Non-destructive measurement of fruit and vegetable quality by means of NIR spectroscopy: A review. *Postharvest Biology and Technology*, **46**, 99–118.

Nicolaï, B.M., Theron, K.I. & Lammertyn, J. (2007b). Kernel PLS regression on wavelet transformed NIR spectra for prediction of sugar content of apple. *Chemometrics and Intelligent Laboratory*, **85**, 243–252.

Nicolaï, B.M., Bulens, I., De Baerdemaker, J., De Ketelaere, B., Hertog, M.L.A.T.M., Verboven, P. & Lemmertyn, J. (2009). Non-destructive evaluation: detection of external and internal attributes frequently associated with quality and damage. In: *Postharvest Handling: A Systems Approach* (edited by W.J. Florkowiski, R.L. Shewfelt, B. Brueckner & S.E. Prussia). Pp. 421–442. Academic Press, Elsevier, Amsterdam.

Nikbakht, A.M., Hashjin, T.T., Malekfar, R. & Gobadian, B. (2011). Non-destructive determination of tomato fruit quality parameters using Raman spectroscopy. *Journal of Agriculture, Science and Technology*, **13**, 517–526.

Olarewaju, O.O., Bertling, I. & Magwaza, L.S. (2016). Non-destructive evaluation of avocado fruit maturity using near infrared spectroscopy and PLS regression models. *Scientia Horticulturae*, **199**, 229–236.

Stellenbosch University https://scholar.sun.ac.za

Opara, U.L. & Pathare, P.B. (2014). Bruise damage measurement and analysis of fresh horticultural produce–A review. *Postharvest Biology and Technology*, **91**, 9–24.

Pan, L., Zhang, Q., Zhang, W., Sun, Y., Hu, P. & Tu, K. (2016). Detection of cold injury in peaches by hyperspectral reflectance imaging and artificial neural network, *Food Chemistry*, **192**,134–141.

Parker, F.S. (1983). *Applications of Infrared, Raman and Resonance Raman Spectroscopy in Biochemistry*. Plenum Press, New York.

Peiris, K.H.S., Dull, G.G., Leffler, R.G. & Kays, S.J. (1999). Spatial variability of soluble solids or dry-matter content within individual fruits, bulbs, or tubers: Implications for the development and use of NIR spectrometric techniques. *HortScience*, **34**, 114–118.

Qin, J., Burks, T.F., Kim, M.S., Chao, K. & Ritenour, M.A. (2008). Citrus canker detection using hyperspectral reflectance imaging and PCA-based image classification method. *Sensing* and *Instrumentation for Food Quality and Safety*, **2**, 168–177.

Qin, J., Chao. K. & Kim, M.S. (2012). Non-destructive evaluation of internal maturity of tomatoes using spatially offset Raman spectroscopy. *Postharvest Biology and Technology*, **71**, 21–31.

Qin, J., Chao. K., Kim, M.S., Lu, R. & Burks, T. (2013). Hyperspectral and multispectral imaging for evaluating food safety and quality. *Journal of Food Engineering*, **118**, 157–171.

Rajkumar, P., Wang, W., EImasry, G., Raghavan, G.S.V.Y. & Gariepy, Y. (2012). Studies on banana fruit quality and maturity stages using hyperspectral imaging. *Journal of Food Engineering*, **108**, 194–200.

Raman, C.V. & Krishnan, K.S. (1928). A new type of secondary radiation. *Nature*, **121**, 501–502.

Saito, K., Miki, T., Hayashi, S., Kajikawa, H., Shimada, M., Kawate, Y., Nishizawa, T., Ikegaya, D., Kimura, N., Takabatake, K., Sugiura, N. & Suzuki, M. (1996). Application of magnetic resonance imaging to non-destructive void detection in watermelon. *Cryogenics*, **36**, 1027–1031.

Salmanizadeh, F., Nassiri, S.M., Jafari, A. & Bagheri, M.H. (2014). Volume estimation of two local pomegranate fruit (*Punica Granatum* L.) cultivars and their components using non-destructive X-ray computed tomography technique. *International Journal of Food Properties*, **18**, 439–455.

Salvo, L., Cloetens, P., Maire, E., Zabler, S., Blandin, J.J., Buffiere, J.Y., Ludwig, W., Boller, E., Bellet, D. & Josserond, C. (2003). X-ray micro-tomography an attractive

Stellenbosch University https://scholar.sun.ac.za

characterisation technique in materials science. *Nuclear Instruments and Methods in Physics Research Section B*, **200**, 273–286.

Shao, Y., Bao, Y. & He, Y. (2011). Visible/Near-infrared spectra for linear and nonlinear calibrations: A case to predict soluble solids contents and pH value in peach. *Food and Bioprocess Technology*, **4**, 1376–1383.

Shukla, A. & Kot, R. (2016). An overview of hyperspectral remote sensing and its application in various disciplines. *International Journal of Arts and Sciences*, **5**, 85–90.

Sonego, L., Benarie, R., Raynal, J. & Pech, J.C. (1995). Biochemical and physical evaluation of textural characteristics of nectarines exhibiting woolly breakdown – NMR imaging, X-ray computed-tomography and pectin composition. *Postharvest Biology and Technology*, **5**, 187–198.

Sugiyama, J. (1999). Visualization of sugar content in the flesh of a melon by near-infrared imaging. *Journal of Agricultural and Food Chemistry*, **47**, 2715−2718.

Sugiyama, J. & Tsuta, M. (2010). Visualization of sugar distribution of melons by hyperspectral technique. In: *Hyperspectral Imaging for Food Quality Analysis and Control* (edited by D.W. Sun, D.W). Pp. 349–368. Academic Press, Elsevier, Amsterdam, Netherlands.

Tian, H., Ying, Y., Xu, H., Lu, H. & Xie, L. (2009). Study on Vis/NIR spectra detecting system for watermelons and quality predicting in motion. *Spectroscopy and Spectral Analysis*, **29**, 1536–1540.

Van Dael, M., Herremans, E., Verboven, V., Opara, U.L., Nicolaï, B. & Lebotsa, S. (2016a). Automated online detection of granulation in oranges using X-ray radiographs. *Acta Horticulturae*, **1119**, 179–182.

Van Dael. M., Lebotsa, S., Herremans E., Verboven, P., Sijbers, J., Opara, U.L., Cronje, P.J. & Nicolaï, B.M. (2016b). A segmentation and classification algorithm for online detection of internal disorders in citrus using X-ray radiographs. *Postharvest Biology and Technology*, **112**, 205–214.

Wang, G. (2013). Raman spectroscopic characterization and analysis of agricultural and biological systems. PhD Thesis. Iowa State University Ames, Iowa.

Walsh, K.B. (2005). Commercial adoption of technologies for fruit grading, with emphasis on NIRS. Information and technology for sustainable fruit and vegetable production, FRUTIC 05, Montpellier, France, 12–16 September 2005.

Williams, P.J., Geladi, P., Britz, T.J. & Manley, M. (2012). Near-infrared (NIR) hyperspectral imaging and multivariate image analysis to study growth characteristics and differences

Stellenbosch University https://scholar.sun.ac.za

between species and strains of members of the genus Fusarium. *Analytical and Bioanalytical Chemistry*, **404**, 1759–1769.

Xia, J., Li, X., Li, P., Ma, Q. & Ding, X. (2007). Application of wavelet transform in the prediction of 'Navel' orange vitamin C content by near-infrared spectroscopy. *Agricultural Sciences in China*, **6**, 1067–1073.

Xu, H., Qi, B., Sun, T., Fu, X. & Ying, Y. (2012). Variable selection in visible and near-infrared spectra: Application to on-line determination of sugar content in pears. *Journal of Food Engineering*, **109**, 142–147.

Yang, D. & Ying, Y. (2011). Applications of Raman Spectroscopy in Agricultural Products and Food Analysis: A Review. *Applied Spectroscopy Reviews*, **46**, 539–560.

Yuan, Y., Zhao, Y., Yang, J., Jiang, Y., Fei Lu, F., Jia, Y. & Yang, B. (2017). Metabolomic analyses of banana during postharvest senescence by ^{1}H-high resolution-NMR. *Food Chemistry*, **218**, 406–412.

Zhang, B., Huang, W., Li, J., Zhao, C., Fan, S., Wu, J. & Liu, C. (2014). Principles, developments and applications of computer vision for external quality inspection of fruits and vegetables: A review. *Food Research International*, **62**, 326–343.

Zhang, L. & McCarthy, M.J. (2012). Blackheart characterization and detection in pomegranate fruit using NMR relaxometry and MR imaging. *Postharvest Biology and Technology*, **67**, 96–101.

Zhang, L. & McCarthy, M.J. (2013). Assessment of pomegranate postharvest quality using nuclear magnetic resonance. *Postharvest Biology and Technology*, **77**, 59–66.

Zhang, P.X., Zhou, X.F., Chen, A.Y.S. & Fang, Y. (2006). Raman spectra from pesticides on the surface of fruits. *Journal of Physics*, **28**, 7–11.

Zhou, H., Ye, Z., Yu, Z., Su, M. & Du, J. (2016). Application of low-field nuclear magnetic resonance and proton magnetic resonance imaging in evaluation of 'Jinxiu' yellow peach's storage suitability. *Emirates Journal of Food and Agriculture*, **28**, 633–643.

Zion, B., Chen, P. & McCarthy, M.J. (1995). Detection of bruises in magnetic resonance images of apples. *Computers and Electronics in Agriculture*, **13**, 289–299.

Zou, L., Ming, S. & Zhang D. (2015). A new method for rapid detection of the volume and quality of watermelon based on processing of x-ray images. *Computer and Computing Technologies in Agriculture*, **452**, 731–738.

Zur, N., Shlizerman, L., Ben-Ari, G. & Sadka, A. (2016). Use of magnetic resonance imaging (MRI) to study and predict fruit splitting in citrus. *Journal of the Japanese Society for Horticultural Science*, **86**, 151–158.

Stellenbosch University https://scholar.sun.ac.za

Table 1. A comparison of different non-destructive techniques for different thick and thin rind fruit

Fruit type	Non-destructive method	Parameters	Predictors accuracy	References
Thick rind				
Avocado	NIR	Oil content	R^2 = 0.58, RMSEP = 5.44%	Olarewaju *et al.* (2016)
	Hyper/Multispectral	Firmness	R^2 = 0.94 N mm	Maftoonazad *et al.* (2011)
		Weight loss	R^2 = 0.98	
	NMR	Oil content	-	Marigheto *et al.* (2005)
	X-ray CT	-	-	-
Orange	NIR	SSC	R^2 = 0.83, RMSEP = 0.58%	Magwaza *et al.* (2013a)
		TA	R^2 = 0.22, RMSEP = 0.1%4	
		Vitamin C	R^2 = 0.66, RMSEP = 8.10 mg/100 mL	
	Hyper/Multispectral	SSC	r^2 = 0.96	Liu *et al.* (2008)
	NMR	-	-	-
	X-ray CT	Granulation	99%	Van Dael *et al.* (2016a)
Watermelon	NIR	SSC	R^2 = 0.66, RMSEP = 0.39%	Jie *et al.* (2014)
	Hyper/Multispectral	Seed viability	94.7%	Jin *et al.* (2016)
	MRI	Internal cavity	93.3%	Saito *et al.* (1996)
	X-ray CT	Fruit volume	R^2 = 0.99	Zou *et al.* (2015)
Thin rind				
Apple	NIR	SSC	R^2 = 0.90, RMSEP = 0.40 °Brix	Giovanelli *et al.(*2014)
		Firmness	R^2 = 0.90, RMSEP = 0.46 N mm	
		a* value	R^2 = 0.81, RMSEP = 1.36	
		Total phenolics	R^2 = 0.95, RMSEP = 40.63 mg/kg	
		Antioxidant	R^2 = 0.90, RMSEP = 0.40 mmol/kg	
	Hyper/Multispectral	SSC	R^2 = 0.87, SEP = 0.66%	Mendoza *et al.* (2011)
	NMR	SSC	R^2 = 0.50, RMSEP = 1.07%	Møller *et al.* (2013)
		Dry matter	R^2 = 0.58, RMSEP = 1.06	
	X-ray CT	Watercore	89%	Herremans *et al.* (2014)
Pear	NIR	TSS	R^2 = 0.88, RMSEP = 0.46%	Xu *et al.* (2012)
	Hyper/Multispectral	TSS	R^2 = 0.99, RMSEP = 0.06%	Li *et al.* (2016)
	NMR	Core breakdown	-	Lammertyn *et al.* (2003)
	X-ray CT	Core breakdown	-	Lammertyn *et al.* (2003)
Peach	NIR	TSS	R^2 = 0.93, RMSEP = 0.62%	Shao *et al.* (2011)
		pH	R^2 = 0.85, RMSEP = 0.04	
	Hyper/Multispectral	SSC	R^2 = 0.82, RMSEP = 1.1%	Pan *et al.* (2016)
		TA	R^2 = 0.90, RMSEP = 0.02%	
		Firmness	R^2 = 0.88, RMSEP = 8.4 N mm	
	NMR	Firmness	-	Zhou *et al.* (2016)
		Ethylene	-	
	X-ray CT	Insect infestation	96%	Jiang *et al.* (2008)

SSC, soluble solid content; TSS, total soluble solids; TA, titratable acidity; RMSEP, root mean square error of prediction

Stellenbosch University https://scholar.sun.ac.za

Table 2. Overview of applications of NIR spectroscopy to measure fruit quality in selected thick rind fruit

Commodity	Measured parameter	Wavelength range (nm)	Pre-processing	Analysis	R^2	Prediction error	References
Watermelon	SSC	700–1100			0.81	RMSEP = 0.42%	Abebe (2006)
Watermelon	SSC	350–1000	Smoothing 1st der 2nd der	PLS PCR	0.92 0.90 0.75	RMSEP = 0.65% RMSEP = 0.84% RMSEP = 0.97%	Hai-qing *et al.* (2007)
Watermelon	SSC	650–950	Smoothing 1st der	-	0.90	RMSEP = 0.76%	Tian *et al.* (2009)
Watermelon	SSC	687–920	Smoothing MSC	PLS SMLR	0.66	RMSEP = 0.39%	Jie *et al.* (2014)
Melon	SSC	700–1100	-	MLR	0.72	SEP = 0.7–1.32%	Guthrie *et al.* (1998)
Melon	SSC	630–1030	-	PLS	0.30–0.93	RMSEP = 0.7–1.3%	Greensill *et al.* (2001)
Melon	SSC	306–1130	1st der 2nd der	PLS	0.28	RMSEP = 1.0%	Guthrie *et al.* (2006)
Melon	SSC	300–1150	-	PLS PCA	0.59–0.88	RMSECV = 0.4–0.81%	Long and Walsh (2006)

SSC, soluble solid content; 1st der, 1st derivative; 2nd derivative; MSC, multiplicative scattering correction; PLS, partial least squares; PCR principal component regression; MLR, multiple linear regression; SMLR, stepwise multiple linear regression; RMSEP, root mean square error of prediction, RMSECV, root mean square error of cross-validation; SEP, standard error of prediction

Stellenbosch University https://scholar.sun.ac.za

Table 2. Continue overview of applications of NIR spectroscopy to measure fruit quality in selected thick rind fruit

Commodity	Measured parameter	Wavelength range (nm)	Pre-processing	Analysis	R^2	Prediction error	References
Orange	Vitamin C	800–2500	1st der, 2nd der, COE, SLS, SVN, MSC	PLS	0.96	RMSECV = 3.9	Xia *et al.* (2007)
Orange	SSC	578–1850	SNV and detrending	PLS	0.91	RMSEP = 0.51%	Cayuela (2008)
	TA				0.56	RMSEP = 0.33%	
	pH				0.45	RMSEP = 0.49	
Orange	SSC	350–1800	MSC, SNV	PLS, PCA	0.90	RMSEP = 0.68%	Liu *et al.* (2010)
Orange	Mass	780–2500	MSC	PLS	0.97	RMSEP = 10.45 g	Magwaza *et al.* (2013a)
	SSC		SLS		0.83	RMSEP = 0.58%	
	Colour index		1st der		0.83	RMSEP = 0.82	
	Vitamin C		2nd der		0.66	RMSEP = 8.01 mg/100 mL	
	TA		COE		0.22	RMSEP = 0.14%	
Passion fruit	SSC	603–1090	Smoothing	PLS	0.95	RMSEP = 0.64%	Maniwara *et al.* (2014)
	TA		1st der		0.79	RMSEP = 0.22%	
	Ascorbic acid		2nd der		0.81	RMSEP = 2.57 mg/100 g FW	
	Ethanol				0.89	RMSEP = 0.31%	
	Pulp				0.96	RMSEP = 4.32	
Passion fruit	SSC	800–2700	Smoothing	PLS	0.63	RMSEP = 9.82%	de Oliveira *et al.* (2014)
	TA		MSC		0.49	RMSEP = 11.42%	

SSC, soluble solid content; TA, titratable acidity; 1st der, 1st derivative; 2nd derivative; MSC, multiplicative scattering correction; SLS, straight line subtraction; COE, constant offset elimination; PLS, partial least squares; PCR principal component regression; MLR, multiple linear regression; RMSEP, root mean square error of prediction, RMSECV, root mean square error of cross-validation

Stellenbosch University https://scholar.sun.ac.za

Table 2. Continue overview of applications of NIR spectroscopy to measure fruit quality in selected thick rind fruit

Commodity	Measured parameter	Wavelength range (nm)	Pre-processing	Analysis	R^2	Prediction error	References
Pomegranate	SSC	400–1100	MSC, SNV	PLS	0.93	RMSEC = 0.24%	Khodabakhshian *et al.* (2016)
	TA				0.84	RMSEC = 0.064%	
	pH				0.94	RMSEC = 0.25	
Avocado	Oil content	800–2400	MSC, SNV	PLS	0.58	RMSEP = 5.44%	Olarewaju *et al.* (2016)
	Dry matter		1st der, 2nd der		0.84	RMSEP = 2.49%	
	Moisture content				0.85	RMSEP = 2.49%	
Avocado	Dry matter	500–1000	-	PLS, MLR	0.88	RMSEP = 1.30%	Clarke *et al.* (2004b)

SSC, soluble solid content; TA, titratable acidity, 1st der, 1st derivative; 2nd derivative; MSC, multiplicative scattering correction; SNV, vector normalisation; PLS, partial least squares; MLR, multiple linear RMSEP, root mean square error of prediction, RMSEC, root mean square error of calibration

Stellenbosch University https://scholar.sun.ac.za

Table 3. Overview of applications of multispectral and hyperspectral imaging to measure fruit quality in selected thick rind fruit

Commodity	Quality parameter	Imaging technique	Wavelength range (nm)	Data processing	Accuracy	Reference
Banana	SSC	Hyperspectral	400–1000	MLR	$R^2 = 0.85$	Rajkumar *et al.* (2012)
	Moisture content				$R^2 = 0.87$	
	Firmness				$R^2 = 0.91$	
Orange "Nanfeng"	SSC	Hyperspectral	700–1100	PLS	$R^2 = 0.99$	Liu *et al.* (2008)
Orange "Navel"	SSC				$R^2 = 0.96$	
Mango	SSC	Hyperspectral	380–1000	ANN	$R^2 = 0.79$	Makino *et al.* (2013)
Pomegranate	TSS	Multispectral	700–1000	PLS	$R^2 = 0.94$	Khodabakhshian *et al.* (2017)
	pH				$R^2 = 0.88$	
	TA				$R^2 = 0.93$	
Watermelon	SSC	Multispectral	400–1100	PLS	$R^2 = 0.89$	Sugiyama and Tsuta (2010)

SSC, soluble solid content; TSS, total soluble solids, TA, titratable acidity; PLS, partial least squares; PCA principal component analysis; MLR, multiple linear regression; ANN, artificial neural network

Stellenbosch University https://scholar.sun.ac.za

Table 4. Applications of multispectral and hyperspectral imaging to identify external defects and diseases in selected thick rind fruit

Commodity	Quality parameter	Imaging technique	Wavelength range (nm)	Data processing	Accuracy (%)	Reference
Grapefruit	Cranker	Hyperspectral	730 and 830	-	85.30	Qin *et al.* (2008)
Lemon Orange Mandarin	Defects	Multispectral	750	-	94.00	Aleixos *et al.* (2002)
Mandarin	Green mould	Hyperspectral	320–1100	LDA	91.00	Gomez-Sanchis *et al.* (2008)
Mandarin Orange	Defects	Multispectral	(350–400, 400–1800)	LDA	86.00	Blasco *et al.* (2009)
Orange	Bruise	Hyperspectral	400–1000	PCA	93.70	Li *et al.* (2011)

PCA, principal component analysis; LDA, linear discriminate analysis

Stellenbosch University https://scholar.sun.ac.za

Table 5. Applications of X-ray µCT in quantification of pomegranate fruit

Cultivar	Measured parameter	Data processing	Destructive fruit fraction volume (mL)	X-ray µCT prediction accuracy (%)	References
Rabab Malas	Whole fruit	Matlab image processing (version 8.1)	238.96	97.8	Salmanizadeh *et al.* (2014)
	Arils		104.94	95.1	
	Albedo		114.33	97.2	
	Seeds		18.25	93.5	
	Juice		83.5	94.4	
Rabab Torsh	Whole fruit	Matlab image processing (version 8.1)	254.92	97.3	Salmanizadeh *et al.* (2014)
	Arils		128.64	94.4	
	Albedo		100.27	94.7	
	Seeds		23.00	91.8	
	Juice		98.52	91.9	
Shani-Yonay	Whole fruit	Volume graphics (VG Studio Max 2.1)	360.49 ±27.66	99.02	Magwaza and Opara (2014)
	Albedo		166.08 ±14.69	99.23	
	Arils		170.58 ±14.25	93.66	
	Airspace		23.83 ±1.50	30.21	
Wonderful	Whole fruit	Volume graphics (VG Studio Max 2.2)	337.36 ±22.56	99.8	Arendse *et al.* (2016a)
	Peel		161.81 ±20.60	98.7	
	Arils		163.28 ±15.24	99.5	
	Kernels		15.10 ±1.63	92.2	
	Single aril		0.32 ±0.09	96.9	
	Air space		12.28 ±4.44	88.7	
	Juice content		142.73 ±16.41	97.7	
	Arils per fruit		545.50 ±22.78	97.4	
Herskawitz	Whole fruit	Volume graphics (VG Studio Max 2.2)	261.72 ±37.22	99.3	Arendse *et al.* (2016b)
	Arils		159.06 ±33.09	96.5	
	Albedo		102.30 ±11.66	97.8	

Stellenbosch University https://scholar.sun.ac.za

Table 6. Summary of advantages and disadvantages for each non-destructive technique

Technique	Advantages	Disadvantages	Reference
NIR spectroscopy	Non-destructive technique with minimal or no sample preparation required, it allows the determination of chemical and non-chemical (physical) parameters, NIR measurements are rapid and fast providing real-time analytical information from samples, NIR instrumentation is suitable for online use in control processes due to its simplified mechanics and robust components, fiber optics provides robust sensors for on-line and in-line analysis	NIR is barely selective therefore chemometric techniques have to be applied to extract relevant information, accurate and robust models are difficult to obtain as their construction requires large enough number of samples with large variations, NIR requires prior knowledge of the value for a specific parameter which needs to be previously determined using a reference method	Blanco and Villarroya (2002)
Hyperspectral imaging	Hyperspectral imaging provides detailed information about the spectral-spatial models for classification and segmentation, accurate and provides simultaneous analysis of several compounds, potential to detect diseases and defects within agricultural products	Hyperspectral instrumentation are costly, requires high hardware speed and are complex, hyperspectral cubes are large and requires significant amount of storage space due to accumulation of vast amounts of multi-dimensional datasets, hyperspectral imaging requires chemometric techniques to extract relevant information, modeling and data processing is time-consuming	Dale *et al.* (2013); Shukla and Kot (2016)
X-ray computed tomography	X-ray CT is highly accurate in analysis and characterization of internal structures, reproduction of high resolution three dimensional (3-D) visualisation and analysis of microstructures, detection and characterization of internal defects without sample preparation	X-ray CT systems are considerably large, complex and expensive compared with other non-destructive technologies, lengthy data acquisition time required, large amount of storage space required for data acquisition, health and safety issues may arise due to harmful effects of X-ray radiation	Arendse *et al.* (2016a; b)

Stellenbosch University https://scholar.sun.ac.za

Nuclear magnetic resonance	Minimal sample preparation, quantitative analyses even in the absence of an authentic standard, detection of various compounds simultaneously thereby permitting analysis of complex samples without separation	Less sensitive than other analytical methods, NMR systems are expensive and complex, health and safety issues may arise due to maintenance of magnetic field	Kraszni *et al.* (2013); Marcone *et al.* (2013)
Raman spectroscopy	Very small amounts of material size can be studied down to microscopic levels in the range of 10 microns, Raman spectroscopy can be used for samples in solids, liquids or gaseous state gasses, no sample preparation required and sample thickness, shape or size is not a problem, provide information about concentration, structure and interaction of biochemical molecules within intact cells	Low sensitivity when concentrations are very low for a substance, metals and alloys can't be used, sample heating through intense laser can destroy the sample or mask the Raman spectrum	Parker (1983); Nikbakht *et al.* (2011)

Stellenbosch University https://scholar.sun.ac.za

Section II

Chapter 3: Non-destructive characterization and volume estimation of pomegranate fruit external and internal morphological fractions using X-ray computed tomography[1]

Chapter 4: Using Fourier transform near-infrared diffuse reflectance spectroscopy and two spectral acquisition modes for the evaluation of the external and internal quality of intact pomegranate fruit

Chapter 5: Development of calibration models for the evaluation of pomegranate aril quality by Fourier-transform near-infrared spectroscopy combined with chemometrics[2]

Chapter 6: Comparing the analytical performance of near and mid-infrared spectrometers for evaluating pomegranate juice quality

[1.] Journal of Food Engineering. 186: 42–49.

[2.] Biosystems Engineering. 148: 148–156.

Stellenbosch University https://scholar.sun.ac.za

DECLARATION BY THE CANDIDATE

Regarding **Chapter 3 (pp 52-70)**, the nature and scope of my contribution were as follows:

Nature of contribution	Extent of contribution (%)
Data collection, analysis, writing of chapter and final approval of the published version	75

The following co-authors have contributed to **Chapter 3 (pp 52-70)**

Name	e-mail address	Nature of contribution	Extent of contribution (%)
Prof U.L. Opara	opara@sun.ac.za	Conception of the work, critical revision and final approval of the published version	10
Dr O.A. Fawole	olaniyi@sun.ac.za	Research input, editorial suggestion, proof reading and final approval of the published version	10
Dr L.S. Magwaza	Magwazal@ukzn.ac.za	Research input, proof reading and final approval of the published version	5

Stellenbosch University https://scholar.sun.ac.za

E Arendse **Signature of candidate**	29/08/2017 **Date**

DECLARATION BY CO-AUTHORS

The undersigned hereby confirm that:

1. the declaration above accurately reflects the nature and extent of the contributions of the candidate and the co-authors to **Chapter 3 (pp 52-70)**

2. no other authors contributed to **Chapter 3 (pp 52-70)** besides those specified above, and

3. potential conflicts of interest have been revealed to all interested parties and that the necessary arrangements have been made to use the material in **Chapter 3 (pp 52-70)** of this dissertation.

Signature	Institutional affiliation	Date
Prof U.L. Opara	Stellenbosch University	29/08/2017
Dr O.A. Fawole	Stellenbosch University	29/08/2017
Dr L.S. Magwaza	University of KwaZulu-Natal	29/08/2017

Stellenbosch University https://scholar.sun.ac.za

CHAPTER 3

Non-destructive characterization and volume estimation of pomegranate fruit external and internal morphological fractions using X-ray computed tomography

Abstract

In this study, X-ray computed tomography (CT) was used as a non-destructive technique to characterise and quantify the internal structure of pomegranate fruit (cv. Wonderful). A commercial X-ray system with a radiation source of 245 kW and electron current of 300 μA was used to generate two-dimensional (2-D) radioscopic images which were reconstructed into three dimensional (3-D) images for the quantification and volume estimation of internal structural components of fruit. Segmentation of the internal fruit components (arils, peel, kernel, juice content, air space) and single arils was achieved using StudioMax volume graphics software. The calculated volume of each fruit fraction were 162.5 ±16.2, 163.9 ±21.4, 16.4 ±1.8, 10.9 ±2.6 mL for arils, peel, kernel and air space, respectively which accounted for 48.05, 48.46, 4.9 and 3.2% of total fruit volume. Furthermore, the calculated volume of juice content was 146.1 ±16.3 mL per fruit which was equivalent to an average of 89.9% of total aril weight, while a single aril (0.3 ±0.04 mL) accounted for only 0.09% of whole fruit volume. Destructive validation measurements of each fruit fraction showed similar results to non-destructive data, with volumes of 163.3 ±15.2, 161.8 ±20.6, 15.1 ±1.6, and 12.3 ±4.4 mL for arils, peel, kernel, air space, respectively, while volumes of juice and single aril were 142.7 ±16.4 and 0.3 ±0.09 mL per fruit, respectively. The results showed that fruit physical attributes such as length, diameter and peel thickness were underestimated by an average of 0.14%, 1.13% and 5.27%, respectively, although fruit radius was overestimated by 1.75%. Nevertheless, no significant differences were observed for length, diameter, radius and peel thickness between X-ray CT predicted values and actual measurements. This work has demonstrated the capability of X-ray CT as a non-destructive technique to suitably estimate the fruit volume and its fractions which could be employed in fruit quality management systems.

Keywords: *Punica granatum* L., Fruit quality, Image analysis, Image segmentation, Fruit fractions, Volume estimation, Juice content, Kernel size.

Stellenbosch University https://scholar.sun.ac.za

1. Introduction

Pomegranate (*Punica granatum* L.) is an important tree of the tropical and subtropical regions which is valued for its delicious edible fruit. The fruit has leathery exocarp and the interior is separated by membranous walls and white spongy tissue into compartments (Holland *et al*., 2009). Each compartment is packed with an edible portion (aril) which is surrounded by a translucent sac containing juice and each aril contains a kernel (woody portion) (Holland *et al*., 2009; Aindongo *et al*., 2014). The fruit is a rich source of organic acids, polyphenols, vitamins, polysaccharides, and important minerals compounds (Miguel *et al*., 2010; Viuda-Martos *et al*., 2010; Opara *et al*., 2009; Fawole & Opara, 2012). Scientific studies have linked potent pharmacological activities of pomegranates to several groups of phytochemicals found in the fruit (Viuda-Martos *et al*., 2010; Fawole *et al*., 2012). Consequently, there has gained renewed global interest in pomegranate fruit consumption in relation to human health due to increased consumer awareness of its medicinal properties and nutritional value. This has consequently spurred an increase in global growth of pomegranate fruit for production, consumption and research (Arendse *et al*., 2014).

The evaluation of the internal and external quality of fresh produce is extremely important in the agricultural industry. The bio-physical parameters that are conventionally used for quality determination are flavour, size, shape, colour, appearance, texture and freedom from internal and external defects (Holland *et al*., 2009; Fawole & Opara, 2013a). Physical properties such as the volume of whole fruit, arils and juice content relative to the peel are important in the marketing and processing of pomegranate fruit because these attributes influence industrial processing value as well as consumer preference (Holland *et al*., 2009; Fawole & Opara, 2013a). However, the proportion of aril content (number of kernels, volume and juice content) relative to the peel fraction varies depending on the variety, maturity and growing region (Al-Said *et al*., 2009; Fawole & Opara, 2014; Al-Maiman & Ahmad, 2002). Currently, destructive practices are commonly employed to evaluate the internal quality attributes as well as the characteristics and proportion of individual components of fruit including pomegranates. However, these methods are labour intensive, time-consuming, require specialised sample preparation and are inapplicable for in-line grading and sorting in commercial pack-houses. Furthermore, both internal and external fruit quality attributes may exhibit significant differences due to variability amongst cultivars, orchard, preharvest management practices, fruit maturity and growing region (Magwaza *et al*., 2013a; Fawole & Opara, 2014; Mphahlele *et al*., 2014a, b). Consequently, the high variability in quality attributes amongst cultivars or even the same cultivar has promoted the development of non-destructive techniques for

Stellenbosch University https://scholar.sun.ac.za

detection, prediction and segmentation of fruit quality for laboratory and grading that can both visualise and quantify internal and external structures.

Several non-destructive techniques have been used for the assessment of internal and external quality attributes of fresh produce. These include visible to near-infrared spectroscopy (Vis/NIRS, Nicolaï *et al*., 2007), Vis/NIRS-based systems such as hyperspectral imaging (Zhang *et al*., 2014) and optical coherence tomography (OCT, Magwaza *et al*., 2013b), magnetic resonance imaging (MRI, Lammertyn *et al*., 2003a) and X-ray computed tomography (X-ray CT, Donis-González *et al*., 2014a). The use of X-ray CT as a non-destructive technique for studying the external and internal morphological characteristics and defects of horticultural products is well documented (Cantre *et al*., 2014; Donis-González *et al*., 2014b; Magwaza & Opara, 2014; Kotwaliwale *et al*., 2014). X-ray CT measures variation in material density of the sample and is based on the attenuation of X-ray that depends on the density of the irradiated object. Jha *et al*. (2010) reported the potential of X-ray CT to measure the external (size, shape) and internal (pulp, moisture) morphological characteristics of mango (*Mangifera indica*). Using high resolution CT, Mendoza *et al*. (2007) successfully measured the pore space within apples (*Malus domestica*). Lammertyn *et al*. (2003a,b) applied X-ray CT to study the development of core breakdown in 'Conference' pears (*Pyrus communis*) and found that X-ray CT was able to differentiate between unaffected tissue, brown tissue and cavities. Shahin *et al*. (2002) reported that bruising was detectable in 'Golden Delicious' apples using X-ray CT imaging. The use of X-ray CT imagery for inspection of horticultural produce offers considerable advantages including its large field of view, which allows scanning the entire sample without preparation (Léonard *et al*., 2008). Secondly, the internal structure of an object can be reconstructed into three-dimensional (3-D) images from stacked series of 2-D images allowing for characterization of physical and physiological structures.

Recently, a preliminary study by Magwaza & Opara (2014) investigated the feasibility of X-ray CT imaging as a non-destructive technique for the quantification of internal structures of pomegranate fruit cv. Shani-Yonay. These authors successfully demonstrated the potential of X-ray CT with image analysis as a non-destructive technique to study the quantity and distribution of edible (arils) and non-edible (albedo) portions of pomegranates. Significantly ($p < 0.001$) high accuracy was obtained using linear regression models to predict destructively measured volumes of albedo (external skin plus internal soft tissue) and arils, with R^2 values of 0.83 and 0.89, respectively. However, the authors did not quantify several key parameters such as juice content and kernel size which are of considerable economic importance in the food and beverage industry.

Stellenbosch University https://scholar.sun.ac.za

Pomegranate cultivar Wonderful is the most widely grown and consumed pomegranate cultivar globally (Holland *et al*., 2009) and during the past ten years, South Africa has seen increase in its commercial production, with cv. Wonderful accounting for over 56% of total production of 8000 tons (Pomegranate Association of South Africa, 2012). Therefore, non-destructive estimation of different components for Wonderful cultivar would be immense importance and understanding there relative contribution of these different components to total mass is relevant to consumers, growers and processors. In the food and beverage industry, pomegranates cultivars are commonly selected on the basis of juice content, fruit size, colour, aril yield, and taste (Holland *et al*., 2009). Juice is produced industrially by either crushing whole pomegranate fruit or extracted arils. The by-products of the fresh aril and juice industries are the remnants of the fruit skin (peel), membranes, and kernels. The fruit skin is rich in elagitannins, which have been reported to possess a wide array of health-promoting bioactivities while the kernel oil has a rare combination of unsaturated fatty acids and sterols, the extracts of which have commercial health importance for humans (Viuda-Martos *et al*., 2010; Seeram *et al*., 2006). Therefore, the quantification of pomegranate fruit components, including seeds and juice content, is of considerable economic important for breeders, growers, and food process technologists. The objective of this study was to validate the use of X-ray CT to quantify volumes of key parts of pomegranate fruit cv. Wonderful relevant to the food and beverage industry.

2. Materials and Methods

2.1. *Fruit sampling*

A sample of 23 pomegranate fruit (*Punica granatum* L. cv. Wonderful) without external defects selected for analysis were obtained from Sonlia Pack-house (33°34′851″S, 19°00′360″E) in Western Cape, South Africa. Fruit were packed inside Xtend® bags and carton boxes with the following dimensions: width 0.3 m, length 0.4 m, height 0.133 m and a total of 22 perforations and transported to the Postharvest Technology Research Laboratory at Stellenbosch University.

2.2. *X-ray computed tomography scanning*

X-ray CT images of whole pomegranate fruit were obtained using a commercial X-ray computed tomography system (V|Tome|X L240, General Electric Sensing & Inspection Technologies GmbH, Phoenix, Wun-storf, Germany) situated in the Central Analytical Facility at the University of Stellenbosch, South Africa. The X-ray CT system constituted of an X-ray tube, collimators, turntable and a multi-channel detector mounted into a shield chamber. A collimated X-ray beam is focused on the product and the remainder radiation is captured by a

Stellenbosch University https://scholar.sun.ac.za

multi-channel detector, which transmits a response signal to a computer which is used to analyse the signal and reconstruct a cross-sectional image based on the X-ray transmission data (Lammertyn *et al*., 2003a; Magwaza & Opara, 2014). The standard unit for measuring X-ray absorption with CT systems has been expressed in X-ray CT numbers. The CT number is based on linear X-ray absorption coefficients and, in general, is expressed by the brightness data in an image (Kotwaliwale *et al*., 2011). The CT number is defined in Eq. 1:

$$\text{CT number} = \frac{(\mu s - \mu w)\ \text{x}\ k}{\mu w} \qquad (1)$$

Where μs is an object linear X-ray absorption coefficient (m^{-1}), μw is a linear X-ray absorption coefficient of water (m^{-1}) and k is a constant equal to 1,000. The measuring range for k is from −1.000 to +4.000. CT numbers use a normalization of zero for water and –1000 for air (Ogawa *et al*., 1998). The computer makes an image in grey scale based on these numbers, with higher CT numbers in an image approach to white. To optimise the fruit scan quality several system settings were tested. Optimal CT settings were obtained with an isotropic voxel size of 71.4 μm based on the X-ray radiation generated from a source voltage of 245 kV and the electron current was set at 300 μA. The X-ray CT system was equipped with a copper filter to remove low energy X-rays. Pomegranate samples were mounted on a translation stage which was at a fixed physical distance of 250 mm from the X-ray source and 700 mm from the detector with a scanning resolution of 71.4 μm. Two dimensional X-ray images were acquired as the fruit was rotated 360 degrees in one slow stepwise rotation, with 250 milliseconds of exposure time, recording a total of 2100 images in one rotation, depending on the size of sample and resolution. The total scan time for each sample was approximately 1 h.

2.3. *Image processing*

In order to characterise and quantify internal structures, 16-bit greyscale tagged image files (tiff) were imported and reconstructed to 3-D images using commercially available volume graphics software (VG StudioMax 2.1. and 2.2, Volume Graphics GmbH, Heidelberg, Germany). VG StudioMax is the version of the high-end software used for the visualisation and analysis of industrial computed tomography (CT) data and provides unique functionality for precise and fast analysis of voxel data. Further information on the software and optional add on modules are available from the user manual (www. volumegraphics.com). Pomegranate fruit encompasses a wide range of grey values required for effective analysis and segmentation of internal components due to variation in density or even similar density. The internal

Stellenbosch University https://scholar.sun.ac.za

components could not be segmented using traditional standard thresholding (Salmanizadeh *et al*., 2015); therefore, segmentation of internal components with a universal (single) threshold proved challenging.

To resolve this problem, an adaptive segmentation algorithm based on the grey level frequency from 4,000 to 60,000 was applied. The average grey values for each internal component was determined by manual segmentation. X-ray data was first filtered and smoothed using adaptive (5x5) Guass method. The removal of background pixels (external air and cardboard) was required before image segmentation could occur. Fruit were then separated from the background using an appropriate threshold of grey values averaging a tolerance ranging from 2,34 to 5,548 for external air and 6,302 to 32,875 units for cardboard. Surface determination was applied to the background (cardboard) in order to calculate the material boundary in sub-voxel accuracy defined by one grey value applied globally to the object before dilation was applied at positive 3 units to eliminate any remaining artefacts. In order to non-destructively quantify volumes of air spaces, peel, arils, kernels and single aril an appropriate threshold of grey values averaging a tolerance range from 4,532 to 20,482 units for air spaces, from 4,499 to 39,716 units for peel, from 6,680 to 53,481 for bulk arils and single aril, from 6,680 to 44,270 for kernels and from 8,629 to 42,408 for juice content was executed. Surface determination of the data was performed using interactive thresholding of these grey values. To ensure the surface was well defined, the advance mode was activated from surface determination and the local vicinity of each selected surface was investigated for the sharpest slope. The advanced surface determination is a re-evaluation of the material boundary defined by adapted grey values from the region of interest. Advanced surface determination reconstructs the component geometry more closely compared to standard surface determination because deviations are compensated from beam hardening or artefacts. Noises were removed by the procedure of erosion and dilation.

2.4. *Image analysis and segmentation of the internal components*

The different steps of image analysis and segmentation for separating the internal components of the pomegranate fruit are shown in (Fig. 1). Firstly, the representative 2-D image slice (Fig. 1a) was segmented to estimate the volume and eliminate the airspaces within the fruit (Fig. 1b). In order to visually distinguish arils from the non-edible material, the selected 2-D image slices for arils were segmented based on their grey values and assigned a red colour (Fig 1c) and while the non-edible portion was assigned white and black colours (Fig. 1c).To extract the arils, surface fitting was applied followed by morphological opening and closing (Fig. 1d). After aril extraction, peel area was determined by applying a perimeter using surface determination (Fig.

Stellenbosch University https://scholar.sun.ac.za

1e). In order to extract the kernels from the arils, surface determination was applied to the perimeter of the kernels and morphological opening and closing was applied to the area occupied by the kernels (Fig. 1f). Juice content was determined by removing the area occupied by kernels from arils (Fig. 1g). A single aril was extracted from the total aril volume by manual segmentation (Fig. 1h). 3-D models (Fig. 2) of arils and kernels were reconstructed by appropriately stacking floating image slices. Total number of arils per fruit was calculated by dividing the total aril volume by the single aril volume. Non-destructive measurement of the physical attributes including length, diameter and peel thickness using X-ray CT was estimated with a caliper instrument. The caliper instrument can be regarded as a distance instrument function enhanced by an additional line at each end. The additional lines are in a fixed right angle to the distance measurement line which was used to measure the fruit diameter and length and peel thickness. Fruit radius was calculated using a reference sphere which was based on attaching four or more fitting points to the fruit sample. The time required for image analysis of a sample set was approximately 2 h.

2.5. *Determination of physical parameters*

Fruit weight was measured using an electronic scale (Mettler Toledo, model ML3002E, Switzerland, 0.0001 g accuracy). Fruit length, diameter and peel thickness were measured using a Vernier caliper (Mitutoyo, model CD-6 CX, Japan) with 0.01 mm accuracy. Fruit volumetric measurements were determined at room temperature using the liquid displacement method based on Archimedes' Principle (Lang & Thorpe, 1989). For this purpose, toluene was used as an appropriate liquid for the tests because of its low absorption by the fruit and its low surface tension (Aydin, 2002).

In order to validate results from X-ray CT image analysis, fruit samples used for the scanning experiments were manually cut open and separated into peel and arils and each fraction was weighted. The volumes of whole arils and peel per fruit were determined. Fruit juice extraction from arils was performed with a cheese cloth and the volume of juice was measured using a graduated cylinder (± 1 cm^3). The kernels per fruit were carefully cleaned to remove surface moisture and fleshy pulp, and the weight and volume were measured. The volumetric measurements made allowed us to confirm if measured morphological features of the fruit corresponded with X-ray CT estimated data.

3. Statistical Analysis

Statistical analysis was carried out using Statistica software (Statistical version 10, StatSoft Inc., Tulsa, OK, USA). The accuracy of non-destructive prediction was assessed by subjecting the data calculated by X-ray CT and destructive measurements to linear regression analysis.

Stellenbosch University https://scholar.sun.ac.za

The significant difference between the two methods was subjected to paired t-test ($p = 0.05$) to determine statistical differences. GraphPad Prism software version 4.03 (GraphPad Software, Inc., San Diego, USA) was used for the graphical presentations.

4. Results and Discussion

4.1. *Volume analysis of different fruit fractions*

After image analysis, it was possible to determine volumes of pomegranate morphological structures. The results showing volumes occupied by arils, peel, kernels, juice content, air space and single aril is presented in Table 1. Results showed that using X-ray CT coupled with image analysis technique, on average; arils occupied 162.5 ±16.2 mL (48.05%) of the total pomegranate fruit volume (338.2 ±22.4 mL). The calculated volumes per fruit of peel, kernels, air space, and single aril were 163.9 ±21.4 mL (48.46%), 16.4 ±1.8 mL (4.9%), 10.9 ±4.1 mL (3.2%) and 0.3 ±0.04 mL (0.09%), respectively. In addition, the juice content was 146.1 ±16.3 mL, which accounted for 89.9% of the total estimated volume of arils. Destructive validation results were similar to X-ray CT non-destructive data, showing the volume of peel, arils, kernels, and single arils of 161.8 ±20.6, 163.3 ±15.2, 15.1±1.6 and 0.3 ±0.09 mL, respectively, corresponding to 47.95, 48.40, 4.48 and 0.09% of the total volume (337.4 ±22.6 mL) (Table 1). The remaining 3.66% (12.28 ±4.44) of the total fruit volume in destructive results could be due to air spaces. The results on volume of different fruit fractions obtained in this study are comparable to those reported by Shulman *et al*. (1984) for 'Mule's Head' and 'Wonderful' cultivars, where fruit arils constituted about 50% of total fruit mass. Our findings agree with aril yields previously reported in the literature. For instance, Al-Said *et al*. (2009) reported a yield of 50% for Jabal 1 and Jabal 3 cultivars, while aril yield of 47.5% was reported Wonderful cultivar grown in South African (Fawole & Opara, 2014). However, aril yields ranging between 52 and 68% for 7 other commercial cultivars grown in South Africa are contrary to our findings (Fawole & Opara, 2014).

The results in Table 1 also showed that the total volume of whole fruit, peel, kernels and juice content were underestimated by an average of 0.25%, 1.27%, 7.8% and 2.29%, respectively, while arils, single aril and airspace were overestimated by 0.51%, 3.13% and 11.31%, respectively. The results also showed that the difference between X-ray calculated and destructively measured mean volume for whole fruit, peel, arils, kernels, juice content and airspace were not significantly ($p > 0.05$) different. These results demonstrated that X-ray CT and associated image analysis were accurate in predicting whole fruit, arils, peel, kernels, air space, single arils and juice content. The average number of arils per fruit was non-destructively estimated to be 531.82 ±25.79 compared to destructive validation results of 545.50 ±22.78.

Stellenbosch University https://scholar.sun.ac.za

Furthermore, total aril number was overestimated by 2.51% with no significant difference ($p > 0.05$). These values fall within the range reported by several researchers on pomegranates grown in region of California (488 ±167; Wetzstein *et al*., 2011), Oman (378.04 ±24.68-651.23 ±50.43; Al-Said *et al*., 2009) and South Africa (271.6 ±17.24-815.5 ±55.24; Fawole & Opara, 2014).

Physical properties such as length, diameter and radius have been used to describe the shape index and fruit volume which could potentially be used for packaging of a particular produce (Fawole & Opara, 2013b; Al-Yahyai *et al*., 2009). The usage of X-ray CT coupled with image analysis technique for analysis of physical parameters showed that average fruit length, diameter, radius and peel thickness were 76.67 ±2.93 mm, 86.82 ±3.34 mm, 44.19 ±2.93 mm and 4.67±0.60 mm, respectively (Table 2). Furthermore, validation results were similar to X-ray CT non-destructive data, with fruit average length being (76.78 ±2.61 mm), diameter (85.86 ±3.04 mm), radius (42.93 ±0.99 mm) and peel thickness (4.93±0.50 mm) (Table 2). The results on physical parameters such as length, diameter and peel thickness obtained in this study are lower (13.34%, 13.88% and 38.38%) than those reported by Fawole & Opara (2014) for 'Wonderful' at harvest maturity grown in South Africa during the 2010 season from Western Cape region. However, similar results for peel thickness were in the range (5.30 mm) reported by Arendse *et al*. (2014) for 'Wonderful' cultivar at harvest maturity during 2012 season. Furthermore, the results in Table 2 also showed that fruit physical attributes such as length and peel thickness were overestimated by an average of 0.14% and 5.27% respectively, while diameter and fruit radius was overestimated by 1.11% and 2.8 5%. Nevertheless, no significant differences were observed for length, diameter, radius and peel thickness between X-ray CT predicted values and actual measurements.

The results of X-ray CT predicted and destructively measured data on the amount of fruit fractions were further subjected to linear regression analysis. Fig. 3 showed predicted X-ray CT values plotted against the destructively measured values for the volume of peel, arils, kernels, juice content, airspace and single aril with R^2 values of 0.97, 0.84, 0.90, 0.87, 0.82, and 0.80, respectively (Fig. 3a-e). The high R^2 provides a statistical measure of how close the predicted and measured data are to the fitted regression line and the low residual observed between predicted and measured volume for these 2 methods are similar indicating the accuracy of this method.

5. Conclusions

This work has shown the potential use of X-ray CT and image analysis as a promising tool for non-destructive characterization of internal and external structures. This non-destructive

Stellenbosch University https://scholar.sun.ac.za

approach could classify different pomegranate fruit cultivars on the basis of their contents of relevant fruit morphological fractions such as aril, peel, kernel and juice. Considering that high aril yield and juice content, in particular, are desirable properties which are of particular interest to breeders, growers, postharvest technologists, food process engineer's and consumers, understanding the relative contribution of different fruit fractions to total harvest is essential. Furthermore, the application of X-ray CT as a non-destructive tool could be used as a reliable method for tracking of maturity index by classifying different pomegranate cultivars based on their density and morphological fractions.

Although X-ray CT image analysis shows potential as a non-invasive analytical tool for internal fruit quality measurement and prediction, it is still currently available only to researchers for experimental purposes due to high cost. Furthermore, this non-destructive method has the potential to detect unidentified constituents based on the density of fruit tissues such as decay, disease infection and insect larva. Despite its potential as a technique for inspection of individual fruit with capabilities of detecting internal defects that goes beyond the traditional inspection of the human eye, X-ray CT have a series of problems that must be considered before they can be used for in-line application. For instance, X-ray CT systems are expensive and complex compared with other technologies such as Vis/NIRS and hyperspectral imaging. On the other hand, the current data acquisition times and image analysis are high and thus do not allow them to be readily applicable for commercial in-line or real-time inspection systems. Future research needs to consider reducing the amount of images acquired during data acquisition in order to provide a solution for a more automated process. Although a reduction in amount of images would result in low resolution quality and problems in segmentation this, therefore, provides novel research opportunities for future reductions in computing and image analysis cost.

Stellenbosch University https://scholar.sun.ac.za

References

Aindongo, W.V., Caleb, O.J., Mahajan, P.V., Manley, M. & Opara, U.L. (2014). Effects of storage conditions on transpiration rate of pomegranate aril-sacs and arils. *South African Journal of Plant and Soil*, **31**, 7–11.

Al-Maiman, S.A. & Ahmad, D. (2002). Changes in physical and chemical properties during pomegranate (*Punica granatum* L.) fruit maturation. *Food Chemistry*, **76**, 437–441.

Al-Said, F.A., Opara, U.L. & Al-Yahyai, R.A. (2009). Physico-chemical and textural quality attributes of pomegranate cultivars (*Punica granatum* L.) grown in the Sultanate of Oman. *Journal of Food Engineering*, **90**, 129–134.

Al-Yahyai, R., Al-Said, F. & Opara, L. (2009). Fruit growth characteristics of four pomegranate cultivars from northern Oman. *Fruits*, **64**, 335–341.

Arendse, E., Fawole, O.A. & Opara, U.L. (2014). Influence of storage temperature and duration on postharvest physico-chemical and mechanical properties of pomegranate fruit and arils. *CyTA-Journal of Food*, **12**, 389–398.

Aydin, C. (2002). Physical properties of hazel nuts. *Biosystems Engineering*, **82**, 297–303.

Cantre, D., Herremans, E., Verboven, P., Ampofo-Asiama, J. & Nicolaï, B.M. (2014). Characterization of the 3-D microstructure of mango (*Mangifera indica* L. cv. Carabao) during ripening using X-ray computed microtomography. *Innovative Food Science* and *Emerging Technologies*, **24**, 28–39.

Donis-González, I.R., Guyer, D.E., Pease, A. & Barthel, F. (2014a). Internal characterization of fresh agricultural products using traditional and ultrafast electron beam X-ray computed tomography imaging. *Biosystems Engineering*, 117, **104**–113.

Donis-González, I.R., Guyer, D.E., Fulbright, D.W. & Pease, A. (2014b). Postharvest non-invasive assessment of fresh chestnut (*Castanea* spp.) internal decay using computer tomography images. *Postharvest Biology and Technology*, **94**, 14–25.

Fawole, O.A., Makunga, N.P. & Opara, U.L. (2012). Antibacterial, antioxidant and tyrosine-inhibition activities of pomegranate fruit peel methonolic extract. *BioMed Central Complementary and Alternative Medicine*, **12**, 200–225.

Fawole, O.A. & Opara, U.L. (2012). Composition of trace and major minerals in different parts of pomegranate (*Punica granatum*) fruit cultivars. *British Food Journal*, **114**, 1518–1532.

Fawole, O.A. & Opara, U.L. (2013a). Developmental changes in maturity indices of pomegranate fruit: A descriptive review. *Scientia Horticulturae*, **159**, 152–161.

Stellenbosch University https://scholar.sun.ac.za

Fawole, O.A. & Opara, U.L. (2013b). Fruit growth dynamics, respiration rate and physico-textural properties during pomegranate development and ripening. *Scientia Horticulturae*, **157**, 90–98.

Fawole, O.A. & Opara, U.L. (2014). Physicomechanical, phytochemical, volatile compounds and free radical scavenging properties of eight pomegranate cultivars and classification by principal component and cluster analyses. *British Food Journal*, **116**, 544–567.

Holland, D., Hatib, K. & Bar-Ya'akov, I. (2009). Pomegranate: botany, horticulture, breeding. *Horticultural Reviews*, **35**, 127–191.

Jha, S.N., Narsaiah, K., Sharma, A.D., Singh, M., Bansal, S. & Kumar, R. (2010). Quality parameters of mango and potential of non-destructive techniques for their measurement - a review. *Journal of Food Science and Technology*, **47**, 1–14.

Kotwaliwale, N., Kalne, A. & Singh, K. (2011). Radiography, CT and MRI. In: *Book chapter in non-destructive evaluation of food quality theory and practice* (edited by S.N. Jha). Springer, Berlin.

Kotwaliwale, N., Singh, K., Kalne, A., Jha, S.N., Seth, N. & Kar, A. (2014). X-ray imaging methods for internal quality evaluation of agricultural produce. *Journal of Food Science and Technology*, **51**, 1–15.

Lammertyn, J., Dresselaers, T., Van Hecke, P., Jancsók, P., Wevers, M. & Nicolaï, B.M. (2003a). MRI and X-ray CT study of spatial distribution of core breakdown in 'Conference' pears. *Journal of Magnetic Resonance Imaging*, **21**, 805–815.

Lammertyn, J., Dresselaers, T., Van Hecke, P., Jancsók, P., Wevers, M., De Baerdemaeker, J. & Nicolaï, B.M. (2003b). Analysis of the time course of core breakdown in 'Conference' pears by means of MRI and X- ray CT. *Postharvest Biology and Technology*, **29**, 19–28.

Lang, A. & Thorpe, M.R. (1989). Xylem, phloem and transpiration flows in a grape: Application of a technique for measuring the volume of attached fruits to high resolution using Archimedes' Principle. *Journal of Experimental Botany*, **40**, 1069–1078.

Léonard, A., Blacher, S., Nimmol, C. & Devahastin, S. (2008). Effect of far-infrared radiation assisted drying on microstructure of banana slices: an illustrative use of X-ray microtomography in microstructural evaluation of a food product. *Journal of Food Engineering*, **85**, 154–162.

Magwaza, L.S., Opara, U.L., Terry, L.A., Landahl, S., Cronje, P.J.R., Nieuwoudt, H.H., Hanssens, A., Saeys, W. & Nicolaï, B.M. (2013a). Evaluation of Fourier transform-

Stellenbosch University https://scholar.sun.ac.za

NIR spectroscopy for integrated external and internal quality assessment of 'Valencia' oranges. *Journal of Food Composition and Analysis*, **31**, 144–154.

Magwaza, L.S., Ford, H.D., Cronje, P.J.R., Opara, U.L., Landahl, S., Tatam, R.P. & Terry, L.A. (2013b). Application of optical coherence tomography to non-destructively characterise rind breakdown disorder of 'Nules Clementine' mandarins. *Postharvest Biology and Technology*, **84**, 16–21.

Magwaza, L.S. & Opara, U.L. (2014). Investigating non-destructive quantification and characterization of pomegranate fruit internal structure using X-ray computed tomography. *Postharvest Biology and Technology*, **95**, 1–6.

Mendoza, F., Verboven, P., Mebatsion, H.K., Kerckhofs, G., Wevers, M. & Nicolaï, B. (2007). Three-dimensional pore space quantification of apple tissue using X-ray computed microtomography. *Planta*, **226**, 559–570.

Miguel, M.G., Nevesa, M.A. & Antunes, M.D. (2010). Pomegranate (*Punica granatum* L.): A medicinal plant with myriad biological properties- a short review. *Journal* of *Medicinal Plants Research*, **4**, 2836–2847.

Mphahlele, R.R., Stander, M.A., Fawole, O.A. & Opara, U.L. (2014a). Effect of fruit maturity and growing location on the postharvest contents of flavonoids, phenolic acids, vitamin C and antioxidant activity of pomegranate juice (cv. Wonderful). *Scientia Horticulturae*, **179**, 36–45.

Mphahlele, R.R., Fawole, O.A., Stander, M.A. & Opara, U.L. (2014b). Preharvest and postharvest factors influencing bioactive compounds in pomegranate (*Punica granatum* L.)-A review. *Scientia Horticulturae*, **178**, 114–123.

Nicolaï, B.M., Beullens, K., Bobelyn, E., Peirs, A., Saeys, W., Theron, I.K. & Lammertyn, J. (2007). Non-destructive measurement of fruit and vegetable quality by means of NIR spectroscopy: a review. *Postharvest Biology and Technology*, **46**, 99–118.

Opara, L.U., Al-Ani, M.R. & Al-Shuaibi, Y.S. (2009). Physiochemical properties, vitamin C content, and antimicrobial properties of pomegranate fruit (*Punica granatum* L.). *Food and Bioprocess Technology*, **2**, 315–321.

Ogawa, Y., Morita, K., Tanaka, S., Setoguchi, M. & Thai, C.N. (1998). Application of X-ray CT for detection of physical foreign materials in foods. *Transactions of the American Society of Agricultural Engineers*, **41**, 157–162.

Pomegranate Association of South Africa (POMASA) (2012). Pomegranate industry statistics. Paarl, South Africa [Internet document] URL http://www.sapomegranate.co.za/focus-areas/statistics-and-information/. Accessed 04/01/2016.

Stellenbosch University https://scholar.sun.ac.za

Salmanizadeh, F., Nassiri, S.M., Jafari, A. & Bagheri, M.H. (2015). Volume estimation of two local pomegranate fruit (*Punica granatum* L.) cultivars and their components using non-destructive X-ray computed tomography technique. *International Journal of Food Properties*, **18**, 439–455.

Seeram, N.P., Zhang, Y., Reed, J.D., Krueger, C.G. & Vaya, J. (2006). Pomegranate phytochemicals. In: *Pomegranates: ancient roots to modern medicine* (edited by N.P. Seeram, R.N. Schulman, & D. Heber). Pp. 3–29. CRC Press Taylor & Francis Group, Boca Raton, FL.

Shahin, M.A., Tollner, E.W., Gitaitis, R.D., Sumner, D.R. & Maw, B.W. (2002). Apple classification based on surface bruises using image processing and neural networks. *Transactions of the American Society of Agricultural Engineers*, **45**, 1619–1627.

Viuda-Martos, M., Fernández-López, J. & Pérez-Álvarez, J.A. (2010). Pomegranate and its many functional components as related to human health: A Review. *Comprehensive Reviews in Food Science and Food Safety*, **9**, 635–654.

Volume Graphics Solutions about Voxels [Internet document] URL http://www.volumegraphics.com/fileadmin/user_upload/flyer/VGStudioMAX_22_en_pdf/. Accessed 03/03/2016.

Wetzstein, H.Y., Zhang, Z., Ravid, N. & Wetzstein, M.E. (2011). Characterization of attributes related to fruit size in pomegranate. *HortScience*, **46**, 908–912.

Zhang, B., Huang, W., Li, J., Zhao, C., Fan, S., Wu, J. & Liu, C. (2014). Principles, developments and applications of computer vision for external quality inspection of fruits and vegetables: A review. *Food Research International*, **62**, 326–343.

Stellenbosch University https://scholar.sun.ac.za

Table 1. Volumes of whole fruit and fruit fractions (peel, arils, kernel, juice, single aril and airspace) of pomegranate fruit (cv. Wonderful).

Fruit fraction	Non-destructively calculated volume (mL)	Destructively measured volume (mL)	Mean of difference (mL)	Paired t-test *p*-value
Whole fruit	338.19 ±22.41	337.36 ±22.56	0.83 ±4.85	0.99
Peel	163.87 ±21.42	161.81 ±20.60	2.06 ±6.65	0.74
Arils	162.45 ±16.21	163.28 ±15.24	-0.83 ±6.55	0.85
Kernels	16.38 ±1.81	15.10 ±1.63	2.45 ±1.69	0.42
Single aril	0.31 ±0.04	0.32 ±0.09	-0.01 ±0.04	0.83
Airspace	10.89 ±2.57	12.28 ±4.44	-1.39 ±1.90	0.27
Juice content	146.07 ±16.28	142.73 ±16.41	3.34 ±7.49	0.49
Count of arils per fruit	531.82 ±25.79	545.50 ±22.78	-13.68 ±2.81	0.15

Values are presented as the mean ± Std dev for 23 fruit with p value < 0.05 indicating significant difference according to t-test.

Stellenbosch University https://scholar.sun.ac.za

Table 2. Lineal size parameters of whole pomegranates fruit and peel (cv. Wonderful).

Size parameter	Non-destructively calculated measurement (mm)	Destructively measured (mm)	Mean of difference (mm)	Paired t-test *p*-value
Length	76.67 ±2.93	76.78 ±2.61	-0.11 ±2.51	0.86
Diameter	86.82 ±3.34	85.86 ±3.04	0.96 ±3.64	0.18
Radius	44.19 ±2.93	42.93 ±0.99	1.26 ±9.59	0.08
Peel thickness	4.67 ±0.60	4.93 ±0.50	-0.26 ±0.40	0.23

Values are presented as the mean ± Std dev for 23 fruit with p value < 0.05 indicating significant difference according to t-test.

Stellenbosch University https://scholar.sun.ac.za

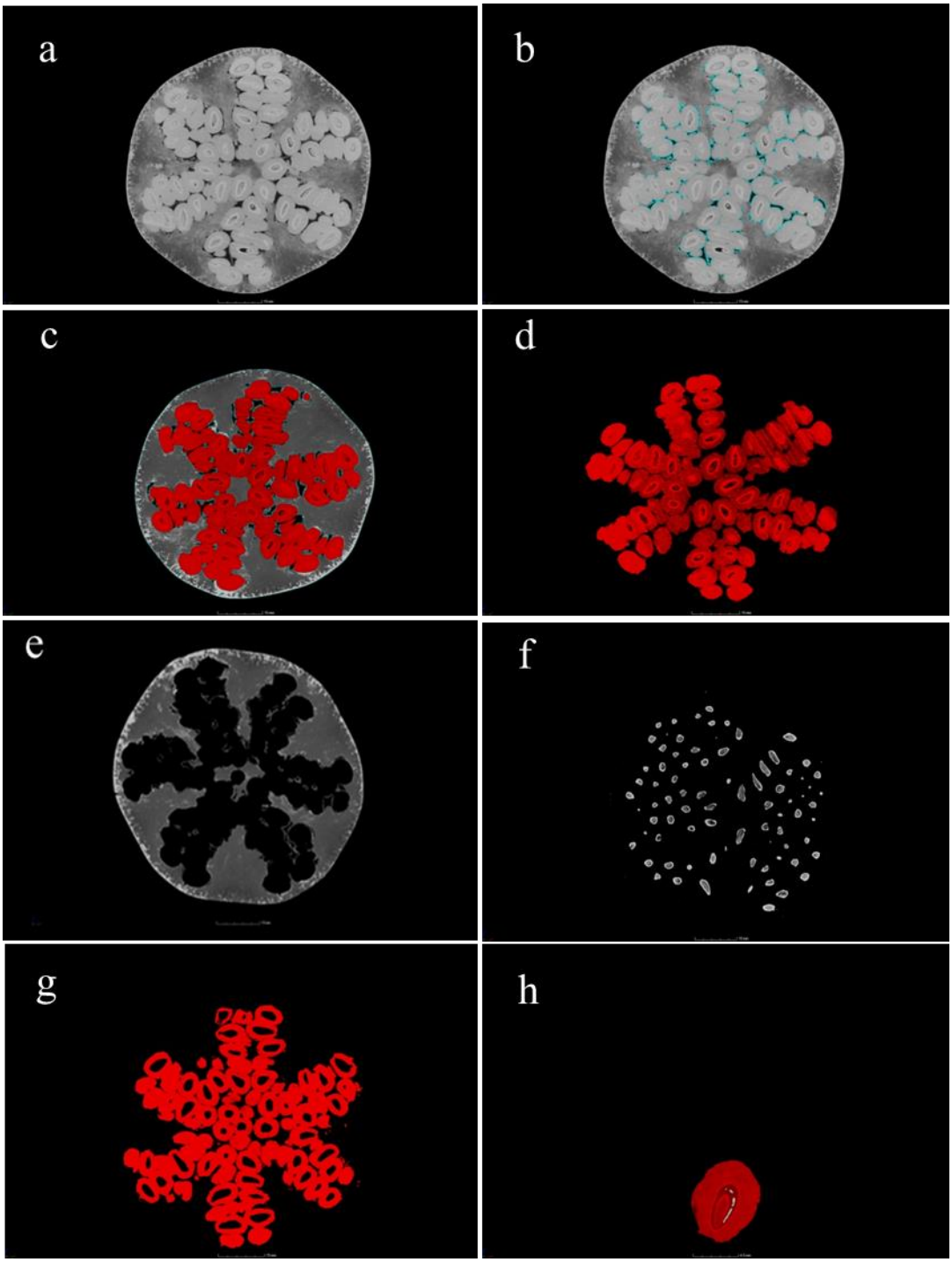

Fig. 1. Image analysis procedure for X-ray computed tomography images of pomegranate fruit samples: (a) representative raw X-ray image slice was filtered; (b) airspace was estimated and removed (c) arils were colour-coded based on density; area occupied by aril and peel were extracted (d and e); (f) kernels were extracted from arils using surface determination; (g) juice content was estimated by removing kernels from arils; and (h) single arils were separated from aril sac.

Stellenbosch University https://scholar.sun.ac.za

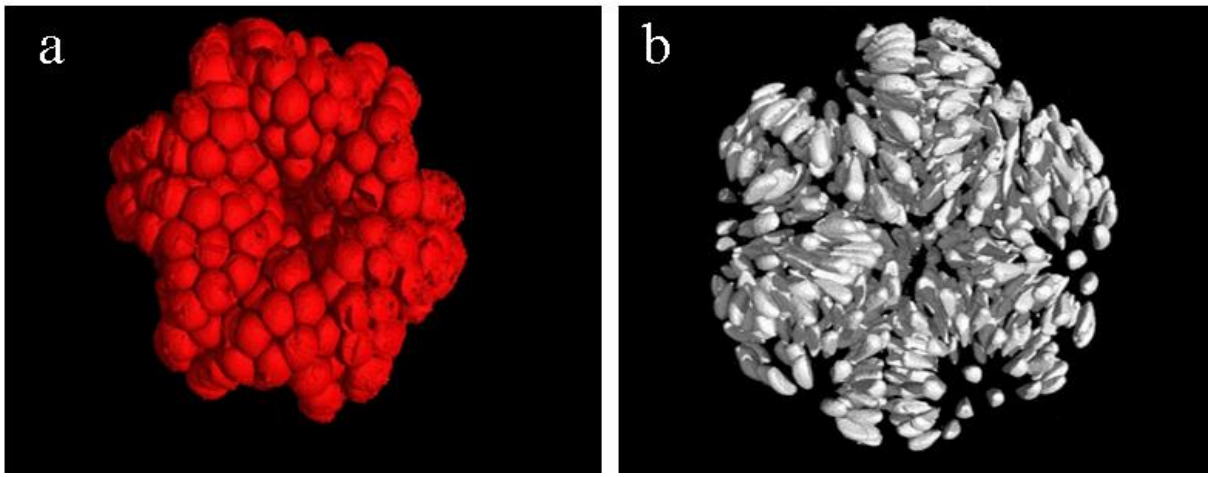

Fig. 2. 3-D models of (a) pomegranate arils and (b) kernels reconstructed by stacking floatation.

Stellenbosch University https://scholar.sun.ac.za

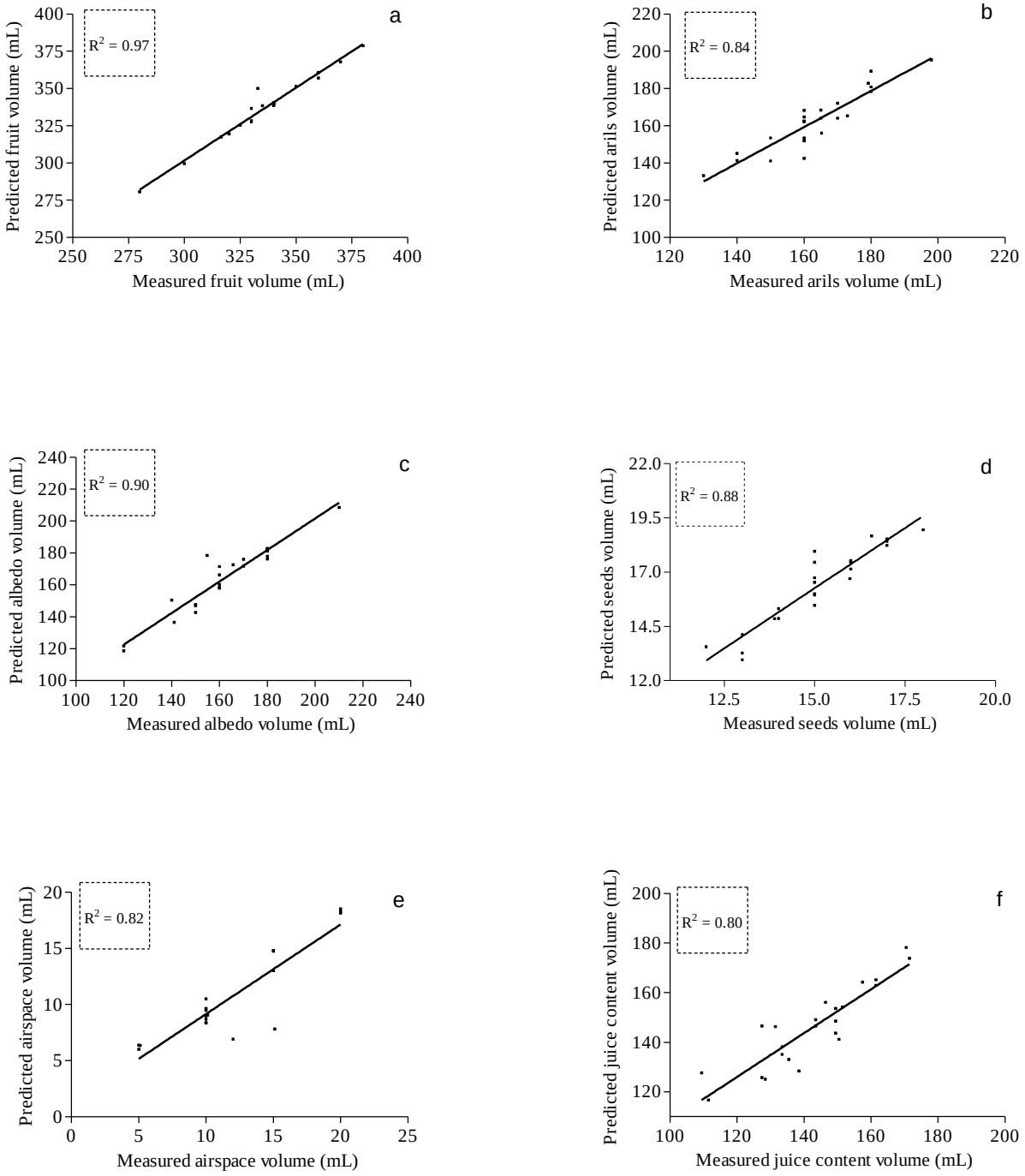

Fig. 3. Scatter plots of non-destructively calculated (X-ray CT) versus destructively measured volumes of (a) whole pomegranate fruit and fruit fraction (b) arils, (c) peel, (d) kernels, (e) airspace, and (f) juice content (cv. Wonderful).

Stellenbosch University https://scholar.sun.ac.za

DECLARATION BY THE CANDIDATE

With regard to **Chapter 4 (pp 73-95)**, the nature and scope of my contribution were as follows:

Nature of contribution	Extent of contribution (%)
Research, data collection, analysis and writing of chapter	70

The following co-authors have contributed to **Chapter 4 (pp 73-95)**

Name	e-mail address	Nature of contribution	Extent of contribution (%)
Prof U.L. Opara	opara@sun.ac.za	Conception of the work and proof reading	10
Dr O.A. Fawole	olaniyi@sun.ac.za	Research input, editorial suggestion and proof reading	10
Dr L.S. Magwaza	Magwazal@ukzn.ac.za	Research input, editorial suggestion and proof reading	5
Dr H. Nieuwoudt	hhn@sun.ac.za	Research input, editorial suggestion and analysis	5

Stellenbosch University https://scholar.sun.ac.za

E Arendse **Signature of candidate**	29/08/2017 **Date**

DECLARATION BY CO-AUTHORS

The undersigned hereby confirm that:

1. the declaration above accurately reflects the nature and extent of the contributions of the candidate and the co-authors to **Chapter 4 (pp 73-95)**

2. no other authors contributed to **Chapter 4 (pp 73-95)** besides those specified above, and

3. potential conflicts of interest have been revealed to all interested parties and that the necessary arrangements have been made to use the material in **Chapter 4 (pp 73-95)** of this dissertation.

Signature	Institutional affiliation	Date
Prof U.L. Opara	Stellenbosch University	29/08/2017
Dr O.A. Fawole	Stellenbosch University	29/08/2017
Dr L.S. Magwaza	University of KwaZulu-Natal	29/08/2017
Dr H. Nieuwoudt	Stellenbosch University	29/08/2017

Stellenbosch University https://scholar.sun.ac.za

CHAPTER 4

Using Fourier transform near-infrared diffuse reflectance spectroscopy and two spectral acquisition modes to evaluate external and internal quality of intact pomegranate fruit

Abstract

This paper evaluated Fourier transform near-infrared diffuse reflectance spectroscopy as a non-destructive method for the development of calibration models to assess the quality of whole pomegranate fruit. Two FT-NIR diffuse reflectance spectrometers with different spectral acquisition modes were evaluated; namely, by direct contact between the sample and the integrating sphere (IS), and by a contact-less measurement using an optic fibre coupled emission head (EH) to scan fruit over a distance of 17 cm. External quality parameters assessed include fruit weight, firmness and colour components (a*, Chroma, hue angle), while internal quality parameters were total soluble solids (TSS), pH, titratable acidity (TA), sugar to acid ratio (TSS:TA), BrimA, total phenolics, total anthocyanin and vitamin C. The best prediction statistics obtained from calibration models of the EH were firmness (R^2 = 85.03, RPD = 2.43), fruit colour components (a*: R^2 = 92.65, RPD = 3.34); Chroma: R^2 = 86.00, RPD = 2.58), TSS (R^2 = 83.48, RPD = 2.37), TA (R^2 = 77.67, RPD = 2.12), BrimA (R^2 = 79.18, RPD = 2.21), total phenolics (R^2 = 88.16, RPD = 2.91) and vitamin C (R^2 = 83.39, RPD = 2.06). The best prediction statistics obtained from calibration models of the IS were colour component Hue (R^2 = 94.68, RPD = 2.50), TSS:TA (R^2 = 99.54, RPD = 2.72) and total anthocyanin (R^2 = 99.45, RPD = 1.64). Overall, good prediction statistics were observed for both the EH and IS; however, better prediction performance was obtained with the EH which gave the best prediction for 9 of the 13 quality parameters evaluated. These findings have demonstrated that the EH (a contactless option of the Matrix-F) can be implemented as an online tool for the analysis of pomegranate fruit quality.

Keywords: *Punica granatum* L., Fruit quality, Partial least squares, Non-destructive measurement, FT-NIR, Total phenolics, Vitamin C

Stellenbosch University https://scholar.sun.ac.za

1. Introduction

Pomegranate (*Punica granatum* L) fruit has gained popularity for its high nutritional content, potent pharmacological and antioxidant properties linked to its consumption (Viuda-Martos *et al*., 2010). Literature suggests that these health benefits have been linked to a group of phytochemical compounds such as phenolics, tannins, anthocyanins and flavinoids found within the fruit (Viuda-Martos *et al*., 2010; Fawole *et al*., 2012; Seeram *et al*., 2006). Pomegranate fruit has a thick leathery rind which has been reported to range between 4 to 8 mm in thickness (Fawole & Opara, 2014; Arendse *et al*., 2014a) and the fruit interior is separated into compartments. The edible portion of the fruit contains arils are packed in compartments and each aril contains a kernel (woody portion) (Holland *et al*., 2009; Aindongo *et al*., 2014; Arendse *et al*., 2016).

External quality evaluation of pomegranate fruit is based on the measurement of parameters such as fruit weight, rind colour and firmness. Internal fruit quality related to organoleptic aspects include total soluble solids (TSS), titratable acidity (TA), TSS:TA ratio and total phenolic content. The traditional method of measuring these internal quality attributes are destructive in nature, require specialised sample preparation, labour intensive and inapplicable during grading and sorting in commercial packing operations. Moreover, fruit quality determined destructively may display significant variation due to difference in maturity, growing region and fruit canopy position (Magwaza *et al*., 2013). In order to supply high quality fruit to the international market, an alternative non-destructive approach is required.

Near-infrared (NIR) spectroscopy is a non-destructive technique that interacts with molecular groups which consist of C-H, O-H and N-H bonds providing information about the proportion of each including scattering from microstructures which can be indirectly related to physical properties (Nicolaï *et al*., 2007). Furthermore, NIR spectroscopy is regarded as one of the most advances in chemometric software packages and commercial application compared to other non-destructive techniques such as NMR and X-ray CT (Nicolaï *et al*., 2007; Magwaza *et al*., 2012a). Published NIR based research on different quality attributes for pomegranate fruit is limited to one study. Khodabakhshian *et al*. (2016) focused on the use of Vis/NIR for the measurement of sugar and acidity content. However, several key parameters used to evaluate pomegranate quality still needs to be assessed such as fruit weight, fruit colour, firmness, TSS:TA ratio and more recently BrimA (Fawole & Opara, 2013a). BrimA index is a variant of TSS/TA and a criterion for acceptance of fruit juice, relating to the sensorial properties of the fruit. The index allows smaller amounts of acid than sugar to make the same numerical change to BrimA (Fawole & Opara, 2013b). Therefore, evaluation of these

Stellenbosch University https://scholar.sun.ac.za

parameters could contribute to the implementation of suitable management strategies to predict and control desired pomegranate quality attributes. Furthermore, the pomegranate is a rich source of vitamin C and several other active polyphenolic compounds (Viuda-Martos *et al*., 2010; Ismail *et al*., 2012; Opara *et al.*, 2009). Accurate and reliable prediction of these chemical constituents during postharvest handling and processing could contribute in providing high quality fruit rich in vitamin C and phytochemicals to consumers.

In industrial applications, conventional spectrometers can only be installed close to the stage where the product such as fruit is measured, whereas the fibre optic probes make it possible to reach measurement points that are difficult to access. The application of FT-NIRS in process control has the potential for on-line analysis of fruit quality. The objective of this study was, therefore, to evaluate two different spectral acquisition modes, namely direct contact between the sample using a rotating integrating sphere (IS) and a contact-less measurement using an optic fibre coupled emission head (EH) for the prediction of external and internal quality parameters of intact pomegranate fruit. The contactless option simulates the situation in the pack-house for online application, whereas direct contact provides an ideal tool to meet the requirements for research applications.

2. Materials and Methods

2.1. *Fruit supply*

This research was carried out during the 2015 season using pomegranate (cv. Wonderful) procured from two commercial orchards in the area of Western Cape province, South Africa (33°34′851″S, 19°00′360″E). A total of 200 fruit was obtained from Heinrich Frederich Schaefer (HFR) orchard, while another set of 100 fruit was obtained from Porterville to add orchard location variability. The fruit were transported to the Postharvest Technology Research Laboratory at Stellenbosch University. On arrival, fruit were equilibrated for 12 h at ambient conditions (23 ±3 °C) before being sorted out for size uniformity.

2.2. *Spectral acquisition*

Two different spectral preselection methods were used to obtain NIR spectra of pomegranate fruit, namely, the Multi-Purpose Analyser (MPA) FT-NIR spectrophotometer (Bruker Optics, Ettlingen, Germany) and MATRIX^{TM}-F FT-NIR spectrophotometer (Bruker Optics, Ettlingen, Germany). NIR spectral data were acquired on opposite equilateral sides of each fruit over a spectral wavelength range of 800-2500 nm. The acquired spectra for each fruit were averaged to obtain a single spectrum. During NIR spectral acquisition the same fruit samples were

Stellenbosch University https://scholar.sun.ac.za

measured sequentially using two different spectral acquisition methods at room temperature. The MPA was equipped with an integrating sphere (IS) for direct contact with the sample and measure diffuse reflectance. Fruit samples were placed on a 50 mm width accessory sample holder which is used for measurement of highly scattering solid media. The MPA is equipped with a permanently aligned and highly stable RockSolid^{TM} interferometer which consist of gold-coated mirrors with a beam splitter which is made of a quartz substrate (Magwaza *et al*., 2013). The NIR beam is directed into the gold-coated sphere and through the centre of the sphere into the pomegranate sample. Due to the gold coating, the reflected light re-enters the sphere and are collected and directed towards the detector. The integrating sphere uses a PbS detector with nonlinearity correction. The wavelength range scanned was from 800-2500 nm (12500-4000 cm^{-1}) with a scanning resolution of 8 cm^{-1} and scanner velocity of 10 kHz. For each spectrum a total of 128 scans were acquired which averaging about 120 s per sample and after 30 min reference measurements were performed against air background.

The MATRIX^{TM}-F (Q410/A) FT-NIR spectrometer was equipped with a fibre optic emission head (EH) (230 mm diameter, 185 mm height and 170 mm focus depth) mounted 185 mm above the sampling platform for contactless measurement of the fruit. The EH contains 4 air cooled tungsten NIR light sources (tungsten halogen, 12 V, 20 W). The diffused reflected light was collected via an optic fibre cable connected to the spectrometer which is equipped with a thermoelectrically cooled and temperature-controlled TE InGaAs diode detector. Prior to scanning pomegranate fruit, reference measurements were taken against air background and periodically at intervals of 30 min between measurements. The wavelength range, scanning resolution and a number of scans per spectrum were the same as the MPA FT-NIR spectrophotometer. In both instruments, the measurement the NIR spectra system was operated was achieved using OPUS software (OPUS v. 7.0 for Microsoft, Bruker Optics, Ettlingen, Germany). Illustration of the two different spectrometers is presented in appendix chapter 6, Fig. 1.

2.3. *Reference measurements*

The weight of each fruit was determined using an electronic scale (Mettler Toledo, Model ML3002E, Switzerland, 0.01 g accuracy). A fruit texture analyser (GÜSS-FTA, South Africa) fitted with a cylindrical probe (5 mm) which was used to measure fruit firmness. Rind colour components were performed using a calibrated colour Chroma Meter (CR-400 Minolta Corp, Osaka, Japan). Chroma (C*) and Hue angle (h°) were derived from the colour components L*, a*and b* as described by Pathare *et al*. (2013): Individual fruit were manually peeled and the

Stellenbosch University https://scholar.sun.ac.za

extracted arils were juiced using a Liquafresh juice extractor. The juice was filtered through a 1 mm sieve and immediately used measure the TSS, pH and TA and the remainder of the juice was stored in a freezer (VF720 -86, SNIJDER LABS, Netherlands) at -80 °C for further analysis of phytochemicals and vitamin C concentration.

A hand-held digital refractometer (0-32%) was used to assess the percentage of total soluble solids in the juice. A titro-sampler (Metrohm, Switzerland) was used to assess the acidity (citric acid %) by titration of 2 mL fresh juice with 0.1 M NaOH solution. The pH values were determined using a calibrated pH meter (Crison, Model 924, Barcelona, Spain). The sugar to acidity ratio was assessed by calculating the ratio between TSS to TA. BrimA index, a variation of TSS and TA was assessed using TSS-k*TA, where k equals 2 thereby avoiding negative BrimA values (Arendse *et al*., 2014a).

The total phenolic content assay was done in duplicate using Folin-Ciocalteu colorimetric method according to Makkar *et al*. (2007) with slight modification according to (Fawole *et al*., 2012). Briefly, 50 µL of fruit juice supernatant was diluted with 500 µL of 1 N Folin C reagent and 2.5 mL of 2% sodium carbonate solution and the mixture was stored in a dark environment for 40 min before being measured at 725 nm against 50% blank aqueous methanol and results were expressed as grams gallic acid equivalents (GAE) per liter of pomegranate juice.

Total monomeric anthocyanin concentration was measured using pH differential method (Giusti & Wrolstad, 2001) and recently applied by Arendse *et al*. (2014b). Juice supernatant (1 mL) was diluted with 9 mL pH 1 KCL buffer solution and pH 4.5 sodium acetate buffer solution respectively. After 10 min the absorbance was measured spectrophotometrically (Thermo Scientific Technologies, Madison, WI, USA) at 510 nm and 700 nm against 50% blank aqueous methanol. Total monomeric anthocyanin was expressed as cyanidin-3-glucoside equivalents per litre of pomegranate juice. The vitamin C assay was performed in duplicate as described by Klein and Perry (1982) with slight modification by Barros, (2007) and recently been applied by Arendse *et al*. (2017). The results were expressed as grams ascorbic acid equivalent per litre crude juice.

2.4. *Precision and accuracy of destructive reference measurements*

Reference measurements were subjected to intra- and inter-day variability testing to evaluate their repeatability. Intra-day variability was determined on five replicates within 1 day, and the inter-day was determined for 3 consecutive days. In order to determine their repeatability, the relative standard derivation (RSD) was calculated using Eq 1:

Stellenbosch University https://scholar.sun.ac.za

$$\text{RSD} = \frac{SD}{X} \times 100 \quad (1)$$

where RSD is relative standard deviation, SD and X are standard deviation and the average obtained from replicate measurements respectively. RSD values for quality parameters ranged from 0.30 to 0.90% indicating acceptable accuracy as reported by Olarewaju *et al.* (2016).

2.5. *Chemometric data analysis*

In order to construct calibration models NIR spectral data was subjected to principal component analysis (PCA) and partial least squares regression (PLSR) using OPUS version 7.0 software Spectral data were subjected to different spectral pre-processing methods that included multiplicative scattering correction (MSC), first derivative, second derivative, and vector normalization (SNV). Combinations of FD+MSC and FD+SNV were also tested. OPUS software was used to investigate the spectral variation using PCA, samples with high residual and located far away from the zero line of the residual variance was perceived as potential outliers (Goodacre *et al*., 2007). A dataset of both orchards was randomly split into calibration (70%) and validation (30%) each set containing sufficient samples of both orchards. The development of calibration models was selected based on the pre-processing method that provided the lowest root mean square error of estimation (RMSEE) and higher residual predictive deviation (RPD) value.

The model's performance was evaluated using the following regression statistics:

- R^2 Eq. (2), the coefficient of determination explains the proportion of variation in the dependent variable (reference data) that is predictable from the independent variable. R^2 shows how well the regression model fits the data.

$$R^2 = 1 - \frac{\sum(y_{cal} - y_{act})^2}{\sum(y_{cal} - y_{mean})^2} \quad (2)$$

- RMSEE Eq. (8) used to evaluate modeling error or calibration variance (Bruker Optik, 2006).

$$RMSEE = \sqrt{\frac{1}{M-R-1} \times SSE} \quad (3)$$

With M, the number of calibration samples; R, the rank; and SSE, the Sum of Squared Errors.

$$SSE = \sum[Res]^2 \quad (4)$$

With Res, the residual (the difference between the true and the fitted value).

Stellenbosch University https://scholar.sun.ac.za

- RMSEP Eq. (10) used to evaluate the prediction error or validation variance. (Bruker Optik, 2006).

$$RMSEP = \sqrt{\sum \frac{(y_{pred} - y_{act})^2}{n}} \quad (5)$$

- The bias Eq. (11) (systematic variation between the predicted and reference data) and

$$Bias = \frac{1}{n}\sqrt{\sum (y_{pred} - y_{act})^2} \quad (6)$$

- RPD Eq. (12) residual predictive deviation has been used to assess the predictive ability of the developed models. RPD is the ratio of standard error of prediction to the standard deviation (Williams, 2014).
- $$RPD = \frac{SD}{RMSEP} \quad (7)$$

Where:

n = number of spectra

y_{act} = actual value

y_{mean} = mean value

y_{cal} = calculated value

y_{pred} = predicted value of the attribute

3. **Results and discussion**

3.1. *Spectral characteristics*

The average absorbance spectra of cv. Wonderful pomegranate for the two different spectral acquisition modes are, presented in Fig. 2. The spectral range (800-2500 nm) was trimmed to the region of 800-2400 nm to remove noise. Considerable variation in absorbance values was observed during the different spectral preselection modes with higher absorbance values for the IS of MPA compared to the EH of the Matrix-F spectrophotometer. The offset in absorbance values may be due to the difference in focus depth between the two instruments. However, both spectral acquisition methods displayed similar wavelength bands. The spectral bands for the respective acquisition methods displayed contours having prominent absorbance bands in the region 950, 1200, 1450, 1780 and 1930 nm. Band assignment was done according to literature (Nicolaï *et al*., 2007; Shenk *et al*., 2008; Magwaza *et al*., 2012a). The spectral profile for pomegranate fruit is similar to those reported for fruit such as mango (Guthrie & Walsh, 1997), kiwifruit (McGlone & Kawano, 1998), passion fruit (De Oliveira *et al*., 2014)

Stellenbosch University https://scholar.sun.ac.za

and tomatoes (De Oliveira *et al*., 2014). The NIR absorption bands in the region of 950 and 1450 correspond to second and first vibrational overtones associated with O-H stretching related to water (Lestander & Geladi, 2005; Clément et al., 2008). Bands observed in the region of 1200 and 1930 nm corresponded to the second and first overtones of C-H stretching including the third overtone related to deformation of OH, CH and CH_2 bonds found in sugar solution. Sugars and organic acids have been reported to display bands in the wavelength regions of 1100-1600 and 1700-2300 nm (Gómez *et al*., 2006; Louw & Theron, 2010).

3.2. *Distribution of calibration and validation reference data*

In order to ensure that samples of both orchards had sufficient variation in TSS and TA, their distribution frequency was assessed. Pomegranate fruit samples (n = 300) were categorised into four groups (high TSS high TA, high TSS low TA, low TSS high TA and low TSS low TA) according to Arendse *et al*. (2017). The distribution frequency of the variation in TSS and TA in pomegranate fruit samples (n = 300) are presented in Fig 1. The sample collection showed a wide range of variability in TSS and TA within the sample set. The statistics (mean, standard deviation, coefficient of variation) for external and internal parameters of pomegranate fruit are presented in Table 1. In this study, the reference data for all parameters were normally distributed around the mean. Lu *et al*. (2006) stated that the validation and accuracy of calibration models would depend on enough variation present within the sample set in the physical and biochemical reference data. Furthermore, a large sample variation within the calibration and validation data sets have been shown to be predicted better by NIR spectroscopy (Magwaza *et al*., 2013; Magwaza *et al*., 2014). It was apparent from the standard deviation, minimum-to-maximum range and CV% statistics that most parameters had high CV% values of up to 20.95% with both calibration and validation data sets covered a wide range of values.

3.3. *Model development of two FT-NIR acquisition modes*

The development of calibration models for each parameter was performed by evaluating different wavelength ranges that gave higher R^2 and RPD values including lower RMSEE values (Appendix chapter 6, Tables 1-13). The best selected FT-NIR calibration models for external and internal quality parameters are presented in Table 2-4. Scatter plots of FT-NIR predicted data plotted against destructively acquired reference data are presented in Figs. 2 and 3. The statistical data for model development showed that EH gave higher prediction statistics than the IS for most parameters.

Stellenbosch University https://scholar.sun.ac.za

Fruit weight is a physical parameter which cannot be measured directly by NIR spectroscopy but can be quantified indirectly by measuring water content (Louw & Theron, 2010). The prediction statistics for fruit weight were R^2 = 81.07, RMSEE = 9.70 g, RMSEP = 11.90 g and RPD = 1.63 for IS and R^2 = 63.57, RMSEE = 13.70 g, RMSEP = 13.10 g and RPD = 1.63) for EH. The model developed for fruit weight was relatively poor as characterised by the high RMSEE and low RPD for both spectral acquisition modes. Nicolaï *et al*. (2007) stated that fruit firmness is a physical parameter which can be determined indirectly by the light scattering properties of tissue, which are associated with fruit firmness. The prediction statistics for fruit firmness acquired using the EH (R^2 = 85.03, RMSEE = 6.43 N, RMSEP = 7.45 N and RPD = 2.43) were comparable to the IS (R^2 = 82.99, RMSEE = 6.71 N, RMSEP = 7.31 N and RPD = 2.40). The wavelength range used for the development of calibration model for fruit firmness was found to be within the region of 1064-2355 nm. The wavelength region for model development of firmness is within the range reported by Gómez *et al*. (2006).

The calibration models developed for predicting the external colour components (a*, *C**, h°) of pomegranate fruit are shown in Table 2. The prediction statistics for model development using the EH provided relatively better prediction accuracy for a* (R^2 = 92.65, RMSEE = 1.40, RMSEP = 1.61 and RPD = 3.34) and *C** (R^2 = 86.65, RMSEE = 1.87, RMSEP = 2.15 and RPD = 2.43) than the models developed from the IS. The colour component h° for the IS (R^2 = 94.68, RMSEE = 0.96, RMSEP = 1.67 and RPD = 2.50) were superior to those of the EH (R^2 = 75.74, RMSEE = 1.73, RMSEP = 2.05 and RPD = 1.91). The wavelength range used for model development for colour components ranged between 1064 to 2355 nm. Fruit colour have been reported to less likely be directly detected outside the visible range (Clément *et al*., 2008; Ruiz *et al*., 2008; Magwaza *et al*., 2013), the detection of colour components within the region of 1064 to 2355 nm may represent secondary correlation related to biochemical constituents that could be active in the visible or NIR region. The higher correlation between NIR spectra and colour components could be related to anthocyanin pigments (Table 5). Furthermore, several studies have reported a high correlation between colour and anthocyanin concentration within pomegranate fruit (Fawole & Opara, 2013c). Since a large number of LVs (13) were used for model development there is a possibility of model overfitting.

Calibration models developed for the measurement of TSS using the EH (R^2 = 83.84, RMSEE = 0.26, RMSEP = 0.28 and RPD = 2.17) were comparable with the IS (R^2 = 83.64, RMSEE = 0.25, RMSEP = 0.32 and RPD = 1.92). Superior predictive statistics for model development of pH were observed using the EH (R^2 = 86.39, RMSEE = 0.06, RMSEP = 0.06 and RPD = 2.57). Similarly, prediction statistics for model development of TA were best

Stellenbosch University https://scholar.sun.ac.za

predicted using the EH (R^2 = 77.67, RMSEE = 0.11%, RMSEP = 0.13% and RPD = 2.12) with lower amount of LVs used for model development and higher RPD compared to IS. The development of calibration models for indirect prediction of TSS:TA is based on correlation between the acquired spectra for each sample and the value between sugar to acid ratio. BrimA was best predicted using the EH (R^2 = 81.81, RMSEE = 0.31, RMSEP = 0.39 and RPD = 2.08), while the IS gave the best prediction of TSS: TA (R^2 = 99.54, RMSEE = 0.12, RMSEP = 0.74 and RPD = 2.72). The optimal waveband region best reflecting TSS and TA of pomegranate fruit using the EH was between 1064 and 1835 nm, this wavelength region is within the regions reported by De Oliveira *et al*. (2014).

The calibration statistics for phytochemicals such as total phenolics were best predicted with the EH (R^2 = 88.16, RMSEE = 0.09, RMSEP = 0.11 and RPD = 2.91), while the calibration statistics for total anthocyanin for both the IS and EH were characterised by high LVs (17 and 16 respectively) and a lower RPD (1.64-1.59) indicated poor predictability with (R^2 = 99.45, RMSEE = 0.12, RMSEP = 0.09 and RPD = 1.64) and (R^2 = 73.18, RMSEE = 0.07, RMSEP = 0.08 and RPD = 1.59), respectively. The waveband range for total phenolic and total anthocyanin content obtained by EH was within the region of 1064-2355 nm which is in agreement with the waveband range reported by Arendse *et al*. (2017) for pomegranate arils. Similarly, vitamin C concentration showed better model performance with the EH (R^2 = 83.39, RMSEE = 0.06, RMSEP = 0.10 and RPD = 2.06). The model development of vitamin C was within the wavelength range of 1064-1333 nm which is in agreement with the wavelength regions reported by Magwaza *et al*. (2013).

For fruits and vegetables, Williams (2014) suggested that RPD value which are less than 1.5 would indicate that the model is unreliable and cannot be used, RPD values that are between 1.5 and 2.0 indicates that the developed model is appropriate for rough predictions, while for quantitative predictions the RPD values should be between 2.0 and 2.5, those between 2.5 and 3.0 are considered good models. Satisfactory models should have an RPD value of above 3. The RPD values for the developed external quality models parameters (fruit weight, firmness, a*, *C**, h°) ranged from (1.63 to 3.34). The RPD values for fruit weight fit those of rough predictions (1.63). In the case of colour components (*C** and a*), the RPD values for model development using the EH was 2.43 and 3.34 providing good and satisfactory predictions respectively. Whilst, calibration model developed using the IS for colour component h° gave RPD value for good model predictions. The model prediction for fruit firmness for the EH was similar (RPD = 2.43) to those of the IS (RPD = 2.40), providing quantitative predictions. The RPD values for the developed internal quality model parameters

Stellenbosch University https://scholar.sun.ac.za

ranged from (1.64-2.91). Furthermore, the RPD values for maturity parameters (TSS, TA, BrimA) developed using the EH were appropriate for quantitative prediction (Table 3). Based on the RPD (2.72) for TSS:TA the model developed using EH is considered good for prediction. The model prediction of total phenolics for the EH was superior (RPD = 2.91) to those of the IS (RPD = 2.09). Similarly, the RPD value of 2.06 for vitamin C indicate a fit model for quantitative prediction, while the RPD value of 1.64 for total anthocyanin shows the model was appropriate for rough prediction.

The high predictive power for measurement of internal quality parameters such as TSS and TA may suggest a high penetration depth of NIR radiation. In thin rind fruit such as apple, FT-NIR has been reported to have a light penetration depth of up to 4 mm (Lammertyn *et al*., 2000). However, pomegranates have thick rind, are heterogeneous and therefore the penetration depth may differ compared to thin rind fruit such as apples. Considering that the IS spectral acquisition method irradiated a smaller section of the fruit it is therefore not surprising that EH which radiates a larger surface area performed better, had the best predictive power of nine of the thirteen measured parameters.

4. Conclusions

In this study, FT-NIR diffuse reflectance spectroscopy combined with chemometric analysis was successfully used to develop calibration models to predict internal and external quality parameters of intact pomegranate fruit. Two spectral acquisition methods were explored and distinct effects on the prediction performance were observed. The emission head of the MATRIX-F gave the best results for fruit firmness, colour components (a* and *C**), TSS, pH, TA, BrimA, total phenolics and vitamin C. The integrating sphere of the Multi-Purpose Analyser gave the best results for colour component (h°) and TSS:TA. Considering that fruit weight, colour, firmness, TSS and acidity content are desirable properties which are of particular interest to breeders, growers, postharvest engineers and consumers, the application of high throughput non-invasive measurement technologies (such as NIRS) could provide a holistic approach to classify fruit into different quality tiers. These findings can be utilised by the pomegranate industry to develop online grading systems for the analysis of various pomegranate fruit quality attributes.

References

Stellenbosch University https://scholar.sun.ac.za

Aindongo, W.V., Caleb, O.J., Mahajan, P.V., Manley, M. & Opara, U.L. (2014). Effects of storage conditions on transpiration rate of pomegranate aril-sacs and arils. *South African Journal of Plant and Soil*, **31**, 7–11.

Arendse, E., Fawole, O.A. & Opara, U.L. (2014a). Influence of storage temperature and duration on postharvest physico-chemical and mechanical properties of pomegranate fruit and arils. *CyTA-Journal of Food*, **12**, 389–398.

Arendse, E., Fawole, O.A. & Opara, U.L. (2014b). Effects of postharvest storage conditions on phytochemical and antioxidant properties of pomegranate fruit (cv. Wonderful). *Scientia Horticulturae*, **169**, 125–129.

Arendse, E., Fawole, O.A., Magwaza, L.S. & Opara, U.L. (2016). Non-destructive characterization and volume estimation of pomegranate fruit external and internal morphological fractions using X-ray computed tomography. *Journal of Food Engineering*, **186**, 42–49.

Arendse, E., Fawole, O.A., Magwaza, L.S., Nieuwoudt, H.H. & Opara, U.L. (2017). Development of calibration models for the evaluation of pomegranate aril quality by Fourier-transform near infrared spectroscopy combined with chemometrics. *Biosystems Engineering*, **159**, 22–32.

Barros, L., Ferreira, M.J., Queiros, B., Ferreira, I.C.F.R. & Baptista, P. (2007). Total phenols, ascorbic acid, ß-carotene and lycopene in Portuguese wild edible mushroom and their antioxidant activities. *Food Chemistry*, **103**, 413–419.

Clément, A., Dorais, M. & Vernon, M. (2008). Non-destructive measurement of fresh tomato lycopene content and other physicochemical characteristics using visible-NIR spectroscopy. *Journal of Agricultural and Food Chemistry*, **56**, 9813–9818.

Davey, M.W., Saeys, W., Hof, E., Ramon, H., Swennen, R.L. & Keulemans, J. (2009). Application of visible and near-infrared reflectance spectroscopy (Vis/NIRS) to determine carotenoid contents in banana (Musa spp.) fruit pulp. *Journal of Agricultural and Food Chemistry*, **57**, 1742–1751.

De Oliveira, G.A., Bureau, S., Renard, C.M.G.C., Pereira-Netto, A.B. & de Castilhos, F. (2014). Comparison of NIRS approach for prediction of internal quality traits in three fruit species. *Food Chemistry*, **143**, 223–230.

Fawole, O.A., Opara, U.L. & Theron, K.I. (2012). Chemical and phytochemical properties and antioxidant activities of three pomegranate cultivars grown in South Africa. *Food and Bioprocess Technology*, **5**, 2934–2940.

Stellenbosch University https://scholar.sun.ac.za

Fawole, O.A. & Opara, U.L. (2013a). Harvest discrimination of pomegranate fruit: postharvest quality changes and relationships between instrumental and sensory attributes during shelf life. *Journal of Food Science*, **78**, 1264–1272.

Fawole, O.A. & Opara, U.L. (2013b). Changes in physical properties, chemical and elemental composition and antioxidant capacity of pomegranate (cv. Ruby) fruit at five maturity stages. *Scientia Horticulturae*, **150**, 37–46.

Fawole, O.A. & Opara, U.L. (2013c). Seasonal variation in chemical composition, aroma volatiles and antioxidant capacity of pomegranate during fruit development. *African Journal of Biotechnology*, **12**, 4006–4019.

Fawole, O.A. & Opara, U.L. (2014). Physicomechanical, phytochemical, volatile compounds and free radical scavenging properties of eight pomegranate cultivars and classification by principal component and cluster analyses. *British Food Journal*, **116**, 544–567.

Giusti, M.M. & Wrolstad, R.E. (2001). Characterization and measurement of anthocyanins by UV–visible spectroscopy. In: *Current Protocols in Food Analytical Chemistry* (edited by R.E. Wrolstad, T.E. Acree & H. An). F1.2.1-F.1.2.13. John Wiley & Sons, Inc., New York, NY.

Goodacre, R., Broadhurst, D., Smilde, A.K., Kristal, B.S., Baker, J.D., Beger, R., Bessant, C., Connor, S., Capuani, G., Craig, A., Ebbels, T., Kell, D.B., Manetti, C., Newton, J., Paternostro, G., Somorjai, R., Sjöström, M., Trygg, J. & Wulfert, F. (2007). Proposed minimum reporting standards for data analysis in metabolomics. *Metabolomics*, **3**, 231–241.

Gómez, A.H., He, Y. & Pereira, A.G. (2006). Non-destructive measurement of acidity, soluble solids and firmness of Satsuma mandarin using vis–NIR spectroscopy techniques. *Journal of Food Engineering*, **77**, 313–319.

Guthrie, J. & Walsh, K. (1997). Non-invasive assessment of pineapple and mango fruit quality using near infrared spectroscopy. *Australian Journal of Experimental Agriculture*, **37**, 253–263.

Holland, D., Hatib, K. & Bar-Ya'akov, I. (2009). Pomegranate: Botany, Horticulture, Breeding. In: *Horticultural Reviews* (edited by J. Janick). Pp. 127–191. John Wiley & Sons, Inc.

Ismail, T., Sestili, P. & Akhtar, S. (2012). Pomegranate peel and fruit extracts: A review of potential anti-inflammatory and anti-infective effects. *Journal of Ethnopharmacology*, **143**, 397–405.

Khodabakhshian, R., Emadi, B., Khojastehpour, M., Golzarian M.R. & Sazgarnia, A. (2016). Non-destructive evaluation of maturity and quality parameters of pomegranate fruit by

Stellenbosch University https://scholar.sun.ac.za

visible/near infrared spectroscopy. *International Journal of Food Properties*, **20**, 41–52.

Klein, B.P. & Perry, A.K. (1982). Ascorbic acid and vitamin A activity in selected vegetables from different geographical areas of United States. *Journal of Food Science*, **47**, 941–945.

Lammertyn, J., Peirs, J., De Baerdemaeker, J. & Nicolaï, B.M. (2000). Light penetration properties of NIR radiation in fruit with respect to non-destructive quality assessment. *Postharvest Biology and Technology*, **18**, 121–132.

Lestander, T.A. & Geladi, P. (2005). NIR spectral information used to predict water content of pine seeds from multivariate calibration. *Canadian Journal of Forest Research*, **35**, 1139–1148.

Louw, E.D. & Theron, K.I. (2010). Robust prediction models for quality parameters in Japanese plums (*Prunus salicina* L.) using NIR spectroscopy. *Postharvest Biology and Technology*, **58**, 176–184.

Lu, H., Xu, H., Ying, Y., Fu, X., Yu, H. & Tian, H. (2006). Application of Fourier transform near infrared spectrometer in rapid estimation of soluble solids content of intact citrus fruits. *Journal of Zhejiang University Science*, **7**, 794–799.

Magwaza, L.S., Opara, U.L., Nieuwoudt, H., Cronje, P.J., Saeys, W. & Nicolaï, B. (2012a). NIR spectroscopy applications for internal and external quality analysis of citrus fruit–a review. *Food and Bioprocess Technology*, **5**, 425–444.

Magwaza, L.S., Opara, U.L., Terry, L.A., Landahl, S., Cronje, P.J., Nieuwoudt, H., Mouazen, A.M., Saeys, W. & Nicolaï, B.M. (2012b). Prediction of 'nules clementine' mandarin susceptibility to rind breakdown disorder using VIS/NIR spectroscopy. *Postharvest Biology and Technology*, **74**, 1–10.

Magwaza, L.S., Opara, U.L., Terry, L.A., Landahl, S., Cronje, P.J.R., Nieuwoudt, H.H., Hanssens, A., Saeys, W. & Nicolaï, B.M. (2013). Evaluation of Fourier transform-NIR spectroscopy for integrated external and internal quality assessment of 'Valencia' oranges. *Journal of Food Composition and Analysis*, **31**, 144–154.

Magwaza, L.S., Opara, U.L., Cronje, P.J.R., Landahl, S., Nieuwoudt, H.H., Mouazen, A.M., Nicolaï, B.M. & Terry, L.A. (2014). Assessment of rind quality of 'Nules Clementine' mandarin fruit during postharvest storage: 2. Robust Vis/NIRS PLS models for prediction of physico-chemical attributes. *Scientia Horticulturae*, **165**, 421–432.

Makkar, H.P.S., Siddhuraju, P. & Becker, K. (2007). *Plant secondary metabolites* (pp. 74–75). Totowa: Humana Press.

Stellenbosch University https://scholar.sun.ac.za

Nicolaï, B.M., Beullens, K., Bobelyn, E., Peirs, A., Saeys, W., Theron, K.I. & Lammertyn, J. (2007). Non-destructive measurement of fruit and vegetable quality by means of NIR spectroscopy: a review. *Postharvest Biology and Technology*, **46**, 99–118.

Nicolaï, B.M., Verlinden, B.E., Desmet, M., Saevels, S., Saeys, W., Theron, I.K., Cubeddub, R., Pifferi, A. & Torricelli, A. (2008). Time-resolved and continuous wave NIR reflectance spectroscopy to predict soluble solids content and firmness of pear. *Postharvest Biology and Technology*, **47**, 68–74.

Olarewaju, O.O., Bertling, I. & Magwaza, L.S. (2016). Non-destructive evaluation of avocado fruit maturity using near infrared spectroscopy and PLS regression models. *Scientia Horticulturae*, **199**, 229–236.

Pathare, P.B., Opara, U.L. & Al-Said, F.A.J. (2013). Colour measurement and analysis in fresh and processed foods: A review. *Food and Bioprocess Technology*, **6**, 36–60.

Ruiz, D., Reich, M., Bureau, S., Rebard, C.M.G.C. & Audergon, J.M. (2008). Application of reflectance colorimeter measurements and infrared spectroscopy methods to rapid and non-destructive evaluation of carotenoids content in apricot (*Prunus armeniaca* L.). *Journal of Agricultural and Food Chemistry*, **56**, 4916–4922.

Seeram, N.P., Zhang, Y., Reed, J.D., Krueger, C.G. & Vaya, J. (2006). Pomegranate phytochemicals. In: *Pomegranates: Ancient Roots to Modern Medicine* (edited by N.P. Seeram, R.N. Schulman & D. Heber). Pp. 3–29. CRC Press Taylor & Francis Group, Boca Raton, London & New York.

Shenk, J.S., Workman, J.J. & Westerhaus, M.O. (2008). Application of NIR spectroscopy to agricultural products. In: *Handbook of NIR analysis* (edited by D.A. Burns, & E.W. Ciurczik). Pp. 349–360. CRC Press.

Shiroma, C. & Rodriguez-Saona, S. (2009). Application of NIR and MIR spectroscopy in quality control of potato chips. *Journal of Food Composition and Analysis*, **22**, 596–605.

Tewari, J.C., Dixit, V., Chi, B.K. & Malik, K.A. (2008). Determination of origin and sugars of citrus fruit using genetic algorithm, correspondence analysis and partial least square combined with fibre optic NIR spectroscopy. *Spectrochim Acta Part A*, **71**, 1119–1127.

Viuda-Martos, M., Fernández-López, J. & Pérez-Álvarez, J.A. (2010). Pomegranate and its many functional components as related to human health: A Review. *Comprehensive Reviews in Food Science and Food Safety*, **9**, 635–665.

Williams. P. (2014). The RPD statistic: a tutorial note. *NIR news*, **25**, 22–26.

Stellenbosch University https://scholar.sun.ac.za

Table 1

Mean, standard deviation (SD) range and coefficient of variation for calibration and validation subsets for external and internal parameters for pomegranate fruit

Quality Parameter	Calibration			Validation			Overall CV (%)
	Mean	SD	Range	Mean	SD	Range	
Fruit weight (g)	390.97	21.89	341.97-448.38	390.88	19.54	353.50-440.17	5.31
Firmness (N)	98.19	16.39	57.78-126.87	96.95	18.16	58.61-125.71	17.71
a*	5.077	12.83	31.20-50.03	39.94	5.37	32.20-49.39	13.14
Chroma	42.11	4.96	28.09-51.30	41.41	5.24	29.62-48.68	12.22
Hue	36.18	4.01	26.42-47.99	35.78	4.19	26.64-44.67	11.40
TSS (%)	14.52	0.63	12.77-16.00	14.69	0.60	13.00-15.80	4.22
pH	3.17	0.15	2.84-3.48	3.20	0.15	2.84-3.46	4.83
TA (%)	1.58	0.26	0.93-2.00	1.53	0.28	0.94-1.87	17.31
TSS:TA	9.35	1.79	5.49-15.10	9.13	2.03	6.10-15.10	20.72
BrimA	11.43	0.70	9.48-13.60	11.57	0.79	9.54-13.02	6.51
Total Phenolics (g/L)	1.57	0.25	1.15-2.38	1.60	0.32	1.19-2.29	17.94
Total Anthocyanin (g/L)	0.73	0.15	0.38-1.13	0.71	0.15	0.40-1.09	20.95
Vitamin C (g/L)	1.59	0.16	1.21-2.03	1.59	0.19	1.24-2.00	10.96

TSS, total soluble solids; TA, titratable acidity; SD, standard deviation; CV, coefficient of variation

Stellenbosch University https://scholar.sun.ac.za

Table 2

Model performance for external parameters using different FT-NIR instruments

Parameter	NIR probe	Wavelength range (nm)	Calibration			Validation					
			LV	R^2	RMSEE	R^2	RMSEP	RPD	Bias	Slope	Corr.
Fruit weight (g)	IS	1064-1333, 2064-2355	8	81.07	9.70	62.36	11.90	1.63	0.40	0.57	0.79
	EH	1064-2183	11	63.57	13.70	62.11	13.10	1.63	0.64	0.67	0.79
Firmness (N)	IS	1064-1333, 1835-2355	9	82.99	6.71	82.57	7.31	2.40	-0.63	0.82	0.91
	EH	1064-1333, 1639-1835	5	85.03	6.43	83.01	7.45	2.43	0.19	0.85	0.91
a* (redness)	IS	1064-1333, 2062-2355	8	91.38	1.56	87.02	1.72	2.86	0.42	0.83	0.94
	EH	1064-1836	6	92.65	1.40	90.90	1.61	3.34	0.19	0.98	0.97
Chroma	IS	1064-2355	14	85.53	1.84	73.65	2.29	2.03	-0.66	0.77	0.87
	EH	1064-2355	11	86.65	1.87	82.97	2.15	2.43	-0.18	0.90	0.91
Hue	IS	1064-1836, 2174-2355	13	94.68	0.96	83.94	1.67	2.50	-0.10	0.85	0.92
	EH	1064-1333, 2174-2355	8	75.74	1.73	71.66	2.05	1.91	-0.39	0.68	0.86

LV, latent variables; R^2, coefficient of determination; RMSEE, root mean square error of estimation; RPD, residual predictive deviation; RMSEP, root mean square error of prediction; Corr, correlation coefficient; IS, integrating sphere; EH, emission head

Stellenbosch University https://scholar.sun.ac.za

Table 3

Model performance for internal quality parameters using different FT-NIR instruments

Parameter	NIR probe	Wavelength range (nm)	Calibration			Validation					
			LV	R^2	RMSEE	R^2	RMSEP	RPD	Bias	Slope	Corr.
TSS (%)	IS	1064-1836, 2174-2355	7	83.64	0.25	71.87	0.32	1.92	0.06	0.78	0.86
	EH	1064-1333, 1640-1836	9	83.84	0.26	78.12	0.28	2.17	0.05	0.86	0.89
pH	IS	1064-1333, 1640-1732	11	95,87	0.04	75.73	0.07	2.13	0.02	0.90	0.89
	EH	1064-2355	7	86.39	0.06	84.86	0.06	2.57	0.00	0.81	0.92
TA (%)	IS	1064-1333, 1640-2174	8	85.58	0.10	73.34	0.14	2.00	-0.03	0.64	0.88
	EH	1064-1333, 1640-1836	7	77.67	0.11	76.78	0.13	2.12	-0.02	0.71	0.89
TSS:TA	IS	1064-1333, 1640-2174	17	99.54	0.12	86.28	0.74	2.72	0.10	0.81	0.93
	EH	1064-1333, 1640-1836	12	65.10	0.71	52.13	0.81	1.50	-0.09	0.56	0.73
BrimA	IS	1064-1836, 2174-2260	6	80.52	0.33	68.89	0.47	1.86	0.13	0.66	0.85
	EH	1064-1640, 1836-2355	8	80.81	0.31	76.16	0.39	2.08	0.06	0.79	0.88

LV, latent variables; R^2, coefficient of determination; RMSEE, root mean square error of estimation; RPD, residual predictive deviation; RMSEP, root mean square error of prediction; Corr, correlation coefficient; IS, integrating sphere; EH, emission head; TSS, total soluble solids; TA, titratable acidity

Stellenbosch University https://scholar.sun.ac.za

Table 4

Model performance for internal parameters for phytochemical and antioxidant activity using different FT-NIR instruments

Parameter	NIR probe	Wavelength range (nm)	Calibration			Validation					
			LV	R^2	RMSEE	R^2	RMSEP	RPD	Bias	Slope	Corr.
Total phenolics (g/L)	IS	1064-1640, 1836-2355	10	88.09	0.07	77.12	0.15	2.09	0.64	0.67	0.89
	EH	1064-1640, 1836-2355	13	88.16	0.09	87.97	0.11	2.91	-0.57	0.80	0.94
Total anthocyanin (g/L)	IS	1064-1836, 2174-2355	17	99.45	0.12	62.59	0.09	1.64	-0.68	0.62	0.79
	EH	1064-1836, 2174-2355	16	73.18	0.07	59.92	0.08	1.59	0.93	0.70	0.79
Vitamin C (g/L)	IS	1333-1640, 1836-2175	9	74.11	0.08	72.19	0.09	1.99	-1.77	0.76	0.86
	EH	1064-1333, 1640-732	11	85.48	0.06	76.16	0.09	2.06	-0.90	0.74	0.87

LV, latent variables; R^2, coefficient of determination; RMSEE, root mean square error of estimation; RPD, residual predictive deviation; RMSEP, root mean square error of prediction; Corr, correlation coefficient; IS, integrating sphere; EH, emission head

Stellenbosch University https://scholar.sun.ac.za

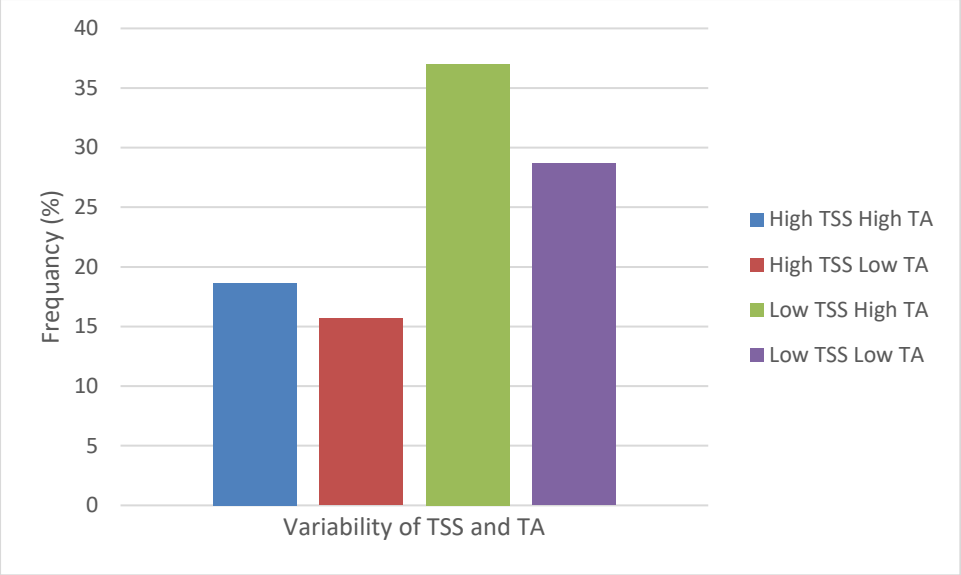

Fig. 1. Sample frequency (%) vs variability of TSS and TA for pomegranate fruit samples (n = 300) with high TSS ≥15 ºBrix and high TA ≥ 1.5%.

Stellenbosch University https://scholar.sun.ac.za

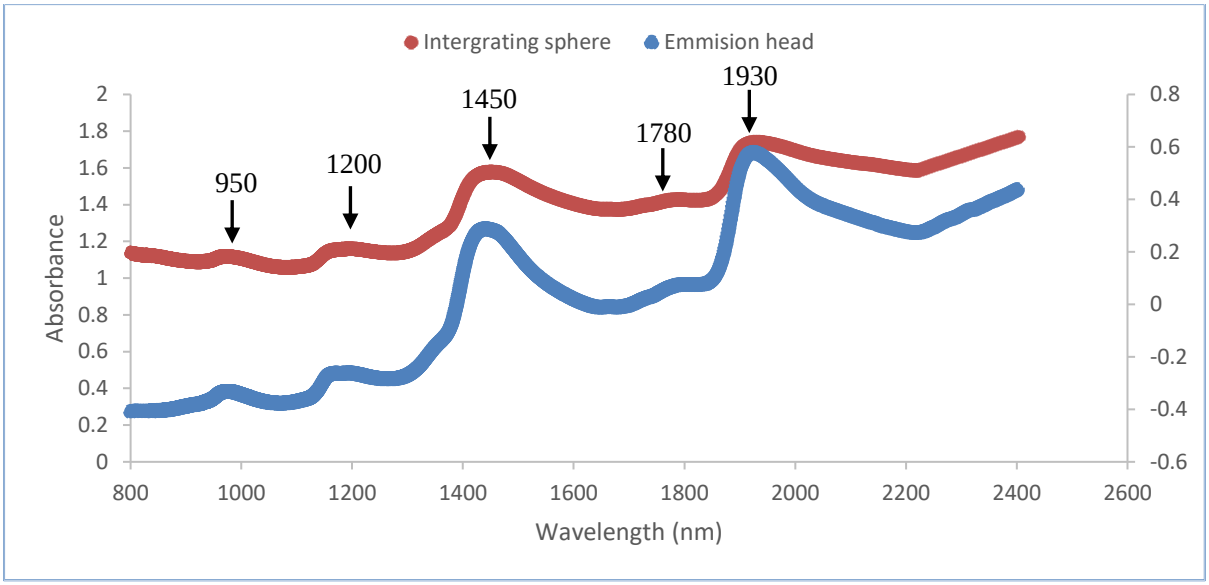

Fig. 2. Absorbance spectra of pomegranate fruit obtained using two different spectral acquisition modes integrating sphere (orange solid line) and emission head (blue solid line).

Stellenbosch University https://scholar.sun.ac.za

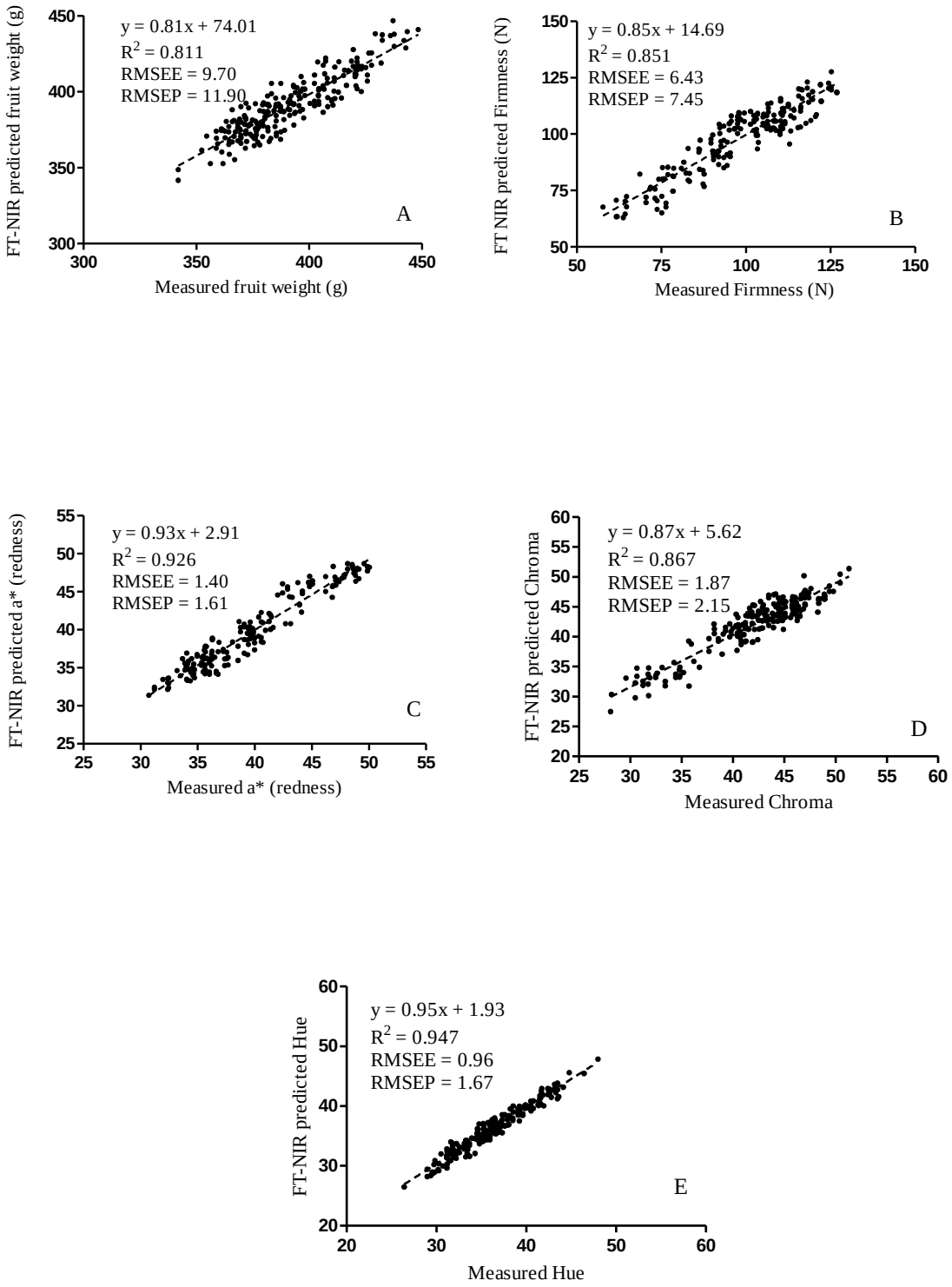

Fig. 3. Scatter plots of FT-NIR predicted fruit weight (A), firmness (B), a* (redness) (C), Chroma (D) and Hue (E) plotted against destructively acquired reference data.

Stellenbosch University https://scholar.sun.ac.za

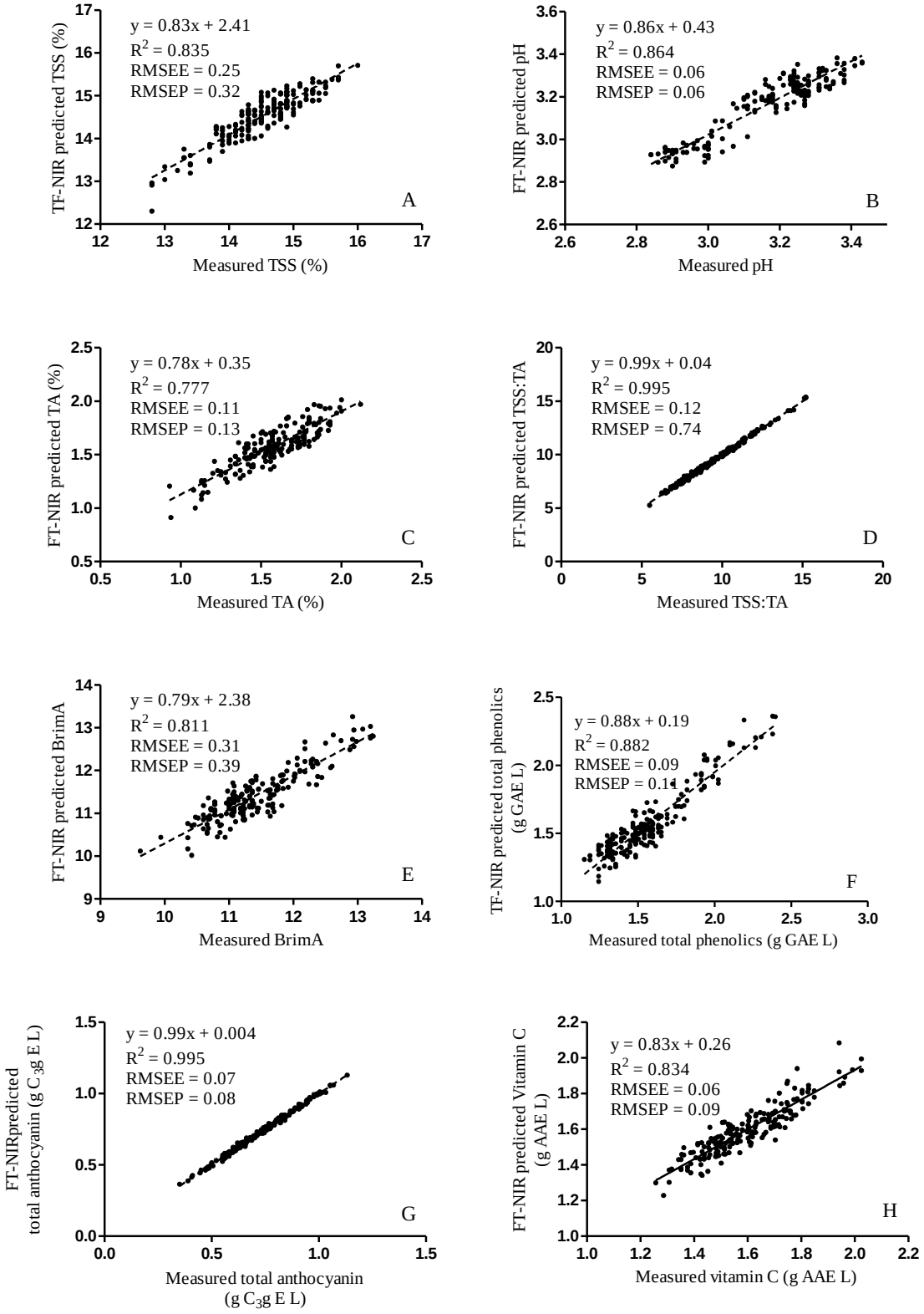

Fig. 4. Scatter plots of FT-NIR predicted TSS (A), pH (B), TA (C), TSS:TA (D), BrimA (E), total phenolics (F), total anthocyanin (G) and Vitamin C (H) plotted against destructively acquired reference data

Stellenbosch University https://scholar.sun.ac.za

DECLARATION BY THE CANDIDATE

With regard to **Chapter 5 (pp 99-124)**, the nature and scope of my contribution were as follows:

Nature of contribution	Extent of contribution (%)
Research, data collection, analysis, writing of chapter and final approval of the published version	70

The following co-authors have contributed to **Chapter 5 (pp 99-124)**

Name	e-mail address	Nature of contribution	Extent of contribution (%)
Prof U.L. Opara	opara@sun.ac.za	Conception of the work, editorial suggestion and final approval of the published version	10
Dr O.A. Fawole	olaniyi@sun.ac.za	Research input, editorial suggestion, proof reading and final approval of the published version	10
Dr L.S. Magwaza	Magwazal@ukzn.ac.za	Research input, editorial suggestion, proof reading and final	5

Stellenbosch University https://scholar.sun.ac.za

		approval of the published version	
Dr H. Nieuwoudt	hhn@sun.ac.za	Research input, editorial suggestion, analysis and final approval of the published version	5

E Arendse **Signature of candidate**	29/08/2017 **Date**

DECLARATION BY CO-AUTHORS

The undersigned hereby confirm that:

1. the declaration above accurately reflects the nature and extent of the contributions of the candidate and the co-authors to **Chapter 5 (pp 99-124)**

2. no other authors contributed to **Chapter 5 (pp 99-124)** besides those specified above, and

3. potential conflicts of interest have been revealed to all interested parties and that the necessary arrangements have been made to use the material in **Chapter 5 (pp 99-124)** of this dissertation.

Stellenbosch University https://scholar.sun.ac.za

Signature	Institutional affiliation	Date
Prof U.L. Opara	Stellenbosch University	29/08/2017
Dr O.A. Fawole	Stellenbosch University	29/08/2017
Dr L.S. Magwaza	University of KwaZulu-Natal	29/08/2017
Dr H. Nieuwoudt	Stellenbosch University	29/08/2017

Stellenbosch University https://scholar.sun.ac.za

CHAPTER 5

Development of calibration models for the evaluation of pomegranate aril quality using Fourier-transform near-infrared spectroscopy combined with chemometrics

Abstract

A Fourier transform NIR (FT-NIR) spectroscopy method was developed combining chemometrics for prediction of organoleptic and phytochemical parameters of pomegranate arils using two different data acquisition methods over a spectral region 800-2500 nm; namely, an integrating sphere (IS) and an emission head (EH) used. Several pre-processing methods were investigated and those that yielded higher coefficient of determination (R^2) and residual predictive deviation (RPD), lower root mean square error estimation (RMSEE) and root mean square error of prediction (RMSEP) values were used for model development. Models developed using the EH gave the best prediction of total soluble solids (R^2 = 87.55, RMSEP = 0.30%), pH (R^2 = 85.18, RMSEP = 0.10), titratable acidity (R^2 = 85.59, RMSEP = 0.10%), BrimA (R^2 = 83.43, RMSEP = 0.43), aril hue (R^2 = 88.59, RMSEP = 4.19), total phenolic concentration (R^2 = 86.48, RMSEP = 0.11 g/L), total anthocyanin concentration (R^2 = 70.50, RMSEP = 0.13 g/L) and vitamin C concentration (R^2 = 84.86, RMSEP = 0.09 g/L), while the IS provided the best results for TSS:TA (R^2 = 82.20, RMSEP = 1.03), aril firmness (R^2 = 68.40, RMSEP = 6.71 N), aril colour components (a* (R^2 = 73.54, RMSEP = 1.67) and Chroma (R^2 = 78.37, RMSEP = 2.31). Good prediction was observed for both the models based on EH and IS data acquisition methods. However, better prediction performance was obtained with the model based on EH data acquisition method, resulting in accurate prediction of eight quality parameters. This study demonstrated that FT-NIR and associated chemometric analysis can holistically evaluate the quality parameters of pomegranate arils.

Keywords: *Punica granatum*, Fruit quality, Near-infrared, Partial least squares, Chemometrics

Stellenbosch University https://scholar.sun.ac.za

1. Introduction

Pomegranate (*Punica granatum* L.) has gained global recognition and has been extensively documented for its potential health benefits such as antioxidant, anti-hypertension, anti-mutagenic and anti-inflammatory activities (Seeram *et al*., 2012a; Ismail *et al*., 2012). Scientific evidence has linked these potential health benefits to active polyphenolic compounds derived from fruit consumption (Seeram *et al*., 2006; Miguel *et al.*, 2010; Fawole *et al*., 2012b). Furthermore, pomegranate fruit contains considerable amounts of soluble solids, organic acids, vitamins, polysaccharides, mineral elements, fatty acids and vitamin C content (Opara *et al*., 2009). Despite the nutritional and health benefits, consumption is still limited due to the difficulties of extracting the arils. Therefore, minimally processed fresh pomegranate arils have become popular due to their convenience to consumers, increasing both prospects of production and consumption (Ayhan & Eştürk, 2009; Caleb *et al*., 2012). The growing pomegranate industry requires non-invasive methods that allow accurate, rapid and cost-effective analysis of fruit quality. Non-invasive assessment of fruit quality can contribute to the implementation of suitable management strategies to predict and control desired pomegranate quality attributes such as sugar content, acidity, colour and content of phytochemical components.

Several non-destructive techniques have been used for the assessment of the internal and external quality of fresh fruit. These include visible to near-infrared spectroscopy (Vis/NIRS, Magwaza *et al*., 2012; Ghosh *et al*., 2016), Vis/NIRS-based systems such as multispectral and hyperspectral imaging (Khodabakhshian *et al*., 2016), nuclear magnetic resonance imaging (NMR/MRI; Zhang & McCarthy, 2013), and X-ray computed tomography (CT; Magwaza & Opara, 2014; Arendse *et al*., 2016). Amongst the non-destructive methods, NIRS combined with chemometric techniques are the most widely used due to its accuracy, rapidity and cost-effectiveness for quantification of chemical constituents (Nicolaï *et al*., 2007; Huang *et al*., 2008; Magwaza *et al*., 2012; Magwaza *et al*., 2016). NIR spectroscopy is appropriate for the measurement of compounds containing polar functional groups such as –OH, C–O, and N–H (Blanco & Villarroya, 2002) and provides a non-invasive alternative for predicting the presence and/or concentration of specific chemical constituents in fruit and vegetables without prior sample preparation (Musingarabwi *et al*., 2016). To our knowledge, there is no reported use of FT-NIR spectroscopy in the analysis of pomegranate aril quality. The ability to assess pomegranate aril composition using high-throughput technologies such as FT-NIR spectroscopy would support the practical implementation of comprehensive analysis for predicting aril quality for on-line grading and sorting systems in commercial pack-houses.

Stellenbosch University https://scholar.sun.ac.za

The objective of this study was to develop a FT-NIR method for accurate prediction of organoleptic and phytochemical quality parameters of pomegranate arils.

2. Materials and Methods

2.1. *Fruit sampling*

Pomegranate fruit (cv. Wonderful) used in this study were obtained from Sonlia commercial packhouse (33°34′851″S, 19°00′360″E), located in the Western Cape Province, South Africa. A sample of 200 fruit were obtained from HRF orchard while another set of 100 fruit was obtained from Portville to add orchard location variability. Procured fruit were packed in open-top telescopic carton boxes and immediately transported to the Postharvest Technology Research Laboratory at Stellenbosch University, South Africa. On arrival, Fruit were equilibrated for 12 h at ambient conditions (23 ±3 °C) before sorting by removing any fruit with external damage. Fruit were processed at 23 ±3 °C by separating the arils from the husk. Surface moisture on the arils was removed by gently applying sterile paper towels after which 100 g of arils per fruit were weighed using an electronic scale (Mettler Toledo, Switzerland, 0.01 g) for analysis.

2.2. *NIR spectral acquisition*

During NIR spectral acquisition the same aril samples were measured sequentially using two different spectral acquisition methods. The first NIR data set was acquired over a spectral wavelength range of 800-2500 nm using a Multi-Purpose Analyser (MPA) FT-NIR spectrometer (Bruker Optics, Ettlingen, Germany) equipped with a gold-coated integrating sphere (IS) accessory for the measurement of heterogeneous samples. The IS measures diffuse reflectance and has a 50 mm width sample holder for highly scattering solid materials. Approximately 50 g arils of each fruit were transferred to the IS sample holder. Prior to scanning aril samples, reference measurements were taken against air background and periodically at intervals of 30 min between subsequent measurements. The IS sample holder was cleaned with lens tissue paper and distilled water. The second set of spectral data was obtained over the wavelength range 800-2500 nm using a MATRIX-F FT-NIR spectrometer (Bruker Optics, Ettlingen, Germany) equipped with emission head (EH) (230 mm diameter, 185 mm height and 170 mm focus depth). The EH provided contactless measurements and contained 4 air cooled tungsten light sources (tungsten halogen, 12 V, 20 W) which illuminate the sample. The diffused reflected light was collected via an optic fibre cable connected to the

Stellenbosch University https://scholar.sun.ac.za

spectrophotometer which is equipped with a thermoelectrically cooled and temperature-controlled TE InGaAs diode detector. Approximately 50 g arils were placed in a glass Petri dish filled to a depth of 10 mm with arils. The contactless option of the Matrix simulated the situation in the pack-house for online application whereas the MPA provided an ideal tool to meet the requirements for laboratory application.

The NIR spectra acquisition system for both methods was operated and initial spectral processing was achieved using OPUS software (OPUS v. 7.0 for Microsoft, Bruker Optics, Ettlingen, Germany). FT-NIR spectra were obtained with a sample measurement time of 120 s at 2 nm intervals over 800-2500 nm range with an 8 cm^{-1} resolution scan and 10 kHz scanner velocity. For each sample, 64 scans were taken per spectrum.

2.3. *Reference measurements*

2.3.1. *Colour attributes*

Aril colour was measured in CIELAB coordinates (L^*, a^*, b*) with a Minolta Chroma Meter CR-400 (Minolta Corp, Osaka, Japan). Measurements were performed on arils (50 g per fruit) in a glass petri dish. From the L^*, a^*, b^* values, the colour components Chroma (C*) and Hue ($h°$) values were calculated using Eq. 1 and Eq. 2 (Pathare *et al*., 2013):

$$C^* = \sqrt{a^{*2} + b^{*2}} \quad (1)$$

$$h° = \tan^{-1}(b^*/a^*) \quad (2)$$

2.3.2. *Aril firmness*

Aril firmness was measured by a compression test using a texture profile analyser XT Plus (Stable MicroSystem Ltd., Godalming, UK). Optimal operating settings: pre-test speed 1.5 mm s^{-1}, probe test speed 1 mm s^{-1}, post-test speed 10.0 mm s^{-1}, compression force 10 N. and compression distance 10 mm (Chen & Opara, 2013a,b; Arendse *et al*., 2014). The data attained from the texture profile analyser were interpreted using software Exponent v.4 (Stable MicroSystem Ltd., Godalming, UK). Aril compression was performed on 10 individual arils per fruit and the results presented as means ± standard error.

2.3.3. *Sample preparation*

Stellenbosch University https://scholar.sun.ac.za

Prior to biochemical measurements arils were juiced using a Liquafresh juice extractor (Mellerware, South Africa). After juice extraction, TSS was measured with a digital refractometer (Palette, PR-32α, Atago, Tokyo, Japan) using 1 mL of fresh juice and expressed as a percent. Titratable acidity (TA) was measured with compact Metrohm titro-sampler (Herisua, Switzerland) by titrating 2 mL of fresh juice against 0.1 mol L^{-1} NaOH solution to an end point of pH 8.2. The distribution frequency of the variation in TSS and TA in pomegranate aril samples (n = 300) are presented in Fig 1. The sample collection showed a wide range of variability in TSS and TA within the sample set. The pH values were determined using a calibrated pH meter (Crison, Model 00924, Barcelona, Spain). A portion of juice was stored in an ultra-low temperature freezer (VF720 -86, SNIJDER LABS, Netherlands) at -80 ^{0}C for the analysis of phytochemicals and vitamin C. The ratio of TSS to TA was also calculated. BrimA (a variant of TSS and TA and a criterion for the acceptance of juice) was also calculated using Eq. 3.

$$BrimA = TSS - k * TA \quad (3)$$

Where k is the tongue's sensitivity index ranging from 2 to 10. In order to avoid a negative BrimA index k value of 2 was used (Fawole & Opara, 2013; Arendse *et al.,* 2014).

2.3.4. *Phytochemical analysis*

2.3.4.1. *Preparation of sample*

Crude pomegranate juice (PJ) (0.5 mL) samples were extracted with 14.5 mL of cold 50% aqueous methanol. The mixture was vortexed and sonicated in an ice-cold water bath for 20 minutes and then centrifuged at 12,000 g for 10 min at 4 °C. The collected supernatant was stored at -80 °C for further use.

2.3.4.2. *Determination of total phenolic concentration*

Total phenolic concentration was determined in duplicate by the Folin-Ciocalteu (Folin-C) colorimetric method (Makkar, 2000) with a slight modification (Fawole *et al*., 2012a). Briefly, PJ supernatant (50 µL) was mixed with 450 µL of 50% methanol (v/v) before the addition of 500 µL of Folin C and then 2.5 mL of sodium carbonate (2%). The mixture was mixed in a vortex mixer and after 40 min the absorbance was read at 725 nm against 50% blank aqueous methanol using a UV–visible spectrophotometer (Thermo Scientific Technologies, Madison, WI, USA). Final results were expressed as g [gallic acid equivalent] per litre of crude juice.

Stellenbosch University https://scholar.sun.ac.za

2.3.4.3. *Determination of total anthocyanin concentration*

Total monomeric anthocyanin concentration was performed in duplicate using the pH differential method described by Giusti and Wrolstad (2001) and recently applied by Mphahlele *et al*. (2014). Briefly, PJ supernatant (1 mL) was diluted with 9 mL of pH 1.0 (potassium chloride, 0.025 M) and pH 4.5 (sodium acetate, 0.4 M) buffers, separately. After 10 min, the absorbance was measured in a UV–visible spectrophotometer at 510 nm and 700 nm against 50% blank aqueous methanol.

$$A = (A_{520} - A_{700})_{\text{pH 1.0}} - (A_{520} - A_{700})_{\text{pH 4.5}} \quad (4)$$

$$\text{Total anthocyanin} = \frac{A\ MW\ DF\ 100}{\varepsilon\ L} \quad (5)$$

where A is absorbance; MW is molecular weight (for cyanidin-3-glucoside 449.2 g mol^{-1}), DF is dilution factor; L is cell path length (10 mm); ε is the molar extinction coefficient (26900). Final results were expressed as g [cyanidin-3-glucoside equivalent] per litre of crude juice.

2.3.4.4. *Quantification of ascorbic acid*

Ascorbic acid concentration was determined in duplicate according to Klein and Perry (1982) with slight modifications (Barros *et al*., 2007). Briefly, PJ (0.5 mL) was diluted with 1% metaphosphoric acid (14.5 mL), the mixture was vortexed followed by sonication in an ice-cold water bath for 4 min and centrifugation at 12,000 g for 10 min. The collected supernatant (1.0 mL) was mixed with 0.0025% 2, 6-dichlorophenolindophenol dye (9 mL) and incubated in a dark environment for 10 min before measuring the absorbance at 515 nm. Results were expressed as g [ascorbic acid equivalent] per litre of crude juice.

2.4. *Chemometric data analysis*

OPUS version 7.0 (Bruker Optics, Ettlingen, Germany) chemometric software was used to perform principal component analysis (PCA) and partial least squares (PLS) regression analysis in order to construct calibration models. PCA is a technique that transforms an original set of correlated variables to a new set of uncorrelated variables, called principal components. PCA of a data table gives vectors of scores, with values which summarise all the variables entering the analysis was carried out and gives residuals, deviations between the data and the PC model (Jackson, 1991). PLS is commonly used in quantitative spectroscopy to correlate spectroscopic data (X) with related physico-chemical data (Y) (Saiz-Abajo *et al*., 2005). In this

Stellenbosch University https://scholar.sun.ac.za

way, it is ensured that the latent variables are ordered according to their relevance for predicting the Y-variable (Nicolai *et al*., 2007). Spectral data were subjected to various pre-processing methods to correct light scattering and reduce the changes of light path length. Pre-processing methods were tested individually and in combination with others. Pre-processing methods studied included multiplicative scatter spectral filtering methods such as Savitzky–Golay transformation (first derivative and second derivatives), multiplicative scattering correction (MSC) and vector normalisation (SNV). The spectral pre-processing method which provided a higher coefficient of determination (R^2) and residual predictive deviation (RPD) and lowest root mean square error of estimation (RMSEE) and lower amount of latent variables (LV) was selected and used to develop calibration models for predicting quality parameters.

The spectral range (800-2500 nm) was trimmed to the region of 800-2400 nm to remove noise for the purpose of obtaining good prediction models (Olarewaju *et al*., 2016). The removal of outliers and spectral variation was investigated using PCA. Samples with high residual and located far from the zero line of the residual variance plot were identified as potential outliers. Calibration and test set validation were selected on a 2:1 split using multivariate sampling; calibration (70%) and prediction (30%) sets. The developed PLS models were described by the values coefficient of determination (R^2, Eq. (6)); the root mean square error of estimation (RMSEE, Eq. (7)); and SSE, Eq. (8)), (Bruker Optik, 2006)); root mean square error of prediction (RMSEP, Eq. (9)) and residual predictive deviation (RPD, Eq. (10)). The regression statistics used to evaluate the model's performance was selected for its higher R^2 and RPD values including lower RMSEE and RMSEP values. Other statistical parameters explaining selected model were based on the Bias (Eq. (11)) systematic difference between the predicted and reference data.

$$R^2 = 1 - \frac{\sum(y_{cal} - y_{act})^2}{\sum(y_{cal} - y_{mean})^2} \quad (6)$$

$$RMSEE = \sqrt{\frac{1}{M-R-1} \times SSE} \quad (7)$$

$$SSE = \sum[Res]^2 \quad (8)$$

$$RMSEP = \sqrt{\sum \frac{(y_{pred} - y_{act})^2}{n}} \quad (9)$$

Stellenbosch University https://scholar.sun.ac.za

$$RPD = \frac{SD}{RMSEP} \quad (10)$$

$$Bias = \frac{1}{n}\sqrt{\sum(y_{pred} - y_{act})^2} \quad (11)$$

Where n is number of spectra, y_{act} is actual value, y_{mean} is mean value, y_{cal} is calculated value, y_{pred} is predicted value of the attribute, M is number of calibration samples, R is the rank, SSE is the sum of squared error, Res is the residual (the difference between the true and the fitted value) and SD is the standard deviation of reference values.

2.5. *Statistical analysis*

In order to demonstrate that the prediction of different phytochemicals such as phenolics, anthocyanins and vitamin C is from the actual IR spectra and not due to possible correlations with total soluble solids and organic acids, the reference data was subjected to Pearson's correlation test using Statistica software (Statistica 13.0, StatSoft Inc., Tulsa, OK, USA).

3. **Results and discussion**

3.1. *FT-NIR spectral characteristics*

The average absorbance spectrum of pomegranate arils after spectral pre-processing (first derivative + MSC) from a batch of 50 fruit for two different spectral acquisition modes is presented in Fig 2. The spectral peaks are comparable to those obtained for other fruits such as apricots (Bureau *et al*., 2009) and grape berries (Musingarabwi *et al*., 2016). Slight variation in absorbance values was observed during the different modes of spectral acquisition with higher absorbance values for the IS of MPA compared to the EH of the Matrix F spectrophotometer. Peak assessment was done according to literature (Nicolaï *et al*., 2007; Musingarabwi *et al*., 2016). The contours of the spectral curves for the respective acquisition modes were similar having prominent absorbance peaks in the region at 950, 1200, 1400, 1789 and 1876 nm. The peaks for the IS were more prominent at 950 and 1200 nm compared to the EH which had more pronounced peaks at 1400 nm. The peaks at 950 and 1400 nm correspond to the second and first vibrational overtones of closely associated with the OH stretching modes of water absorption (Lestander & Geladim, 2005; Clément *et al*., 2008; Magwaza *et al*., 2013), while the peaks at 1200 and 1942 nm corresponded to the second and first overtones of CH stretching as well as the third overtone of OH, CH and CH_2 deformation associated with sugar

Stellenbosch University https://scholar.sun.ac.za

solution (Golic *et al*., 2003). Sugars are known to display bands in the wavelength regions of 1100-1600 and 1700-2300 nm (Tewari *et al*., 2008).

3.2. *Distribution of calibration and validation reference data*

The distribution statistics (mean, standard deviation and coefficient of variation (CV %)) used for the calibration and validation reference data for all parameters in this study are presented in Table 1. During data exploration, the reference data for calibration and validation data set for all parameters in this study were normally distributed around the mean. The interpretation of calibration models depends on the precision of physical and biochemical reference data and enough variation within the calibration and validation data set should be present (Lu *et al*., 2006). Preferably, calibration and validation data sets should display enough variation within the sample set in order to better predict NIRS (Pérez-Marín *et al*., 2005; Clément *et al*., 2008, Magwaza *et al*., 2013). It was apparent from the standard deviation, minimum-to-maximum range and CV% statistics that most parameters in this study had high CV% values of up to 30.53% suggesting that both calibration and validation data sets covered a wide range of values.

Pearson correlation was used to investigate the interrelationships between selected reference data of pomegranate arils (Table 2). In order to demonstrate convincingly the prediction of these phytochemicals (phenolics, anthocyanins, vitamin C) their concentrations should not correlate with each other. Correlation tests indicate that no correlation was observed between any chemical indices (TSS, TA) and phytochemical and antioxidant compounds (Table 2). However, correlation tests indicated a significantly ($p < 0.01$) high relationship between TSS and BrimA (r = 0.86). Furthermore, a significant positive correlation between BrimA and TSS:TA (r = 0.75) indicated that BrimA, a variant of TSS and TA and a criterion for the acceptance of juice could be used as an indicator for the measurement of pomegranate aril flavour. Furthermore, there was a significantly ($p < 0.01$) high correlation for TSS:TA ratio and TA (r = -0.91) and a moderate correlation between BrimA and TA (r = -0.62). This relationship clearly shows that a decrease in fruit titratable acidity may bring an increase in fruit flavour. There were strong positive correlations between Chroma and aril redness (r = 0.86) and Chroma and hue (r = 0.66). Another interesting relationship was the moderate correlation between anthocyanin concentration and colour component hue (r = -0.50). This indirect correlation between colour component hue and colour pigment anthocyanin may suggest that anthocyanin could be used as a potential indicator for aril colour.

Stellenbosch University https://scholar.sun.ac.za

3.3. *PLS regression models of two FT-NIR acquisition modes*

The best FT-NIR models were developed using either no pre-processing, MSC or FD+MSC. The development of best models for each quality parameter was performed by critically evaluating different wavelength ranges that gave the higher R^2 and RPD, least RMSEE and RMSEP (Appendix chapter 5, Tables 1-12). The calibration models for organoleptic quality and phytochemical parameters are shown in Tables 3-5. Scatter plots representing the relationships between measured quality parameters and model predictions are presented in Fig.3 and Fig. 4. The spectral acquisition mode had a major influence on the calibration and prediction regression statistics (Tables 3-5). The statistical data for model development showed that both EH and IS acquisition modes gave reasonably accurate calibration models. The models developed using spectra acquired with EH gave better prediction statistics for TSS (R^2 = 87.55, RMSEE = 0.24%, RMSEP = 0.30%, RPD = 2.65) compared to the IS (R^2 = 85.75, RMSEE = 0.23%, RMSEP = 0.31% RPD = 2.19). Similarly, good models were developed for prediction of TA (R^2 = 85.59, RMSEE = 0.10%, RMSEP = 0.10%, RPD = 2.34) using the EH spectral acquisition mode. The prediction statistics for pH using EH were also comparable (R^2 = 85.18, RMSEE = 0.14, RMSEP = 0.10 and RPD = 2.40) to those of IS (R^2 = 83.49, RMSEE = 0.12, RMSEP = 0.10 and RPD = 2.32). BrimA was also predicted better using EH spectral data (R^2 = 83.43, RMSEE = 0.46, RMSEP = 0.43 and RPD= 2.22). The best predictive statistics for TSS: TA ratio (R^2 = 82.20, RMSEE = 0.87, RMSEP = 1.03 and RPD = 2.13) were developed using the IS (Table 3). Despite the large amount of LVs (7) used for model development, the good agreement between the values of RMSEE and RMSEP in the models developed by the EH and IS suggest that overfitting noise modelling were not evident. Furthermore, the developed models had low bias values (0.02 - 0.08) indicating robust fitting and stability and therefore not sensitive to the external factors such as growing location. The optimal wavebands for spectral acquisition to best predict TSS and TA concentration of pomegranate arils were determined to be in the region of 1064-1333 nm and 1587-1835 nm using the EH (Table 3). The wavelength region for model development of TSS and TA are similar to those reported by Musingarabwi *et al*. (2016).

PLS calibration models developed for predicting colour components of pomegranate arils such as, aril redness (a*) (R^2 = 73.54, RMSEE = 1.69, RMSEP = 1.67 and RPD = 1.86) and colour intensity chroma (R^2 = 78.37, RMSEE = 2.24, RMSEP = 2.31 and RPD = 1.79) showed moderate model performances using the IS, whereas colour hue (R^2 = 88.59, RMSEE = 4.07, RMSEP = 4.19 and RPD = 1.88) were best predicted using ES (Table 4). In this study,

Stellenbosch University https://scholar.sun.ac.za

the development of models for colour components used a wavelength ranged from 800-2500 nm. The high predictability in colour components could be related to an indirect correlation between biochemical constituents or pigments such as anthocyanins related to colour which are active in the NIR region. Magwaza *et al*. (2013) showed that the spectral range from 800 - 2500 nm was suitable in developing models for prediction of the colour index of 'Valencia' oranges. Previous studies suggest that extending the wavelength range below to the visible region is beneficial to determine colour parameters and related pigments including anthocyanins, chlorophyll, carotenoids and lycopene (Williams & Sobering, 1993). A study executed by Clément *et al*. (2008) evaluated the use of visible NIR spectroscopy for the measurement of lycopene and colour parameters (L*, a*, b*) using short wave (400-1000 nm) and long wave (900-1500 nm). These authors reported that the visible and short wavelength region (400-1000 nm) were required to accurately predict lycopene content and colour parameters. Similarly, Ruiz et al. (2008) used the visible reflectance spectra (380-770 nm) to assess the carotenoid content in apricots, the authors observed a correlation between colour parameters and carotenoid content. This suggests that pigments would produce some influences on the variation of absorbance in the spectra and this could be directly related to the colour parameters.

Nicolaï *et al*. (2007) stated that fruit firmness cannot be determined directly; however, it can give a measurement of the NIR light scattering properties of tissue, such as the cell wall, associated with fruit firmness. In the current study the performance of the calibration models for firmness were reasonable with the IS (R^2 = 68.40, RMSEE = 6.05 N, RMSEP = 6.71 N and RPD = 1.62) outperforming the EH (R^2 = 62.27, RMSEE = 8.06 N, RMSEP =7.62 N and RPD = 1.60) acquisition mode (Table 4). Similar results were reported by Louw and Theron (2010) for the prediction of fruit firmness for three South African plum cultivars (R^2 = 0.623-0.791; RMSEE = 12.459-22.760 N). The best wavelength region for the prediction of aril firmness was determined to be from 1064-2355 nm which is within the wavelength regions reported Louw and Theron (2010). The best stable models for phytochemicals such as total phenolic (R^2 = 86.48, RMSEE = 0.11 g/L, RMSEP = 0.11 g/L and RPD = 2.47) and anthocyanin content (R^2 = 70.50, RMSEE = 0.16 g/L, RMSEP = 0.13 g/L and RPD = 1.79) was obtained using the EH spectral acquisition mode (Table 5). The RMSEE and RMSEP values for total phenolic and total anthocyanin concentration were very similar indicating robust fitting. Similarly, the model development for vitamin C was best predict using EH (R^2 = 84.86, RMSEE =0.10 g/L, RMSEP = 0.09 g/L and RPD = 1.63). The ideal waveband range for total phenolic and total anthocyanin content obtained by EH was 1064-1835 nm. This is in agreement with the

Stellenbosch University https://scholar.sun.ac.za

waveband range used in previous studies to develop models for sorghum grains (Dykes *et al*., 2014). The best prediction of vitamin C was within the wavelength range of 1064-1333 nm which is in agreement with the wavelength regions reported by Magwaza *et al*. (2013). Furthermore, the results suggested that the prediction of these compound is from the actual IR spectra as no correlation was observed with total soluble solids or due to the maturation program from the pomegranate. Since both FT-NIR spectral acquisition modes (EH and IS) are contactless, smaller fruit sample would send less light towards the detector due to the rapidly changing angle of reflection. Therefore, with this regard slightly higher prediction were obtained from the EH as it irradiates a larger surface area compared to IS and therefore receives more information resulting in better model prediction with lower RMSEE and RMSEP.

Several studies suggest that it is important to confirm the reliability of the model by checking the RPD even when high correlation occurs between NIR predicted and actual reference measurements (Williams, 2014). Calibration models that gave RPD value <1.5 means that the model is unreliable, those between 1.5 and 2.0 are appropriate for rough predictions, those between 2.0 and 2.5 are fit for quantitative predictions, those between 2.5 and 3.0 are considered good models while those >3.0 are regarded as satisfactory models (Williams, 2014). In the case of maturity parameters (TSS, pH, TA, TSS: TA, BrimA) the RPD values developed using the EH which ranged between (1.95 and 2.65) and was higher than that of IS (Table 3). Furthermore, the RPD values for these parameters (TSS, pH, TA, TSS:TA, BrimA) fit those of quantitative predictions. The RPD values for the developed models using the IS for the prediction of firmness and colour components (a*, Chroma and Hue) were 1.62, 1.86, 1.79 and 1.88 respectively, providing rough predictions. RPD value of 2.47 for total phenolic concentration (Table 5) clearly indicate a fit model for quantitative prediction, while the RPD values 1.79 and 1.63 for total anthocyanin and vitamin C shows that the models are appropriate for rough predictions. Additionally, considering that the EH irradiated a larger surface of pomegranate arils compared to the IS, it is therefore not surprising that EH had the best predictive power in 8 of the 12 quality parameters considered.

4. **Conclusions**

This study has demonstrated that non-destructive FT-NIR spectroscopy and associated chemometric analysis can be used to develop prediction models for quantifying quality parameters of pomegranate arils. Clear effects of the different spectral acquisition modes on the prediction performance of various quality parameters were observed with the emission head of Matrix^{TM}-F spectrometer outperforming the integrating sphere of Multi-Purpose Analyser.

Stellenbosch University https://scholar.sun.ac.za

The emission head the gave the best results for TSS, pH, TA, BrimA, colour hue, total phenolics, total anthocyanin and vitamin C, while the integrating sphere provided the best results for TSS:TA, firmness, arils redness (a*) and colour intensity (chroma). These findings can holistically be employed by the pomegranate industry to develop a grading/sorting system to rapidly evaluate organoleptic and phytochemical quality parameters of pomegranate arils.

References

Arendse, E., Fawole, O.A., Magwaza, L.S. & Opara, U.L. (2016). Non-destructive characterization and volume estimation of pomegranate fruit external and internal morphological fractions using X-ray computed tomography. *Journal of Food Engineering*, **186**, 42–49.

Arendse, E., Fawole, O.A. & Opara, U.L. (2014). Influence of storage temperature and duration on postharvest physico-chemical and mechanical properties of pomegranate fruit and arils. *CyTA Journal of Food*, **12**, 389–398.

Ayhan, Z. & Eştürk, O. (2009). Overall quality and shelf life of minimally processed and modified atmosphere packaged "ready-to-eat" pomegranate arils. *Journal of Food Science*, **74**, 399–405.

Barros, L., Ferreira, M.J., Queiros, B., Ferreira, I.C.F.R. & Baptista, P. (2007). Total phenols, ascorbic acid, ß-carotene and lycopene in Portuguese wild edible mushroom and their antioxidant activities. *Food Chemistry*, **103**, 413–419.

Blanco, M. & Villarroya, I. (2002). NIR spectroscopy: A rapid-response analytical tool. *Trends in Analytical Chemistry*, **21**, 240–250.

Bruker Optik GmbH: User Manual III NIR/Process, Opus Spectroscopy Software, Version 6, Ettlingen, 2006.

Bureau, S., Ruiz, D., Reich, M., Gouble, B., Bertrand, D., Audergon, J. & Renard, C.M.G.C. (2009). Rapid and non-destructive analysis of apricot fruit quality using FT-near infrared spectroscopy. *Food Chemistry*, **113**, 1323–1328.

Caleb, O.J., Opara, U.L. & Witthuhn, C. (2012). Modified atmosphere packaging of pomegranate fruit and arils: A review. *Food and Bioprocess Technology*, **5**, 15–30.

Chen, L. & Opara, U.L. (2013a). Texture measurement approaches in fresh and processed foods - a review. *Food Research International*, **51**, 823–835.

Chen, L. & Opara, U.L. (2013b). Approaches to analysis and modeling texture in fresh and processed foods - a review. *Journal of Food Engineering*, **119**, 497–507.

Stellenbosch University https://scholar.sun.ac.za

Clément, A., Dorais, M. & Vernon, M. (2008). Non-destructive measurement of fresh tomato lycopene content and other physicochemical characteristics using visible-NIR spectroscopy. *Journal of Agricultural and Food Chemistry*, **56**, 9813–9818.

Dykes, L., Hoffmann, L., Portillo-Rodriguez, O., Rooney, W.L. & Rooney, L.W. (2014). Prediction of total phenols, condensed tannins, and 3-deoxyanthocyanidins in sorghum grain using near-infrared (NIR) spectroscopy. *Journal of Cereal Science*, **60**, 138–142.

Fawole, O.A., Makunga, N.P. & Opara, U.L. (2012a). Antibacterial, antioxidant and tyrosine-inhibition activities of pomegranate fruit peel methonolic extract. *BMC Complementary and Alternative Medicine*, **12**, 200–225.

Fawole, O.A., Opara, U.L. & Theron, K.I. (2012b). Chemical and phytochemical properties and antioxidant activities of three pomegranate cultivars grown in South Africa. *Food and Bioprocess Technology*, **5**, 2934–2940.

Fawole, O.A. & Opara, U.L. (2013). Changes in physical properties, chemical and elemental composition and antioxidant capacity of pomegranate (cv. Ruby) fruit at five maturity stages. *Scientia Horticulturae*, **150**, 37–46.

Ghosh, S., Mishra, P., Mohamad, S.N.H., de Santos, R.M., Iglesias, B.D. & Elorza, P.B. (2016). Discrimination of peanuts from bulk cereals and nuts by near infrared reflectance spectroscopy. *Biosystems Engineering*, **151**, 178–186.

Giusti, M.M. & Wrolstad, R.E. (2001). Characterization and measurement of anthocyanins by UV–visible spectroscopy. In: *Current Protocols in Food Analytical Chemistry* (edited by R.E. Wrolstad, T.E. Acree & H. An). John Wiley & Sons, Inc., New York, NY.

Golic, M., Walsh, K.B. & Lawson, P. (2003). Short-wavelength near infrared spectra of sucrose, glucose, and fructose with respect to sugar concentration and temperature. *Applied Spectroscopy*, **57**, 139–145.

Huang, H., Yu, H., Xu, H. & Ying, Y. (2008). Near infrared spectroscopy for on/in-line monitoring of quality in foods and beverages: a review. *Journal of Food Engineering*, **87**, 303–313.

Ismail, T., Sestili, P. & Akhtar, S. (2012). Pomegranate peel and fruit extracts: A review of potential anti-inflammatory and anti-infective effects. *Journal of Ethnopharmacology*, **143**, 397–405.

Jackson, J.E. (1991). *A User's Guide to Principal Components*, John Wiley, New York. ISBN 0-471-62267-2.

Stellenbosch University https://scholar.sun.ac.za

Khodabakhshian, R., Emadi, B., Khojastehpour, M., Golzarian, M.R. & Sazgarnia, A. (2016). Development of a multispectral imaging system for online quality assessment of pomegranate fruit. International *Journal of Food Proprieties*, **20**, 107–118.

Klein, B.P. & Perry, A.K. (1982). Ascorbic acid and vitamin A activity in selected vegetables from different geographical areas of United States. *Journal of Food Science*, **47**, 941–945.

Lestander, T.A. & Geladi, P. (2005). NIR spectral information used to predict water content of pine seeds from multivariate calibration. *Canadian Journal of Forest Research*, **35**, 1139–1148.

Louw, E.D. & Theron, K.I. (2010). Robust prediction models for quality parameters in Japanese plums (*Prunus salicina* L.) using NIR spectroscopy. *Postharvest Biology and Technology*, **58**, 176–184.

Lu, H., Xu, H., Ying, Y., Fu, X., Yu, H. & Tian, H. (2006). Application of Fourier transform near infrared spectrometer in rapid estimation of soluble solids content of intact citrus fruits. *Journal of Zhejiang University Science*, **7**, 794–799.

Magwaza, L.S., Opara, U.L., Nieuwoudt, H., Cronje, P., Saeys, W. & Nicolaı, B. (2012). NIR spectroscopy applications for internal and external quality analysis of citrus fruit – a review. *Food and Bioprocess Technology*, **5**, 425–444.

Magwaza, L.S., Opara, U.L., Terry, L.A., Landahl, S., Cronje, P.J.R., Nieuwoudt, H.H., Hanssens, A., Saeys, W. & Nicolaï, B.M. (2013). Evaluation of Fourier transform-NIR spectroscopy for integrated external and internal quality assessment of 'Valencia' oranges. *Journal of Food Composition and Analysis*, **31**, 144–154.

Magwaza, L.S. & Opara, U.L. (2014). Investigating non-destructive quantification and characterization of pomegranate fruit internal structure using X-ray computed tomography. *Postharvest Biology and Technology*, **95**, 1–6.

Magwaza, L.S., Naidoo, S.I.M., Laurie, S.M., Laing, M.D. & Shimelis, H. (2016). Development of NIRS models for rapid quantification of protein content in sweetpotato [*Ipomoea batatas* (L.) LAM.]. *LWT-Food Science and Technology*, **72**, 63–70.

Makkar, H.P.S. (2000). Quantification of tannins in tree foliage. In: A Laboratory Manual for the FAO/IAEA Coordinated Research Project on 'Use of Nuclear and Related Techniques to Develop Simple Tannin Assay for Predicting and Improving the Safety and Efficiency of Feeding Ruminants on the Tanniniferous Tree Foliage'. Joint FAO/IAEA Division of Nuclear Techniques in Food and Agriculture, Vienna, Austria.

Stellenbosch University https://scholar.sun.ac.za

Miguel, M.G., Neves, M.A. & Antunes, M.D. (2010). Pomegranate (*Punica granatum* L.): A medicinal plant with myriad biological properties - a short review. *Journal of Medicinal Plants Research*, **4**, 2836–2847.

Mphahlele, R.R., Stander, M.A., Fawole, O.A. & Opara, U.L. (2014). Effect of fruit maturity and growing location on the postharvest contents of flavonoids, phenolic acids, vitamin C and antioxidant activity of pomegranate juice (cv. Wonderful). *Scientia Horticulturae*, **179**, 36–45.

Musingarabwi, D.M., Nieuwoudt, H.H., Young, P.R., Eyéghè-Bickong, H.A. & Vivier, M.A. (2016). A rapid qualitative and quantitative evaluation of grape berries at various stages of development using Fourier-transform infrared spectroscopy and multivariate data analysis. *Food Chemistry*, **190**, 253–262.

Nicolaï, B.M., Beullens, K., Bobelyn, E., Peirs, A., Saeys, W., Theron, K.I. & Lammertyn, J. (2007). Non-destructive measurement of fruit and vegetable quality by means of NIR spectroscopy: a review. *Postharvest Biology and Technology*, **46**, 99–118.

Olarewaju, O.O., Bertling, I. & Magwaza, L.S. (2016). Non-destructive evaluation of avocado fruit maturity using near infrared spectroscopy and PLS regression models. *Scientia Horticulturae*, **199**, 229–236.

Opara, U.L., Al-Ani, M.R. & Al-Shuaibi, Y.S. (2009). Physicochemical properties, vitamin C content, and antimicrobial properties of pomegranate fruit (*Punica granatum* L.). *Food and Bioprocess Technology*, **2**, 315–321.

Pérez-Marín, D., Garrido-Varo, A. & Guerrero, J.E. (2005). Implementation of LOCAL algorithm with near-infrared spectroscopy for compliance assurance in compound feeding stuffs. *Applied Spectroscopy*, **59**, 69–77.

Pathare, P.B., Opara, U.L. & Al-Said, F.A.J. (2013). Colour measurement and analysis in fresh and processed foods: a review. *Food and Bioprocess Technology*, **6**, 36–60.

Ruiz, D., Reich, M., Bureau, S., Rebard, C.M.G.C. & Audergon, J.M. (2008). Application of reflectance colorimeter measurements and infrared spectroscopy methods to rapid and non-destructive evaluation of carotenoids content in apricot (*Prunus armeniaca* L.). *Journal of Agricultural and Food Chemistry*, **56**, 4916–4922.

Saiz-Abajo, M.J., Mevick, B.H., Segtnan, V.H. & Naes, T. (2005). Ensemble methods and data augmentation by noise addition applied to the analysis of spectroscopic data. *Analytica Chimica Acta*, **533**, 147–159.

Seeram, N.P., Zhang, Y., Reed, J.D., Krueger, C.G. & Vaya, J. (2006). Pomegranate phytochemicals. In: *Pomegranates: ancient roots to modern medicine* (edited by N. P.

Stellenbosch University https://scholar.sun.ac.za

Seeram, R. N. Schulman, & D. Heber). Pp. 3–29. CRC Press Taylor & Francis Group, Boca Raton, FL.

Tewari, J.C., Dixit, V., Chi, B.K. & Malik, K.A. (2008). Determination of origin and sugars of citrus fruit using genetic algorithm, correspondence analysis and partial least square combined with fibre optic NIR spectroscopy. *Spectrochimica Acta Part A*, **71**, 1119–1127.

Williams, P.C. & Sobering, D.C. (1993). Comparison of commercial near infrared transmittance and reflectance instruments for the analysis of whole grains and seeds. *Journal of Near Infrared Spectroscopy*, **1**, 25–32.

Williams, P. (2014). The RPD statistic: a tutorial note. *NIR news*, **25**, 22–26.

Zhang, L. & McCarthy, M.J. (2013). Assessment of pomegranate postharvest quality using nuclear magnetic resonance. *Postharvest Biology and Technology*, **77**, 59–66.

Stellenbosch University https://scholar.sun.ac.za

Table 1. Mean, standard deviation (SD) and range for calibration and validation subsets for organoleptic and phytochemical quality parameters of pomegranate arils.

Quality Parameter	Calibration			Validation			Overall CV %
	Mean	SD	Range	Mean	SD	Range	
TSS (%)	14.42	0.65	12.6-16.1	14.45	0.77	12.6-15.9	4.92
pH	3.10	0.28	2.78-3.83	3.09	0.20	2.79-3.81	7.67
TA (%)	1.30	0.24	0.81-2.00	1.32	0.23	0.81-1.97	17.86
TSS:TA	10.72	1.98	4.57-15.44	10.28	2.30	5.51-14.69	20.45
BrimA	11.58	0.84	9.38-13.34	11.53	0.93	9.56-13.20	7.66
Firmness (N)	120.82	10.88	102.53-148.98	123.24	10.53	102.94-147.97	8.78
a*	18.72	3.20	11.18-25.79	19.76	3.11	11.23-25.66	16.42
Chroma	20.90	4.68	11.72-32.90	23.35	4.11	13.32-31.39	20.00
Hue	30.42	11.52	14.40-51.05	26.39	7.03	15.80-34.48	27.43
Total Phenolics (g/L)	1.72	0.28	1.22-2.40	1.67	0.26	1.24-2.31	15.80
Total Anthocyanin (g/L)	0.82	0.28	0.33-1.64	0.83	0.23	0.34-1.35	30.53
Vitamin C (g/L)	1.60	0.26	1.01-1.96	1.53	0.15	1.09-1.94	13.05

TSS, total soluble solids; TA, titratable acidity; SD, standard deviation; CV, coefficient of variation

Stellenbosch University https://scholar.sun.ac.za

Table 2. Pearson correlation coefficient matrix between chemical indices measured in pomegranate arils

	Variables	1	2	3	4	5	6	7	8	9	10	11	12
1	TSS	1.00											
2	pH	0.16	1.00										
3	TA	-0.13	-0.43	1.00									
4	TSS:TA	0.36	0.46	**-0.91**	1.00								
5	BrimA	**0.86**	0.34	**-0.62**	**0.75**	1.00							
6	a*	-0.06	0.24	0.03	-0.03	-0.07	1.00						
7	Chroma	-0.08	0.41	-0.18	0.16	0.03	**0.86**	1.00					
8	Hue	-0.09	0.45	-0.42	0.37	0.14	0.23	**0.66**	1.00				
9	Firmness	-0.05	0.04	-0.06	0.04	0.00	-0.16	-0.11	0.01	1.00			
10	Total phenolics	0.04	-0.18	0.22	-0.19	-0.08	-0.21	-0.28	-0.31	0.09	1.00		
11	Total anthocyanins	0.26	-0.21	0.36	-0.29	0.02	-0.21	-0.31	**-0.50**	0.03	0.45	1.00	
12	Vitamin C	0.03	0.23	-0.17	0.13	0.11	0.00	0.15	0.25	0.21	-0.01	-0.06	1.00

Correlation values in bold are significant at $p < 0.05$

Stellenbosch University https://scholar.sun.ac.za

Table 3. Model performance for organoleptic parameters using different FT-NIR instruments

Parameter	NIR probe	Wavelength range (nm)	Calibration			Validation					
			LV	R^2	RMSEE	R^2	RMSEP	RPD	Bias	Slope	Corr.
TSS (%)	IS	1064-1333	6	85.75	0.23	79.07	0.31	2.19	-0.024	0.66	0.85
	EH	1064-1333, 1587-1724	7	87.55	0.24	84.64	0.30	2.65	0.079	0.79	0.93
pH	IS	1064-1640	7	83.49	0.12	80.59	0.10	2.32	0.002	0.95	0.91
	EH	1064-2100	6	85.18	0.14	80.30	0.10	2.40	-0.036	0.81	0.91
TA (%)	IS	1064-1585, 2100-2353	5	80.44	0.10	79.96	0.13	2.29	0.013	0.82	0.90
	EH	1064-1333, 1740-1835	8	85.59	0.10	81.75	0.10	2.34	0.000	0.76	0.91
TSS:TA	IS	1064-2355	7	82.20	0.87	77.83	1.03	2.13	0.083	0.86	0.89
	EH	1064-1333, 1740-1840,	7	75.67	0.96	73.62	1.10	1.95	0.008	0.62	0.87
BrimA	IS	1064-1586, 1725-2355	7	77.61	0.42	78.68	0.45	2.17	0.022	0.71	0.89
	EH	1064-1333, 1640-1835	7	83.43	0.36	78.79	0.43	2.22	0.020	0.73	0.89

LV, latent variables; R^2, coefficient of determination; RMSEE, Root mean square error of estimation; RPD, residual predictive deviation; RMSEP, root mean square error of prediction; Corr, correlation coefficient; IS, integrating sphere; EH, emission head; TSS, total soluble solids; TA, titratable acidity

Stellenbosch University https://scholar.sun.ac.za

Table 4. Model performance for colour parameters and firmness using different FT-NIR instruments

Parameter	NIR probe	Wavelength range (nm)	Calibration			Validation					
			LV	R^2	RMSEE	R^2	RMSEP	RPD	Bias	Slope	Corr.
Firmness (N)	IS	1064-2355	3	68.40	6.05	61.47	6.71	1.62	-0.79	0.59	0.79
	EH	1064-1333, 1640-1835	3	62.27	8.06	60.34	7.62	1.60	-0.90	0.64	0.78
a*	IS	1064-1183, 1640-1732	4	73.54	1.69	70.83	1.67	1.86	-0.16	0.72	0.84
	EH	1064-1360	7	67.71	2.31	62.36	1.92	1.67	0.42	0.69	0.80
Chroma	IS	1064-1333, 2000-2174	4	78.37	2.24	67.96	2.31	1.79	0.37	0.65	0.83
	EH	1064-1333, 1465-1725	6	69.70	3.74	65.56	2.50	1.72	0.32	0.74	0.81
Hue	IS	1064-1333, 2000-2174	5	78.91	5.77	70.60	4.99	1.92	1.37	0.78	0.85
	EH	1064-1333, 1465-1584	9	88.59	4.07	70.69	4.19	1.88	0.73	0.87	0.86

LV, latent variables; R^2, coefficient of determination; RMSEE, Root mean square error of estimation; RPD, residual predictive deviation; RMSEP, root mean square error of prediction; Corr, correlation coefficient; IS, integrating sphere; EH, emission head

Stellenbosch University https://scholar.sun.ac.za

Table 5. Model performance for phytochemicals and Vitamin C using different FT-NIR instruments

Parameter	NIR probe	Wavelength range (nm)	Calibration			Validation					
			LV	R^2	RMSEE	R^2	RMSEP	RPD	Bias	Slope	Corr.
Total phenolics (g/L)	IS	1064-1333	7	76.82	0.14	72.41	0.12	1.97	3.01	0.76	0.86
	EH	1064-1333	9	86.48	0.11	82.61	0.11	2.47	0.25	0.82	0.91
Total anthocyanin (g/L)	IS	1064-1333, 1640-1835	7	68.81	0.13	68.77	0.14	1.79	-0.08	0.74	0.83
	EH	1064-1333, 1640-1835	6	70.50	0.16	68.79	0.13	1.79	0.35	0.70	0.83
Vitamin C (g/L)	IS	1064-1333, 1640-2100	7	85.40	0.08	61.24	0.09	1.64	-1.82	0.60	0.79
	EH	1064-1333	4	84.86	0.10	62.20	0.09	1.63	-0.44	0.74	0.80

LV, latent variables; R^2, coefficient of determination; RMSEE, Root mean square error of estimation; RPD, residual predictive deviation; RMSEP, root mean square error of prediction; Corr, correlation coefficient; IS, integrating sphere; EH, emission head.

Stellenbosch University https://scholar.sun.ac.za

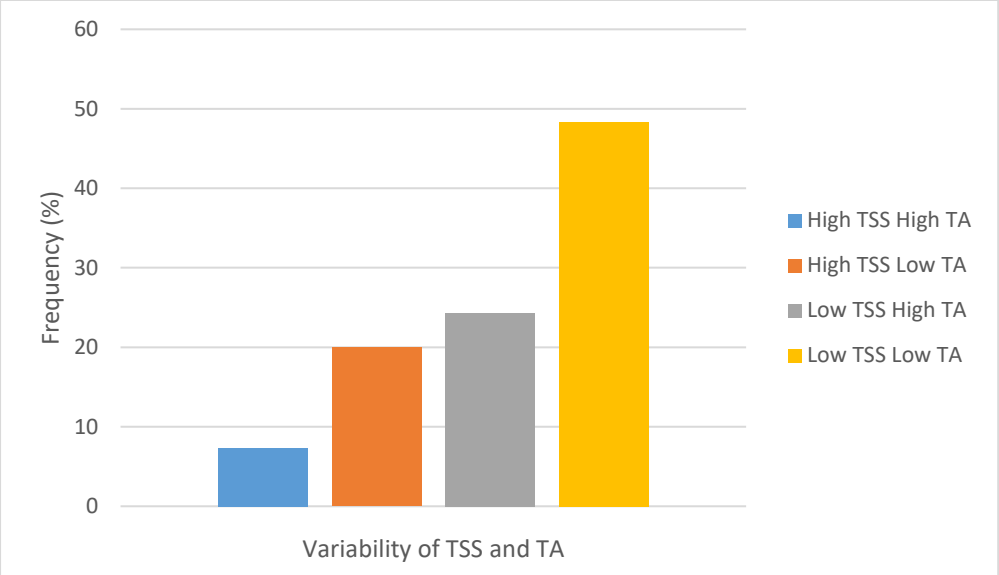

Fig. 1. Sample frequency (%) vs variability of TSS and TA for pomegranate aril samples (n = 300) with high TSS ≥15°Brix and high TA ≥ 1.5%.

Stellenbosch University https://scholar.sun.ac.za

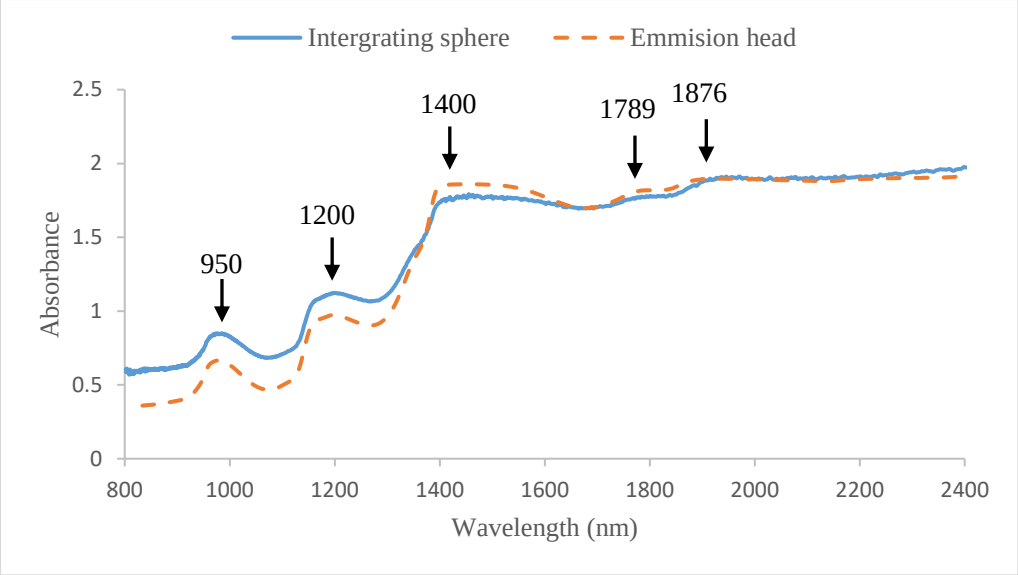

Fig. 2. Absorbance spectra of pomegranate arils obtained using two different spectral acquisition modes integrating sphere (blue solid line) and emission head (broken orange line).

Stellenbosch University https://scholar.sun.ac.za

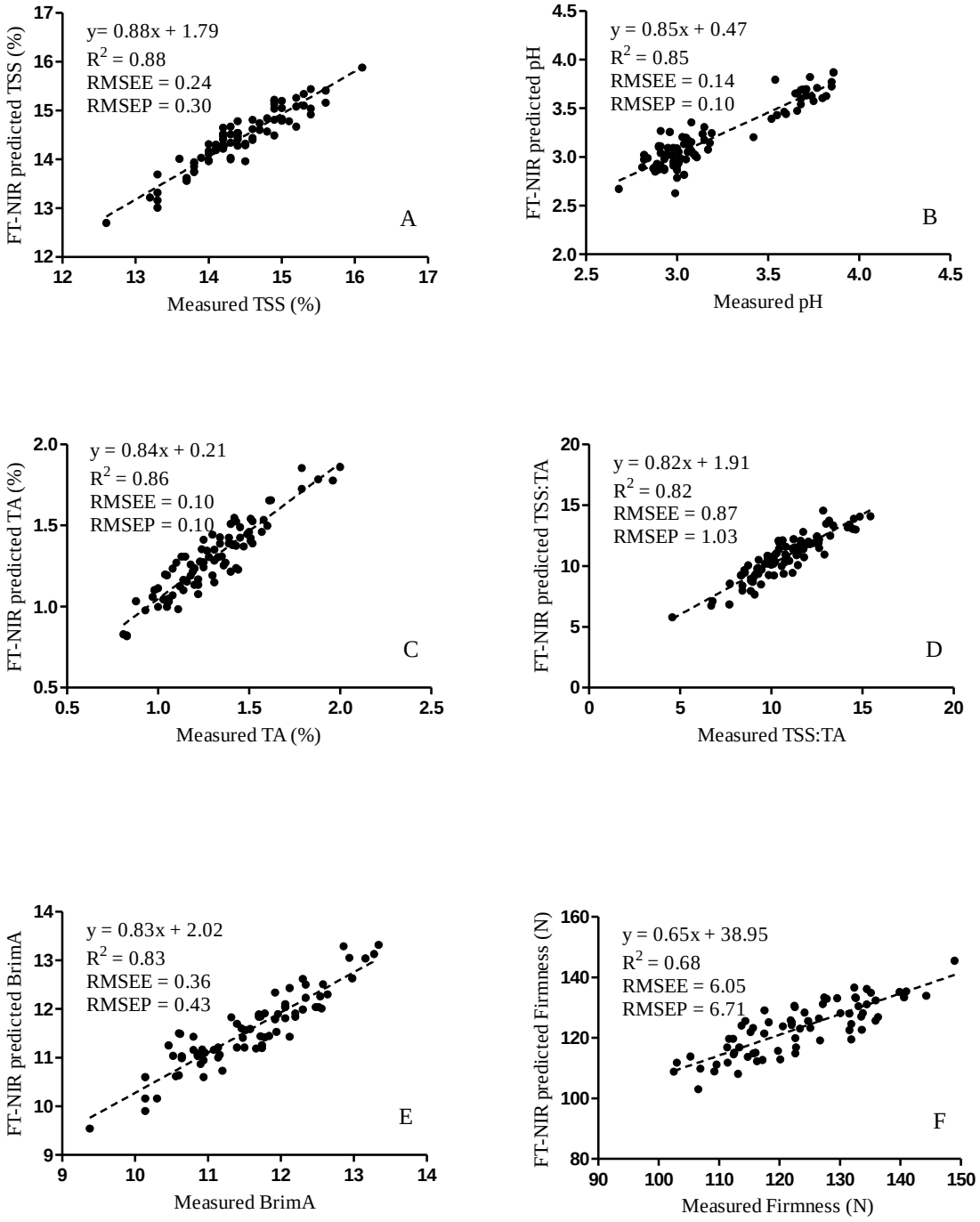

Fig. 3. Scatter plots of FT-NIR predicted TSS (A), pH (B), TA (C), TSS:TA (D), BrimA (E) and firmness (F) plotted against destructively acquired reference data.

Stellenbosch University https://scholar.sun.ac.za

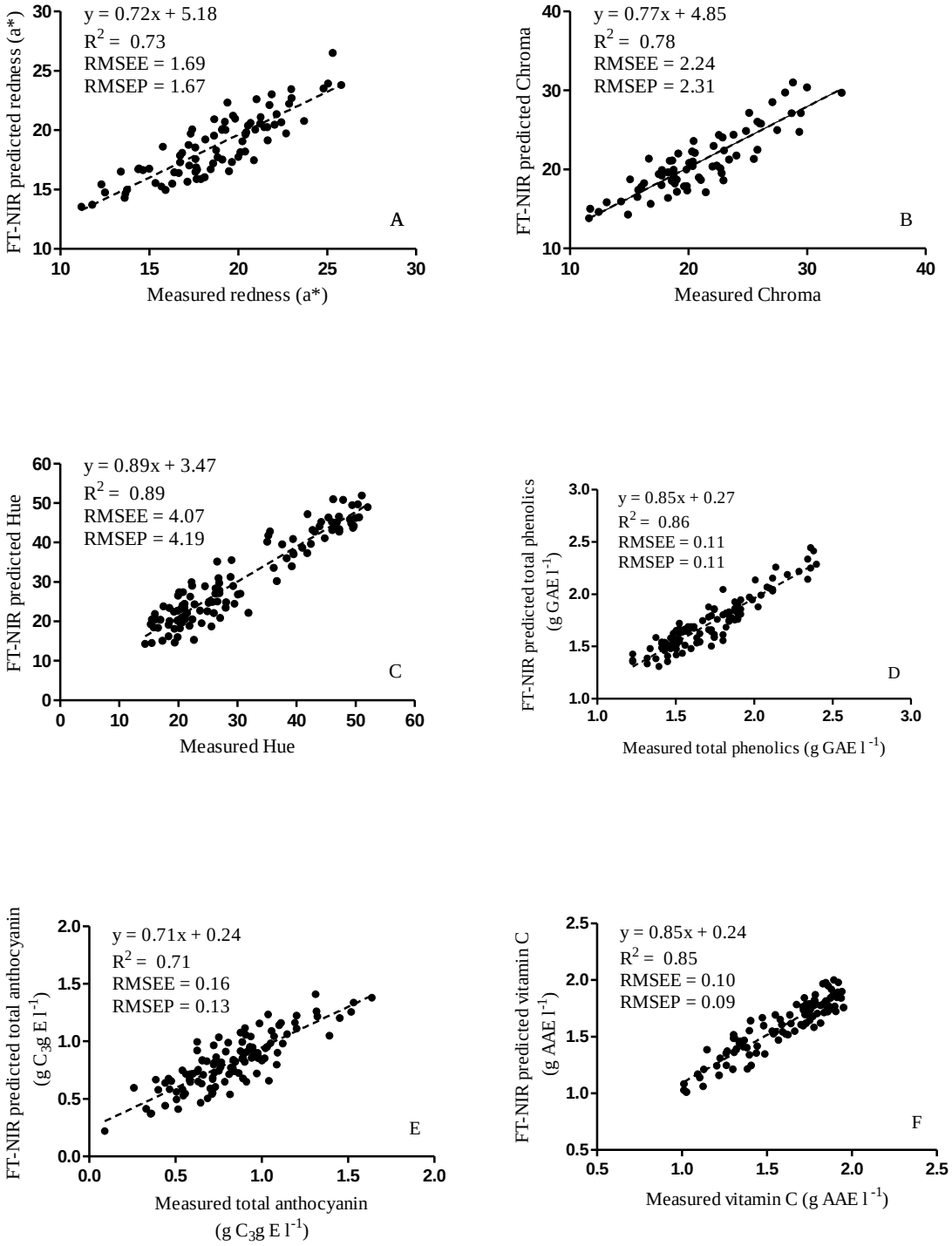

Fig. 4. Scatter plots of FT-NIR predicted aril redness (A), Chroma (B), Hue (C), total phenolics (D), total anthocyanin (E) and vitamin C (F) plotted against destructively acquired reference data.

Stellenbosch University https://scholar.sun.ac.za

DECLARATION BY THE CANDIDATE

With regard to **Chapter 6 (pp 127-151)**, the nature and scope of my contribution were as follows:

Nature of contribution	Extent of contribution (%)
Research, data collection, analysis and writing of chapter	70

The following co-authors have contributed to **Chapter 6 (pp 127-151)**

Name	e-mail address	Nature of contribution	Extent of contribution (%)
Prof U.L. Opara	opara@sun.ac.za	Conception of the work, editorial suggestion and proof reading	10
Dr O.A. Fawole	olaniyi@sun.ac.za	Research input, editorial suggestion and proof reading	10
Dr L.S. Magwaza	Magwazal@ukzn.ac.za	Editorial suggestion and proof reading	5
Dr H. Nieuwoudt	hhn@sun.ac.za	Research input, editorial suggestion and analysis	5

Stellenbosch University https://scholar.sun.ac.za

E Arendse **Signature of candidate**	29/08/2017 **Date**

DECLARATION BY CO-AUTHORS

The undersigned hereby confirm that:

1. the declaration above accurately reflects the nature and extent of the contributions of the candidate and the co-authors to **Chapter 6 (pp 127-151)**

2. no other authors contributed to **Chapter 6 (pp 127-151)** besides those specified above, and

3. potential conflicts of interest have been revealed to all interested parties and that the necessary arrangements have been made to use the material in **Chapter 6 (pp 127-151)** of this dissertation.

Signature	Institutional affiliation	Date
Prof U.L. Opara	Stellenbosch University	29/08/2017
Dr O.A. Fawole	Stellenbosch University	29/08/2017
Dr L.S. Magwaza	University of KwaZulu-Natal	29/08/2017
Dr H. Nieuwoudt	Stellenbosch University	29/08/2017

Stellenbosch University https://scholar.sun.ac.za

CHAPTER 6

Comparing the analytical performance of near and mid-infrared spectrometers for evaluating pomegranate juice quality

Abstract

In this study, near-infrared (NIR) and mid-infrared (MIR) spectral acquisition modes were investigated and compared for predicting organoleptic and phytochemical quality attributes of pomegranate juice using three Fourier transform infrared (FT-IR) spectrometers; namely, a Multi-Purpose Analyser (MPA) FT-NIR spectrometer, Alpha-P FT-MIR spectrometer and WineScan FT-MIR spectrometer. Model development over the NIR region of 12500-4000 cm^{-1} using the MPA gave the best prediction statistics for titratable acidity (R^2 = 93.43, RMSEP = 0.11%) and vitamin C concentration (R^2 = 79.72, RMSEP = 0.11 g/L). In the NIR/MIR region of 5000-930 cm^{-1}, models developed using the WineScan gave the best prediction statistics for total soluble solids (R^2 = 96.70, RMSEP = 0.31%), TSS:TA ratio (R^2 = 91.12, RMSEP = 0.82), BrimA (R^2 = 90.58, RMSEP = 0.55), total phenolic concentration (R^2 = 81.48, RMSEP = 0.15 g/L), total anthocyanin concentration (R^2 = 82.47, RMSEP = 0.21 g/L) and colour component hue (R^2 = 77.02, RMSEP = 2.10 g/L). However, developed models over a spectral region of 4000-600 cm^{-1} using the Alpha-P spectrometer provided good prediction statistics for pH (R^2 = 81.93, RMSEP = 0.14), and colour components a* (R^2 = 87.53, RMSEP = 3.22) and Chroma (R^2 = 87.13, RMSEP = 4.17). Prediction ability of the three instruments for selected juice quality attributes were statistically compared using two different regression algorithms (Bland and Altman, and Passing-Bablok). The outcomes are critically discussed together with the regression models, which showed the suitability of the WineScan FT-MIR spectrometer for predicting selected quality attributes of pomegranate juice.

Keywords: *Punica granatum* L., Juice quality, Partial least squares, Chemometrics, Bland and Altman, Passing-Bablok

Stellenbosch University https://scholar.sun.ac.za

1. Introduction

Pomegranate (*Punica granatum* L.) belongs to the *Punicaceae* family. Currently, less than 10% of the global commercial production of pomegranate fruit occurs in the Southern Hemisphere, with South Africa being one of the few producers competing with Chile and Peru to fill the counter season window during spring and early summer months in Northern Hemisphere (Fawole & Opara, 2013 a,b). The increased growth of the global pomegranate industry has coincided with consumer demand for the consistent supply of safe, nutritious and traceable fruit and juice products. This need for quality assured juice has spurred the need for the development and application of accurate, fast and cost-effective non-destructive assessment methods for field and laboratory measurement as well as in-line sorting and grading. The fruit consist of an edible portion known as arils which contain a considerable amount of juice with each aril containing a kernel (Al-Said *et al.*, 2009; Magwaza & Opara, 2014a; Arendse *et al.*, 2016). The juice is a rich source of sugars, organic acids, mineral elements, vitamin C and bioactive compounds (Arendse *et al.*, 2015). Pomegranate juice has been described to possess a diverse array of complex biochemical constituents (Seeram *et al.*, 2006) which have been reported to improve human health as result of several groups of phytochemicals and polyphenolic compounds (e.g. phenolics and anthocyanins). Thus, the fruit juice has been extensively documented for its high antimicrobial effects (Opara *et al.*, 2009) and antioxidant contents (Fawole *et al.*, 2012 a,b; Fawole & Opara, 2013c; Mphahlele *et al.*, 2014a,b).

Infrared (IR) spectroscopy (IRS), which includes visible to near-infrared (Vis/NIR) and mid-infrared (MIR) region of the electromagnetic spectrum, in combination with multivariate data analysis, has become one of the most widely used methods for analysis, providing accurate, fast and cost-effective non-destructive quantification of major components in agricultural materials (de Oliveira *et al.*, 2014; Magwaza *et al.*, 2012, 2014b). IR spectroscopy is appropriate for the prediction of compounds containing polar functional groups such as –OH, C–O, and N–H (Blanco & Villarroya, 2002). In the agricultural industry, IR spectroscopy in the near-infrared (NIR, 12500-4000 cm^{-1}) and the mid-infrared (MIR, 4000-400 cm^{-1}) spectral region have been applied as a non-destructive analytical tool. In combination with chemometrics, NIR spectroscopy has several advantages it is rapid has cheaper instrumentation cost and more robust components than MIR. NIR has the additional versatility of penetrating fruit a finite distance and provides spectral information of surfaces and internal characteristics (Nicolaï *et al.*, 2007). Whereas, MIR spectroscopy contains more spectral information due to the higher resolution of the fundamental vibrational absorption bands compared to the broad overtone and combination absorption bands in the NIR region (Kelly *et al.*, 2004). Limited studies have assessed the potential use of MIR and NIR spectrophotometric methods for the evaluation and

Stellenbosch University https://scholar.sun.ac.za

characterization of juice and the present study performs for the first time, a critical comparison between the Fourier transform (FT)-NIR and FT-MIR spectrometers are considered. The objective of this research was, therefore, to compare three FT-IR spectrometers for the evaluation of organoleptic and phytochemical quality parameters of pomegranate juice.

2. Materials and Methods

2.1. *Fruit sampling and processing*

During the 2015 season, a total of two hundred pomegranate fruit (cv. Wonderful) were procured from Heinrich Frederich Schaefer orchard, while another one hundred fruit of the same cultivar were procured from Porterville orchard (33°01'00"_S, 18°58'59"_E) to provide orchard variability. The individual fruit was manually peeled at 23 ±3 °C by removing the arils. Arils per fruit were juiced individually using a juice extractor (Mellerware, South Africa). Prior to spectral acquisition juice was filtered with a Filtration Unit (type 79500, Foss Electric, Denmark) using Whatman filter paper (20-25 µm and with diameter 185 mm) this was performed to remove particles from the juice that might disturb the optical path length during spectral acquisition.

2.2. *FT-IR spectral measurements of pomegranate juice*

FT-IR spectra were generated in transmission mode from the Multi-Purpose Analyser (MPA) FT-NIR spectrometer (Bruker Optics, Ettlingen, Germany) over a spectral region of 12500-4000 cm^{-1}. The MPA incorporates a high energy air cooled NIR source (20 W tungsten-halogen lamp) and a permanently aligned Rocksolid interferometer, which is equipped with gold-coated mirrors (high reflective surface and inert). The permanent interferometer provides constant high quality results which have a wave number reproducibility superior to 0.04 cm^{-1} and a wavenumber accuracy superior to 0.1 cm^{-1}. The MPA was fitted with a sample compartment for the measurement of liquids. The background absorbance prior to scanning of the juice sample was taken against air background and periodically at intervals of 30 min between subsequent measurements. Approximately 0.5 mL of filtered juice fruit was transferred into a cuvette. Sample measurement time was 120 s for each fruit obtaining a total of 128 scans averaged per spectrum using a scanning resolution of 4 cm^{-1} and scanner velocity of 10 kHz. The NIR spectra system was operated and initial spectral processing was achieved using OPUS version 7 software (Bruker Optics, Ettlingen, Germany). The cuvette was cleaned between measurements with the subsequent juice sample.

The second type of instrument used to acquire FT-IR spectra was the Alpha-P ATR FT-MIR spectrometer (Bruker Optics, Ettlingen, Germany) over a spectral region of 12500-4000

Stellenbosch University https://scholar.sun.ac.za

cm^{-1} and measured diffuse reflectance. The Alpha-P spectrometer was fitted with a single bounce diamond crystal sample plate (area 2 mm^2) with the temperature maintained at 40 °C. Prior to obtaining FT-MIR spectra, reference measurements were performed against air background and periodically at intervals of 30 min during sample spectra acquisition. The scanning stage was cleaned with distilled H_2O and tissue paper after subsequent measurements. Sample measurement time was 120 s using the following operating parameters 4 cm^{-1} resolution scan and 10 kHz scanner velocity with a total of 128 averaged background and sample scans per spectrum.

The third type of instrument used to acquire FT-IR spectra was the automated WineScan FT120 (Foss Electric, Denmark) spectrometer. The WineScan instrument was specifically designed to generate quantitative data against a background of matrix wine. Operating settings (wavenumber selection and pre-processing) were pre-selected by the manufacturer and therefore were not available for selection. Juice (10 mL) per sample was pumped through a CaF2-lined cuvette (optical path length 37 µm) housed by a heater unit which increased the temperature of the samples to 40 °C before being analysed. The background absorbance prior to scanning of the juice sample was taken using Foss Zero Liquid S-6060. Juice samples were scanned from the wavelength range of 5000-925 cm^{-1} at 4 cm^{-1} intervals. The WineScan FT120 scans a small section of the near-IR spectrum and the mid-IR spectrum. The generation of the final transmittance spectrum was achieved by usage of the ratio of the sample spectrum to the zero liquid spectrum at each recorded data point. Through a series of mathematical procedures, the transmittance spectra were finally converted into linearised absorbance spectra with an average of 20 replicate scans per spectrum for each sample (Nieuwoudt *et al.*, 2004).

2.3. *Reference measurements*

Total soluble solids (TSS) was performed using a digital refractometer (Palette, PR-32α, Otago, Japan) and results were expressed as a percentage (Magwaza & Opara, 2015). The titratable acidity (citric acid %) of the juice was assessed by the method of titration using 2 mL juice against 0.1 M sodium hydroxide solution using a compact titro-sampler (Metrohm, Herisua, Switzerland). Pomegranate flavour was expressed as the ratio between TSS and TA. BrimA which is a variation of sugar to acid ratio was calculated from Eq 1.

$$BrimA = TSS - k * TA \quad (1)$$

Where k equal 2 representing the tongue sensitivity. (Fawole & Opara 2013b; Arendse *et al.,* 2014a). The pH values were determined using a calibrated pH meter (Crison, Barcelona, Spain).

Stellenbosch University https://scholar.sun.ac.za

Pomegranate juice absorbance colour was assessed at 520 nm using UV-vis spectrophotometer. Colour attributes (L*, a*, b*) of juice were recorded using a Chroma Meter CR-400 (Minolta Corp, Japan). Colour components Chroma (C^*) and Hue angle ($h°$) were derived from the CIE coordinates (L*, a*, b*) as reviewed by Pathare and Opara (2013) and applied by Arendse *et al.* (2017).

Total phenolic concentration was quantified using Folin-Ciocalteu method (Makker *et al.,* 2007) with modification according to Fawole *et al.* (2012b). Briefly, in duplicate 50 µL of juice supernatant was diluted with 450 µL of 50% methanol (v/v) before the addition of 1 N Folin C (500 mL) and 2% sodium carbonate (2.5 mL). The mixture was stored in a dark environment for 40 min before the absorbance was measured at 725 nm against blank aqueous methanol. The final results were expressed as grams gallic acid equivalents per litre of pomegranate juice. The quantification of total anthocyanin concentration was performed using the pH differential method (Giusti & Wrolstad, 2001) with modification according to Arendse *et al.* (2014b). Pomegranate juice supernatant (1 mL) were diluted with 9 mL of pH 1.0 (potassium chloride, 0.025 M) and pH 4.5 (sodium acetate, 0.4 M) buffers respectively. Subsequently, samples were stored in dark for 10 min before the absorbance was measured at 510 and 700 nm respectively against 50% blank aqueous methanol using a UV–visible spectrophotometer. Results were expressed as cyanidin-3-glucoside equivalents per litre of juice.

Vitamin C assay was performed according to Klein and Perry (1982) with slight modifications (Barros *et al.,* 2007) as recently applied by Arendse *et al.* (2017). Briefly, 0.5 mL pomegranate juice was diluted with 14.5 mL metaphosphoric acid (1%), the extraction solution was vortexed and sonicated in an ice-cold bath for 5 min followed by centrifugation at 10 000 rpm (G = 11.5) for 5 min at 4 °C. The collected supernatant (1 mL) was mixed with 0.0025% 2, 6-dichlorophenolindophenol dye (9 mL) followed by incubation in the dark for 10 min. The absorbance was measured at 515 nm using a UV–vis spectrophotometer (Thermo Scientific Technologies, Madison, WI, USA) against the 1% metaphosphoric acid solution blank and the results were expressed as grams of ascorbic acid equivalent per litre of crude juice.

2.4. *Chemometric data analysis*

OPUS version 7.0 software (Bruker Optics) was used for multivariate analysis. Spectral parameters were optimised by subjecting spectral data to the software's "Optimise" function which analyse combinations of different pre-processing methods and wavelength regions. The optimise function yields a combination of possible parameters with RMSECV value, number of latent variables, pre-processing methods and wavelength frequency regions. A method was

Stellenbosch University https://scholar.sun.ac.za

selected based on the best overall performance (lower RMSCEV, the number of latent variables, frequency region). Calibration models were constructed by subjecting NIR spectral data to principal component analysis (PCA) and partial least squares (PLS) regression analysis (including mean centering) Spectral outliers and variation were explored by OPUS software using PCA. Spectral data with high residual and located far away from the zero line of the residual variance was perceived as potential outliers. To construct calibration models with high robustness, the data for both orchards were combined and randomly split into 2:1 subset i.e. calibration (70%) and prediction (30%) sets, each subset containing sufficient samples of both orchards.

The regression statistics used to evaluate the model's performance were described by the coefficient of determination (R^2, Eq. (2)); the root mean square error of estimation (RMSEE, Eq. (3)); and SSE, Eq. (4)), (Bruker Optik, 2006)); root mean square error of prediction (RMSEP, Eq. (5)), residual predictive deviation (RPD), Eq. (6)) and models Bias (Eq. (7);

$$R^2 = 1 - \frac{\sum(y_{cal} - y_{act})^2}{\sum(y_{cal} - y_{mean})^2} \quad (2)$$

$$RMSEE = \sqrt{\frac{1}{M-R-1} \times SSE} \quad (3)$$

$$SSE = \sum[Res]^2 \quad (4)$$

$$RMSEP = \sqrt{\sum \frac{(y_{pred} - y_{act})^2}{n}} \quad (5)$$

$$RPD = \frac{SD}{RMSEP} \quad (6)$$

$$Bias = \frac{1}{n}\sqrt{\sum(y_{pred} - y_{act})^2} \quad (7)$$

Where n is number of spectra, yact is actual value, ymean is mean value, ycal is calculated value, ypred is predicted value of the attribute, M is number of calibration samples, R is the rank, SSE is the sum of squared error, Res is the residual (the difference between the true and the fitted value) and SD is the standard deviation of reference values.

RPD is a statistic used for the evaluation of calibration models in spectroscopy. The RPD evaluates the standard error prediction in terms of standard deviation of the reference data

Stellenbosch University https://scholar.sun.ac.za

(Williams, 2014). Several studies have suggested for fruits and vegetables that RPD values below 1.5 indicate that the developed model is unreliable, while RPD values ranging between 1.5 and 2.0 can be used for rough predictions, those between 2.0 and 2.5 are considered adequate for quantitative predictions, RPD values between 2.5 and 3.0 are considered good models, satisfactory models can be regarded when the RPD values are above 3.0 (Williams, 2014).

2.5. *Statistical analysis*

Spectral and reference data were subjected to statistical analysis using Statistica version 13 software (StatSoft Inc., Tulsa, OK, USA). In order to test the repeatability of the three instruments data were subjected to 10 randomly fitted models of test and train subsets, there average mean square error (MSE) between the predicted and actual values for the three instruments was compared. The comparison between the estimation abilities of three instruments was performed using Bland and Altman and Passing-Bablock regression algorithms (Bland & Altman, 1986; 1999). Bland and Altman's plot is a developed method used to evaluate the agreement amongst two different instruments. Their approach is based on quantifying any systematic difference between the measurements (i.e., the bias). The 95% limits of agreement, estimated by mean difference ± 1.96 standard deviations and these values define the range within which most differences between measurements by the two methods would occur. Thus, the smaller the range between these two limits the better the agreement between the measurements (Bland & Altman, 1986; 1999). Passing-Bablok is a robust statistical method for non-parametric regression analysis suitable for methods comparison. In order to assess two methods using Passing-Bablok regression analysis, the requirements needed are a large variation within the dataset and a linear relationship between the two methods (Passing & Bablok, 1983). Since analytical methods are affected by some non-negligible experimental error, the three instruments (MPA-NIR, Alpha-MIR and WineScan-MIR) were subjected to a joint statistical test on slopes and intercepts of the developed linear regression models. In order for the two or more instruments to have the same prediction ability at a 95% confidence level, this study uses a null hypothesis (H_0). The null hypothesis (H_0) for this study is based on the slope and the intercept for the regression models. It states that the slope should not be significantly different from 1 and that the intercept is not significantly different from 0. The hypothesis is accepted if the value of l is enclosed within the confidence interval for the slope, otherwise, it is rejected. This rejection demonstrates at least a proportional difference between the two methods. Similarly, the hypothesis is accepted if the confidence interval for the intercept

Stellenbosch University https://scholar.sun.ac.za

contains the value of 0. However, if the hypothesis is rejected both methods differ at least by a constant amount (Passing & Bablok, 1983; Bilić-Zulle, 2011).

3. Results and discussion

3.1. *FT-NIR spectral characteristics*

Typical average absorbance spectra for all the juice samples using three different spectral acquisition modes are presented in Fig. 1. The MPA spectrum displayed contours having prominent absorbance peaks in the region 6950 and 5600 cm^{-1} respectively (Fig 1.a). The peak at 6950 cm^{-1} corresponded to the absorption of water as result of second and first vibrational overtones closely associated with the O-H stretching. The peak at 5600 cm^{-1} has been reported to be associated with sugars and organic acids as result of second and first overtones of C-H stretching as well as deformation of the third overtone of O-H, C-H and C-H_2 (Golic *et al.*, 2005). The MIR absorbance spectra for Alpha and WineScan spectral acquisition are presented in Fig. 1. b and c. Some characteristic features of the FT-Alpha spectrum were observed included peaks at 3300 and 1650 cm^{-1} corresponding to the O-H stretch in water (Fig. 1. b). The Winescan spectrum showed bands associated with the -OH group located in regions of 3695, 3280 and 1650 cm^{-1} (Fig. 1. c). MIR spectra for both spectral acquisition modes had a distinct region of systematic variation with Alpha (1050-1450 cm^{-1}) and WineScan (1157-1370 cm^{-1}). The systematic variation is known as a fingerprint region as previously reported by Nieuwoudt *et al.* (2004). This fingerprint region has been reported to be associated with C-O and C-C stretches in sugars and organic acids amongst other compounds (Nieuwoudt *et al.*, 2004).

3.2. *Distribution statistics for calibration and validation reference data*

Table 1 shows the distribution statistics for calibration and validation reference datasets for all parameters. It was observed that the reference data for all parameters in this study were normally distributed around the means. In order to better predict a variable using NIRS, the dataset for both calibration and validation subsets should have sufficient variation (Clément *et al.*, 2008; Magwaza *et al.*, 2013). According to the minimum-to-maximum range and CV% observed in this study, most parameters showed large variability amongst the data subsets with CV% values of up to 38.69% with the exception of prediction of colour absorbance at 520 nm (1.72%).

3.3. *Model development of three FT-IR acquisition modes*

The best model for each parameter was selected based on the lowest root mean square error, lower latent variables, and higher residual predictive deviation. Distribution of reference and predicted values for models developed with NIR and MIR spectroscopy are presented in Fig. 2

Stellenbosch University https://scholar.sun.ac.za

and Fig. 3. Model development using three different FT-IR acquisition modes had a major influence on the regression statistics and the prediction accuracy (Tables 2-4). The model developed for the spectra acquired in the MIR region using the WineScan spectral acquisition mode gave the best prediction for TSS (R^2 = 96.70, RMSEE = 0.25%, RMSEP = 0.31% and RPD = 3.32) followed by the MPA (R^2 = 94.76, RMSEE = 0.32%, RMSEP = 0.31% and RPD = 3.62) in the NIR region (Table 2). The model developed using the Alpha-P gave better prediction statistics for pH (R^2 = 81.93, RMSEE = 0.14, RMSEP = 0.14 and RPD = 2.18). The best predictive statistics for TA (R^2 = 93.43, RMSEE = 0.08%, RMSEP = 0.11% and RPD = 2.70) were developed in the NIR region using the MPA. Calibration models developed using the WineScan spectral acquisition mode in the MIR region gave relatively superior prediction statistics for TSS:TA ratio (R^2 = 91.12, RMSEE = 0.79, RMSEP = 0.82 and RPD = 2.64) and BrimA (R^2 = 90.58, RMSEE = 0.47, RMSEP = 0.55 and RPD = 2.09) than models developed from the MPA and Alpha-P. The wavelength range used during the development of calibration model for TSS was 5000-932 cm^{-1} which is within the range reported by de Oliveira *et al.* (2014), whereas the wavelength region for the prediction of TA was from 7500-5450 cm^{-1} which is within the wavelength region reported by Chen et al. (2006) for apricot juice. The models developed in Table 2 were characterised by low bias values (<0.08) which suggest that the developed models were stable and non-sensitive to external factors such as growing location and seasonality. Furthermore, the RMSEE and RMSEP values were very similar indicating robust fitting regardless of the large amount of LVs (9) used for development of some models this suggest that overfitting noise to models were not evident.

The calibration models developed for predicting phytochemical and vitamin C concentration are presented in Table 3. PLS calibration models developed for predicting total phenolic (R^2 = 81.48, RMSEE = 0.13 g/L, RMSEP = 0.15 g/L and RPD = 1.78) and total anthocyanin concentration (R^2 = 82.47, RMSEE = 0.13 g/L, RMSEP = 0.21 g/L and RPD = 1.95) showed good performance using the WineScan, whereas vitamin C concentration (R^2 = 79.72, RMSEE = 0.09 g/L, RMSEP = 0.11 g/L and RPD = 1.85) were predicted using MPA in the NIR region. In this study, the development of models for total phenolic and anthocyanin concentration used a wavelength ranged from 4000-609 cm^{-1}. This is in agreement with the wavelength range used in previous studies to develop models for blueberries (Sinelli *et al.*, 2008). The ideal waveband range for model development of vitamin C obtained by MPA was 9400-4250 cm^{-1} which is in agreement with the wavelength region used in previous studies to develop models for oranges (Magwaza *et al.*, 2013). The RPD values for total phenolic, total anthocyanin and vitamin C concentration are between 1.5 and 2.0 which are appropriate for rough predictions.

Stellenbosch University https://scholar.sun.ac.za

The calibration statistics for predicting pomegranate juice colour components are presented in Table 4. Colour components (a* and *C**) .were best predicted in the MIR region using the Alpha-P spectral acquisition mode with calibration statistics of (R^2 = 87.53, RMSEE = 2.92, RMSEP = 3.22 and RPD = 2.66) and (R^2 = 87.13, RMSEE = 3.46, RMSEP = 4.17 and RPD = 1.85), respectively. The model developed for the spectra acquired by the WineScan gave the best prediction statistics for h° (R^2 = 77.02, and RPD = 1.73), whilst the calibration statistics for measurement of colour at 520 nm for all three acquisition modes were characterised by low R^2 and a lower RPD (1.23-1.27) values indicating poor predictability. The waveband range from 4000-609 cm^{-1} was used to develop models for colour components which is in agreement with the wavebands reported by He *et al.* (2007).

3.4. *Comparison of the three different instruments*

Replicated and repeatability of methods in method comparison is an important aspect of method comparability which is often disregarded. If only one measurement is used for each method, it is difficult to know which method is more repeatable (precise) and if one method has poor repeatability due to considerable variation in repeated measurements, the agreement between the two or more is bound to be poor (Bland and Altman, 1999). For this reason, the estimation of repeatability and agreement between replicated data for the three instruments were investigated (Fig. 4). A high estimation of repeatability was observed with a low mean square error between the three instruments. Furthermore, a significant difference was only observed with the WineScan compared to the Alpha and MPA instrument suggesting that the WineScan is highly repeatable with a lower mean square error for the measurement of TSS. The differences amongst the three instruments were statistically compared using Bland and Altman and Passing–Bablok regression. TSS was used as a parameter for method comparison due to its superior predictive statistics (Table 2) for all three instruments compared to other measured parameters Statistical comparison of titratable acidity and sugar to acid ratio were included in Appendix chapter 6. The Bland and Altman plot for the measurement of TSS using three instruments are presented in Fig. 5. The comparison of the MPA vs Alpha for the measurement of TSS provided a mean difference of 0.21 between the two instruments and the standard deviation of the differences were 1.06 and -1.48 Fig. 5a. Similarly, the comparison of Alpha vs WineScan and MPA vs WineScan for the measurement of TSS provided a mean difference of 0.09 and 0.12 respectively (Fig. 5b and Fig. 5c). Since the measurement points for TSS lie between -1.96_{sd} and $+1.96_{sd}$ nearly all pairs of measurements by the two methods are closer together than these extreme values or 95% limits of agreement. Therefore, Bland and Altman analysis suggest that there is no statistical difference between the instruments with comparable

Stellenbosch University https://scholar.sun.ac.za

and accurate results obtained for all three instruments. The results for Passing-Bablok comparison for different instruments are presented in Table 5. The comparison of Alpha vs MPA, Alpha vs WineScan and MPA vs WineScan for the prediction of TSS showed that the values of the slope are within the lower and upper CI for each comparison respectively. The value of zero falls within its lower and upper CI for the intercept, therefore, we accept the hypothesis for both the slope and the intercept and can infer that the methods used for the prediction of TSS are identical. Although, the prediction statistics (RMSEP and RPD) for the three instruments may vary, the statistical analyses used for methods comparison indicated that none of the three instruments were statistically different.

4. **Conclusions**

This work has demonstrated that IR spectroscopy combined with chemometrics as a non-destructive tool can be utilised for the prediction of quality parameters of pomegranate juice. The spectral acquisition modes had affected the ability to accurately predict various pomegranate quality attributes, with the WineScan and the Alpha-P instruments in the mid infrared region outperforming the MPA instrument in the near-infrared region. This may be attributed primarily to the fact that the mid-infrared spectrum contains wavelengths for fundamental rotational molecular vibration which is highly sensitive to specific chemical composition, whereas the near-infrared spectrum is associated mainly with overtone and combination bands of fundamental transition, making it less reproducible and specific. Regarding the comparison between the three instruments, the developed models showed reliability in predicting total soluble solids of pomegranate juice, with no statistical differences found between the Bland and Altman and Passing-Bablok analytical algorithms.

References

Al-Said, F.A., Opara, U.L. & Al-Yahyai, R.A. (2009). Physico-chemical and textural quality attributes of pomegranate cultivars (*Punica granatum* L.) grown in the Sultanate of Oman. *Journal of Food Engineering*, **90**, 129-134.

Arendse, E., Fawole, O.A. & Opara, U.L. (2014a). Influence of storage temperature and duration on postharvest physico-chemical and mechanical properties of pomegranate fruit and arils. *CyTA Journal of Food*, **12**, 389–398.

Arendse, E., Fawole, O.A. & Opara, U.L. (2014b). Effects of postharvest storage conditions on phytochemical and antioxidant properties of pomegranate fruit (cv. Wonderful). *Scientia Horticulturae*, **169**, 125-129.

Stellenbosch University https://scholar.sun.ac.za

Arendse, E., Fawole, O.A. & Opara, U.L. (2015). Effects of postharvest handling and storage on physiological attributes and quality of pomegranate fruit (*Punica granatum* L.): A review. *International Journal of Postharvest Technology and Innovation*, **5**, 13–31.

Arendse, E., Fawole, O.A., Magwaza, L.S. & Opara, U.L. (2016). Non-destructive characterization and volume estimation of pomegranate fruit external and internal morphological fractions using X-ray computed tomography. *Journal of Food Engineering*, **186**, 42–49.

Arendse, E., Fawole, O.A., Magwaza, L.S., Nieuwoudt, H.H. & Opara U.L. (2017). Development of calibration models for the evaluation of pomegranate aril quality by Fourier-transform near infrared spectroscopy combined with chemometrics. *Biosystems Engineering*, **159**, 22–32.

Barros, L., Ferreira, M.J., Queiros, B., Ferreira, I.C.F.R. & Baptista, P. (2007). Total phenols, ascorbic acid, ß-carotene and lycopene in Portuguese wild edible mushroom and their antioxidant activities. *Food Chemistry*, **103**, 413–419.

Bilić-Zulle, L. (2011). Comparison of methods: Passing and Bablok regression, *Biochemia Medica*, **21**, 49–52.

Bland, J.M. & Altman, D.G. (1986). Statistical methods for assessing agreement between two methods of clinical measurement. *Lancet*, **1** (8476), 307–310.

Bland, J.M. & Altman, D.G. (1999). Measuring agreement in method comparison studies. *Statistical Methods in Medical Research*, **8**, 135–160.

Chen, J.Y., Zhang, H. & Matsunaga, R. (2006). Rapid determination of the main organic acid composition of raw Japanese apricot fruit juices using near-infrared spectroscopy *Journal of Agricultural and Food Chemistry*, **54**, 9652–965.

Clément, A., Dorais, M. & Vernon, M. (2008). Non-destructive measurement of fresh tomato lycopene content and other physicochemical characteristics using visible-NIR spectroscopy. *Journal of Agricultural and Food Chemistry*, **56**, 9813–9818.

De Oliveira, G.A., Bureau, S., Renard, C.M.G.C., Pereira-Netto, A.B. & de Castilhos, F. (2014). Comparison of NIRS approach for prediction of internal quality traits in three fruit species. *Food Chemistry*, **143**, 223–230.

Fawole, O.A., Makunga, N.P. & Opara, U.L. (2012a). Antibacterial, antioxidant and tyrosine-inhibition activities of pomegranate fruit peel methonolic extract. *BMC Complementary and Alternative Medicine*, **12**, 200–225.

Fawole, O.A., Opara, U.L. & Theron, K.I. (2012b). Chemical and phytochemical properties and antioxidant activities of three pomegranate cultivars grown in South Africa. *Food and Bioprocess Technology*, **5**, 2934–2940.

Stellenbosch University https://scholar.sun.ac.za

Fawole, O.A. & Opara, U.L. (2013a). Changes in physical properties, chemical and elemental composition and antioxidant capacity of pomegranate (cv. Ruby) fruit at five maturity stages. *Scientia Horticulturae*, **150**, 37–46.

Fawole, O.A. & Opara, U.L. (2013b). Developmental changes in maturity indices of pomegranate fruit: A descriptive review. *Scientia Horticulturae*, **159**, 152–161.

Fawole, O.A. & Opara, U.L. (2013c). Effects of storage temperature and duration on physiological responses of pomegranate fruit. *Industrial Crops and Products*, **47**, 300–309.

Giusti, M.M. & Wrolstad, R.E. (2001). Characterization and measurement of anthocyanins by UV–visible spectroscopy. In: Wrolstad, R.E., Acree, T.E., An, H., et al. (Eds.), Current Protocols in Food Analytical Chemistry. John Wiley & Sons, Inc., New York, NY, F1.2.1-F.1.2.13.

Golic, M., Walsh, K.B. & Lawson, P. (2003). Short-wavelength near infrared spectra of sucrose, glucose, and fructose with respect to sugar concentration and temperature. *Applied Spectroscopy*, **57**, 139–145.

He, J., Rodriguez-Saona, L.E. & Giusti M.M. (2007). Mid infrared spectroscopy for juice authentication rapid differentiation of commercial juices. *Journal of Agricultural and Food Chemistry*, **55**, 4443–4452.

Kelly, J.F.D., Downey, G. & Fourtier, V. (2004). Initial study of honey adulteration by sugar solutions using mid-infrared (MIR) spectroscopy and chemometrics. *Journal of Agricultural and Food Chemistry*, **52**, 33–39.

Klein, B.P. & Perry, A.K. (1982) Ascorbic acid and vitamin A activity in selected vegetables from different geographical areas of United States. *Journal of Food Science*, **47**, 941–945.

Lu, H., Xu, H., Ying, Y., Fu, X., Yu, H. & Tian, H. (2006). Application of Fourier transform near infrared spectrometer in rapid estimation of soluble solids content of intact citrus fruits. *Journal of Zhejiang University Science*, **7**, 794–799.

Makkar, H.P.S., Siddhuraju, P. & Becker, K. (2007). Plant secondary metabolites (pp. 74–75). Totowa: Humana Press.

Magwaza, L.S., Opara, U.L., Terry, L.A., Landahl, S., Cronje, P.J., Nieuwoudt, H., Mouazen, A.M., Saeys, W. & Nicolaï, B.M. (2012). Prediction of 'Nules Clementine' mandarin susceptibility to rind breakdown disorder using Vis/NIR spectroscopy. *Postharvest Biology and Technology*, **74**, 1–10.

Magwaza, L.S., Opara, U.L., Terry, L.A., Landahl, S., Cronje, P.J.R., Nieuwoudt, H.H., Hanssens, A., Saeys, W. & Nicolaï, B.M. (2013). Evaluation of Fourier transform-NIR

Stellenbosch University https://scholar.sun.ac.za

spectroscopy for integrated external and internal quality assessment of 'Valencia' oranges. *Journal of Food Composition and Analysis*, **31**, 144–154.

Magwaza, L.S. & Opara, U.L. (2014a). Investigating non-destructive quantification and characterization of pomegranate fruit internal structure using X-ray computed tomography. *Postharvest Biology and Technology*, **95**, 1–6.

Magwaza, L.S., Opara, U.L., Cronje, P.J.R., Landahl, S., Nieuwoudt, H.H., Mouazen, A.M., Nicolaï, B.M. & Terry, L.A. (2014b). Assessment of rind quality of 'Nules Clementine' mandarin fruit during postharvest storage: 2. Robust Vis/NIRS PLS models for prediction of physico-chemical attributes. *Scientia Horticulturae*, **165**, 421–432.

Magwaza, L.S. & Opara, U.L. (2015). Analytical methods for determination of sugars and sweetness of horticultural products-A review. *Scientia Horticulturae*, **184**, 179–192.

Mphahlele, R.R., Fawole, O.A., Stander, M.A. & Opara, U.L. (2014a). Preharvest and postharvest factors influencing bioactive compounds in pomegranate (*Punica granatum* L.)-A review. *Scientia Horticulturae*, **178**, 114–123.

Mphahlele, R.R., Stander, M.A., Fawole, O.A. & Opara, U.L. (2014b). Effect of fruit maturity and growing location on the postharvest contents of flavonoids, phenolic acids, vitamin C and antioxidant activity of pomegranate juice (cv. Wonderful). *Scientia Horticulturae*, 179, 36–45.

Musingarabwi, D.M., Nieuwoudt, H.H., Young, P.R., Eyéghè-Bickong, H.A. & Vivier, M.A. (2016). A rapid qualitative and quantitative evaluation of grape berries at various stages of development using Fourier-transform infrared spectroscopy and multivariate data analysis. *Food Chemistry*, **190**, 253–262.

Nieuwoudt, H.H., Prior, B.A., Pretorius, I.S., Manley, M. & Bauer, F.F. (2004).Principal component analysis applied to Fourier transform infrared spectroscopy for the design of calibration sets for glycerol prediction models in wine and for the detection and classification of outlier samples. *Journal of Agricultural and Food Chemistry*, **52**, 3726–3835.

Nicolaï, B.M., Beullens, K., Bobelyn, E., Peirs, A., Saeys, W. & Theron, I.K. (2007). Non-destructive measurement of fruit and vegetable quality by means of NIR spectroscopy: A review. *Postharvest Biology and Technology*, **46**, 99–118.

Pathare, P.B., Opara, U.L. & Al-Said, F.A.J. (2013). Colour measurement and analysis in fresh and processed foods: a review. *Food and Bioprocess Technology*, **6**, 36–60.

Passing, H. & Bablok, W. (1983). A new biometrical procedure for testing the equality of measurements from two different analytical methods. *Journal of Clinical Chemistry and Clinical Biochemistry*, **21**, 709–720.

Stellenbosch University https://scholar.sun.ac.za

Seeram, N.P., Zhang, Y., Reed, J.D., Krueger, C.G. & Vaya, J. (2006). Pomegranate phytochemicals. In: N.P. Seeram, R.N. Schulman, & D. Heber (Eds.), Pomegranates: ancient roots to modern medicine (pp. 3–29). CRC Press Taylor & Francis Group, Boca Raton, FL.

Sinelli, N., Spinardi, A., Di Egidio, V., Mignani, I. & Casiraghi, E. (2008). Evaluation of quality and nutraceutical content of blueberries (*Vaccinium corymbosum* L.) by near and mid-infrared spectroscopy. *Postharvest Biology and Technology*, **50**, 31–36.

Vardin, H., Tay, A., Ozen, B. & Mauer, L., (2008). Authentication of pomegranate juice concentrate using FTIR spectroscopy and chemometrics. *Food Chemistry*, **108**, 742–748.

Williams. P. (2014). The RPD statistic: a tutorial note. *NIR news*, **25**, 22–26.

Stellenbosch University https://scholar.sun.ac.za

Table 1

Mean, standard deviation (SD), range and coefficient of variation (CV) for calibration and validation subsets for organoleptic and phytochemical parameters of pomegranate juice.

Parameters	Calibration			Validation			Overall CV (%)
	Mean	SD	Range	Mean	SD	Range	
TSS (%)	14.11	1.37	8.20-17.40	14.49	1.05	12.00-17.38	8.49
pH	3.23	0.32	2.64-3.93	3.26	0.31	2.68-3.92	9.71
TA (%)	1.38	0.32	0.66-2.39	1.35	0.30	0.68-2.36	22.67
TSS:TA	10.63	2.63	4.83-22.57	10.65	2.17	6.71-16.11	22.57
BrimA	11.38	1.52	5.86-15.24	11.64	1.15	9.00-14.64	11.63
Total phenolics (g/L)	1.74	0.28	1.15-2.60	1.75	0.26	1.34-2.30	15.48
Total anthocyanin (g/L)	0.86	0.30	0.14-1.92	0.95	0.40	0.26-1.88	38.69
Vitamin C (g/L)	1.59	0.19	1.22-1.95	1.57	0.19	1.21-1.93	12.34
Colour@520 nm	3.27	0.06	3.09-3.39	3.28	0.05	3.11-3.37	1.72
a*	35.26	8.10	10.97-44.03	34.35	8.53	12.05-43.34	23.91
Chroma	39.79	9.56	11.30-50.95	38.17	10.09	12.30-49.69	25.23
Hue	26.06	3.37	13.06-30.21	25.65	3.63	13.19-30.45	13.54

TSS, total soluble solids; TA, titratable acidity; SD, standard deviation; CV, coefficient of variation

Stellenbosch University https://scholar.sun.ac.za

Table 2

Model performance for quality parameters using different infrared spectroscopy instruments

Parameter	Instruments	Wavenumber range (cm^{-1})	Calibration			Validation						Pre-processing
			LV	R^2	RMSEE	R^2	RMSEP	RPD	Bias	Slope	Corr.	
TSS (%)	MPA-NIR	9400-5450, 4600-4250	4	94.76	0.32	92.34	0.31	3.62	0.02	0.94	0.96	MSC
	Alpha-MIR	4000-610	8	94.29	0.32	91.80	0.33	3.49	0.00	0.92	0.96	SNV
	WineScan-MIR	5000-930	4	96.70	0.25	90.78	0.31	3.32	0.04	0.89	0.95	None
pH	MPA-NIR	9400-7500, 6098-5450	10	81.56	0.14	67.04	0.17	1.74	0.01	0.75	0.82	MSC
	Alpha-MIR	3320-1285, 950-609	9	81.93	0.14	78.98	0.14	2.18	0.00	0.78	0.89	None
	WineScan-MIR	5000-4583, 4183-3774	5	51.34	0.22	40.51	0.25	1.30	-0.01	0.44	0.64	Straight line
TA (%)	MPA-NIR	7500-5450	6	93.43	0.08	86.23	0.11	2.70	-0.01	0.84	0.93	FD+MSC
	Alpha-MIR	2500-16400	8	86.66	0.12	82.60	0.12	2.40	0.00	0.92	0.91	SNV
	WineScan-MIR	2000-2650, 3375-4662	4	83.90	0.13	77.09	0.13	2.13	0.03	0.87	0.89	None
TSS:TA	MPA-NIR	9400-7500, 6098-5450	6	83.37	1.00	76.86	1.00	2.08	-0.05	0.92	0.89	FD+SNV
	Alpha-MIR	4000-610	8	81.79	1.03	81.76	1.04	2.35	-0.08	0.79	0.91	SNV
	WineScan-MIR	5000-4583, 2558-1740	2	91.12	0.79	85.55	0.82	2.64	0.08	0.94	0.93	FD+MSC
BrimA	MPA-NIR	9400-5450, 4600-4250	5	92.84	0.40	90.66	0.40	3.28	-0.02	0.93	0.95	MSC
	Alpha-MIR	2500-16400	8	93.91	0.36	90.64	0.40	3.27	-0.02	0.90	0.95	SNV
	WineScan-MIR	5000-930	1	90.58	0.47	79.11	0.55	2.09	-0.02	0.79	0.88	FD+SNV

LV, latent variables; R^2, coefficient of determination; RMSEE, Root mean square error of estimation; RPD, residual predictive deviation; RMSEP, root mean square error of prediction; Corr, correlation coefficient; FD, first derivative; MSC, multiplicative scattering correction; SNV, vector normalisation; MPA, Multi-Purpose Analyser; TSS, total soluble solids; TA, titratable acidity

Stellenbosch University https://scholar.sun.ac.za

Table 3

Model performance for phytochemical and antioxidant parameters using different infrared spectroscopy instruments

Parameter	Instruments	Wavenumber range (cm^{-1})	Calibration			Validation						Pre-processing
			LV	R^2	RMSEE	R^2	RMSEP	RPD	Bias	Slope	Corr.	
T P	MPA-NIR	8375-7855, 6309-5800	13	89.24	0.09	59.19	0.18	1.57	-0.83	0.67	0.77	SNV
	Alpha-MIR	3660-905	8	58.75	0.18	34.10	0.22	1.25	3.24	0.41	0.60	None
	WineScan-MIR	5000-930	13	81.48	0.13	68.17	0.15	1.78	0.92	0.75	0.83	None
T Ant	MPA-NIR	9400-5777	12	77.20	0.17	66.37	0.19	1.73	-0.76	0.68	0.82	SNV
	Alpha-MIR	4000-610	9	59.66	0.19	58.74	0.19	1.56	-1.65	0.57	0.77	None
	WineScan-MIR	5000-930	16	82.47	0.13	73.67	0.21	1.95	-0.11	0.60	0.88	None
Vitamin C	MPA-NIR	9400-5450, 4600-4250	5	79.72	0.09	70.90	0.11	1.85	0.19	0.68	0.84	SD
	Alpha-MIR	4000-610	9	72.28	0.12	68.04	0.13	1.77	-0.32	0.63	0.83	None
	WineScan-MIR	4580-2214	15	76.36	0.09	69.41	0.09	1.82	-0.86	0.67	0.84	SD

LV, latent variables; R^2, coefficient of determination; RMSEE, Root mean square error of estimation; RPD, residual predictive deviation; RMSEP, root mean square error of prediction; Corr, correlation coefficient; SD, second derivative; SNV, vector normalisation; MPA, Multi-Purpose Analyser; T P, total phenolics; T Ant, total anthocyanin

Stellenbosch University https://scholar.sun.ac.za

Table 4

Model performance for colour parameters using different infrared spectroscopy instruments

Parameter	Instruments	Wavenumber range (cm^{-1})	Calibration			Validation						Pre-processing
			LV	R^2	RMSEE	R^2	RMSEP	RPD	Bias	Slope	Corr.	
a*	MPA-NIR	9400-4425	7	87.14	3.20	81.61	3.78	2.33	-0.17	0.80	0.90	FD+SNV
	Alpha-MIR	4000-610	7	87.53	2.92	85.57	3.22	2.66	-0.45	0.90	0.93	None
	WineScan-MIR	4184-2145	8	72.15	3.84	72.11	3.52	1.91	0.42	0.72	0.85	FD
Chroma	MPA-NIR	9400-7752, 4600-4425	11	94.41	2.68	83.23	3.81	2.44	-0.16	0.93	0.92	MSC
	Alpha-MIR	4000-610	7	87.13	3.46	82.76	4.17	2.45	-0.75	0.87	0.91	None
	WineScan-MIR	4600-2145	8	86.16	3.61	81.09	3.78	2.31	0.32	0.82	0.90	FD+SNV
Hue	MPA-NIR	9400-7423, 4600-4425	12	87.75	0.96	46.60	1.65	1.37	0.09	0.73	0.73	MSC
	Alpha-MIR	4690-610	5	58.87	2.27	49.95	2.49	1.43	0.36	0.59	0.72	None
	WineScan-MIR	4600-2145	9	77.02	1.67	66.13	2.10	1.73	-0.28	0.65	0.82	None
Colour@520 nm	MPA-NIR	9400-5450	8	51.78	0.04	27.18	0.04	1.23	0.01	0.40	0.59	MSC
	Alpha-MIR	3660-946	9	66.39	0.04	37.41	0.04	1.27	0.01	0.48	0.63	None
	WineScan-MIR	2962-930	3	41.37	0.04	34.68	0.03	1.24	0.00	0.39	0.59	FD

LV, latent variables; R^2, coefficient of determination; RMSEE, Root mean square error of estimation; RPD, residual predictive deviation; RMSEP, root mean square error of prediction; Corr, correlation coefficient; MPA, Multi-Purpose Analyser; FD, first derivative; MSC, multiplicative scattering correction; SNV, vector normalisation

Stellenbosch University https://scholar.sun.ac.za

Table 5
Passing-Bablok regression results for comparison of three FT-IR spectrometers to predict total soluble solids. A joint test on slope and intercept values of the regression lines, at a 95% confidence level.

Alpha predicted vs MPA predicted

PASSING-BABLOK REGRESSION FIT:

	EST	SE	LCI	UCI
Intercept	-1.355235	NA	-4.2478651	0.776049
Slope	1.109038	NA	0.9559837	1.314067

Alpha predicted vs WineScan predicted

PASSING-BABLOK REGRESSION FIT:

	EST	SE	LCI	UCI
Intercept	-0.02211613	NA	-2.3246324	2.145520
Slope	1.00328970	NA	0.8524576	1.163262

MPA predicted vs WineScan predicted

PASSING-BABLOK REGRESSION FIT:

	EST	SE	LCI	UCI
Intercept	1.3147269	NA	-0.3174326	2.946960
Slope	0.9056937	NA	0.7898301	1.019244

Stellenbosch University https://scholar.sun.ac.za

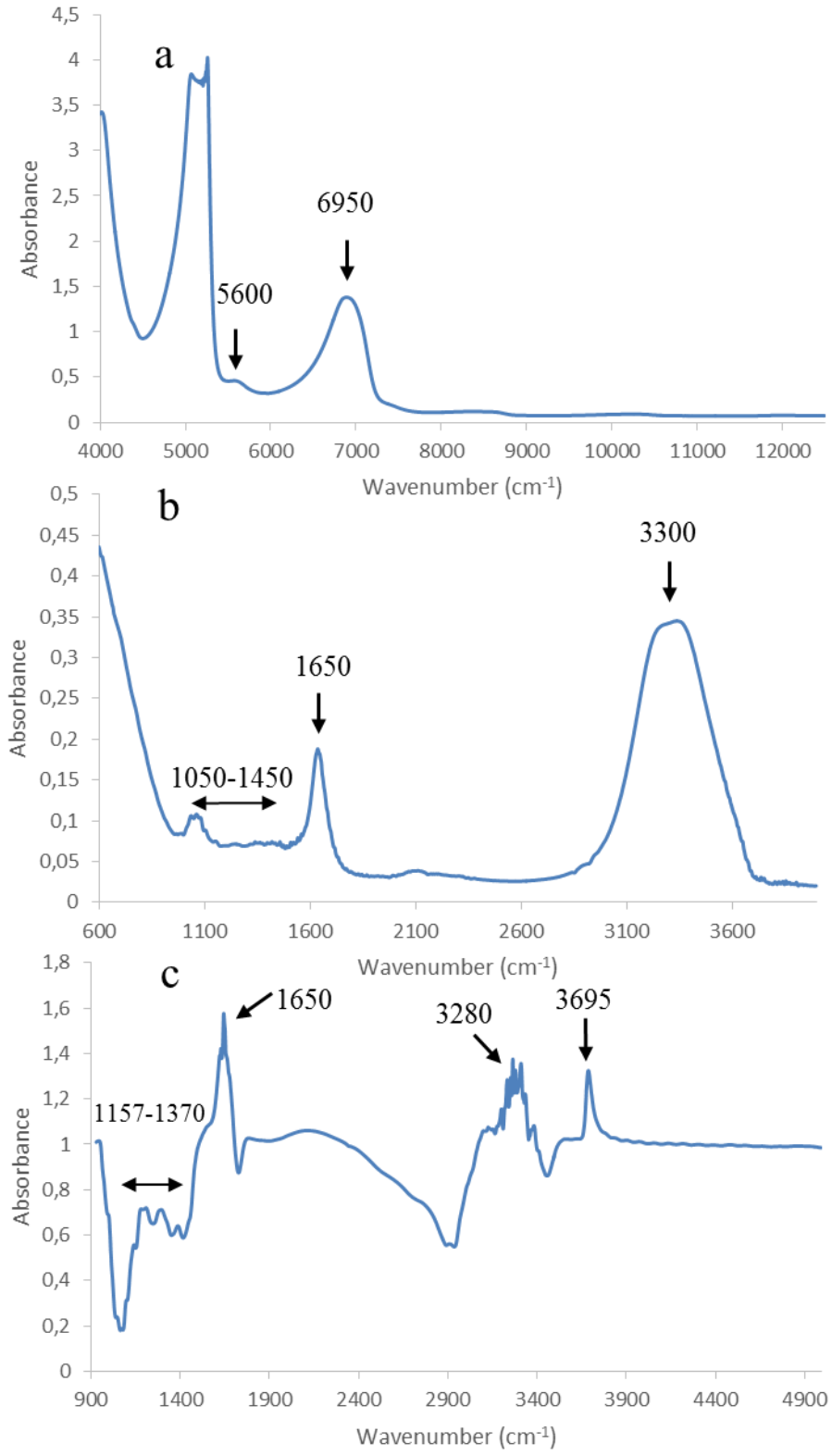

Fig. 1. Absorbance spectra of three spectrometers using MPA NIR spectra (a), Alpha MIR spectra (b) and WineScan MIR spectra (c) of pomegranate juice.

Stellenbosch University https://scholar.sun.ac.za

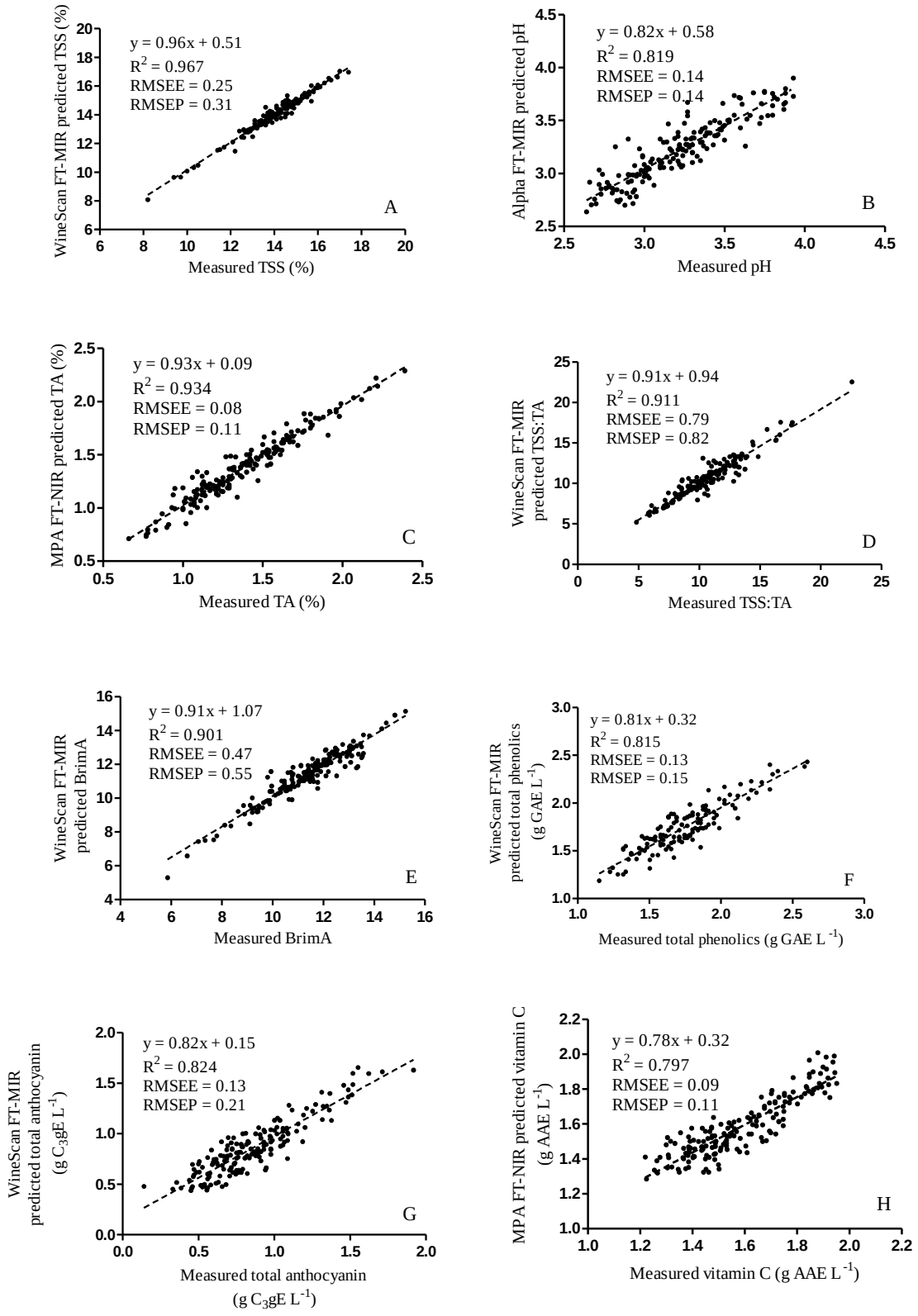

Fig. 2. Scatter plots of FT-NIR predicted TSS (A), pH (B), TA (C), TSS:TA (D), BrimA (E), total phenolic (F), total anthocyanin (G) and Vitamin C (H) plotted against destructively acquired reference data.

Stellenbosch University https://scholar.sun.ac.za

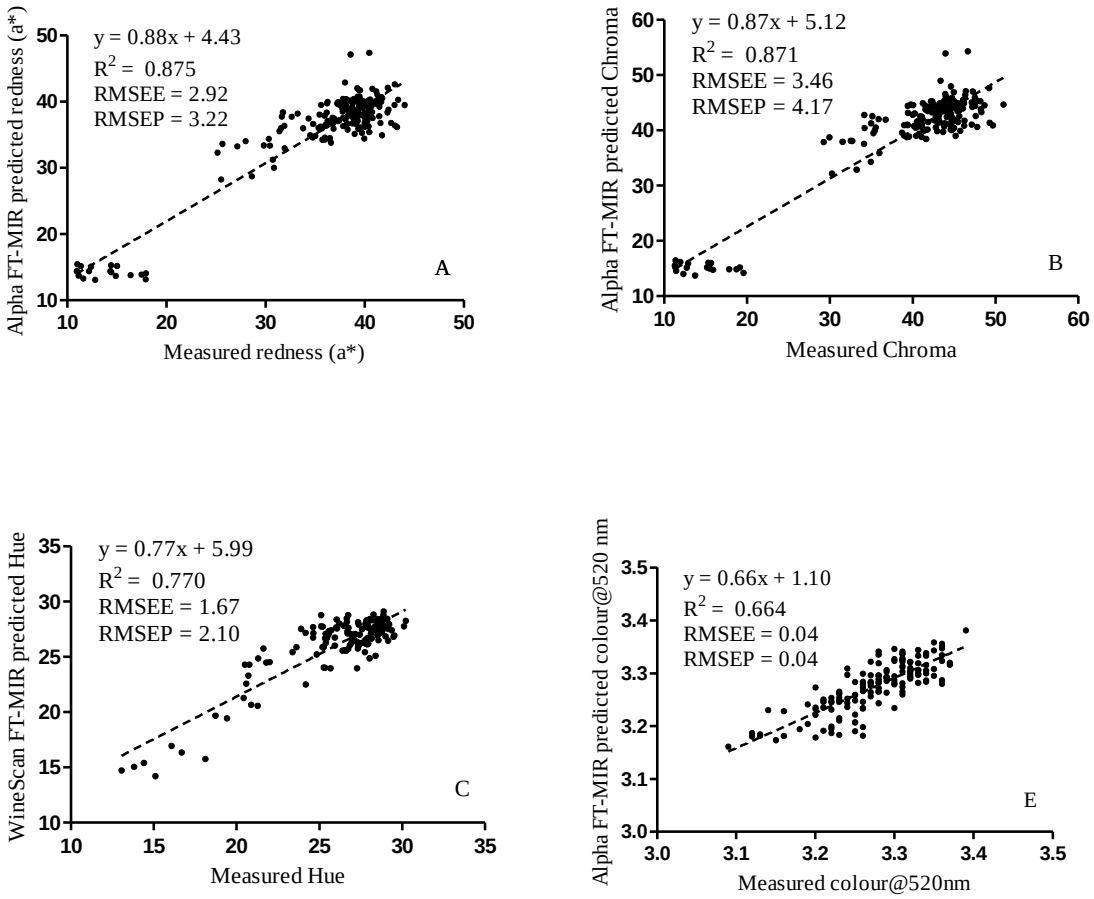

Fig. 3. Scatter plots of FT-NIR predicted colour a* (A), chroma (B), hue (C) and colour at 520 nm (D) plotted against destructively acquired reference data

Stellenbosch University https://scholar.sun.ac.za

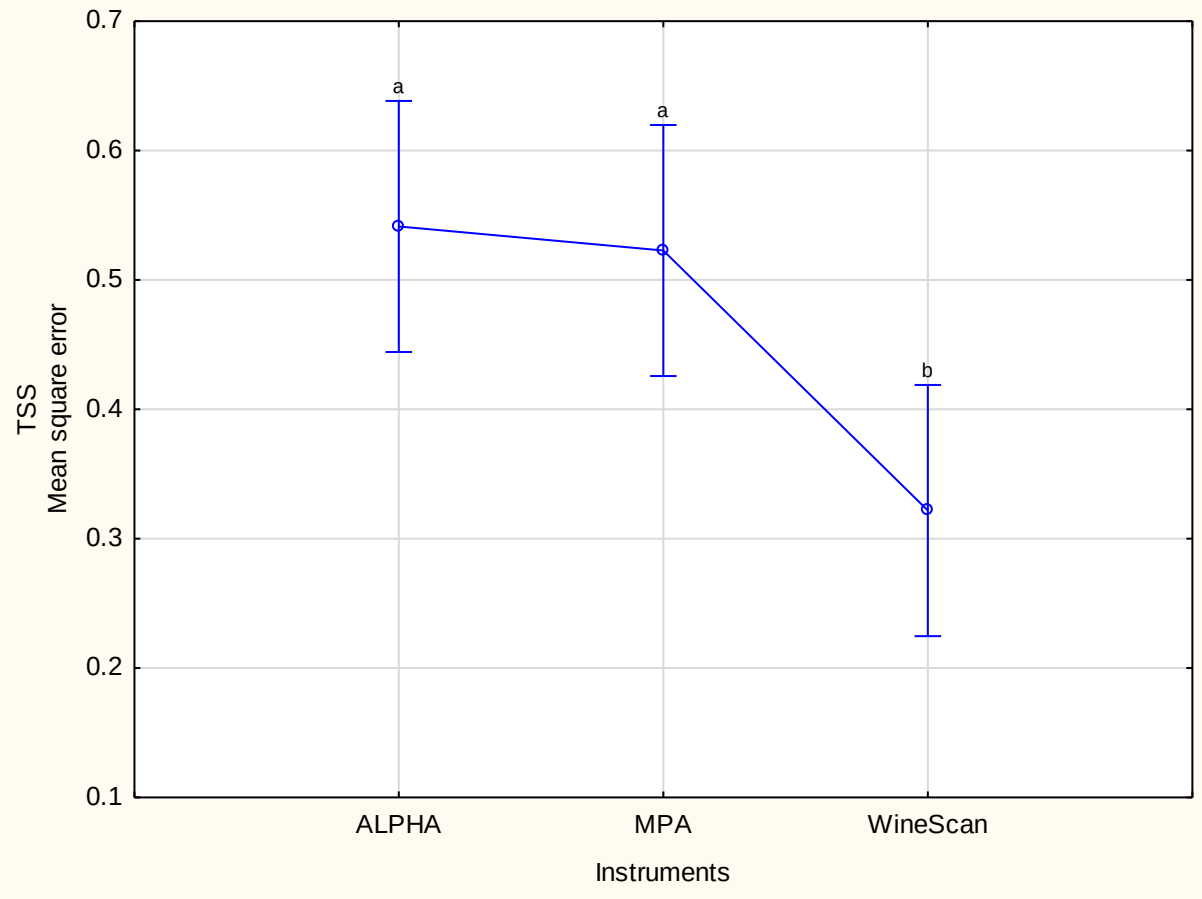

Fig.4. The estimation of repeatability and agreement between replicated data with an average mean square error between the predicted and actual values for measurement of TSS using three instruments.

Stellenbosch University https://scholar.sun.ac.za

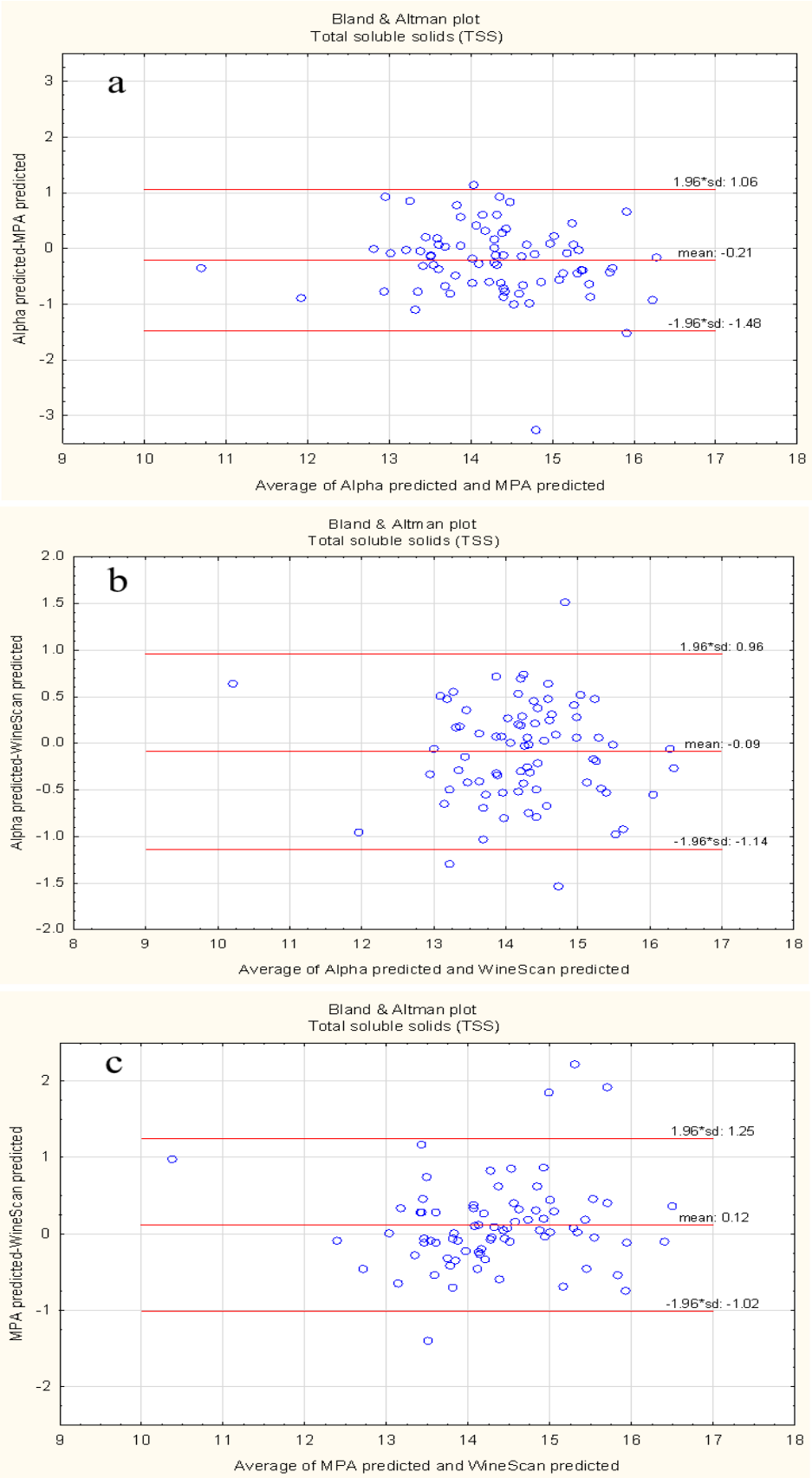

Fig. 5. Bland and Altman plot for TSS data with the representation of the limits of agreement (a) Alpha vs MPA (b) Alpha vs WineScan and (c) MPA vs WineScan

Stellenbosch University https://scholar.sun.ac.za

Section III

Chapter 7: Estimation of the density of pomegranate whole fruit and fruit fractions and detecting the presence of internal pests using X-ray computed tomography calibrated with polymeric materials[1]

Chapter 8: Evaluation of biochemical markers associated with the development of husk scald and the use of diffuse reflectance NIR spectroscopy to predict husk scald in pomegranate fruit

[1.] Journal of Food Engineering. 186: 42–49.

Stellenbosch University https://scholar.sun.ac.za

DECLARATION BY THE CANDIDATE

With regard to **Chapter 7 (pp 155-178)**, the nature and scope of my contribution were as follows:

Nature of contribution	Extent of contribution (%)
Research, data collection, analysis, writing of chapter and final approval of the published version	70

The following co-authors have contributed to **Chapter 7 (pp 155-178),**

Name	e-mail address	Nature of contribution	Extent of contribution (%)
Prof U.L. Opara	opara@sun.ac.za	Conception of the work, editorial suggestion, proof reading and final approval of the published version	15
Dr O.A. Fawole	olaniyi@sun.ac.za	Research input, editorial suggestion, proof reading and final approval of the published version	10
Dr L.S. Magwaza	Magwazal@ukzn.ac.za	proof reading and final approval of the published version	5

Stellenbosch University https://scholar.sun.ac.za

E Arendse **Signature of candidate**	29/08/2017 **Date**

DECLARATION BY CO-AUTHORS

The undersigned hereby confirm that:

1. the declaration above accurately reflects the nature and extent of the contributions of the candidate and the co-authors to **Chapter 7 (pp 155-178)**

2. no other authors contributed to **Chapter 7 (pp 155-178)** besides those specified above, and

3. potential conflicts of interest have been revealed to all interested parties and that the necessary arrangements have been made to use the material in **Chapter 7 (pp 155-178)** of this dissertation.

Signature	Institutional affiliation	Date
Prof U.L. Opara	Stellenbosch University	29/08/2017
Dr O.A. Fawole	Stellenbosch University	29/08/2017
Dr L.S. Magwaza	University of KwaZulu-Natal	29/08/2017

Stellenbosch University https://scholar.sun.ac.za

CHAPTER 7

Estimation of the density of pomegranate whole fruit and fruit fractions and detecting the presence of internal pests using X-ray computed tomography calibrated with polymeric materials

Abstract

This study investigated the application of microfocus X-ray computed tomography (µCT) to quantity pomegranate fruit fractions (albedo and arils) and detect the presence of false codling moth and blackheart disease in inside fruit. A commercial microfocus X-ray (µCT) system in combination with image analysis techniques was used to generate two-dimensional (2-D) radioscopic images which were reconstructed into three dimensional (3-D) images. Optimum µCT settings were obtained using an isotropic voxel size of 71.4 µm based on a radiation source generated from a voltage of 100 kV with the electric current set at 200 µA. The density of whole pomegranate fruit, its fractions (arils and albedo), and portions affected by false codling moth and blackheart were successfully determined within the calibration range. Furthermore, the density of larva moth (9400 ±40 kg m^{-3}) was found to be significantly ($p < 0.0001$) lower than whole fruit (1070 ±20 kg m^{-3}) and fruit fractions (arils 1120 ±40 kg m^{-3} and albedo 1040 ±30 kg m^{-3}). Similarly, healthy fruit and those affected by blackheart disease were successfully classified within the calibration range. The density of healthy fruit (1070 ±20 kg m^{-3}) was significantly ($p < 0.0001$) higher than that of fruit affected by blackheart (870 to 1000 kg m^{-3}). These results demonstrated that X-ray µCT with an associated algorithm can be used to accurately detect and classify internal defects due to the presence of false codling moth and blackheart disease in pomegranate fruit.

Keywords: *Punica granatum* L., False codling moth, Blackheart, Polymers, Image analysis, Image segmentation; Internal Quality

1. Introduction

Pomegranate (*Punica granatum* L.) is an emerging fruit within the global export industry. The fruit has been long valued for its high nutritional content and potent pharmacological and antioxidant properties (Lansky & Newman, 2007; Viuda-Martos *et al*., 2010). The rising consumer interest has spurred a global increase in production and marketing of pomegranate

Stellenbosch University https://scholar.sun.ac.za

fruit (Fawole & Opara, 2013a). Less than 10% of world commercial pomegranate production occurs in the Southern Hemisphere, and South Africa is one of the few producers in the Southern Hemisphere, competing with Chile and Peru to fill the counter season window during spring and early summer months in Northern Hemisphere (Fawole & Opara, 2013a, b). Consequently, this has encouraged large scale production to increase exports of pomegranate fruit allowing producers in the Southern Hemisphere to fill the counter season export opportunity. However, pomegranates are a fruit that is particularly susceptible to pest and disease infestations (Holland *et al*., 2009). One pest, the false codling moth (FCM) (*Thaumatotibia leucotreta*) is endemic, in parts of Africa such as Ethiopia, Madagascar, Senegal, Ivory Coast, Southern Africa, and has been found in the islands of the Atlantic and Indian Oceans such as Mauritius (Newton, 1998; Carpenter *et al*., 2007). FCM has been reported to cause loss of entire pomegranate orchards within South Africa (Wohlfarter *et al*., 2010). The FCM feeds on a wide range of cultivated crops including deciduous, subtropical and tropical fruits (Stotter & Terblanche, 2009; Manrakhan *et al*., 2014). The adult female FCM lays its eggs on the fruit surface and emerging larvae penetrate and feed inside the fruit leading to fruit decay, premature ripening and abscission or fruit drop (Newton, 1998). Furthermore, FCM can enter through the crown/calyx of the fruit and pomegranate fruit can harbour FCM till maturity making it extremely difficult to detect.

Blackheart, also known as heart rot, is a major disease impacting the production of pomegranate fruit worldwide (Kader, 2006). Although blackheart is recognised as a postharvest quality problem, infection begins during fruit growth in an orchard. In blackheart infection, *Alternaria* spp. and *Aspergillus* spp. have been reported as the major pathogens (Caleb *et al*., 2012; Yehia, 2013; Munhuweyi *et al*., 2016). These pathogens enter the fruit during the bloom and early fruit set, grow and spread as affected fruit develops (Zhang & McCarthy, 2012; Arendse *et al*., 2015). These fungi cause a mass of blackened arils within the fruit ranging from sections of the pomegranate fruit to all the arils within the rind without external symptoms (Kader, 2006). The lack of external symptoms on blackheart infected pomegranate fruit is a major challenge for sorters in the packinghouse or processing lines. Furthermore, the occurrence of FCM and blackheart within pomegranate fruit are dependent the cultivar, climate and agricultural practices (Carpenter *et al*., 2007). Pomegranate fruit, destined for the export market, are subjected to stringent inspection for any pest or diseases that are detected during inspection would result in rejection of total fruit consignments resulting in huge financial losses for producers and the export industry. For the South African pomegranate industry to supply

Stellenbosch University https://scholar.sun.ac.za

high quality fruit without internal defects to consumers and processors, an alternative non-destructive technology is required to assist in discrimination of fruit into different quality tiers.

Microfocus X-ray computed tomography (µCT) is a non-destructive technique that measures the variation in density and it is principally based on the attenuation of X-rays which depends on mass density and mass absorption coefficient of the irradiated object (Maire *et al*., 2001; Salvo *et al*. 2003). Therefore, X-ray attenuation for a particular material is approximately proportional to its density (Guelpa *et al*., 2015). The advantage of the X-ray µCT technique is that it allows reproduction of high resolution three dimensional (3-D) visualisation and analysis of microstructures without sample preparation or chemical fixation (Léonard *et al*, 2008; Magwaza & Opara, 2014; Guelpa *et al*., 2015). X-ray µCT has been applied for the measurement of density variation in various materials including pharmaceutical tablets (Sinka *et al*., 2004), commercial plastics (du Plessis *et al*., 2013) and wood pieces (Meincken & du Plessis, 2013). Furthermore, the analysis and 3-D reconstruction and visualisation for internal characterisation and defect detection of different horticultural produce have been intensively researched and reviewed (Mendoza *et al*., 2007; Nicolaï *et al*., 2009; Donis-González *et al*., 2014; Kotwaliwale *et al*., 2014; Magwaza & Opara, 2014). Several studies have been focused on the use of µCT for determining the absolute density using a density calibration function (du Plessis *et al.*, 2013; Guelpa *et al*., 2015). A recent study by Guelpa *et al*. (2015) on whole maize (*Zea mays* L.) kernels demonstrated that µCT has the potential to differentiate between kernel hardness using a density calibration function. Similarly, du Plessis *et al*. (2013), assessed the accuracy and repeatability associated with the use of absolute density values for commercial plastics. The authors reported that the absolute density could be successfully determined within the calibration range of different homogenous polymeric materials with relatively low standard error and variation occurring over time.

In Chapter three, µCT was successfully used to characterised and quantify pomegranate fruit fractions. However, volume segmentation based on grey values for pomegranate fruit and its fractions was very difficult and time consuming. Therefore, a calibration function was considered within this chapter. The use of a linear transformation would allow us to characterise fruit based on its actual density and separate fruit based on its weight, allowing for a more industrial reliable method which would be faster than volume estimation due to problems associated with manual thresholding. Additionally, the use of a calibration function would allow for the identification of internal disorders associated with pomegranate fruit. This research is the first application of the technique using a density calibration function to detect internal disorders in fresh fruit. The objectives of this study were to (1) investigate the potential

Stellenbosch University https://scholar.sun.ac.za

of using µCT to differentiate fruit fractions and detect the presence of false codling larva moth in pomegranate fruit (cv. Herskawitz) and (2) identify pomegranate fruit (cv. Wonderful) affected by blackheart disease for classification purposes.

2. Materials and Methods

2.1. *Fruit sampling*

Historical orchard production units code (PUC) was used to identify orchards affected with false codling moth and blackheart disorder in the Western Cape Province, South Africa. During the 2015 season, pomegranate (cv. 'Wonderful' and cv. 'Herskawitz') were procured from Sonlia Pack-house (33°34′851″S, 19°00′360″E) in Western Cape region, South Africa. A total of 60 fruits was used (5 healthy, 10 containing codling larva moth, 25 blackheart). Average of 4 to 6 fruit were used per blackheart index. In addition, fruit without any external damage were selected and transported to the Postharvest Technology Research Laboratory at Stellenbosch University. Thereafter, fruit were equilibrated at ambient conditions (23 ±3 °C) prior non-destructive scanning.

2.2. *Polymeric materials used for density calibration*

The calibration function used was adopted as reported by du Plessis *et al*. (2013). Polymeric materials of different homogenous densities used for calibration standards were obtained from Maizey Plastics (Cape Town, South Africa). These polymeric materials included the following ultra-high molecular weight polyethylene (UHMW PE) (920 kilogram per cubic metre (kg m^{-3})), polytetrafluoroethylene (PTFE) (2150 kg m^{-3}), sustanat polycarbonate (PC) (1200 kg m^{-3}) polypropylene (PP) (910 kg m^{-3}), high density polyethylene (HDPE) (910 kg m^{-3}), polyethylene terephthalate (PET) (1380 kg m^{-3}) and sustarin C acetal/nylon (1150 kg m^{-3}) (du Plessis *et al*., 2013; Guelpa *et al*., 2015). These polymers disks were 10 millimetre (mm) in thickness and 25 mm in diameter and the density of these calibration polymers ranged from 910 to 2150 kg m^{-3}.

2.3. *Microfocus X-ray computed tomography*

X-ray µCT scans were acquired using a commercial microfocus X-ray µCT system (V|Tome|X L240, General Electric Sensing & Inspection Technologies GmbH, Phoenix, Germany) which was integrated with Phoenix acquisition and reconstruction software (Datos|x® 2.2, General Electric Sensing & Inspection Technologies GmbH, Phoenix, Germany). The sample distance from the X-ray source and detector influence the amount of X-ray radiation reaching the

Stellenbosch University https://scholar.sun.ac.za

detector and therefore affects the calibration function. The polymer discs were stacked on each other and placed on floral foam, along with pomegranate fruit. Pomegranate fruit and polymer disks could therefore easily be distinguished from the florist oasis due to the low density of the mounting material. Pomegranate samples, polymeric disks and mounting material were fixed onto a specimen stage at a physical distance of 250 mm from the X-ray radiation source and 700 mm from the detector with a scanning resolution of 71.4 micrometre (µm). In this study, CT settings were first optimised using an isotropic voxel size of 71.4 µm based on a radiation source generated from a voltage of 100 kilovolt (kV) with the electric current set at 200 microampere (µA). Two dimensional (2-D) X-ray projection images were acquired at 250 ms per image, attaining 3100 images in one 360 º stepwise rotation of the sample along the axis, perpendicular to the beam direction. Throughout, X-ray µCT scanning phase pomegranate fruit were scanned concurrently with the polymeric discs to facilitate calibration and direct comparison of different scans. Total scanning time for each sample was approximately 1 h.

2.4. *Data processing and image analysis*

A series 16-bit greyscale tagged image files (Tiff) were imported and reconstructed into a three-dimensional (3-D) image using Datos|x® 2.2 reconstruction software. X-ray µCT image processing and analysis were performed using volume graphics software (VG Studio Max 2.2 software, Heidelberg, Germany). The procedure for 3-D image reconstruction contains filtered back algorithms and the grey values in each µCT image represent the attenuation in each pixel (Guelpa *et al*., 2015). Thereby, using µCT, the obtained grey values would, therefore, depend on the densest object in the scan volume (PTFE polymeric disc with a density of 2150 kg m^{-3}). The average grey values were obtained from Studio Max 2.2 software, with the density being calculated using the calibration function.

The density was calculated by using the average sum of grey values obtained from 2-D images for each component. This was accomplished by applying an adaptive segmentation algorithm based on the grey level frequency from 4,000 to 60,000 was applied (Arendse *et al*., 2016). The first step in data processing was to reduce random noise using the Gaussian filtered method. Background pixels (i.e. surrounding air) was removed before image analysis could occur. Fruit and polymer disks were then separated from the background using an appropriate threshold of grey values averaging a tolerance ranging from 234 to 5,548 for external air (Fig 1). In order to non-destructively estimate the density, the ellipse function was used to determine the average grey values of each polymeric disk. Each voxel related to a sample had an associated grey value dependent on the samples atomic weight and density. Therefore, the

Stellenbosch University https://scholar.sun.ac.za

average grey values of each homogeneous polymer disc is consequently a measure of its density. The average grey values for whole fruit were 35,047 ±2,432, total arils were 36,027 ±2,638, albedo were 34,136 ±2,353 and codling larva moth were 32,552 ±2,193. In order to obtain a calibration function, a linear function was used to calculate the density (Eq. 1) (Guelpa *et al*., 2015).

$$\text{Density} = m \times \text{grey value} + c \quad (1)$$

where m is the slope and c is the intercept.

Examples of a linear calibration function for different polymeric materials are presented in Fig. 2.

The removal of calibration polymers was required before image analysis could occur. This was done by application of surface fitting function followed by the procedure of opening in order to determine the perimeter of the polymers before small specks of noise was removed by the procedure of erosion and dilation. A representative 2-D sliced image for analysis and segmentation of fruit fractions and differentiation of larva moth in pomegranate fruit are shown in (Fig. 3). The first step in image analysis was to determine the volume and grey values for the whole fruit (Fig. 3a). In order to distinguish and extract false codling moth from pomegranate fruit, a surface extraction process was applied. Surface determination of the larva moth was performed using adaptive thresholding with the region of interest (ROI). The advance mode was activated from surface determination and the surface of the larva moth was investigated for the sharpest slope in order to calculate the material boundary in sub-voxel accuracy defined by one grey value. The advanced surface determination is a re-evaluation of the material boundary defined by adapted grey values from the ROI. The advanced surface determination compensates for deviations created from beam hardening or artefacts by reconstructing the component geometry more closely compared to the standard surface determination. Thereafter, segmentation was applied and the larva moth was assigned a green colour in order to extract the larva moth (Fig. 3b). The next step in image analysis was to determine the volume and grey values of arils. This was accomplished first by manual segmentation and application of surface determination using the advanced tab function which investigates the sharpest slope to ensure that the surface of the arils is accurately defined (Fig. 3c). After aril extraction, albedo volume and grey values were determined by applying a perimeter to its surface using surface determination (Fig. 3d). Any remaining artefacts were removed using the procedure of erosion and dilation. Figure 4 shows a 2-D image slice (Fig.4a)

Stellenbosch University https://scholar.sun.ac.za

and 3-D model of larva moth reconstructed by appropriately stacking floating image slices (Fig. 4b).

A representative 2-D sliced image for analysis of healthy and blackheart fruit in pomegranate cv. Wonderful are shown in (Fig. 5). In healthy fruit, the X-ray CT image shows the arils as uniformly light-grey area (Fig. 5a). However, in blackheart fruit (Fig. 5b), X-ray CT images revealed arils were partially or fully damaged as evidenced by dark areas corresponding to the disintegrated aril tissue. Furthermore, the darker area within the blackheart fruit represents less dense regions, therefore, an increase in the severity of blackheart may result in a decrease in fruit density. Reconstruction of 2-D data was performed to produce 3-D models of blackheart fruit (Fig.5). A 3-D clipping image of fruit affected with blackheart (Fig. 5c), and 3-D clipping image based on density showing whole fruit assigned with a red colour while internal air was assigned a green colour (Fig. 5d). Once the algorithm was developed for a single data set, it was automatically used to determine the density of the rest of the sample set.

2.5. *Validation of X-ray µCT data*

Validation of pomegranate fruit, its fractions (arils and albedo), false codling moth and blackheart fruit was achieved by comparing predicted and measured (actual) masses. Density is generally calculated by measuring the volume of the object using liquid displacement method based on Archimedes' Principle (Lang & Thorpe, 1989). However, if the volume of the sample is too complex to determine experimentally, it is therefore possible to calculate the density of the sample by quantifying the volume of the 3-D object from the µCT data and thereby calculating its mass from the CT determined density and the CT determined volume (du Plessis *et al*., 2013). In order to validate the density calibration developed using non-destructive µCT, each fruit was first weighed using an electronic scale (Mettler Toledo, Switzerland, 0.01 g). Fruit were manually cut opened, inspected for larva moth and separated into fractions (albedo and arils), each fruit fraction and larva moth was weighted respectively (Fig. 6). The mass (g) obtained from the destructive measurements were compared to the estimated masses (Gustin *et al*., 2013). By analysing µCT data for each fruit, the mass (g) of whole fruit, albedo, arils and larva moth was calculated from the volume (cm^3) using volume analysis tool (VG Studio Max 2.2). In addition, the density was acquired from the µCT images using the density calibration function. The mathematical relationship between mass, volume and density was used to calculate the predicted masses.

Stellenbosch University https://scholar.sun.ac.za

For blackheart, fruit samples used for the scanning experiment were manually cut open and inspected (Fig. 7). The severity of blackheart was evaluated subjectively using a scale, where 0 = none; 1 = ≤ 25%; 2 = between 26 and 50%; 3 = between 51 and 75%; 4 = > 75%. The severity of blackheart infected fruit was compared to their respective absolute density obtained from the µCT images.

2.6. *Statistical analysis*

The comparison between estimated µCT data and destructive measurements were subjected to paired t-test (p = 0.05) using Statistica software (Statistica version 10, StatSoft Inc., Tulsa, OK, USA). One-way analysis of variance (ANOVA) was used to evaluate the difference in density. The difference between mean values of parameters was investigated using Duncan's Multiple Range Test.

3. Results

3.1. *False codling larva (FD larva)*

After data processing and image analysis, densities of whole pomegranate fruit, arils, albedo and larva moth were determined (Table 1). µCT technique in combination with calibration polymers and image analysis technique determined highly significantly ($p < 0.0001$) different densities for fruit parts of interest and FD larva (whole fruit = 1070 ±20 kg m^{-3}, arils = 1120 ±40 kg m^{-3}, albedo = 1040 ±30 kg m^{-3} FD larva = 940 ±40 kg m^{-3}). The average density of FD larva was found to be lower than those of the whole fruit and fruit fractions. Furthermore, the arils had the highest density compared to albedo and whole fruit. This may be due to the seed within the arils which appeared to be denser on X-ray µCT images.

Validation of density was done by comparing µCT estimated values with the measured mass. The results obtained from µCT showed on average predicted the mass of albedo and arils occupied 104.73 ±14.56 g and 153.42 ±34.58 g, which are respectively estimated to be 40 and 59% of the total pomegranate fruit mass (259.84 ±36.90 g). The predicted average mass of the FD larva moth was estimated to be 0.030 ±0.01 g. The destructive mass measurements were in similar range to the predictive data with albedo and arils being 102.30 ±11.66 g and 159.06 ±33.09 g, corresponding to 39% and 61% of the total fruit mass. The use of destructive methods showed similar mass values (0.031 ±0.01 g) for FD larva moth. The results for the proportion of non-edible (albedo) and edible (arils) fractions were in the similar range to those reported by Fawole and Opara (2014) for 'Herskawitz' cultivar at harvest maturity in 2012 season Western Cape region, South Africa. The results in Table 1 showed that the mass of whole fruit,

Stellenbosch University https://scholar.sun.ac.za

arils and FD larva moth were overestimated by an average of 0.69, 3.54 and 1.61%, respectively, while albedo was underestimated by 2.38%. The low residual values confirmed that the two methods were very similar, indicating the accuracy of X-ray μCT. Furthermore, the results from the paired t-test showed no significant difference between μCT predicted and destructively measured mass for whole fruit, albedo, arils and FD larva moth. Therefore, this study confirmed that μCT is capable of differentiating between FD larva moth and pomegranate fractions (albedo and arils) by developing a density calibration function from polymers. Furthermore, it was observed from X-ray μCT predicted and destructive values that 10 fruit from a batch of 30 contained false codling moth larva. The consequences of a high percentage of affected fruit by false codling moth larva may result in the introduction of these damaging pest into exporting countries with the potential of affecting other orchards and crops resulting in huge financial losses for growers and exporters.

3.2. *Blackheart*

The results showing the density of healthy fruit and blackheart infested fruit are presented in Table 2. The use of μCT combined with calibration polymers and image analysis technique predicted the density for healthy fruit being (1070 ±20 kg m^{-3}) and blackheart infested fruit ranged from (870-1000 kg m^{-3}). The density of healthy fruit was found to be higher compared to blackheart infected fruit (Table 2). A decrease in density was observed with an increase in the severity of blackheart infestation. Furthermore, significant differences were mainly observed between the density of healthy and blackheart fruit that constituted greater than 75% blackheart infestation.

The results for the predicted and actual measured mass are presented in Table 3. The average mass of X-ray μCT predicted of healthy fruit was higher (400.70 ±4.50 g) than that of blackheart infected fruit (356.28 ±44.08 g). The actual measured mass of healthy and blackheart fruit was in the similar range to μCT predicted data which was 402.50 ±2.69 g and 360.50 ±46.81 g, respectively. The results indicated that the mass of healthy and blackheart fruit were overestimated by 0.44 and 1.17%, respectively. The relevance of this to fruit mass is that with an increase in the severity of blackheart the less dense fruit become and hence the lighter fruit weight. Furthermore, no significant differences ($p > 0.05$) were observed between the predicted and actual weight measurements. Due to the low residual values and non-significant difference observed between the two methods suggest that the two methods were very similar in accuracy. Previous work suggests that μCT has been shown to be highly accurate in detecting and quantifying foreign material and defects in various agricultural

Stellenbosch University https://scholar.sun.ac.za

produce (Lammertyn *et al*., 2003a; Lammertyn *et al*, 2003b; Lim & Barigou, 2004; Haff & Slaughter, 2004; Haff & Toyofuku, 2008; Kotwaliwale *et al*., 2014). Therefore this study confirmed that μCT has the potential to differentiate between healthy and blackheart infected fruit in pomegranate cv. Wonderful based on absolute density.

From a scientific viewpoint, the application of non-destructive discriminative power of X-ray μCT combined with image analysis and homogenous polymeric materials could successfully differentiate densities in tissues and detect internal disorders such as pest or disease infestation including internal defects associated with physiological disorders. Furthermore, results reported in the present study showed that the developed algorithm could be successfully used to quantify different proportions of the fruit. Considering that the edible proportion of pomegranate fruit varies depending on the variety it may account for less than 50% of the fruit weight. Therefore, X-ray μCT as a non-destructive technique could be helpful to identify cultivars suitable for marketing either a whole fruit or processed into arils. Considering pomegranates are non-climacteric it would be interesting in future studies to assess the accuracy of X-ray μCT to classify fruit based on changes during fruit growth and maturation. Despite its potential as a non-destructive tool X-ray μCT is only available to researchers for experimental purposes. However, with steady improvements in instrumentation design and computational power, it is expected that the application of X-ray μCT for commercial in-line or real-time inspection systems would become more field-worthy in times to come.

4. **Conclusions**

This study has demonstrated that the use of X-ray μCT with a calibration function of polymers and image analysis could non-destructively identify and differentiate between internal disorders such as false codling larva moth, blackheart and pomegranate fruit fractions based on absolute density. Furthermore, X-ray μCT as a non-destructive technique has shown to be highly accurate with similar mass for predicted and actual measurements. Additionally, optimising fruit parts such as aril yield is a desirable property for growers, breeders and processors and therefore understanding and non-destructively predicting their relative distribution between the edible and non-edible portion with regards to the total mass is pertinent. However, the drawback of using X-ray μCT is its considerable large equipment size, harmful effects of X-rays radiation for operators and large data set and lengthy processing time required for analysis. Additionally, health and safety issues may arise from using an open X-ray μCT system for the industrial application due to escape or leak out of X-ray radiation,

Stellenbosch University https://scholar.sun.ac.za

creating a health hazard. Although, this provides novel opportunities that warrant further research in properly designed shielding can prevent human exposure, reducing large data size and image analysis in order to provide rapid real-time non-destructive detection of internal defects.

References

Arendse, E., Fawole, O.A. & Opara, U.L. (2015). Effects of postharvest handling and storage on physiological attributes and quality of pomegranate fruit (*Punica granatum* L.): A review. *International Journal of Postharvest Technology and Innovation*, **5**, 13–31.

Arendse, E., Fawole, O.A., Magwaza, L.S. & Opara, U.L. (2016). Non-destructive characterization and volume estimation of pomegranate fruit external and internal morphological fractions using X-ray computed tomography. *Journal of Food Engineering*, **186**, 42–49.

Caleb, O.J., Opara, U.L. & Witthuhn, C.R. (2012). Modified atmosphere packaging of pomegranate fruit and arils: A Review. *Food and Bioprocess Technology*, **5**, 15–30.

Carpenter, J., Bloem, S. & Hofmeyer, H. (2007). Area-Wide Control Tactics for the False Codling Moth *Thaumatotibia leucotreta* in South Africa: a Potential Invasive Species. In: *Area Wide Control of Insect Pest* (edited by M.J.B. Vreysen, A.S. Robinson & J. Hendrichs). Pp.351–359. Springer Netherlands.

Donis-González, I.R., Guyer, D.E., Pease, A. & Barthel, F. (2014). Internal characterisation of fresh agricultural products using traditional and ultrafast electron beam X-ray computed tomography imaging. *Biosystems Engineering*, **117**, 104–113.

du Plessis, A., Meincken, M. & Seifert, T. (2013). Quantitative determination of density and mass of polymeric materials using microfocus computed tomography. *Journal of Non-destructive Evaluation*, **32**, 413–417.

Fawole, O.A. & Opara, U.L. (2013a). Harvest discrimination of pomegranate fruit: postharvest quality changes and relationships between instrumental and sensory attributes during shelf life. *Journal of Food Science*, **78**, 1264–1272.

Fawole O.A. & Opara U.L. (2013b). Effects of storage temperature and duration on physiological responses of pomegranate fruit. *Industrial Crops and Products*, **47**, 300–309.

Fawole, O.A. & Opara, U.L. (2014). Physico-mechanical, phyto-chemical and free radical scavenging properties and volatile compounds in eight pomegranate cultivars and

Stellenbosch University https://scholar.sun.ac.za

classification by principle component and cluster analyses. *British Food Journal*, **116**, 544–567.

Guelpa, A., du Plessis, A., Kidd, M. & Manley, M. (2015). Non-destructive estimation of maize (*Zea mays* L.) kernel hardness by means of an X-ray micro-computed tomography (µ CT) density calibration. *Food Bioprocess Technology*, **8**, 1419–1429.

Gustin, J.L., Jackson, S., Williams, C., Patel, A., Armstrong, P.R. & Peter, G.F. (2013). Analysis of maize (*Zea mays*) kernel density and volume using micro-computed tomography and single-kernel near infrared spectroscopy. *Journal of Agricultural and Food Chemistry*, **61**, 10872–10880.

Haff, R.P. & Slaughter, D.C. (2004). Real-time X-ray inspection of wheat for infestation by the granary weevil, *Sitophilus granarius* (L.). *Transactions of the American Society of Agricultural Engineers*, **47**, 531–537.

Haff, R.P. & Toyofuku, N. (2008). X-ray detection of defects and contaminants in the food industry. *Sensing and Instrumentation for Food Quality and Safety*, **2**, 262–273.

Holland, D., Hatib, K. & Bar-Ya'akov, I. (2009). Pomegranate: Botany, Horticulture, Breeding. In: *Horticultural Reviews* (edited by J. Janick). Pp. 127–191. John Wiley & Sons, Inc.

Kader, A.A. (2006). Postharvest Biology and Technology of Pomegranates. In: *Pomegranates: Ancient Roots to Modern Medicine* (edited by N. P. Seeram, R. N. Schulman & D. Heber). Pp. 211–220. CRC Press, Boca Raton, FL.

Kotwaliwale, N., Singh, K., Kalne, A., Jha, S. N., Seth, N. & Kar, A. (2014). X-ray imaging methods for internal quality evaluation of agricultural produce. *Journal of Food Science and Technology*, **51**, 1–15.

Maire, E., Salvo, L., Blandin, J.J., Ludwig, W. & Létang, J.M. (2001). On the application of X-ray microtomography in the field of material science. *Advanced Engineering Materials*, **3**, 539–546.

Magwaza, L.S. & Opara, U.L. (2014). Investigating non-destructive quantification and characterization of pomegranate fruit internal structure using X-ray computed tomography. *Postharvest Biology and Technology*, **95**, 1–6.

Manrakhan, A., Daneel, J.H. & Moore, S.D. (2014). The impact of naturally occurring entomopathogenic nematodes on false codling moth, *Thaumatotibia leucotreta* (Lepidoptera: Tortricidae), in citrus orchards. *Biocontrol Science and Technology*, **24**, 241–245.

Stellenbosch University https://scholar.sun.ac.za

Meincken, M. & du Plessis, A. (2013). Visualising and quantifying thermal degradation of wood by computed tomography. *European Journal of Wood and Wood Products*, **71**, 387–389.

Mendoza, F., Verboven, P., Mebatsion, H.K., Kerckhofs, G., Wevers, M. & Nicolaï, B. (2007). Three-dimensional pore space quantification of apple tissue using X-ray computed microtomography. *Planta*, **226**, 559–570.

Munhuweyi, K., Lennox, C.L., Meitz-Hopkins, J.C., Caleb, O.J. & Opara, U.L. (2016). Major diseases of pomegranate (*Punica granatum*, L.), their causes and management—A review. *Scientia Horticulturae*, **211**, 126–139.

Newton, P.J. (1998). False codling moth, *Cryptophlebia leucotreta* (Meyrick). In: *Citrus pests in the Republic of South Africa* (edited by E.C.G. Bedford, M.A. Van Den Berg & E.A. De Villiers). Pp. 192–200. Nelspruit: Agricultural Research Council, Republic of South Africa.

Nicolaï, B.M., Bulens, I., De Baerdemaker, J., De Ketelaere, B., Hertog, M.L.A.T.M., Verboven, P., & Lammertyn, J. (2009). Non-destructive evaluation: detection of external and internal attributes frequently associated with quality and damage. In: *Postharvest Handling: A Systems Approach* (edited by W.J. Florkowiski, R.L. Shewfelt, B. Brueckner & S.E. Prussia). Pp. 421–442. Academic Press, Elsevier, Amsterdam.

Lammertyn, J., Jancsok, P., Dresselaers, T., Van Hecke, P., Wevers, M., De Baerdemaeker, J. & Nicolaï, B.M. (2003a). Analysis of the time course of core breakdown in 'Conference' pears by means of MRI and X- ray CT. *Postharvest Biology and Technology*. **29**, 19–28.

Lammertyn, J., Dresselaers, T., Van Hecke, P., Jancsok, P., Wevers, M. & Nicolaï, B.M. (2003b). MRI and X-ray CT study of spatial distribution of core breakdown in "Conference" pears. *Journal of Magnetic Resonance Imaging*, **21**, 805–815.

Lang, A. & Thorpe, M.R. (1989). Xylem, phloem and transpiration flows in a grape: Application of a technique for measuring the volume of attached fruits to high resolution using Archimedes' Principle. *Journal of Experimental Botany*, **40**, 1069–1078.

Lansky, E.P. & Newman, R.A. (2007). *Punica granatum* (pomegranate) and its potential for prevention and treatment of inflammation and cancer. *Journal of Ethnopharmacology*, **109**, 177–206.

Stellenbosch University https://scholar.sun.ac.za

Léonard, A., Blacher, S., Nimmol, C. & Devahastin, S. (2008). Effect of far-infrared radiation assisted drying on microstructure of banana slices: an illustrative use of X-ray micro tomography in microstructural evaluation of a food product. *Journal of Food Engineering*, **85**, 154–162.

Lim, K.S. & Barigou, M. (2004). X-ray micro-computed tomography of cellular food products. *Food Research International*, **37**, 1001–1012.

Salvo, L., Cloetens, P., Maire, E., Zabler, S., Blandin, J.J., Buffiere, J.Y., Ludwig, W., Boller, E., Bellet, D. & Josserond, C. (2003). X-ray micro-tomography an attractive characterisation technique in materials science. *Nuclear Instruments & Methods in Physics Research Section B-Beam Interactions with Materials and Atoms*, **200**, 273–286.

Sinka, I.C., Burch, S.F., Tweed, J.H. & Cunningham, J.C. (2004). Measurement of density variations in tablets using X-ray computed tomography. *International Journal of Pharmaceutics*, **271**, 215–224.

Stotter, R.L. & Terblanche, J.S. (2009). Low-temperature tolerance of false codling moth *Thaumatotibia leucotreta* (Meyrick) (Lepidoptera: Tortricidae) in South Africa. *Journal of Thermal Biology*, **34**, 320–325.

Viuda-Martos, M., Fernandez-Lopez, J. & Perez-Alvarez, J.A. (2010). Pomegranate and its many functional components as related to human health: a review. *Comprehensive Reviews in Food Science and Food Safety*, **9**, 635–654.

Wohlfarter, M., Giliomee, J.H. & Venter, E. (2010). A survey of the arthropod pests associated with commercial pomegranates, *Punica granatum* (Lythraceae), in South Africa. *African Entomology*, **18**, 192–199.

Yehia, H.M. (2013). Heart rot caused by *Aspergillus* niger through splitting in leathery skin of pomegranate fruit. *African Journal of Microbiology Research*, **7**, 834–837.

Zhang, L. & McCarthy, M.J. (2012). Blackheart characterization and detection in pomegranate fruit using NMR relaxometry and MR imaging. *Postharvest Biology & Technology*, **67**, 96–101.

Stellenbosch University https://scholar.sun.ac.za

Table 1. Density (kg m^{-3}) and mass (g) of whole fruit, arils, albedo and false codling larva moth of pomegranate fruit cv. Herskawitz

Parameter	Density (kg m^{-3})	Predicted mass (g)	Actual mass (g)	Mean difference	Paired t-test
Whole fruit	1070 ±20b	259.84 ±36.90	261.72 ±37.22	-1.88	0.90
Arils	1120 ±40a	153.42 ±34.58	159.06 ±33.09	-5.63	0.91
Albedo	1040 ±30c	104.73 ±14.56	102.30 ±11.66	2.43	0.71
Codling larva	940 ±40d	0.030 ±0.01	0.031 ±0.01	-0.00048	0.68
P-value	0.0001				

Mean ± Standard deviation presented. Different letter(s) indicate significant difference ($p < 0.05$) according to Duncan's multiple range test

Stellenbosch University https://scholar.sun.ac.za

Table 2. Blackheart index and density (kg m^{-3}) of healthy and blackheart infected pomegranate fruit cv. Wonderful

Index	Density (kg m^{-3})
0	1070 ±20a
1	1000 ±50b
2	980 ±20bc
3	940 ±10c
4	870 ±20d
p-value	0.0001

Blackheart was evaluated on a subjectively using a scale of 0 – 4, where 0 = none; 1 = below 25%; 2 = between 25 and 50%; 3 = between 50 and 75%; 4 = > 75%. Mean ± Standard deviation presented. Different letter(s) indicate significant difference ($p < 0.05$) according to Duncan's multiple range test.

Stellenbosch University https://scholar.sun.ac.za

Table 3. Predicted and actual mass (g) of pomegranate fruit cv. Wonderful

Parameter	Predicted fruit mass (g)	Actual fruit mass (g)	Mean difference	Paired t-test
Healthy fruit	400.70 ±4.50	402.50 ±2.69	-1.80	0.46
Blackheart fruit	356.28 ±44.08	360.50 ±46.81	-4.21	0.80

Mean ± Standard deviation presented

Stellenbosch University https://scholar.sun.ac.za

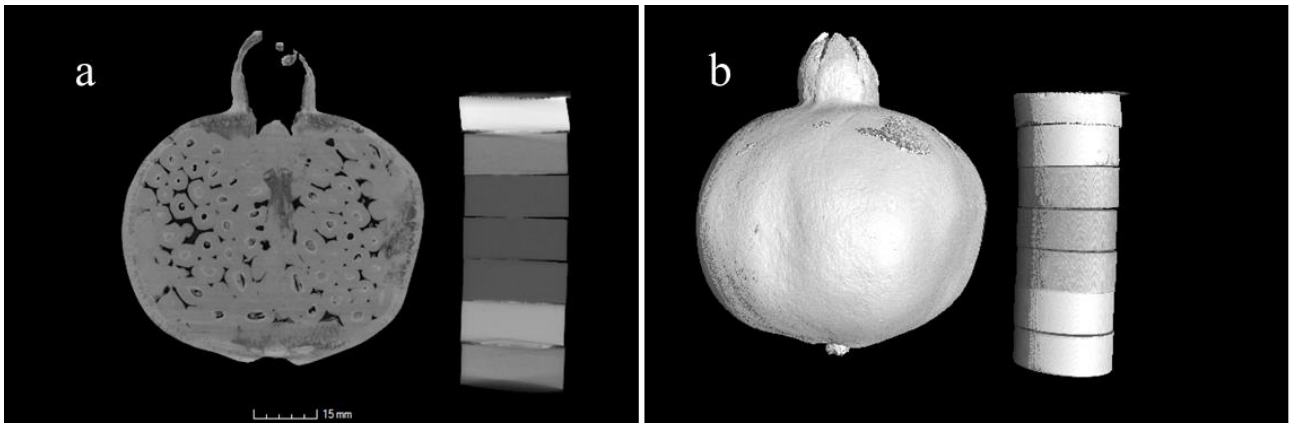

Fig.1. Representative 2-D (a) and 3-D (b) image of pomegranate fruit and polymer disks after removal of background.

Stellenbosch University https://scholar.sun.ac.za

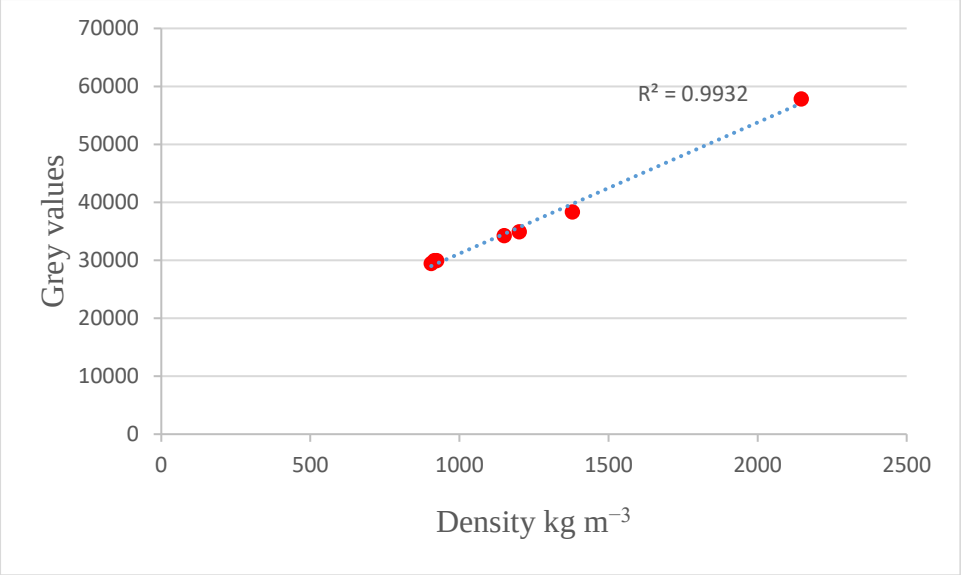

Fig.2. Linear calibration function for a series of 7 different polymers, $R^2 = 0.99$

Stellenbosch University https://scholar.sun.ac.za

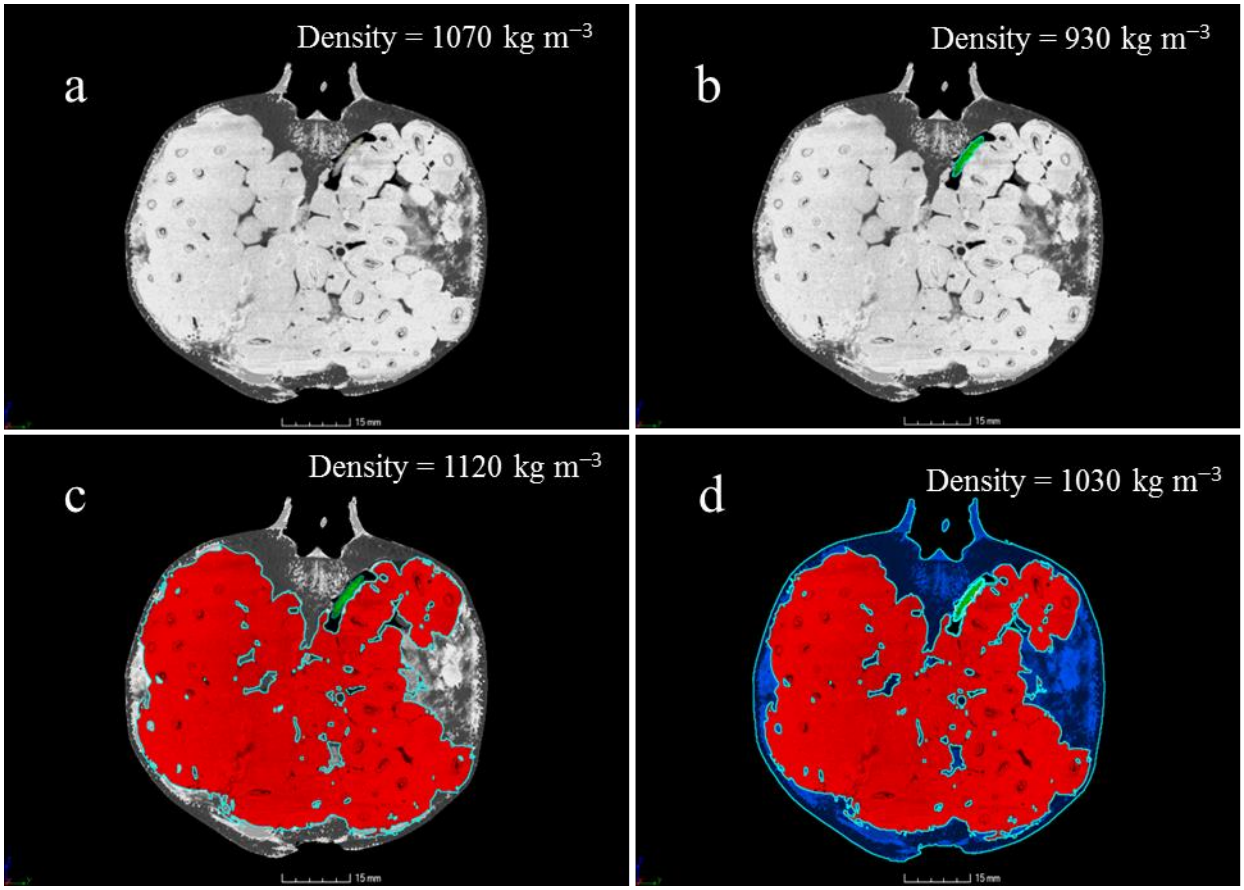

Fig. 3. Image analysis procedure using X-ray computed tomography for a single pomegranate fruit cv. Herskawitz with calculated density (kg m^{-3}). Raw representative X-ray image slice of a fruit containing false codling lava moth (a). Segmentation of lava moth with image slice being colour coded green (b). Segmentation and application of surface determination for arils with image slice being colour coded red (c). Albedo area were determined after aril extraction and colour coded blue (d).

Stellenbosch University https://scholar.sun.ac.za

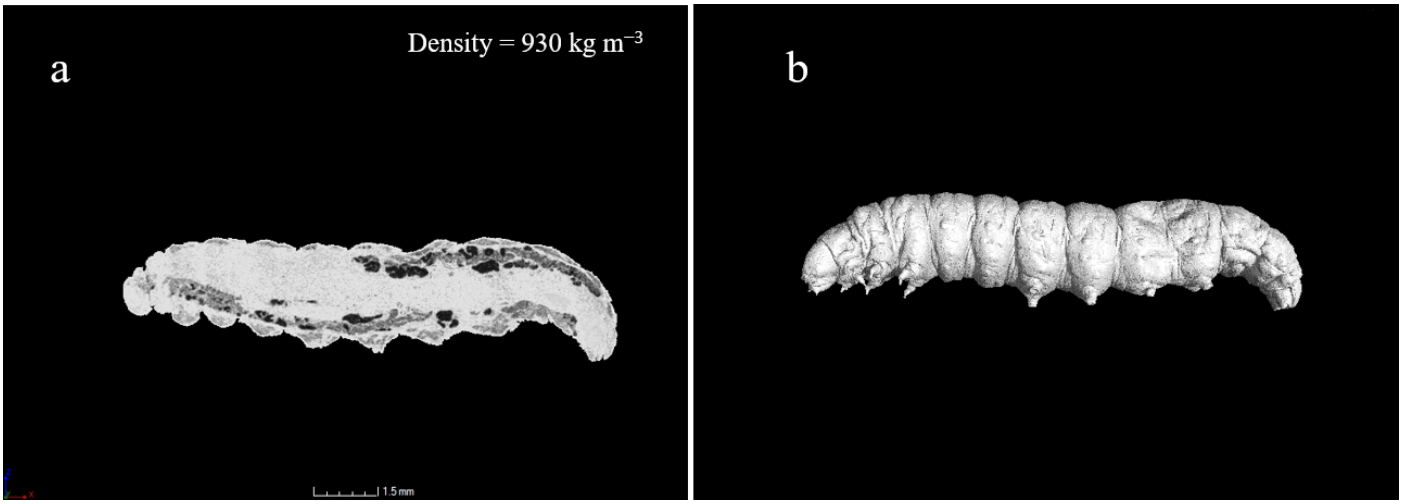

Fig. 4. False codling larva moth with calculated density (kg m^{-3}). 2-D image slice (a) and 3-D model reconstructed by appropriately stacking floating image slices (b)

Stellenbosch University https://scholar.sun.ac.za

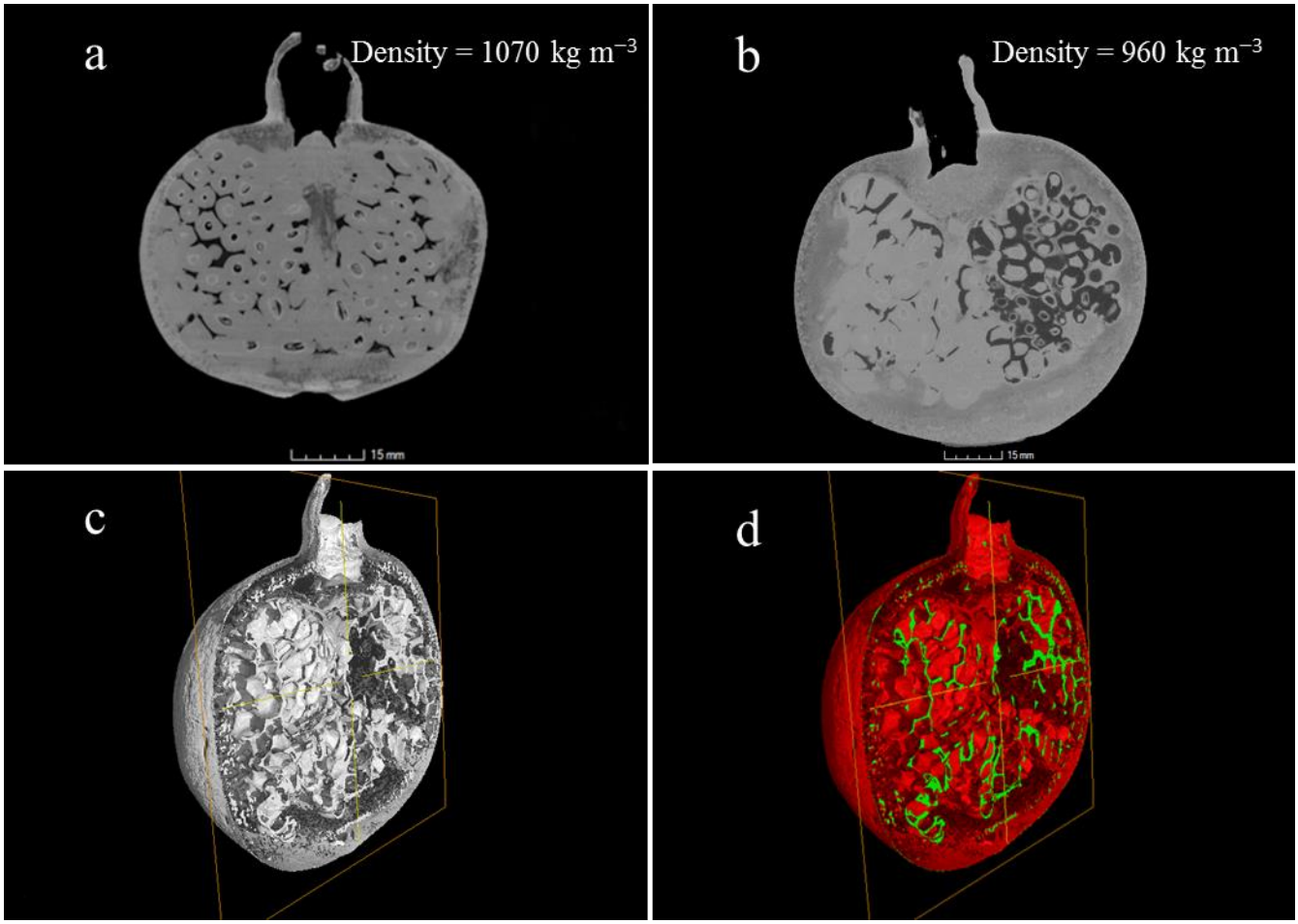

Fig. 5. Image analysis procedure using X-ray computed tomography for pomegranate fruit cv. Wonderful with calculated density (kg m^{-3}). Raw representative X-ray image slice of a healthy fruit (a). Raw representative X-ray image slice of a fruit containing blackheart (b). 3-D clipping image of fruit infected with blackheart (c). 3-D clipping image showing fruit area colour coded red and internal air colour coded green (d)

Stellenbosch University https://scholar.sun.ac.za

Fig. 6. Representative image of pomegranate fruit (cv. Herskawitz) containing false codling larva moth

Stellenbosch University https://scholar.sun.ac.za

Fig. 7. Representative image of pomegranate fruit (cv. Wonderful) affected by blackheart disease

Stellenbosch University https://scholar.sun.ac.za

DECLARATION BY THE CANDIDATE

Regarding **Chapter 8 (pp 181-205)**, the nature and scope of my contribution were as follows:

Nature of contribution	Extent of contribution (%)
Research, data collection, analysis and writing of chapter	75

The following co-authors have contributed to **Chapter 8 (pp 181-205)**

Name	e-mail address	Nature of contribution	Extent of contribution (%)
Prof U.L. Opara	opara@sun.ac.za	Conception of the work, editorial suggestion and proof reading	10
Dr O.A. Fawole	olaniyi@sun.ac.za	Research input, editorial suggestion and proof reading	5
Dr L.S. Magwaza	Magwazal@ukzn.ac.za	Editorial suggestion	5
Dr H. Nieuwoudt	hhn@sun.ac.za	Research input, editorial suggestion and analysis	5

Stellenbosch University https://scholar.sun.ac.za

E Arendse **Signature of candidate**	29/08/2017 **Date**

DECLARATION BY CO-AUTHORS

The undersigned hereby confirm that:

1. the declaration above accurately reflects the nature and extent of the contributions of the candidate and the co-authors to **Chapter 8 (pp 181-205)**

2. no other authors contributed to **Chapter 8 (pp 181-205)** besides those specified above, and

3. potential conflicts of interest have been revealed to all interested parties and that the necessary arrangements have been made to use the material in **Chapter 8 (pp 181-205)** of this dissertation.

Signature	Institutional affiliation	Date
Prof U.L. Opara	Stellenbosch University	29/08/2017
Dr O.A. Fawole	Stellenbosch University	29/08/2017
Dr L.S. Magwaza	University of KwaZulu-Natal	29/08/2017
Dr H. Nieuwoudt	Stellenbosch University	29/08/2017

Stellenbosch University https://scholar.sun.ac.za

CHAPTER 8

Evaluation of biochemical markers associated with the development of husk scald and the use of diffuse reflectance NIR spectroscopy to predict husk scald in pomegranate fruit

Abstract

Husk scald is a physiological rind disorder that manifests during storage and commercial shipping of pomegranate fruit. Scald affects the external quality thereby reducing its marketability, causing major economic loss to the industry worldwide. The lack of understanding of the underlying physiological and biochemical mechanisms of this disorder hinders the development of cost-effective solutions to minimise losses and assure a consistent supply of quality fruit. Therefore, this study evaluated several biochemical markers associated with the development of husk scald and to discriminate between healthy and scalded fruit non-destructively. The effects of storage temperature and duration on fruit weight loss, colour attributes (L*, a*, C*, h^o), browning index, total phenolics, total tannins, total anthocyanin content and enzymatic activity (polyphenol oxidase; PPO and peroxidase; POD) were investigated. The results showed that enzymatic browning was the main cause of peel browning with tannin and phenolic compounds acting as substrates for PPO and POD activity. Fruit stored at 10 °C for five months exhibited a higher incidence of scald compared to fruit at 5 °C. Fourier transform near-infrared reflectance spectroscopy was used to qualitatively discriminate between healthy and scalded fruit using orthogonal partial least squares discriminant analysis (OPLS-DA). The fruit were classified into three categories, namely, healthy, moderate scald and severe scald. A classification accuracy of 100% healthy, 92.6% moderate scald and 93% severe scald was achieved. Furthermore, the variable importance of projection (VIP) plot revealed that wavelength regions responsible for discrimination between classes were at 1350-1450, 1830-1950 and 2150-2250 nm, the wavebands attributed to stretching of C–O, O–H and C–C bonds related to phytochemical compounds such as phenolics and anthocyanins. This study demonstrated that PPO activity, total phenolic and total tannins content were associated with the development of husk scald and these biomarkers were used to discriminate pomegranate fruit into different quality tiers.

Keywords: Fruit quality, Postharvest rind disorder, *Punica granatum* L. Discrimination, Multivariate analysis, Non-destructive

Stellenbosch University https://scholar.sun.ac.za

1. Introduction

Pomegranate is a nonclimateric, subtropical fruit that has been cultivated and grown in recent years as a commercial export fruit within the South African agricultural industry. The country's production of pomegranate fruit has increased significantly during the past seven years with a total of 8 000 tons produced in 2016 compared to 350 tons harvested in 2009 (Hortgro, 2017). However, pomegranate fruit is prone to develop various types of diseases and physiological disorders during storage and shipping. Husk scald (browning of the peel surface) is a type of physiological rind disorders that occur during postharvest storage of pomegranate fruit. Scalding of the rind manifests mainly during the later stages of postharvest handing, which usually coincides with commercial shipping period. Scalding has no noticeable and observable internal changes on the arils or on the white astringent membrane surrounding the arils and fruit stored at temperatures above 5 °C are more susceptible to the disorder (Ben-Arie & Or, 1986; Defilippi *et al.*, 2006).

Studies performed by Ben-Arie and Or (1986) suggested that this disorder may be due to the enzymatic oxidation of o-dihydroxyphenols to quinone compounds. These authors observed a correlation between husk scald incidence and a number of extractable o-dihydroxyphenols obtained from the affected husk, however, they concluded that the biochemical changes as result of enzymatic browning remain unclear. Zhang and Zhang (2008) studied the relationship between tannin content and several enzymatic activities occurring during storage of sweet pomegranate fruit. They reported that polyphenol oxidase activity increased while tannin content decreased. The negative co-relationship suggested that the tannin content was the primary substrate for pomegranate peel browning. In a later study, Matityahu *et al.* (2013) studied the effects of husk scald on seven pomegranate cultivars during storage. The authors observed that the severity of scald was negatively correlated with punicalin, an anthocyanin pigment. Limited knowledge on the physiological and biochemical mechanisms underlying this disorder hinders the development of cost-effective solutions to minimise losses, and assure a consistent supply of quality fruit.

The key to extending the storage life and maintain the quality of pomegranate fruit lies in early detection and separation of fruit susceptible to husk scald. Limited research has been conducted to develop non-destructive technology that can assess, predict and monitor fruit rind disorders (Magwaza *et al.*, 2012; 2013; 2014a,b,c). Therefore, for the South African pomegranate industry to maintain its competitive edge in the export industry, there is a need for the development of non-destructive methods. Such methods would permit the evaluation of external and internal quality to ensure minimum levels of acceptance in the market (Magwaza

Stellenbosch University https://scholar.sun.ac.za

& Opara, 2014). A wide range of non-destructive instrumentation has been used for assessment of quality attributes in fresh produce. These include near-infrared spectroscopy (NIR, Nicolaï *et al.*, 2007), hyperspectral imaging (Makino *et al.*, 2013), nuclear magnetic resonance (NMR, Zhang & McCarthy, 2013), X-ray computed tomography (µCT, Arendse *et al.*, 2016a, b) and optical coherence tomography (OCT, Magwaza *et al.*, 2013). NIR has become one of the most used methods for the assessment of fresh fruit according to their external quality attributes (Nicolaï *et al.*, 2007). Therefore, to fully harness the opportunity of existing and future competitive export markets, there is a need for the development and application of objective, fast and non-destructive assessment methods that can be used to accurately detect physiological rind disorders during postharvest handling and storage. The objective of this study was twofold; firstly identify potential biochemical markers associated with the development of husk scald during storage. The second aim was to explore diffuse reflectance near-infrared spectroscopy as a non-destructive technique to discriminate pomegranate fruit based on husk scald.

2. Materials and Methods

2.1. *Fruit sampling and storage conditions*

During the 2015 season, commercially ripe pomegranate fruit (cv. Wonderful) were obtained from two different orchards in the Western Cape Province, South Africa. The first batch of fruit were procured from Heinrich Frederich Schaefer (HFR) orchard, and the second set was obtained from Porterville (33°01'00"_S, 18°58'59"_E). Fruit were then transported to the Postharvest Technology and Research Facility at Stellenbosch University. Upon arrival, fruit were allowed to equilibrate at ambient temperature (23 ±4 ˚C) before being sorted out for size uniformity and then randomly divided into two 2 lots. The two lots were stored respectively at 5 ˚C and 10 ˚C with relative humidity (RH %) of 91 ±4 ˚C for 5 months. Temperature was monitored using Tiny Tag data loggers (TV-4500, Gemini Data Logger, Sussex, UK). The first objective was to identify potential biochemical markers associated with the development of husk scald during storage. A total of 140 fruits were sampled at harvest and monthly intervals for up to a period of 5 months. The second aim was to explore diffuse reflectance near-infrared spectroscopy as a non-destructive technique to discriminate pomegranate fruit based on husk scald. A total of 500 fruit were sampled, fruit were sampled at harvest and end of storage trials followed by a 7d shelf-life period (simulating retailers storage).

2.2. *Physical parameters*

2.2.1. *Weight loss*

Fruit weight loss was determined on ten randomly selected individual fruits of similar size for each storage condition. During storage, the same selected fruit were weighted at monthly

Stellenbosch University https://scholar.sun.ac.za

intervals up to 5 months. Fruit were individually weighed using an electronic weighing scale (Mettler, Switzerland, 0.001 g) and the loss in weight was calculated using Eq. 1.

$$W = [(W_i - W_t) \div Wi] \times 100 \quad (1)$$

where W =weight loss (%) of the fruit, W_i = initial weight (g) at the start of storage, W_t = weight at the time of sampling. The results were expressed as mean ± SE for 10 fruit.

2.2.2. *Colour attributes*

Rind colour was assessed in CIELAB coordinates (L*, a*, b*) using a calibrated colour meter (Chroma Meter, CR-400/410 Minolta Corp, Osaka, Japan). Colour measurements was taken along the equatorial region of the fruit. Chroma (C*) and hue angle (h^o) were derived from the (L*, a*, b*) coordinates as described by Pathare *et al.* (2013).

2.2.3. *Browning Index*

In the case of a physical indicator for browning of the peel in relation to husk scald, the CIE (L*, a*, b*) coordinates have been extensively used to characterise the overall changes in browning colour. In order to capture this variation in brown colour, a browning index (BI) was calculated using Eq. 2 according to Pathare *et al.* (2013).

$$BI = 100 \times \frac{(x-0.31)}{0.17} \quad (2)$$

where x = chromaticity coordinate calculated from the *L**, *a**, *b** values using Eq. 3

$$x = \frac{(a* + 1.75L*)a*}{(5.645L* + a* - 3.012b*)} \quad (3)$$

*L**, *a**, *b** values represent the lightness, redness, and yellowness of the sample.

2.3. *Phytochemical analysis*

2.3.1. *Sample preparation of peel*

Pomegranate fruit were manually peeled. The peels were freeze-dried, ground into powder and stored in airtight sealed containers at -20 °C. The finely powdered peel 0.1 g was diluted with 9.9 mL of 50% (v/v) methanol and distilled water. The samples were vortexed (Model. G560E, Scientific Industries, USA) for 5 min, sonicated (DC400H, MRC Ltd. Israel) and centrifuged (Merk, Eppendorf AG, Germany).at 4 °C for 20 min at 10 000 rpm. The supernatant was collected into clean vials and stored at -80 °C for further use.

Stellenbosch University https://scholar.sun.ac.za

2.3.2. *Total phenolic concentration*

Total phenolic concentration was performed using the Folin-Ciocalteu colorimetric method according to Makkar *et al*. (2007) with modification according to Arendse *et al.* (2017), and the results were expressed as milligram of gallic acid equivalent (GAE) per gram of dry matter.

2.3.3. *Total tannin concentration*

The analysis of total tannin concentration was performed as described by Makker *et al.* (2007) with modification according to Mphahlele *et al.* (2014). Total tannin concentration was expressed as milligram of gallic acid equivalent (GAE) per gram of dry matter.

2.3.4. *Total anthocyanin concentration*

Total monomeric anthocyanin concentration was quantified using pH deferential method (Giusti & Wrolstad, 2001) and with modification, as described by Arendse *et al.* (2017). The results were expressed as milligram of cyanidin 3-glucoside per gram of dry matter.

2.4. *Enzyme assays*

2.4.1. *Sample preparation*

One gram of fine pomegranate peel powder was diluted with 10 mL cold extraction buffer. Samples were vortexed, sonicated and stored at 4 °C in a dark environment for 2 h before being centrifuged at 10 000 rpm for 20 min at 4 °C. The resultant supernatant was collected into clean vials and stored at -80 °C for further use. The extraction buffer comprised of the following: 0.1 M L^{-1} potassium phosphate buffer, pH 7, 0.05 M L^{-1} ethylenediaminetetraacetic acid (EDTA) and 60 g L^{-1} polyvinyl polyprrolidone (PVPP) to the ratio (1:1:1) (Gonzalez *et al.*, 1999).

2.4.2. *Polyphenol oxidase (PPO) assay*

Polyphenol oxidase activity was determined spectrophotometrically at 420 nm by measuring the initial rate of increase in absorbance. The activity was assayed in a 3 mL reaction mixture consisting of 2.5 mL sodium phosphate buffer (0.2 M, pH 6), 0.3 mL pyrocatechol (0.1 M) and 0.2 mL enzyme extract. The reaction was initiated by the addition of 0.1 M pyrocatechol substrate and the activity was expressed as change in absorbance at 420 nm over 5 min period. The blank consisted of 3 mL sodium phosphate buffer pH 6 and results were expressed as unit per gram of fresh weight (Gonzalez *et al.*, 1999).

2.4.3. *Peroxidase assay*

Stellenbosch University https://scholar.sun.ac.za

Peroxidase activity was assayed by measuring the increase in absorbance at 470 nm as described by Meighani *et al.* (2014) with slight modification. Briefly, the reaction mixture consisted of 2.73 mL 0.1 M sodium phosphate buffer (pH 6), 0.1 mL 0.045 M guaiacol, 0.15 mL of 0.225 M H_2O_2 and 0.02 mL enzyme extract. The reaction was initiated by adding the 0.045 M guaiacol substrate and the activity was expressed as change in absorbance at 470 nm over 5 min period. The results were expressed as unit per gram of fresh weight.

2.5. *Statistical analysis*

Collected data were subjected to a two-way analysis of variance (ANOVA) according to Duncan multiple range test and Pearson correlation analysis using Statistica (version 13, StatSoft Inc., Tulsa, USA). The mean and standard errors for all the variable were presented. Where appropriate, graphical presentations were made using GraphPad Prism software version 5.0 (GraphPad Software, Inc., San Diego, USA).

2.6. *Spectral acquisition*

The NIR spectra were generated from the equatorial side of the fruit in reflectance mode using a Fourier transform near-infrared (FT-NIR) Multi-Purpose Analyser (MPA) ((Bruker Optics, Ettlingen, Germany) equipped with a gold-coated rotating integrating sphere which had a sample holder width of 50 mm. Prior to the spectral acquisition, background measurements were taken against air and at regular intervals of 30 min during scanning of the fruit. NIR spectra were acquired over a spectral wavelength region of 800-2500 nm using the following scanning parameters: measurement time of 120 s, scanning resolution 8 cm^{-1}, 10 kHz scanner velocity and a total of 128 scans averaged per spectrum. The FT-NIR spectral system was operated and initiated OPUS software (OPUS v. 7.0).

2.7. *Reference measurements*

2.7.1. *Class separation based on* b*rowning index*

In order to non-destructively discriminate between healthy and fruit displaying husk scald. The severity of husk scald for each fruit was evaluated subjectively and categorised into the following groups where healthy = none, moderate = ≤49% and severe ≥ 50%.

2.8. *Multivariate analysis*

Data processing and discriminant analysis were done using SIMCA version 14 (Umetrics, Umeå, Sweden). Several pre-processing methods were evaluated, baseline correction spectra were subjected to several filtering techniques, which included Savitzky–Golay transformation

Stellenbosch University https://scholar.sun.ac.za

(first derivative), multiplicative scattering correction (MSC), and standard normal variate (SNV) correction. Explorative data analysis was performed using Principal Component Analysis (PCA) and classification of fruit with orthogonal partial least squares discriminant analysis (OPLS-DA). PCA is an unsupervised technique for exploratory data analysis, which maximises the variation within the X data by projecting the spectral variation onto a few latent variables (LVs) (Wold *et al.*, 1987). Spectral data were subjected to PCA in order to investigate the separation of healthy and husk scald fruit. OPLS-DA is a supervised classification technique that isolates a predictive component and integrates an orthogonal correction filter, in order to differentiate the variation within the dataset (Bylesjö *et al.*, 2006).

Validation of the spectral dataset was accomplished by randomly splitting the dataset into test (50%) and train (50%) set with the scale set as mean centring. OPLS-DA dataset was subjected to S-Line plot. An S-line plot is especially suited for spectroscopy data. The plot displays the predictive loading in a form resembling the original spectra with the spectral peaks at the top end of the colour scale influence the separation of the groups. Prediction data set were subjected to variable importance projection (VIP) which summarises the importance of the variables both to explain X and to correlate to Y. Terms with VIP values larger than 1 shows to variables with large importance for model performance.

3. Results and discussion

3.1.1. *Browning index in relation to husk scald*

The browning index derived from the CIE values for pomegranate peel are presented in Figure 1. It was observed that the BI increased throughout storage with significant effects ($p = 0.01$) dependent on storage duration. Although, throughout storage and end of storage trails, fruit at 10 °C had higher BI compared to 5 °C. The consistently higher BI observed at 10 °C suggest that fruit were darker in colour as a result of peel browning. These results were buttressed by the visual appearance of the fruit as we observed a higher scalding incidence in fruit stored at 10 °C compared to 5 °C.

3.1.2. *Colour dynamics in relation to browning index*

The CIE values for L*, a*, C* and h^{o} in relation to the browning index are presented in Fig 2. The peel L* and a*values decreased throughout storage period with significant effects dependent on storage duration ($p < 0.0001$), while temperature only had a significant effect on a* ($p < 0.014$) (Fig. 2A and B). The decrease in lightness and redness of pomegranate peel and subsequent increase in browning index suggest that the severity of peel browning increased with temperature and storage duration. Pathare *et al.* (2013) stated that chroma (C*) is a

Stellenbosch University https://scholar.sun.ac.za

quantitative attribute of colourfulness. The higher the chroma values, the higher is the colour intensity. While hue angle (h°) is considered the qualitative attribute of colour, the higher the h° the more the colour is associated with a lesser yellow-brown character. C* followed a similar trend observed for a* values with significant effects mainly attributed to storage duration ($p < 0.0001$) compared to temperature ($p = 0.81$) (Fig. 1C). The decrease in C* values suggests that the colour intensity of the fruit decreases with increase in peel browning. While, h° of fruit peel increased with significant effects associated with both temperature ($p = 0.001$) and storage duration ($p < 0.001$) (Fig. 1D). The higher h° values observed on fruit stored at 10 °C for 5 months suggests that these fruit were consistently darker in colour as result of peel browning compared to those stored at 5 °C and less associated with colour redness. This was supported by the scald data, which showed that fruit stored at 10 °C exhibited the highest incidence of scald compared to fruit stored at 5 °C. Our results were buttressed by the findings reported by Fawole and Opara (2013), where the authors observed a decrease in a*(redness), C* (colour intensity) with an increase in scald incidence over a 16 week storage period for pomegranate cv. Bhagwa.

3.1.3. *Phytochemistry and weight loss in relation browning index*

Total phenolic concentration gradually decreased after harvest and did not vary significantly with storage temperature (Fig. 3A). However, highly significant differences ($p < 0.0001$) were mainly observed after 4 months of storage compared to harvest. At the end of storage trials, the phenolic concentration was reduced from 288.35 to 224.94 and 203.59 mg/g DM for 5 and 10 °C resulting in a reduced concentration of by 22 and 29%, respectively. Our findings are in agreement with those reported by Fawole and Opara (2013) who observed a decrease in the phenolic concentration for Bhagwa and Ruby cultivars stored at 5 to 10 °C over a period of 16 weeks. Total tannin concentration followed a similar trend as the phenolic concentration (Fig. 3B). The decrease in tannin concentration were significantly correlated to both temperature ($p = 0.031$) and storage duration ($p < 0.0001$). After 5 months of storage, tannin concentration was reduced from 281.52 to 248.97 and 159.66 mg/g DM for 5 and 10 °C, resulting in a to 31.2 and 43.3% reduction in concentration. These results demonstrated that fruit with a higher phenolic and tannin content are more resistant to the development of scald. Similar results were reported by Matityahu *et al.* (2013) who studied the effects of husk scald on seven pomegranate cultivars during storage. The authors suggested that fruit with higher total phenolic content and antioxidant capacity was more resistant to the development of husk scald. Figure 3A and B shows the browning index gradually increased with the decrease in phenolic and tannin

Stellenbosch University https://scholar.sun.ac.za

concentration within pomegranate peel suggesting that the negative interrelationship between phenolics, tannins and peel browning.

In general, total anthocyanin concentration increased from 315.94 mg/g DM to 324.96 and 365.37 mg/g DM for 5 and 10 °C respectively (Fig. 3C), the increase in anthocyanin concentration could be related to biosynthesis of anthocyanins, which is known to be induced at lower temperatures (Arendse *et al.,* 2014; 2015). Anthocyanin concentration gradually decreased after the first month of storage resulting in a total reduction of 1.7 folds of its concentration at the end of storage period with no significant differences being observed between the storage temperatures. Although, the decrease in total anthocyanin concentration were dependent on both storage duration ($p < 0.0001$) and temperature ($p = 0.017$). Significant ($p < 0.0001$) differences in the fruit weight loss were observed amongst the storage temperatures (Fig. 3D). Weight loss for fruit stored at 10 °C was significantly higher throughout storage compared to those stored at 5 °C this may be attributed to higher fruit respiration. At the end of the storage period, fruit stored at 5 and 10 °C loss an average of 18.09 and 34.26% of its weight respectively. Figure 2D shows the browning index increased with fruit weight loss. The increase in weight loss caused visible shrinkage in the fruit resulting in a hardening and browning of the husk (Artés *et al.,* 2000; Caleb *et al.,* 2012). Overall, weight loss increased with significant effect as a result of temperature ($p < 0.0001$), storage duration ($p < 0.0001$) and the interaction between them.

3.1.4. *PPO and POD activity in relation to browning index*

PPO activity has been reported to be the primary enzyme responsible for the oxidation of phenolic compounds into quinone compounds leading to the browning of the peel (Chisari *et al.,* 2007). As shown in Fig. 4A, after harvest (1.62 U/g FW), PPO activity increased with storage temperature and duration with significant ($p < 0.05$) differences being observed after 3 and 4 months for 10 and 5 °C, respectively. Storage of fruit at 10 °C for 5 months exhibited the highest PPO activity (2.27 ±0.03 U/g FW) compared to 5 °C (2.00 ±0.02 U/g FW). These values are with a similar range to those reported by Gonzalez *et al.* (1999) for raspberry fruits. The lower temperature may play a role in the reduction in enzymatic activity as observed within this study. Furthermore, it was observed that the BI followed a similar trend to the PPO activity and increased storage temperature and duration. The observed trend for this study is similar to those reported by Zhang and Zhang (2008) who observed an increase in PPO activity in relation to a browning index. The results of the present study showed that the activity of PPO is dependent on storage duration ($p < 0.0001$) and temperature ($p < 0.0002$).

Stellenbosch University https://scholar.sun.ac.za

POD is another enzyme involved in the enzymatic browning process. It utilises polyphenol substances by oxidation in the presence of H_2O_2 leading to browning and may have a synergistic effect with PPO (Chisari *et al.,* 2007). POD activity within the peel gradually increased from 0.098 to 0.37 and 0.38 U/g FW at the end of 5 month storage period for 5 and 10 °C, respectively (Fig. 4B). However, significant differences were observed at harvest and after 4 months of storage at both storage temperatures. POD activity had a 3.75 and 3.85 fold increase in its activity at the end of storage trials compared to fruit at harvest for 5 and 10 °C, respectively with significant effects occurring as a result of storage duration ($p < 0.0001$). The values for POD activity are within the range reported by Chisari *et al.* (2007) and Ghasemnezhad *et al.* (2015) for strawberries and pomegranates respectively. Similarly, the BI gradually increased suggesting that POD may play a role in the development of husk scald in pomegranate fruit.

3.1.5. *Correlation analysis*

To demonstrate if of the above studied variables may play a role in the development of husk scald. Pearson correlation was used to investigate the interrelationships between selected reference data. Table 1 displays the correlation between variables with values of 0.80 and above were only considered to be associated with one another. Correlation analysis suggested that no correlation was observed between any colour attributes, weight loss, and enzymatic activity. However, correlation analysis indicated a significantly ($p < 0.01$) high negative relationship between PPO activity and total tannins (r = -0.85). Similarly, a significant negative correlation between PPO activity and total phenolic compounds (r = -0.81) were observed. The relationship clearly shows that when total phenolic and total tannin compound decrease while PPO activity increases. The negative interrelationship between them suggests that total phenolic and tannin compounds could act as a substrate of pomegranate peel browning. The increase in the severity of husk scald could be attributed to the degradation of total phenolic and total tannin content to simpler phenolic acids and the oxidation of these simpler phenolic compound by polyphenol oxidase activity during postharvest storage (Tomás-Barberán & Espín, 2001).

3.2. *Non-destructive* d*iscrimination based on susceptibility to husk scald*

3.2.1. *Spectral characteristics*

Preliminary assessment of NIR spectra for healthy and scalded fruit were investigated using PCA. The first two principal components were used in relation to the chemical variation within the samples set. By plotting all 479 scores for the first component with the corresponding values for the second component, the first two PC explained 93% (PC1 = 68%, PC2 = 26%) of the

Stellenbosch University https://scholar.sun.ac.za

total variation within the dataset. The examination of score plots from baseline corrected spectra showed the effects of storage on the spectral and chemical properties of the fruit (Fig. 5A). Two dispersed groups were observed which revealed that the first PC contributed most to the sample distribution where samples were mainly stretched along PC1 region after storage and were clustered before storage. This dispersed clustering after storage may be as result of biochemical changes occurring within the rind associated with senescence such as a decrease in phenolic, anthocyanin and tannin content.

Typical mean baseline corrected spectra for the healthy and fruit associated with husk scald are presented in Fig. 5B. The NIR spectrum for both healthy and scalded fruit displayed similar contours and with bands having prominent absorbance peaks in the region 950, 1200, 1450, 1780, and 1930 nm. The bands observed at 950 and 1450 nm have been reported closely associated with the O-H stretching modes of water absorption (Nicolaï *et al.*, 2007), while prominent bands at 1200, 1780 and 1930 nm corresponds second and first overtones of C-H stretching as well as the third overtone of OH, CH and CH_2 these bands have been associated with the absorption profile of various compounds. Variation in the absorbance bands for healthy and scalded fruit were observed in the region of 1930 to 2400 nm. This region has been reported to be associated with compounds such as moisture, protein, fats and phenolic acids (Manley, 2014). In order to establish if the chemistry data responsible for the separation of healthy versus scalded fruit were significantly different from each other, a t-test independent by variables were performed. Figure 5 displays the results for total phenolic, total tannins and polyphenol oxidase activity. Significant ($p < 0.0001$) differences were observed for polyphenol oxidase activity (Fig. 6A), total phenolic (Fig. 6B) and total tannins (Fig. 6C) between healthy and scalded fruit suggesting that the above chemistry are responsible for the separation of the two classes.

3.2.2. *OPLS-DA between 2 classes*

By applying OPLS-DA, both classes based on healthy and infected fruit were separated in a model consisting of one predictive component and five orthogonal components (Appendix chapter 8, Table 1). OPLS-DA model showed a clear separation between the two classes (Fig.7A) with high statistical values for R^2X (0.89), R^2Y (1), Q^2 (0.88). The high Q^2 value of 0.88 provides a qualitative measure of consistency between the predicted and original data, suggesting good performance for the developed model. Similar R^2 and Q^2 values suggest that overfitting of the model was not evident. The separation of the two classes was investigated using the S-line plot. By examining the S-line in Fig. 7B revealed the wave band responsible for discrimination between the two classes were at 1930 nm which is attributed to C–O, O–H and C–C bond stretches of phenolic compounds as interpreted by Arendse *et al.* (2017).

Stellenbosch University https://scholar.sun.ac.za

Furthermore, the prediction dataset was classified into classes and represented as a misclassification dataset. Figure 7C showed the proportion of correctly classified observations in the prediction dataset with the results suggesting that 100% of healthy and 99% of diseased fruit were correctly classified.

Figure 7D shows the VIP plot with important wavelength regions responsible for model performance was at 1350-1450, 1830-1950 and 2150-2250 nm. These regions have been associated with the absorbance of molecules containing O-H, C-H and C-H_2 groups (Nicolaï *et al.*, 2007; de Oliveira *et al.*, 2014). Therefore, this study demonstrated that NIR spectroscopy as a non-destructive technique could discriminate between healthy fruit and fruit associated with husk scald.

3.2.3. *OPLS-DA between 3 classes*

In order to further investigate the discriminating power of NIR spectroscopy, OPLS-DA were applied to three classes, these include healthy fruit (class 1), fruit associated with moderate scald (class 2) and fruit associated with severe scald (class 3) (Fig. 8A). The development of OPLS-DA model separated the three classes based on two predictive components and five orthogonal components (Appendix chapter 8, Table 2). The prediction statistics responsible for class separation were R^2X (0.88), R^2Y (1), Q^2 (0.77) showing a clear separation between class 1 from class 2 and 3. VIP plot (Fig. 8B) suggest that important wavelength regions responsible for model separation were similar to those observed in Figure 7B. Furthermore, the proportion of correctly classified observations in the prediction dataset were class 1 (100%), class 2 (92.6%) and class 3 (93%) respectively with observed confusion found between class 2 and 3 (Fig. 8C).

Figure 8D displays VIP values for chemistry with the variables sorted in descending order based on the confidence interval. The VIP plot suggests that PPO activity contributes slightly more to the separation of the three classes. Although, VIP plot illustrates that PPO activity, total phenolic and tannin concentration all contribute to the models performance. The results of this study suggest that healthy fruit can clearly be distinguished from fruit susceptible to husk scald. An important observation was that the majority of fruit that was subjected to shelf life conditions displayed severe scald suggesting that a dramatic increase in temperature and reduced relative humidity increases degradation of phenolic and tannin compounds thereby promoting PPO activity, increasing the intensity of husk scald.

4. Conclusion

Stellenbosch University https://scholar.sun.ac.za

This study demonstrated that the development of husk scald was primarily influenced by storage duration rather than temperature. However, storage temperature significantly affected several fruit biochemical properties such as PPO activity and concentrations of total tannin and total anthocyanin. Fruit stored at 10 °C and 91% ±4 ˚C RH showed higher scalding incidence compared to storage at 5 °C and 91% ±4 ˚C RH over 5 months of storage, and this was attributed to the effect of lower temperatures in reducing enzymatic activity. The results suggest that enzymatic browning was the primary cause of peel browning, with tannin and phenolic compounds acting as substrates for PPO and POD activity. Furthermore, fruit with higher phenolic and tannin concentration were more resistant to the development of husk scald. Accurate discrimination of healthy and scalded fruit was obtained from FT-NIR spectra analysis. Non-destructive discrimination between healthy and infected (scalded) fruit was accomplished using PCA and OPLS-DA. Scalded fruit were further segregated into moderate and severe scald categories to discriminate between three classes using OPLS-DA. Classification accuracy of 100% for healthy fruit, 92.6% for moderate scald and 93% severe scald were achieved. VIP and S-line plot revealed that these corresponding wave bands responsible for discrimination between the classes were at 350-1450, 1830-1950 and 2150-2250 nm. Overall, these findings have demonstrated the prospects of diffuse reflectance NIR spectroscopy as a non-destructive technique to detect and classify pomegranate fruit affected by postharvest scald disorder.

References

Arendse, E., Fawole, O.A. & Opara, U.L. (2014). Effects of postharvest storage conditions on phytochemical and antioxidant properties of pomegranate fruit (cv. Wonderful). *Scientia Horticulturae*, **169**, 125–129.

Arendse, E., Fawole, O.A. & Opara, U.L. (2015). Effects of postharvest handling and storage on physiological attributes and quality of pomegranate fruit (*Punica granatum* L.): A review. *International Journal of Postharvest Technology and Innovation*, **5**, 13–31.

Arendse, E., Fawole, O.A., Magwaza, L.S. & Opara, U.L. (2016a). Non-destructive characterization and volume estimation of pomegranate fruit external and internal morphological fractions using X-ray computed tomography. *Journal of Food Engineering*, **186**, 42–49.

Arendse, E., Fawole, O.A., Magwaza, L.S. & Opara, U.L. (2016b). Estimation of the density of pomegranate fruit and their fractions using X-ray computed tomography calibrated with polymeric materials. *Biosystems Engineering*, **148**, 148–156.

Stellenbosch University https://scholar.sun.ac.za

Arendse, E., Fawole, O.A., Magwaza, L.S., Nieuwoudt, H.H. & Opara U.L. (2017). Development of calibration models for the evaluation of pomegranate aril quality by Fourier-transform near infrared spectroscopy combined with chemometrics. *Biosystems Engineering*, **159**, 22–32.

Artés, F., Tudela, J.A. & Villaescusa, R. (2000). Thermal postharvest treatment for improving pomegranate quality and shelf life. *Postharvest Biology and Technology*, **18**, 245–251.

Ben-Arie, R. & Or, E. (1986). The development and control of husk scald on 'Wonderful' pomegranate fruit during storage. *Journal of the American Society for Horticultural Science*, **111**, 395-399.

Bylesjö, M., Rantalainen, M., Cloarec, O., Nicholson, J.K., Holmes, E. & Trygg, J. (2006). OPLS discriminant analysis: combining the strengths of PLS-DA and SIMCA classification. *Journal of Chemometrics*, **20**, 3541–351.

Caleb, O.J., Opara, U.L. & Witthuhn, C.R. (2012). Modified atmosphere packaging of pomegranate fruit and arils: A Review. *Food and Bioprocess Technology*, **5**, 15–30.

Chisari, M., Barbagallo, R.N. & Spagna, G. (2007). Characterization of polyphenol oxidase and peroxidase and influence on browning of cold stored strawberry fruit. *Journal of Agricultural and Food Chemistry*, **55**, 3469–3476

Defilippi, B.G., Whitaker, B.D., Hess-Pierce, B.M. & Kader, A.A. (2006). Development and control of scald on 'Wonderful' pomegranates during long-term storage. *Postharvest Biology and Technology*, **41**, 234–243.

Fawole, O.A. & Opara, U.L. (2013). Effects of storage temperature and duration on physiological responses of pomegranate fruit. *Industrial Crops and Products*, **47**, 300–309.

Ghasemnezhad, M, Zareh, S, Shiri, M.A. & Javdani, Z. (2015). The arils characterization of five different pomegranate (*Punica granatum*) genotypes stored after minimal processing technology. *Journal of Food Science and Technology*, **52**, 2023–2032.

Giusti, M.M. & Wrolstad, R.E. (2001). Characterization and measurement of anthocyanins by UV–visible spectroscopy, in: Wrolstad, R.E., Acree, T.E., An, H., (Eds.), Current Protocols in Food Analytical Chemistry. John Wiley & Sons, Inc., New York, NY, F1.2.1-F.1.2.13.

Gonzalez, E.M, de Ancos, B. & Cano, M.P. (1999). Partial characterization of polyphenol oxidase activity in raspberry fruits. *Journal of Agricultural Food Chemistry*, **47**, 4068–4072.

Hortgro. (2017). Stone fruit, pomegranate & cherry production and export data. Paarl: Information and Market Intelligence Division. https://www.hortgro.co.za. Assessed on (18/07/2017).

Stellenbosch University https://scholar.sun.ac.za

Magwaza, L.S., Opara, U.L., Terry, L.A., Landahl, S., Nieuwoudt, H.H., Mouazen, A.M., Saeys, W. & Nicolaï, B.M. (2012). Prediction of 'Nules Clementine' mandarin susceptibility to rind breakdown disorder using Vis/NIR spectroscopy. *Postharvest Biology Technology*, **74**, 1–10.

Magwaza, L.S., Ford, H.D., Cronje, P.J.R., Opara, U.L., Landahl, S., Tatam, R.P. & Terry, L.A. (2013). Application of optical coherence tomography to non-destructively characterise rind breakdown disorder of 'Nules Clementine' mandarins. *Postharvest Biology and Technology*, **84**, 16–21.

Magwaza, L.S., Opara, U.L., Cronje, P.J.R., Landahl, S., Nieuwoudt, H.H., Mouazen, A.M., Nicolaï, B.M. & Terry, L.A. (2014a). Assessment of rind quality of 'Nules Clementine' mandarin fruit during postharvest storage: 1. Vis/NIRS PCA models and relationship with canopy position. *Scientia Horticulturae*, **165**, 410–420.

Magwaza, L.S., Opara, U.L., Cronje, P.J.R., Landahl, S., Nieuwoudt, H.H., Mouazen, A.M., Nicolaï, B.M. & Terry, L.A. (2014b). Assessment of rind quality of 'Nules Clementine' mandarin fruit during postharvest storage: 2. Robust Vis/NIRS PLS models for prediction of physico-chemical attributes. *Scientia Horticulturae*, **165**, 421–432.

Magwaza, L.S., Landahl, S., Cronje, P.J.R., Nieuwoudt, H.H., Mouazen, A.M., Nicolaï, B.M., Terry, L.A. & Opara, U.L. (2014c). The use of Vis/NIRS and chemometric analysis to predict fruit defects and postharvest behaviour of 'Nules Clementine' mandarin fruit. *Food Chemistry*, 163, 267–274.

Magwaza, L.S. & Opara, U.L. (2014). Investigating non-destructive quantification and characterization of pomegranate fruit internal structure using X-ray computed tomography. *Postharvest Biology and Technology*, **95**, 1–6.

Makino, Y., Isami, A., Suhara, T., Oshita, S., Kawagoe, Y., Tsukada, M., Ishiyama, R., Serizawa, M., Purwanto, Y.A., Ahmad, U., Mardjan, S. & Kuroki, S. (2013). Non-destructive analysis of internal and external qualities of mango fruits during storage by hyperspectral imaging. *Acta Horticulturae*, **1011**, 443–450.

Makkar, H.P.S., Siddhuraju, P. & Becker, K. (2007). Plant secondary metabolites (pp. 74–75). Totowa: Humana Press.

Manley, (2014). Near-infrared spectroscopy and hyperspectral imaging: non-destructive analysis of biological materials. *Chemical Society Reviews*, **3**, 8200-8214.

Matityahu I., Glazer, I., Holland, D., Bar-Ya'akov, I., Ben-Arie, R. & Amir, R. (2014). Total antioxidative capacity and total phenolic levels in pomegranate husks correlate to several postharvest fruit quality parameters. *Food Bioprocess Technology*, DOI 10.1007/s11947-013-1184-7.

Stellenbosch University https://scholar.sun.ac.za

Meighani, H., Ghasemnezhad, M. & Bakhshi, D. (2014). Evaluation of biochemical composition and enzymatic activities in browned arils of pomegranate fruits. *International Journal of Horticultural Science and. Technology*, **1**, 53–65.

Mphahlele, R.R., Stander, M.A., Fawole, O.A. & Opara, U.L. (2014). Effect of fruit maturity and growing location on the postharvest contents of flavonoids, phenolic acids, vitamin C and antioxidant activity of pomegranate juice (cv. Wonderful). *Scientia Horticulturae*, **179**, 36–45.

Nicolaï, B.M., Beullens, K., Bobelyn, E., Peirs, A., Saeys, W., Theron, K.I. & Lammertyn, J. (2007). Non-destructive measurement of fruit and vegetable quality by means of NIR spectroscopy: a review. *Postharvest Biology and. Technology*, **46**, 99–118.

Pathare, P.B., Opara, U.L., Al-Said, F.A.J. (2013). Colour measurement and analysis in fresh and processed foods: A review. *Food Bioprocess Technology*, **6**, 36–60.

Tomás-Barberán, F.A. & Espín, J.C. (2001). Phenolic compounds and related enzymes as determinants of quality in fruits and vegetables. *Journal of the Science of Food and Agriculture*, **81**, 853–876.

Wold, S., Esbensen, K. & Geladi, P. (1987). Principal component analysis. *Chemometrics and Intelligent Laboratory Systems*, **2**, 37–52.

Zhang, L. & McCarthy, M.J. (2013). Assessment of pomegranate postharvest quality using nuclear magnetic resonance. *Postharvest Biology and. Technology*, **77**, 59–66.

Zhang, Y. & Zhang, R. (2008). Study on the mechanism of browning of pomegranate (*Punica granafum* L. cv Ganesh) peel in different storage conditions. *Agricultural Sciences in China*, **7**, 65-73.

Stellenbosch University https://scholar.sun.ac.za

Table 1

Pearson correlation coefficient matrix between chemical indices measured in Wonderful pomegranate 2015 season.

	PPO activity	POD activity	Total phenolics	Total tannins	Total anthocyanin	Weight loss	L*	a*	C*	h°	BI
PPO activity	**1.000000**										
POD activity	0.626866	**1.000000**									
Total phenolics	**-0.814409**	-0.671006	**1.000000**								
Total tannins	**-0.847462**	-0.746271	0.978696	**1.000000**							
Total anthocyanin	-0.436863	-0.605551	0.440721	0.519908	**1.000000**						
Weight loss	-0.617360	-0.697563	0.445072	0.568067	0.590511	**1.000000**					
L*	-0.469504	-0.588298	0.402066	0.494260	0.621304	0.667441	**1.000000**				
a*	-0.497279	-0.563113	0.385431	0.485277	0.530543	0.662996	0.385557	**1.000000**			
C*	-0.460602	-0.566987	0.427802	0.512557	0.576832	0.641927	0.642267	**0.841939**	**1.000000**		
h°	0.333754	0.331049	-0.182127	-0.257445	-0.280058	-0.415758	0.077571	-0.774619	-0.317449	**1.000000**	
BI	0.252436	0.227136	-0.121982	-0.184692	-0.325100	-0.341137	-0.702188	0.089906	-0.024802	-0.191220	**1.000000**

Correlation values in bold are significant at $p < 0.05$

Stellenbosch University https://scholar.sun.ac.za

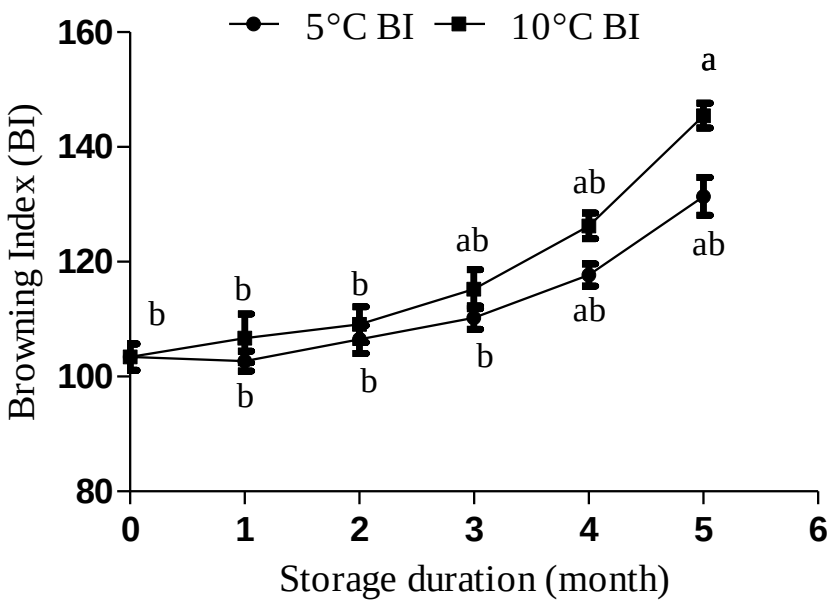

Source	Browning Index
Storage duration (A)	0.010
Temperature (B)	0.420
A*B	0.96

Figure 1. Change in browning index (BI) on pomegranate peel cv. Wonderful in relation to husk scald.

Stellenbosch University https://scholar.sun.ac.za

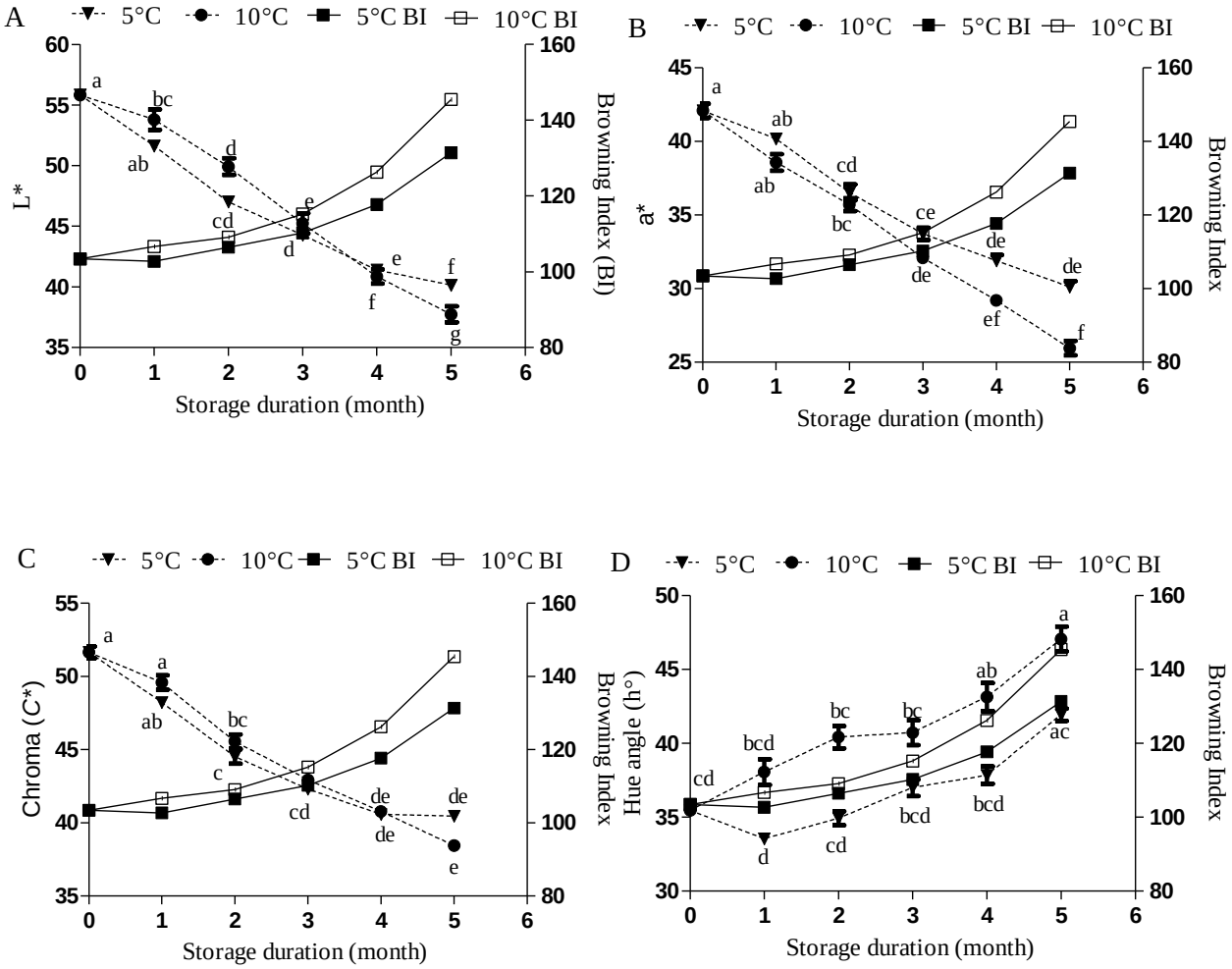

Source	L*	a*	*C**	h°
Storage duration (A)	<0.0001	<0.0001	<0.0001	0.0004
Temperature (B)	0.68	0.014	0.81	0.001
A*B	0.64	0.66	0.68	0.71

p value = 0.05

Figure 2. Change in colour dynamics of pomegranate peel cv. Wonderful in relation to browning index (A) L* lightness, (B) a* redness, (C) C* colour intensity and (D) hº Hue angle.

Stellenbosch University https://scholar.sun.ac.za

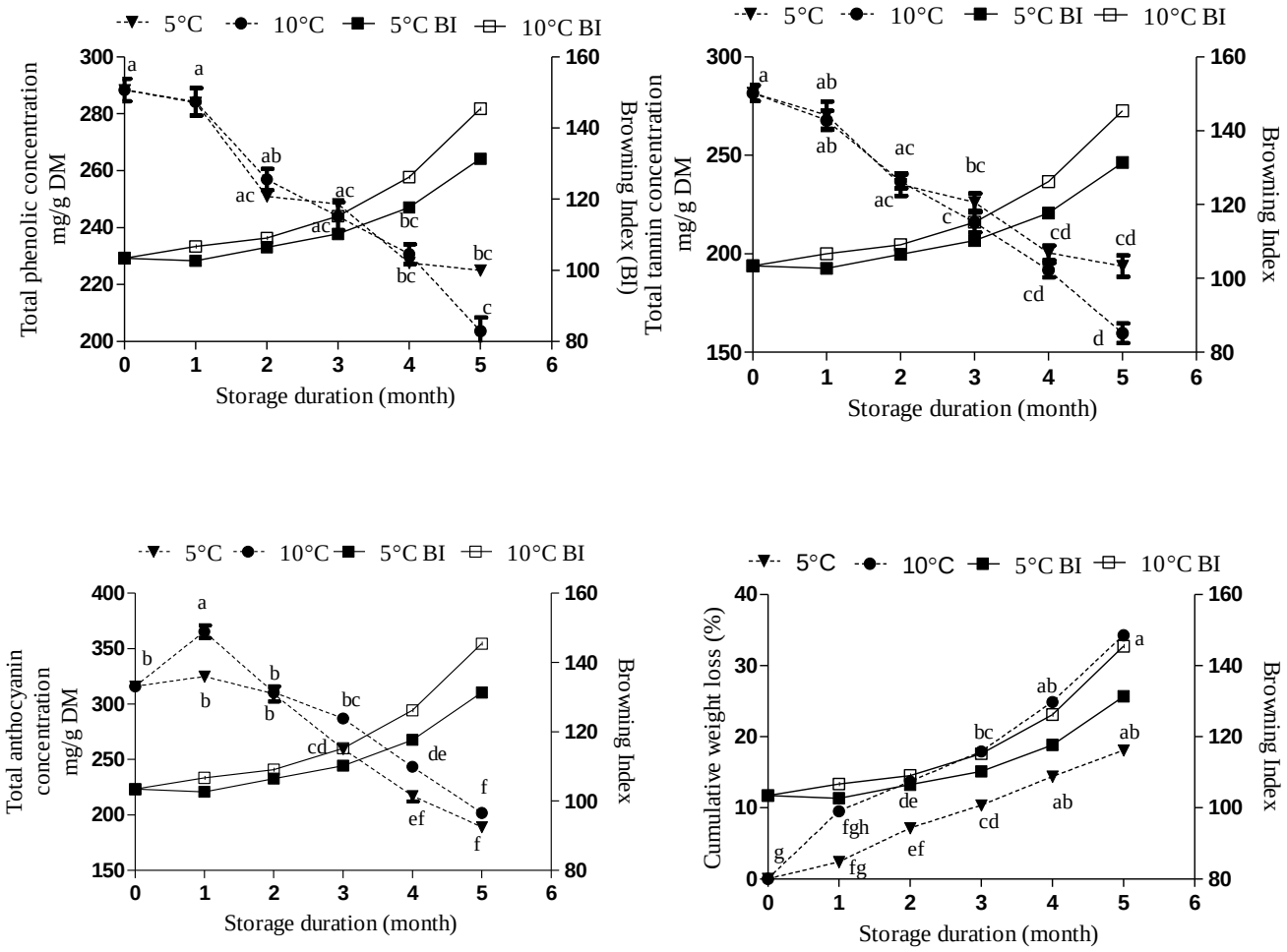

g

Source	Total phenolics	Total tannins	Total anthocyanin	Weight loss
Storage duration (A)	<0.0001	<0.0001	<0.0001	<0.0001
Temperature (B)	0.75	0.031	0.017	<0.0001
A*B	0.96	0.86	0.57	<0.0001

p value = 0.05

Figure 3. Change in phytochemistry and weight in pomegranate peel cv. Wonderful in relation to browning index (A) total phenolic concentration, (B) total tannin concentration, (C) total anthocyanin concentration and (D) cumulative weight loss.

Stellenbosch University https://scholar.sun.ac.za

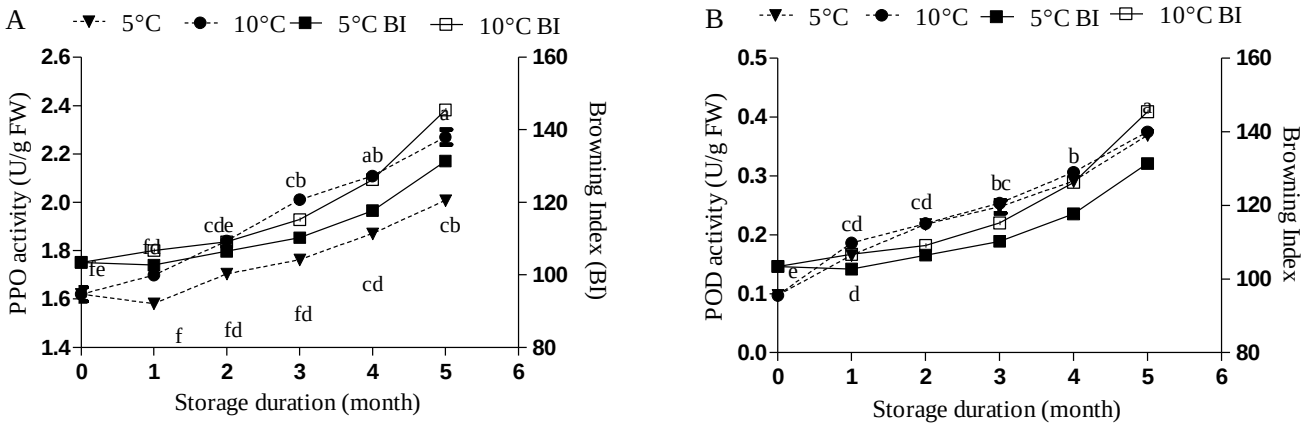

Source	PPO activity	POD activity
Storage duration (A)	<0.0001	<0.0001
Temperature (B)	0.0002	0.51
A*B	0.51	0.99

p value = 0.05

Figure 4. Change in enzymatic activity pomegranate peel cv. Wonderful in relation to browning index (A) polyphenol oxidase and (B) peroxidase.

Stellenbosch University https://scholar.sun.ac.za

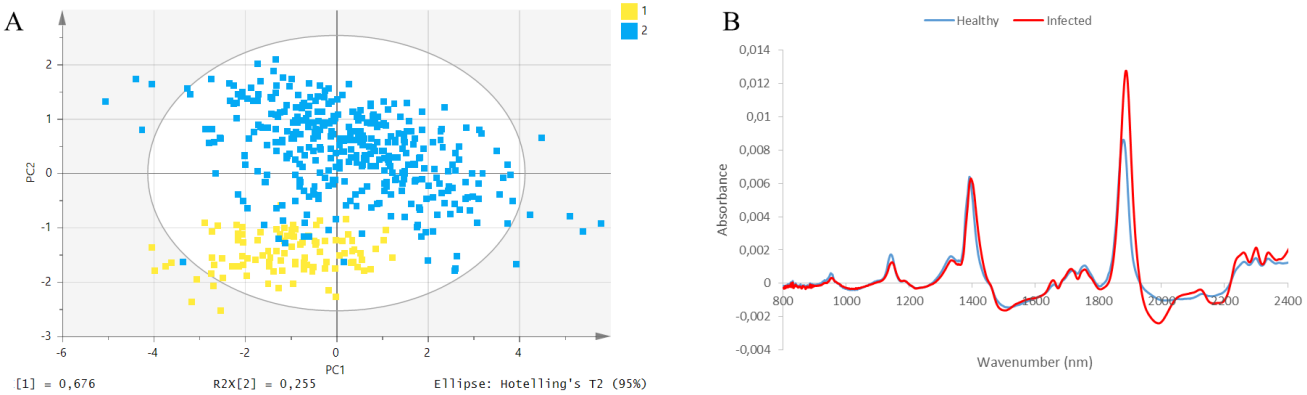

Figure 5. (A) PCA score plot for healthy and fruit associated with scald and (B) NIR baseline corrected spectra for healthy and fruit associated with scald.

Stellenbosch University https://scholar.sun.ac.za

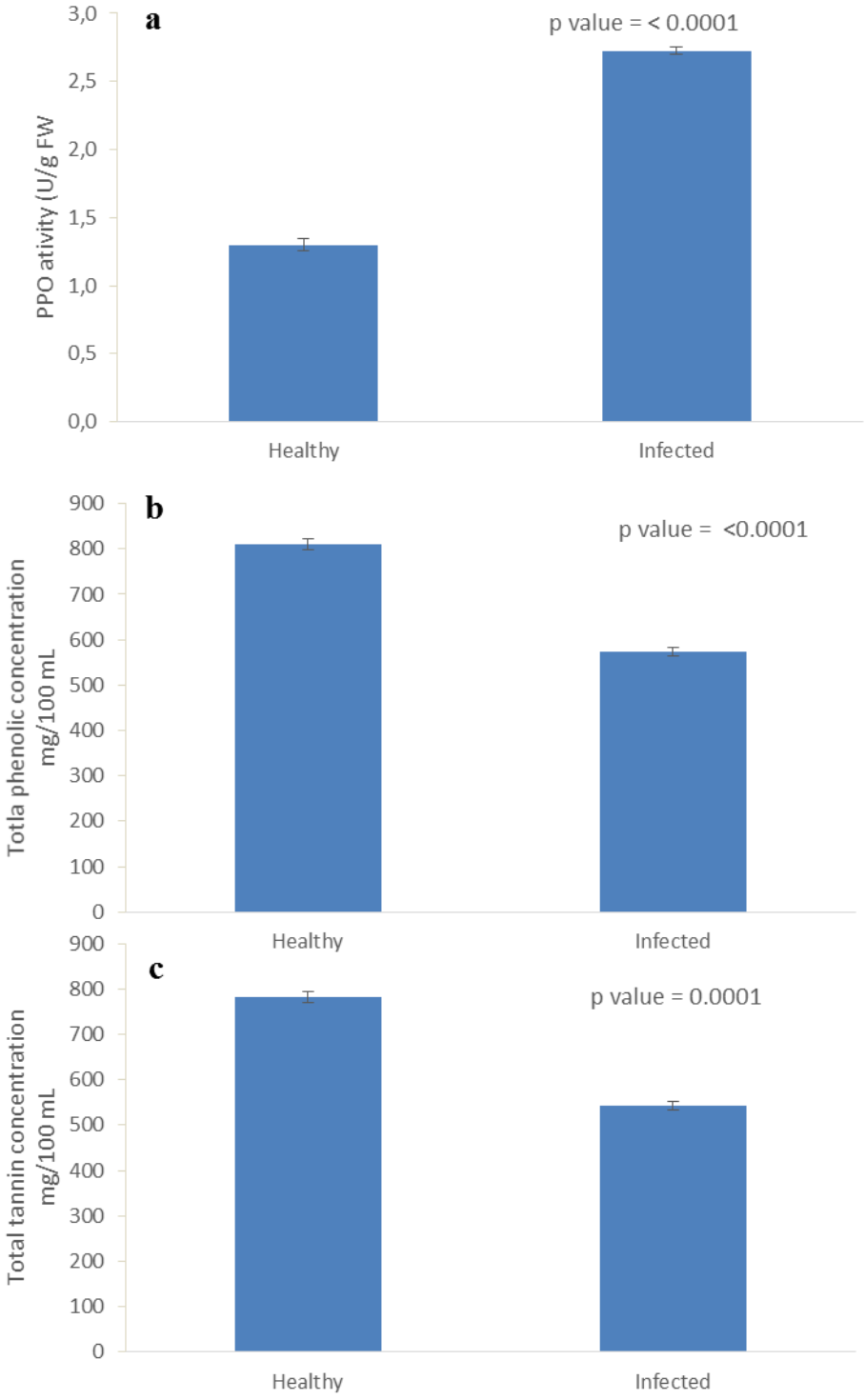

Figure 6. Comparison of chemistry by t-test (A) polyphenol oxidase activity, (B) total phenolic concentration and (C) total tannin concentration between healthy and fruit infected with husk scald.

Stellenbosch University https://scholar.sun.ac.za

A

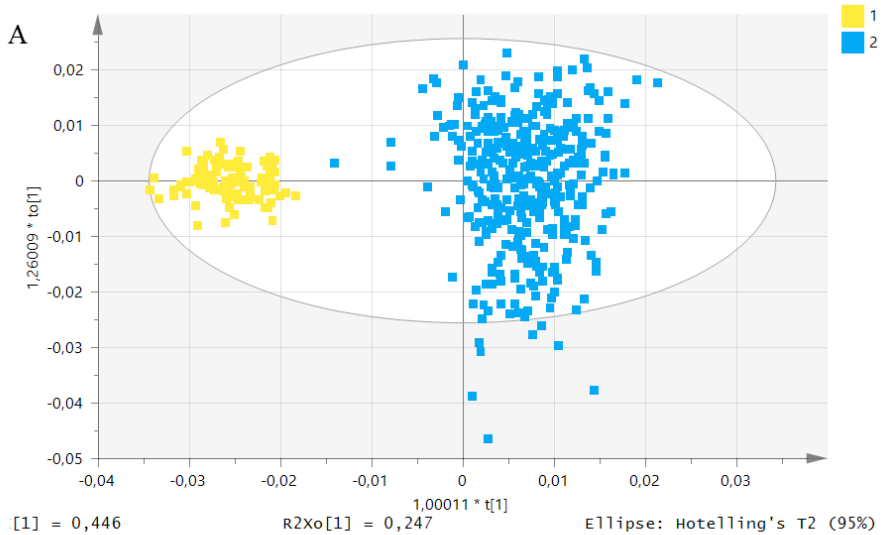

B

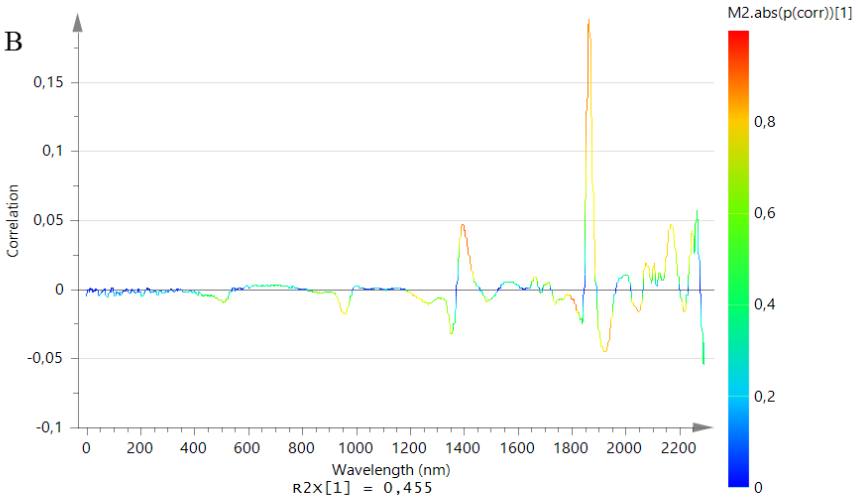

C

Misclassification dataset for OPLS-DA with class 1 = healthy and class 2 = infected

Class	Members	Correct	Class 1	Class 2	No class (YPred <= 0)
1	49	1	49	0	0
2	195	0.9949	1	194	0
No class	0		0	0	0
Total	244		50	194	0
Fisher's prob.	1				

D

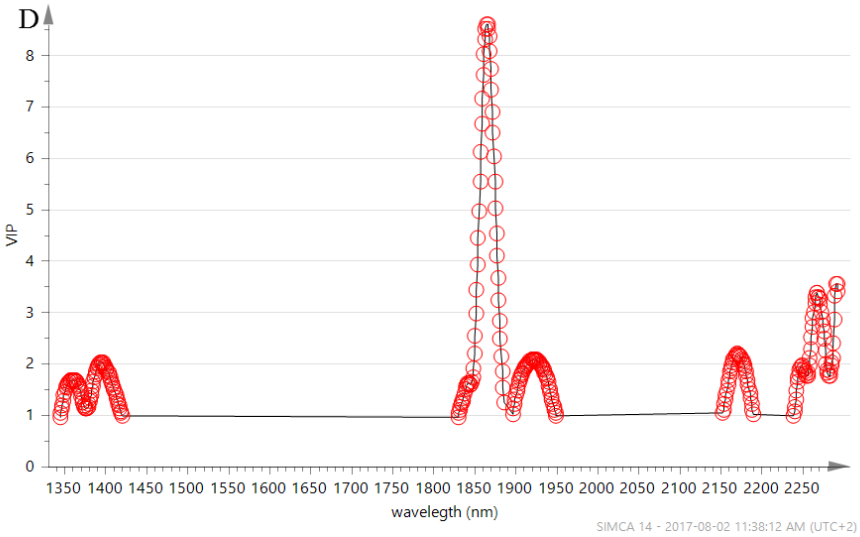

Figure 7. OPLS-DA score plot for all spectra n = 479, class 1 = healthy and class 2 = infected (A), the S-line plot showing wavenumbers responsible for discrimination between two classes (B) misclassification dataset for OPLS-DA (C) variable importance of projection (VIP) summarising the important wavelength regions responsible for model performance (D).

Stellenbosch University https://scholar.sun.ac.za

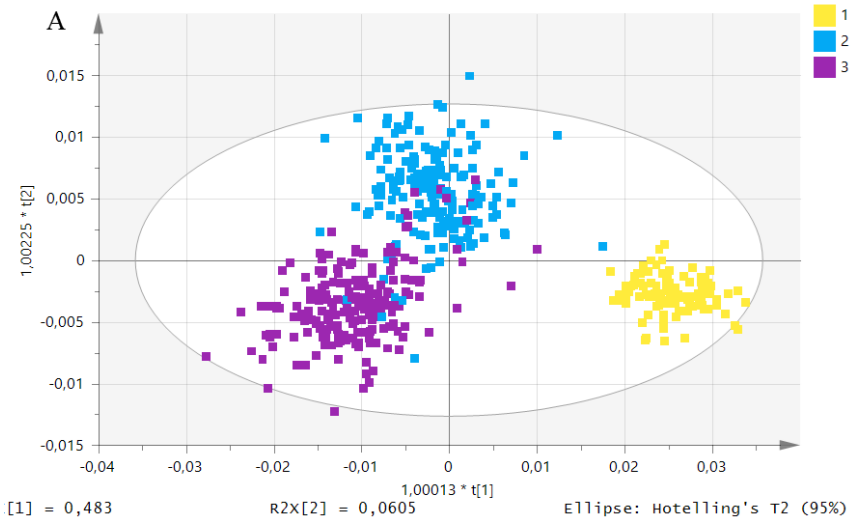

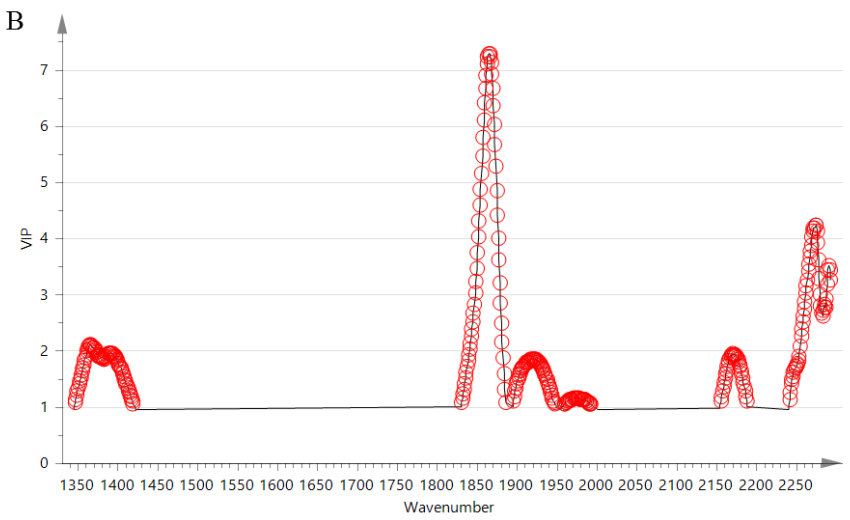

C Misclassification dataset for OPLS-DA with class 1 = healthy, class 2 = moderate scald and class 3 = severe scald

Class	Members	Correct	Class 1	Class 2	Class 3	No class (YPred <= 0)
1	49	100%	49	0	0	0
2	94	92.55%	1	87	6	0
3	101	93%	0	7	94	0
No class	0		0	0	0	0
Total	244		50	87	100	0
isher's prob.	1					

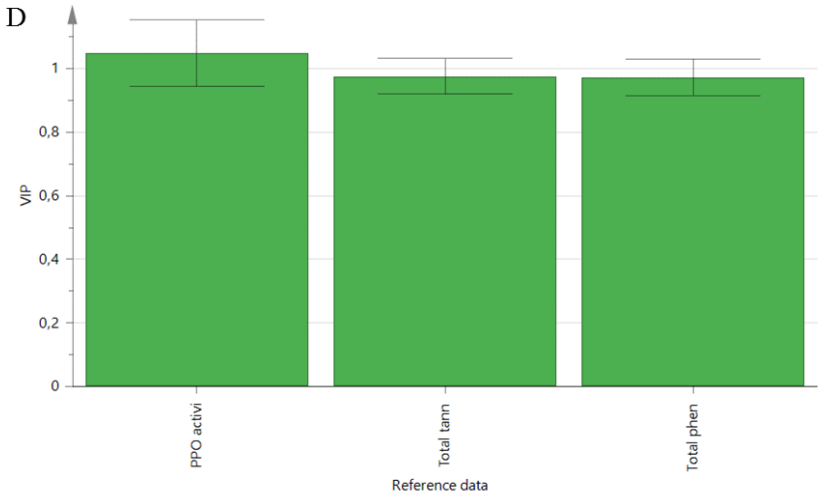

Figure 8. OPLS-DA score plot for all spectra n = 479, class 1 = healthy, class 2 = moderate scald and class 3 = severe scald (A), variable importance of projection (VIP) summarising the important wavelength regions responsible for model performance (B) misclassification dataset for OPLS-DA (C) variable importance of projection (VIP) summarising reference data responsible for model performance (D).

Stellenbosch University https://scholar.sun.ac.za

Section IV

Chapter 9: General discussion and conclusions

Stellenbosch University https://scholar.sun.ac.za

DECLARATION BY THE CANDIDATE

Regarding **Chapter 9 (pp 209-223)**, the nature and scope of my contribution were as follows:

Nature of contribution	Extent of contribution (%)
Writing of chapter	75

The following co-authors have contributed to **Chapter 9 (pp 209-223)**

Name	e-mail address	Nature of contribution	Extent of contribution (%)
Prof U.L. Opara	opara@sun.ac.za	Editorial suggestion and proof reading	10
Dr O.A. Fawole	olaniyi@sun.ac.za	Editorial suggestion and proof reading	10
Dr L.S. Magwaza	Magwazal@ukzn.ac.za	Editorial suggestion	5

E Arendse **Signature of candidate**	29/08/2017 **Date**

Stellenbosch University https://scholar.sun.ac.za

DECLARATION BY CO-AUTHORS

The undersigned hereby confirm that:

1. the declaration above accurately reflects the nature and extent of the contributions of the candidate and the co-authors to **Chapter 9 (pp 209-223)**

2. no other authors contributed to **Chapter 9 (pp 209-223)** besides those specified above, and

3. potential conflicts of interest have been revealed to all interested parties and that the necessary arrangements have been made to use the material in **Chapter 9 (pp 209-223)** of this dissertation.

Signature	Institutional affiliation	Date
Prof U.L. Opara	Stellenbosch University	29/08/2017
Dr O.A. Fawole	Stellenbosch University	29/08/2017
Dr L.S. Magwaza	University of KwaZulu-Natal	29/08/2017

Stellenbosch University https://scholar.sun.ac.za

CHAPTER 9

GENERAL DISCUSSION & CONCLUSIONS

1. Introduction

The commercial production of pomegranate fruit in South Africa has experienced drastic growth from 350 tonnes in 2009 season to 8000 tonnes in 2017, experiencing a 23-fold increase with over 5000 tons currently being exported. The increased growth rate is mainly attributed to fruit export to countries in the Northern Hemisphere during the shortfall period as well as consumer awareness of the potential health benefits linked to its consumption (Fawole & Opara, 2013a). However, the demand for fruit by consumers is principally governed by important external and internal attributes. Internal quality evaluation related to organoleptic and sensorial aspect of the fruit are based on the measurement of parameters such as total soluble solids (TSS), titratable acidity (TA), sugar to acid ratio (TSS:TA), BrimA and total phenolic content, while external attributes include fruit size, shape and skin appearance (colour, free of cracks, scalds and bruises). However, pomegranates are particularly susceptible to pest and disease infestations including the development of progressive physiological rind disorders, namely, husk scald (browning of peel surface) that occur during storage and commercial shipping of pomegranate fruit reducing its marketability (Caleb *et al.*, 2012; Fawole & Opara, 2013b). Pomegranate fruit, destined for the export market, are subjected to stringent inspection, fruit with substandard quality or any pest/diseases that are detected during inspection would result in rejection of total fruit consignments resulting in huge financial losses for the export industry. Hence internal and external quality assessment of pomegranate fruit is held in a high esteem in the export markets. Existing methods for evaluation of internal and external aspects are of destructive nature, time-consuming, and require specialised sample preparation. Therefore, quick screening non-destructive methods are required to evaluate and segregate fruit into different quality tiers. This study evaluated the use of near-infrared spectroscopy (NIRS) and microfocus X-ray computed tomography (X-ray µCT) as non-destructive methods for the evaluation of quality attributes, internal defects and physiological disorders in pomegranate fruit.

Stellenbosch University https://scholar.sun.ac.za

The overall aim of this research study is to develop non-destructive methods to predict the internal and external quality of pomegranate fruit.

This dissertation was structured into three sections each comprising of published or submitted manuscripts addressing a research theme.

- Section I: Review of literature on non-destructive methods for the measurement of fruit quality
- Section II: Non-destructive evaluation of physicochemical quality properties of pomegranate fruit and its fractions.
- Section III: Non-destructive evaluation and prediction of internal defects and postharvest physiological rind disorder.

2. General discussion

2.1. Non-destructive evaluation of physico-chemical quality properties of pomegranate fruit and its fractions (Section II)

Physical properties of pomegranate fruit such as the volume of fruit and arils relative to the peel content are of considerable economic importance for breeders, growers and consumers. Furthermore, volumes of the juice and kernels relative to the arils are important as it influences industrial processing value. These physical characteristics such as aril content (number of kernels, volume and juice content) relative to peel fraction may exhibit significant differences due to variability amongst cultivars, preharvest management practices, maturity and growing location (Fawole & Opara, 2014; Mphahlele *et al.,* 2014; Arendse *et al.,* 2016a). Currently, evaluation of these physical characteristics and the proportion of individual components are of destructive nature. These destructive methods have several drawbacks; they are labour intensive, require specialised sample preparation and are inapplicable for in-line grading and sorting in commercial pack-houses. Consequently, the high variability in quality attributes amongst cultivars or even the same cultivar has promoted the development of non-destructive techniques for detection, prediction and segmentation of fruit quality for laboratory and grading that can both visualise and quantify internal and external structures of individual fruit. **Chapter 3** evaluated the use of microfocus X-ray µCT as a non-destructive method for characterization and volume estimation of pomegranate fruit and its fractions. The ability of µCT to estimate volumes of whole fruit, total arils, peel, juice content and kernels were studied.

Stellenbosch University https://scholar.sun.ac.za

The statistical comparison between µCT and destructive methods provided an insight into the high accuracy of µCT as a non-destructive tool to characterise and quantify intact individual fruit and fruit fractions. This study revealed that the calculated volume using µCT for arils and peel were 162.45 ±16.21 and 163.87 ±21.42 mL respectively, which was equivalent to 48.04 and 48.46% of the total fruit volume (338.19 ±22.41 mL). Calculated juice volume (146.07 ±16.28 mL) and kernel volume (16.38 ±1.81 mL) constituted 89.92% and 10.08% of total aril volume (162.45 ±16.21 mL). Validation results using destructive methods gave volumes for total arils (163.28 ±15.24 mL), peel (161.81 ±20.60 mL), juice content (142.73 ±16.41 mL) and kernels (15.10 ±1.63 mL), respectively, providing similar results as µCT predicted data. Considering that the knowledge of fruit edible and non-edible portion is important to growers and food processors, µCT could be used as a non-destructive tool to accurately characterise the proportion of internal components without application of destructive methods. Furthermore, the application of µCT could contribute to classifying different pomegranate cultivars based on their stage of maturity and morphological fractions allowing the segregation of fruit into different quality tiers based on different fruit characteristics. However, despite the enormous potential displayed by µCT, the systems are expensive and currently only available to researchers due to the lengthy time required for data acquisition and analysis.

A recent trend in postharvest research and analytical chemistry has shifted towards the use of objective techniques that provide accurate, fast and cost-effective solutions for the evaluation of different physical properties and chemical constituents in agricultural materials (Magwaza *et al.*, 2012; de Oliveira *et al.*, 2014). NIRS combined with chemometric software is a powerful non-destructive tool capable of measuring quality attributes at a speed compatible with commercial pack-lines, which may be as high as 10 fruit per second (Nicolaï *et al.*, 2008). Therefore, multifunctional evaluation of NIR spectroscopy for the prediction of physico-chemical and phytochemical parameters in pomegranate fruit and its fractions were investigated and discussed in chapters 4 to 6. The use of NIRS for prediction of internal and external parameters in intact pomegranate fruit was studied in **Chapter 4**. Two Fourier transform near-infrared (FT-NIR) diffuse reflectance spectrometers with different spectral acquisition modes were evaluated, namely, direct contact between the sample with integrating sphere (IS) of the Multi-Purpose Analyser (MPA) and contact-less measurement using an optic fibre coupled emission head (EH) of the MATRIX^{TM}-F. The developed calibration models for the EH provided the best prediction

Stellenbosch University https://scholar.sun.ac.za

statistics for firmness, fruit colour components (a*), Chroma (C), total soluble solids (TSS), titratable acidity (TA), BrimA, total phenolics and vitamin C concentration. Although, the IS provided good prediction statistics for colour component Hue, TSS:TA and total anthocyanin. Furthermore, the contactless EH spectrophotometer gave the best prediction results for 9 of the 13 quality attributes, suggesting its potential for online application for the measurement of integrated fruit quality. Considering that the chances of a successful commercial implementation of non-destructive technology depend on model robustness, fruit from two different locations were included in this study. The results from this study suggested that the sample collection showed a wide range of variability in TSS and TA values. Limited research has been conducted before this current study on assessing the suitability of FT-NIR to predict pomegranate quality attributes (Khodabakhshian *et al.*, 2016). Therefore, this research study provided a significant contribution towards the potential development of an online application for the evaluation of external and internal quality attributes for pomegranate fruit. FT-NIR has several limitations compared to dispersive NIR including the fact that the time to acquire spectra is longer than dispersive NIR. Additionally, fruit that were exposed for longer periods to FT-NIR were burnt due to the high intense heat.

Aside from being the first study on non-destructive evaluation of pomegranate arils, the novelty of the study in **Chapter 5** involved evaluation of two different spectral acquisition modes for optimization of FT-NIRS to predict organoleptic and phytochemical quality parameters in pomegranate arils. The two spectral acquisition methods acquired diffuse reflectance spectra included an integrating sphere (IS) and an emission head (EH) applied over a spectral region of 800-2500 nm. The results of this study demonstrated that the EH, a contactless option of the MATRIX^{TM}-F provided better prediction performance and outperformed the IS of the MPA. The emission head gave the best results for TSS, pH, TA, BrimA, colour hue, total phenolics, total anthocyanin and vitamin C, while the integrating sphere provided the best results for TSS:TA, firmness, arils redness (a*) and colour intensity (chroma). Considering that the EH irradiated a larger surface (180 mm) compared to the IS (50 mm), resulting in the prediction of eight parameters, successful application of the contactless option of the Matrix^{TM}-F could be implemented as an online tool to automatically and simultaneously measure a combination of quality parameters.

Stellenbosch University https://scholar.sun.ac.za

Pomegranate juice has been described to contain a considerable amount of sugars, organic acids, vitamins, mineral elements and a diverse array of complex biochemical constituents (Arendse *et al.,* 2015). Pomegranate juice is obtained by either crushing whole pomegranate fruit or extracted arils. Infrared (IR) spectroscopy in combination with chemometric software either in the near-infrared (NIR, 12500-4000 cm^{-1}) or mid-infrared (MIR, 4000-400 cm^{-1}) spectral region have been extensively applied as an analytical tool in the beverage industry. Limited studies have been conducted to assess the potential use of NIR spectroscopy, MIR and a combination of both NIR/MIR in the assessment of juice quality. Therefore, the use of different spectral acquisition methods was considered in this study. The findings reported in the study of **Chapter 6** provided insight into a critical statistical comparison between near and mid-infrared spectrometers for the evaluation of organoleptic and phytochemical quality attributes of pomegranate juice quality. Three different spectral acquisition methods were considered, including the MPA FT-NIR spectrometer, Alpha-P FT-MIR spectrometer and WineScan FT-NIR/MIR spectrometer. The results of this study suggest that spectrometric instruments in the mid infrared region performed better compared to the near-infrared region this may partially be due to the fact that the mid-infrared spectrum contains wavelengths for fundamental rotational molecular vibration which is highly sensitive to specific chemical composition compared to near-infrared spectrum. The results suggested that model development with the WineScan in the NIR/MIR region of 5000-930 cm^{-1} provided the best prediction statistics for total soluble solids (RPD = 3.32), TSS:TA ratio (RPD = 2.64), BrimA (RPD = 2.09), total phenolic concentration (RPD = 1.78), total anthocyanin concentration (RPD = 1.95) and colour component hue (RPD = 1.73). The Alpha-P in the MIR region of 4000-600 cm^{-1} gave the best prediction statistics for pH (RPD = 2.18), and colour components a* (RPD = 2.66) and Chroma (RPD = 2.45). The MPA in the NIR region of 12500-4000 cm^{-1} gave the best prediction statistics for titratable acidity (RPD = 2.70) and vitamin C concentration (RPD = 1.85).

Since the MIR spectrometers provided better prediction statistics compared to NIR, a statistical comparison between the three instruments was performed on selected parameters using Bland and Altman and Passing-Bablok analytical algorithms. The repeatability of all three instruments was also assessed. The results were found to be highly repeatable with the WineScan providing the lowest mean square error of the three instruments. Furthermore, even though the prediction statistics (RMSEP and RPD) for the three instruments were different, the statistical

Stellenbosch University https://scholar.sun.ac.za

analyses for both Bland and Altman and Passing-Bablok suggest that none of the three instruments were statistically different. This study demonstrated that a combination of near to mid-infrared spectrometer such as the WineScan can potentially be used in the industrial application setting for the simultaneous measurement of multiple quality parameters.

2.2. *Non-destructive evaluation and prediction of postharvest physiological disorders and internal defects (Section III)*

South African pomegranate export industry is currently plagued with huge quality losses due to insect infestation and occurrence of physiological disorders (Munhuweyi *et al.*, 2016). False codling moth is a pest that has been reported to cause loss of entire pomegranate orchards within South Africa. The larva eggs laid on the fruit surface by the female moth emerge and penetrate the fruit causing internal decay, premature ripening and abscission or fruit drop (Arendse *et al.*, 2016b). Blackheart infestation is another major internal disorder impacting the production of pomegranate fruit worldwide. Blackheart infected fruit shows no external symptoms, although internal symptoms include a mass of blackened arils within the fruit ranging from sections of the pomegranate fruit to all the arils. Limited research has been conducted to develop technologies that can assess, predict and monitor disorders and internal defects within pomegranate fruit. The research study conducted in **Chapter 7** was aimed at evaluating the potential use of microfocus X-ray computed tomography (µCT) for differentiating between healthy fruit and internal disorders such as false codling larva moth and blackheart fruit based on its absolute density. In a quest to estimate the absolute density, a calibration function of different homogenous polymeric materials was used with a density ranging from 910 to 2150 kg m^{-3}. The statistical comparison between µCT and destructive methods provided an insight into high accuracy of µCT as a non-destructive tool to differentiate between healthy false codling larva moth and blackheart fruit respectively The results of this study revealed that the estimation of the density of pomegranate fruit, its fractions (arils and albedo), false codling moth and blackheart were successfully determined within the calibration range. µCT in combination with polymeric materials and image analysis showed that the codling larva moth can clearly be differentiated from pomegranate fruit and its factions based on absolute density. The density of the moth larva (940 ±40 kg m^{-3}) was found to be significantly lower compared to fruit fractions (arils 1120 ±40 kg m^{-3} and albedo 1040 ±30 kg m^{-3}). Similarly, different densities were observed for healthy (1070 ±20 kg m^{-3}) and blackheart infected fruit (870 – 1000 kg m^{-3}). Interestingly, with an increase in the severity of blackheart infestation, a decrease

Stellenbosch University https://scholar.sun.ac.za

in absolute density in the fruit were observed. The relevance of the density to fruit mass is that with an increase in the severity of blackheart the less dense fruit become and hence the lighter fruit weight.

The results thus demonstrated that the developed algorithm can be used to accurately characterise fruit internal components and detect the presence of false codling moth within pomegranate fruit. From an industrial viewpoint, discriminative power of X-ray μCT combined with image analysis and homogenous polymeric materials could successfully differentiate between tissues and detect internal disorders and diseases based on absolute density. The application of the developed algorithm would ensure that high quality fruit without any internal defects reaches the export markets, thereby reducing postharvest losses and ensuring quality certified fruit to consumers and industrial processors.

Husk scald is a physiological rind disorder that manifests during storage and commercial shipping of pomegranate fruit. In order to gain better insight into the mechanism of husk scald, Chapter 8 focused on two objectives; first, to evaluate several biochemical markers associated with the development of husk scald; and second, to assess the possibility of FT-NIR to discriminate between healthy and scalded fruit. The effects of temperature and storage duration on several parameters such as weight loss, colour attributes, total phenolics, total tannins, total anthocyanin content and enzymatic activity (polyphenol oxidase (PPO), peroxidase (POD)) in relation to the development of scald were assessed. This study demonstrated that the development of husk scald was primarily influenced by storage duration. Although, fruit stored at 10 °C exhibited higher scalding incidence compared to storage at 5 °C over a 5-month period. The results of this study showed that an increase in peel browning was observed that a decrease in colour attributes (L*, a*, C*), total phenolics, tannins and anthocyanins. The enzymatic activity (PPO and POD) and weight loss increased with storage temperature and duration. Correlation analysis was performed in order to determine if the studied variables may play a role in the development of husk scald. Correlation analysis revealed a significant negative correlation between PPO activity and total phenolic ($r = -0.81$) and total tannins ($r = -0.85$) compounds were observed. The negative interrelationship between these variables suggests that as total phenolic and tannin compounds decrease as enzymatic activity increases. The decrease in these compounds is attributed to their degradation into simpler phenolic acids and the oxidation of these simpler phenolic compounds by PPO. Furthermore, our study is in-line with Zhang and Zhang (2008) who reported that enzymatic

Stellenbosch University https://scholar.sun.ac.za

tannin denaturation was the main cause that led to peel browning of pomegranate fruit during storage. Therefore, the results of this current research study strengthen the hypothesis that the enzyme polyphenol oxidase and degradation of total tannins occurring during storage were responsible for peel browning.

FT-NIR diffuse reflectance spectroscopy was used to non-destructively discriminate between healthy and scalded fruit. The reflectance spectra and biochemical markers associated with scald were subjected to orthogonal partial least squares discriminant analysis (OPLS-DA). Fruit were classified into three categories namely; healthy, moderate scald and severe scald, achieving a classification accuracy of 100% healthy, 92.6% moderate scald and 93% severe scald, respectively. Variable importance (VIP) revealed that PPO activity, total phenolic and tannin concentration all contributed to the model's performance while the wavelength regions responsible for discrimination between classes were at 1350-1450, 1830-1950 and 2150-2250 nm, these regions have been attributed to stretching of C–O, O–H and C–C bonds. Therefore, this study successfully demonstrated the biochemical markers associated with the development of husk scald could potentially be used to non-destructively discriminate between healthy and scalded fruit. The merits of this study could assist researchers towards an in-depth understanding of husk scald mechanism. Furthermore, this research quantified enzymes and substrates involve in the development of scald and the conducted research opens the future possibility of controlling the development of husk scald.

2.3. *Non-destructive evaluation of the prediction accuracy between pomegranate fruit and its fractions*

Two non-destructive methods was assessed within this dissertation for the multi-evaluation of pomegranate fruit (cv. Wonderful) and its fractions. Therefore, this section provides a comprehensive summary and attempts to compare the accuracy of prediction between pomegranate fruit, arils and juice for selected parameters. Since the application of NIR spectroscopy in chapter 4, 5 and 6 included the same quality measurements for model development, only three main parameters used for quality evaluation were selected for comparison, these include TSS, TA and its TSS:TA ratio (Table 1). The results suggest that the prediction statistics for TSS were superior for pomegranate juice (R^2 = 94.76, RPD = 3.62) compared to arils and whole fruit. While, the prediction statistics for arils (R^2 = 85.75, RPD =

Stellenbosch University https://scholar.sun.ac.za

2.19) were better compared to whole fruit (R^2 = 83.64, RPD = 1.92). A similar trend in prediction accuracy for model development was observed for TA and TSS: TA ratio in which the juice had superior prediction ability (Table 1). The order of prediction accuracy were as follows juice > arils > whole fruit. The reduced accuracy of NIR spectroscopy for the measurement of internal quality on whole fruit may be due to limited penetration depth of NIR radiation within the tissue. Since it is known that NIR spectroscopy has a finite penetration distance which is affected by the optical path and density. The thickness of the optical barrier affects the penetration depth. Considering that whole fruit has a larger optical density compared to the arils and juice due to the thickness of its rind, it is therefore not surprising that the prediction accuracy of the juice were better than the arils and the whole fruit. Therefore, it is recommended that the use of NIR spectroscopy would be better suited for the evaluation of juice quality for commercial application.

µCT as a non-destructive tool was used to characterise, quantify and detect internal disorders within pomegranate fruit. Two approaches were considered, chapter 3 characterised fruit based on volume estimation and chapter 7 considered the use of calibration function for fruit characterisation and defect detection. Therefore, this paragraph provides a comprehensive summary and attempts to compare the prediction error between the two methods. The results suggest that the approach using volume estimation for characterisation of fruit fractions provided the lowest prediction error (Table 2). The prediction error using volume estimation were whole fruit (0.25%), arils (0.50%) and albedo (1.27%) compared to the use of calibration function which was observed to have 2.8, 7.0 and 1.9 fold increase in prediction error for whole fruit (0.25%), arils (0.50%) and albedo (1.27%) respectively. However, the results from both approaches suggest that µCT is highly accurate due the low residual with no significant differences being observed as result of the paired t-test. Although, the use of volume estimation approach may have drawbacks compared to the use of calibration function. For instance, segmentation of internal components based on interactive thresholding and grey values alone is time consuming and difficult in comparison to calibration function in which internal components can be differentiated based on its density and mass using adaptive thresholding techniques. Therefore, it is recommended that future research should include a density calibration function for characterisation of fruit internal components.

3. General conclusion and recommendations

Stellenbosch University https://scholar.sun.ac.za

In conclusion, this dissertation contributed to the non-destructive multi evaluation of the external and internal quality of pomegranate fruit. This study showed that the MATRIX^{TM}-F FT-NIR spectrometer fitted with an emission head could be implemented as a rapid online tool for the assessment combination of various quality parameters in intact pomegranate fruit and arils. Although, the assessment of juice quality was best suited using the FT-NIR/MIR WineScan spectrometer. Furthermore, this study evaluated several biochemical markers associated with the development of husk scald and demonstrated the importance of temperature and storage duration of enzymatic activity and phytochemical content. Higher temperature and prolonged storage resulted in a degradation of phytochemical compounds and increase in enzymatic activity which ultimately led to increase in severity in husk scald. Additionally, the use of FT-NIR spectroscopy successfully discriminated between healthy and husk scalded fruit using spectral and reference data. This study demonstrated that microfocus X-ray computed tomography (µCT) as a non-invasive technique could characterise fruit internal components and differentiate between tissues and different internal disorders.

The evaluated non-destructive based methods for assessing desired quality attributes, internal defects and physiological disorders reported in this thesis would ensure the supply of good quality fruit in both local and international markets, thereby reducing losses and waste arising from rejects and claims. The implementation of these methods would provide potential benefits such as maintaining competitive edge of the South African industry in the global markets. Additionally, this thesis provides new understanding and better insights on fruit characteristics of pomegranate fruit grown in South Africa. However, costs of implementation of these non-destructive tools would be high, which ultimately would result in increased premium associated with the commodity. Considering that consumers would receive high quality fruit without any internal defects the increase in the premium may, therefore, be justified. Overall, the study provides new knowledge on non-destructive tools which would help assist fruit packers to segregate fruit based on various quality aspects, internal defects and physiological rind disorders in order to maintain fruit postharvest quality and reduce losses.

One limitation with the use of NIR spectroscopy within this study was that fruit from only two locations, one season and one cultivar were considered. Therefore, the model development within this dissertation may not be applicable to all cultivars. It is, therefore, recommended that for successful commercial online application, future studies need to consider the addition of

Stellenbosch University https://scholar.sun.ac.za

different cultivars, growing locations, and seasonality. Considering, this study only acquired FT-NIR spectra on the equilateral portion of the whole fruit for the development of calibration models. The challenge with acquiring spectra in this manner is that it is not in-line with commercial sorting lines since fruit are randomly rolled onto the conveyor belt. Therefore, in order to holistically apply FT-NIR, it is recommended that a sub-trail be conducted on acquiring spectra at different positions of the fruit in order to test its predictive ability, however, it is noteworthy that a significant increase in the prediction error may be observed as a result of the spatial difference in fruit quality. The use of μCT within this dissertation have several drawbacks and such as expensive equipment and lengthy time required for data acquisition and image analysis. Future research with μCT systems should focus on reducing the number of scans per sample in order to provide faster data acquisition times, including automated processing software which would ultimately allow μCT systems to be cheaper and faster. Additionally, future research should explore the potential use of other non-destructive methods such as hyperspectral imaging and nuclear magnetic resonance for the development and application of objective, fast and non-destructive assessment methods. This will ensure a supply of high quality fruit to the export markets, thereby allowing South Africa's to maintain its competitive edge in the industry.

References

Arendse, E., Fawole, O.A. & Opara, U.L. (2015). Effects of postharvest handling and storage on physiological attributes and quality of pomegranate fruit (*Punica granatum* L.): A review. *International Journal of Postharvest Technology and Innovation*, **5**, 13–31.

Arendse, E., Fawole, O.A., Magwaza, L.S. & Opara, U.L. (2016a). Non-destructive characterization and volume estimation of pomegranate fruit external and internal morphological fractions using X-ray computed tomography. *Journal of Food Engineering*, **186**, 42–49.

Arendse, E., Fawole, O.A., Magwaza, L.S. & Opara, U.L. (2016b). Estimation of the density of pomegranate fruit and their fractions using X-ray computed tomography calibrated with polymeric materials. *Biosystems Engineering*, **148**, 148–156.

Caleb, O.J., Opara, U.L. & Witthuhn, C. (2012). Modified atmosphere packaging of pomegranate fruit and arils: A review. *Food and Bioprocess Technology*, **5**, 15–30.

Stellenbosch University https://scholar.sun.ac.za

De Oliveira, G.A., Bureau, S., Renard, C.M.G.C., Pereira-Netto, A.B. & de Castilhos, F. (2014). Comparison of NIRS approach for prediction of internal quality traits in three fruit species. *Food Chemistry*, **143**, 223–230.

Fawole, O.A. & Opara, U.L. (2013a). Harvest discrimination of pomegranate fruit: postharvest quality changes and relationships between instrumental and sensory attributes during shelf life. *Journal of Food Science*, **78**, 1264-1272.

Fawole, O.A. & Opara, U.L. (2013b). Effects of storage temperature and duration on physiological responses of pomegranate fruit. *Industrial Crops and Products*, **47**, 300–309.

Fawole, O.A. & Opara, U.L. (2014). Physicomechanical, phytochemical, volatile compounds and free radical scavenging properties of eight pomegranate cultivars and classification by principal component and cluster analyses. *British Food Journal*, **116**, 544–567.

Khodabakhshian, R., Emadi, B., Khojastehpour, M., Golzarian M.R. & Sazgarnia A. (2016). Non-destructive evaluation of maturity and quality parameters of pomegranate fruit by visible/near infrared spectroscopy. *International Journal of Food Properties*, **20**, 41–52.

Magwaza, L.S., Opara, U.L., Terry, L.A., Landahl, S., Cronje, P.J., Nieuwoudt, H., Mouazen, A.M., Saeys, W. & Nicolaï, B.M. (2012). Prediction of 'Nules Clementine' mandarin susceptibility to rind breakdown disorder using Vis/NIR spectroscopy. *Postharvest Biology and Technology*, **74**, 1–10.

Mphahlele, R.R., Stander, M.A., Fawole, O.A. & Opara, U.L. (2014). Effect of fruit maturity and growing location on the postharvest contents of flavonoids, phenolic acids, vitamin C and antioxidant activity of pomegranate juice (cv. Wonderful). *Scientia Horticulturae*, **179**, 36–45.

Munhuweyi, K., Lennox, C.L., Meitz-Hopkins, J.C., Caleb, O.J. & Opara, U.L. (2016). Major diseases of pomegranate (*Punica granatum*, L.), their causes and management—A review. *Scientia Horticulturae*, **211**, 126–139.

Nicolaï, B.M., Verlinden, B.E., Desmet, M., Saevels, S., Saeys, W., Theron, I.K., Cubeddub, R., Pifferi, A. & Torricelli, A. (2008). Time-resolved and continuous wave NIR reflectance spectroscopy to predict soluble solids content and firmness of pear. *Postharvest Biology and Technology*, **47**, 68–74.

Stellenbosch University https://scholar.sun.ac.za

Table 1

Comparing the prediction accuracy between models developed for whole fruit, arils and juice for pomegranate (cv. Wonderful) using the Multi-Purpose Analyser

	R^2	RMSEE	RMSEP	RPD	R^2	RMSEE	RMSEP	RPD	R^2	RMSEE	RMSEP	RPD
Sample		TSS (%)				TA (%)				TSS:TA		
Whole fruit	83.64	0.25	0.32	1.92	85.88	0.10	0.14	2.00	65.10	0.71	0.81	1.50
Arils	85.75	0.23	0.31	2.19	80.44	0.10	0.13	2.29	82.2	0.87	1.03	2.13
Juice	94.76	0.32	0.31	3.62	93.43	0.08	0.11	2.70	83.37	1.00	1.00	2.08

R^2, coefficient of determination; RMSEE, root mean square error of estimation; RPD, residual predictive deviation; RMSEP, root mean square error of prediction; TSS, total soluble solids; TA, titratable acidity

Stellenbosch University https://scholar.sun.ac.za

Table 2

Comparing the prediction error between two different approaches for characterisation of pomegranate fruit fractions using microfocus X-ray computed tomography

Parameter	Method	Predicted	Destructive	Residual	Prediction Error (%)	Paired t-test
Whole fruit	Volume estimation	338.19 ±22.41 (mL)	337.36 ±22.56 (mL)	0.83	0.25	0.99
	Calibration function	259.84 ±36.90 (g)	261.72 ±37.22 (g)	1.88	0.69	0.90
Arils	Volume estimation	162.45 ±16.21 (mL)	163.28 ±15.24 (mL)	0.83	0.50	0.85
	Calibration function	153.42 ±34.58 (g)	159.06 ±33.09 (g)	5.63	3.54	0.91
Albedo	Volume estimation	163.87 ±21.42 (mL)	161.81 ±20.60 (mL)	2.06	1.27	0.74
	Calibration function	104.73 ±14.56 (g)	102.30 ±11.66 (g)	2.43	2.38	0.71

Stellenbosch University https://scholar.sun.ac.za

Stellenbosch University https://scholar.sun.ac.za

APPENDIX CHAPTER 4

Table 1
Model performance for fruit weight using different FT-NIR instruments

Parameter	NIR probe	Pre-processing	Spectral range (nm)	Calibration			Validation					
				LV	R^2	RMSEE	R^2	RMSEP	RPD	Bias	Slope	Corr.
Fruit weight (g)	IS	None	1064-1333, 2064-2355	9	79.40	12.30	59.24	16.20	1.57	0.53	0.61	0.77
		FD	1064-1333, 2064-2355	5	63.33	15.90	44.34	19.20	1.34	0.13	0.49	0.67
		SD	1064-1333, 2064-2355	7	87.55	7.57	56.39	15.00	1.52	0.64	0.69	0.76
		MSC	1064-1333, 2064-2355	8	81.07	9.70	62.36	11.90	1.63	0.40	0.57	0.79
		SNV	1064-1333, 2064-2355	9	76.70	10.40	49.83	16.60	1.44	0.69	0.47	0.72
		FD+MSC	1064-1333, 2064-2355	4	51.05	14.80	45.40	14.80	1.36	0.27	0.47	0.67
		FD+SNV	1064-1333, 2064-2355	7	63.04	13.50	41.58	15.00	1.31	-0.37	0.49	0.65
	EH	None	1064-2183	11	63.57	13.70	62.11	13.10	1.63	0.64	0.67	0.79
		FD	1064-2183	10	61.32	13.40	43.97	15.70	1.53	-1.99	0.56	0.68
		SD	1064-2183	6	54.40	13.20	38.47	12.90	1.30	2.27	0.57	0.67
		MSC	1064-2183	11	59.55	11.30	39.96	16.40	1.31	2.48	0.40	0.64
		SNV	1064-2183	7	52.95	14.20	45.09	14.90	1.35	-0.64	0.55	0.68
		FD+MSC	1064-2183	3	50.57	13.50	44.57	14.90	1.34	0.72	0.40	0.67
		FD+SNV	1064-2183	3	44.95	14.50	43.61	13.20	1.37	-2.98	0.58	0.70

LV, latent variables; R^2, coefficient of determination; RMSEE, Root mean square error of estimation; RPD, residual predictive deviation; RMSEP, root mean square error of prediction; Corr, correlation coefficient; IS, integrating sphere; EH, emission head; FD, first derivative; SD, second derivative; MSC, multiplicative scattering correction; SNV, vector normalisation

Stellenbosch University https://scholar.sun.ac.za

Table 2

Model performance for fruit firmness using different FT-NIR instruments

Parameter	NIR probe	Pre-processing	Spectral range (nm)	Calibration			Validation					
				LV	R^2	RMSEE	R^2	RMSEP	RPD	Bias	Slope	Corr.
Firmness (N)	IS	None	1064-1333, 1835-2355	9	82.99	6.71	82.57	7.31	2.40	-0.63	0.82	0.91
		FD	1064-1333, 1835-2355	5	72.89	8.21	73.10	9.17	1.94	0.84	0.70	0.86
		SD	1064-1333, 1835-2355	3	71.32	8.85	64.35	9,98	1.69	1.42	0.67	0.81
		MSC	1064-1333, 1835-2355	5	74.32	8.08	74.93	8.26	2.02	-1.27	0.73	0.87
		SNV	1064-1333, 1835-2355	7	77.48	7.47	77.33	8.14	2.10	-0.47	0.73	0.88
		FD+MSC	1064-1333, 1835-2355	6	79.50	7.04	76.20	8.40	2.05	0.59	0.76	0.87
		FD+SNV	1064-1333, 1835-2355	4	73.95	8.09	75.06	8.36	2.04	-1.54	0.76	0.87
	EH	None	1064-1333, 1639-1835	11	78.49	7.83	77.03	8.67	2.09	0.36	0.92	0.89
		FD	1064-1333, 1639-1835	8	82.84	7.03	78.41	8.40	2.15	-0.29	0.91	0.89
		SD	1064-1333, 1639-1835	5	85.03	6.43	83.01	7.45	2.43	0.19	0.85	0.91
		MSC	1064-1333, 1639-1835	9	77.93	7.89	75.97	8.89	2.04	-0.25	0.87	0.88
		SNV	1064-1333, 1639-1835	11	82.52	7.06	80.23	8.09	2.26	-0.81	0.77	0.90
		FD+MSC	1064-1333, 1639-1835	6	82.07	7.78	73.48	8.53	1.94	0.43	0.74	0.86
		FD+SNV	1064-1333, 1639-1835	7	81.04	7.27	77.39	8.63	2.10	-0.32	0.87	0.88

LV, latent variables; R^2, coefficient of determination; RMSEE, Root mean square error of estimation; RPD, residual predictive deviation; RMSEP, root mean square error of prediction; Corr, correlation coefficient; IS, integrating sphere; EH, emission head; FD, first derivative; SD, second derivative; MSC, multiplicative scattering correction; SNV, vector normalisation

Stellenbosch University https://scholar.sun.ac.za

Table 3

Model performance for a* (redness) using different FT-NIR instruments

Parameter	NIR probe	Pre-processing	Spectral range (nm)	Calibration			Validation					
				LV	R^2	RMSEE	R^2	RMSEP	RPD	Bias	Slope	Corr.
a* (redness)	IS	None	1064-1333, 2062-2355	8	91.38	1.56	87.02	1.72	2.86	0.42	0.83	0.94
		FD	1064-1333, 2062-2355	5	80.77	2.29	80.19	2.06	2.29	-0.40	0.75	0.90
		SD	1064-1333, 2062-2355	5	88.59	1.77	71.07	2.39	1.89	-0.41	0.71	0.85
		MSC	1064-1333, 2062-2355	5	90.86	1.54	80.92	1.99	2.30	0.21	0.88	0.90
		SNV	1064-1333, 2062-2355	6	86.88	1.83	83.76	1.83	2.59	-0.05	0.86	0.93
		FD+MSC	1064-1333, 2062-2355	5	84.77	2.04	79.47	2.26	2.21	-0.10	0.72	0.90
		FD+SNV	1064-1333, 2062-2355	6	88.34	1.77	81.66	2.10	2.43	0.52	0.74	0.92
	EH	None	1064-1836	12	93.31	1.54	90.13	1.41	3.19	-0.12	0.92	0.95
		FD	1064-1836	9	93.58	1.49	87.41	1.59	2.83	0.14	0.93	0.94
		SD	1064-1836	6	92.65	1.40	90.90	1.61	3.34	0.19	0.98	0.97
		MSC	1064-1836	10	92.99	1.55	89.98	1.38	3.13	-0.04	0.94	0.95
		SNV	1064-1836	12	92.31	1.65	87.64	1.63	2.79	-0.29	0.89	0.93
		FD+MSC	1064-1836	8	91.61	1.70	85.11	1.73	2.59	0.01	0.91	0.92
		FD+SNV	1064-1836	9	91.98	1.66	86.60	1.63	2.73	-0.06	0.89	0.93

LV, latent variables; R^2, coefficient of determination; RMSEE, Root mean square error of estimation; RPD, residual predictive deviation; RMSEP, root mean square error of prediction; Corr, correlation coefficient; IS, integrating sphere; EH, emission head; FD, first derivative; SD, second derivative; MSC, multiplicative scattering correction; SNV, vector normalisation

Stellenbosch University https://scholar.sun.ac.za

Table 4

Model performance for Chroma using different FT-NIR instruments

Parameter	NIR probe	Pre-processing	Spectral range (nm)	Calibration			Validation					
				LV	R^2	RMSEE	R^2	RMSEP	RPD	Bias	Slope	Corr.
Chroma	IS	None	1064-2355	14	85.53	1.84	73.65	2.29	2.03	-0.66	0.77	0.87
		FD	1064-2355	6	62.79	2.80	60.22	2.65	1.60	-0.32	0.64	0.78
		SD	1064-2355	5	87.53	1.45	70.08	2.41	1.84	-0.29	0.65	0.84
		MSC	1064-2355	14	97.44	0.73	76.76	2.46	2.08	0.11	0.71	0.88
		SNV	1064-2355	13	94.65	1.05	67.74	2.77	1.76	-0.11	0.66	0.82
		FD+MSC	1064-2355	5	72.36	2.05	58.39	2.58	1.55	-0.03	0.60	0.76
		FD+SNV	1064-2355	5	63.71	2.30	57.56	2.81	1.54	0.09	0.56	0.76
	EH	None	1064-2355	13	85.72	2.07	80.76	2.01	2.28	0.06	0.84	0.90
		FD	1064-2355	11	86.65	1.87	82.97	2.15	2.43	-0.18	0.90	0.91
		SD	1064-2355	10	73.92	2.38	72.68	3.13	1.93	-0.47	0.74	0.86
		MSC	1064-2355	13	80.57	2.17	78.31	2.63	2.19	-0.52	0.83	0.89
		SNV	1064-2355	14	76.55	2.33	75.71	2.81	2.03	-0.05	0.78	0.87
		FD+MSC	1064-2355	7	76.22	2.35	75.92	2.80	2.04	-0.05	0.78	0.87
		FD+SNV	1064-2355	10	76.47	2.12	72.98	2.93	1.95	-0.49	0.67	0.86

LV, latent variables; R^2, coefficient of determination; RMSEE, Root mean square error of estimation; RPD, residual predictive deviation; RMSEP, root mean square error of prediction; Corr, correlation coefficient; IS, integrating sphere; EH, emission head; FD, first derivative; SD, second derivative; MSC, multiplicative scattering correction; SNV, vector normalisation

Stellenbosch University https://scholar.sun.ac.za

Table 5

Model performance for Hue using different FT-NIR instruments

Parameter	NIR probe	Pre-processing	Spectral range (nm)	Calibration			Validation					
				LV	R^2	RMSEE	R^2	RMSEP	RPD	Bias	Slope	Corr.
Hue	IS	None	1064-1836, 2174-2355	13	94.68	0.96	83.94	1.67	2.50	-0.10	0.85	0.92
		FD	1064-1836, 2174-2355	8	88.81	1.34	65.46	2.45	1.72	-0.35	0.66	0.81
		SD	1064-1836, 2174-2355	3	85.03	1.36	44.26	2.90	1.36	0.50	0.41	0.68
		MSC	1064-1836, 2174-2355	10	91.50	1.20	79.50	1.81	2.22	-0.17	0.72	0.90
		SNV	1064-1836, 2174-2355	12	94.08	1.00	68.82	2.20	1.79	0.08	0.70	0.83
		FD+MSC	1064-1836, 2174-2355	5	72.37	2.13	60.21	2.63	1.59	0.01	0.68	0.78
		FD+SNV	1064-1836, 2174-2355	5	67.08	2.30	66.86	2.40	1.74	0.13	0.65	0.82
	EH	None	1064-1333, 2174-2355	10	74.85	1.82	70.57	1.99	2.04	-0.85	0.70	0.87
		FD	1064-1333, 2174-2355	8	72.83	1.89	70.29	2.00	1.96	-0.71	0.66	0.87
		SD	1064-1333, 2174-2355	5	66.47	1.81	62.63	2.31	1.67	-0.48	0.54	0.82
		MSC	1064-1333, 2174-2355	7	74.85	1.76	67.88	2.13	1.84	-0.60	0.68	0.84
		SNV	1064-1333, 2174-2355	8	75.74	1.73	71.66	2.05	1.91	-0.39	0.68	0.86
		FD+MSC	1064-1333, 2174-2355	7	69.89	1.89	65,19	2.16	1.93	-1.04	0.68	0.86
		FD+SNV	1064-1333, 2174-2355	8	70.46	1.88	63.83	2.14	1.85	-0.94	0.67	0.84

LV, latent variables; R^2, coefficient of determination; RMSEE, Root mean square error of estimation; RPD, residual predictive deviation; RMSEP, root mean square error of prediction; Corr, correlation coefficient; IS, integrating sphere; EH, emission head; FD, first derivative; SD, second derivative; MSC, multiplicative scattering correction; SNV, vector normalisation

Stellenbosch University https://scholar.sun.ac.za

Table 6

Model performance for total soluble solids using different FT-NIR instruments

Parameter	NIR probe	Pre-processing	Spectral range (nm)	Calibration			Validation					
				LV	R^2	RMSEE	R^2	RMSEP	RPD	Bias	Slope	Corr.
TSS (%)	IS	None	1064-1836, 2174-2355	11	88.69	0.23	65.42	0.34	1.72	0.06	0.71	0.82
		FD	1064-1836, 2174-2355	5	70.33	0.31	61.23	0.39	1.61	-0.02	0.56	0.79
		SD	1064-1836, 2174-2355	5	77.62	0.25	59.06	0.39	1.57	-0.03	0.59	0.77
		MSC	1064-1836, 2174-2355	7	83.64	0.25	71.87	0.32	1.92	0.06	0.78	0.86
		SNV	1064-1836, 2174-2355	8	75.60	0.31	66.30	0.36	1.72	0.02	0.68	0.82
		FD+MSC	1064-1836, 2174-2355	5	77.35	0.23	60.95	0.38	1.60	-0.01	0.65	0.78
		FD+SNV	1064-1836, 2174-2355	8	70.79	0.34	62.81	0.30	1.76	0.11	0.79	0.83
	EH	None	1064-1333, 1640-1835	13	71.35	0.32	70.97	0.38	1.91	0.09	0.75	0.85
		FD	1064-1333, 1640-1835	12	82.16	0.27	80.84	0.30	2.31	0.04	0.87	0.90
		SD	1064-1333, 1640-1835	10	77.78	0.29	72.06	0.37	1.92	0.07	0.81	0.86
		MSC	1064-1333, 1640-1835	9	74.62	0.30	74.57	0.35	2.03	0.03	0.82	0.87
		SNV	1064-1333, 1640-1835	12	80.99	0.27	78.18	0.32	2.19	0.07	0.85	0.89
		FD+MSC	1064-1333, 1640-1835	8	75.32	0.30	74.86	0.35	2.00	0.02	0.79	0.87
		FD+SNV	1064-1333, 1640-1836	9	83.84	0.26	78.12	0.28	2.17	0.05	0.86	0.89

LV, latent variables; R^2, coefficient of determination; RMSEE, Root mean square error of estimation; RPD, residual predictive deviation; RMSEP, root mean square error of prediction; Corr, correlation coefficient; IS, integrating sphere; EH, emission head; FD, first derivative; SD, second derivative; MSC, multiplicative scattering correction; SNV, vector normalisation; TSS, total soluble solids

Stellenbosch University https://scholar.sun.ac.za

Table 7

Model performance for pH using different FT-NIR instruments

Parameter	NIR probe	Pre-processing	Spectral range (nm)	Calibration			Validation					
				LV	R^2	RMSEE	R^2	RMSEP	RPD	Bias	Slope	Corr.
pH	IS	None	1064-1333, 1640-1732	11	95,87	0.04	75.73	0.07	2.13	0.02	0.90	0.89
		FD	1064-1333, 1640-1732	13	94.60	0.04	77.86	0.07	2.13	0.00	0.88	0.89
		SD	1064-1333, 1640-1732	8	94.12	0.04	62.33	0.09	1.66	0.02	0.74	0.81
		MSC	1064-1333, 1640-1732	7	91.40	0.05	68.30	0.07	1.80	0.01	0.74	0.83
		SNV	1064-1333, 1640-1732	7	87.14	0.06	58.11	0.09	1.55	0.01	0.62	0.76
		FD+MSC	1064-1333, 1640-1732	4	72.39	0.09	56.60	0.10	1.50	0.01	0.69	0.76
		FD+SNV	1064-1333, 1640-1732	5	84.66	0.06	56.31	0.10	1.55	0.02	0.73	0.78
	EH	None	1064-2355	17	88.77	0.05	82.29	0.06	2.38	0.00	0.80	0.91
		FD	1064-2355	14	88.86	0.05	82.31	0.06	2.38	-0.00	0.83	0.91
		SD	1064-2355	7	86.39	0.06	84.86	0.06	2.57	0.00	0.81	0.92
		MSC	1064-2355	16	88.97	0.05	84.80	0.06	2.57	0.00	0.78	0.93
		SNV	1064-2355	14	86.75	0.06	83.76	0.06	2.48	0.00	0.77	0.92
		FD+MSC	1064-2355	10	85.04	0.06	82.95	0.06	2.42	-0.00	0.77	0.91
		FD+SNV	1064-2355	10	83.77	0.06	82.01	0.07	2.36	0.00	0.76	0.91

LV, latent variables; R^2, coefficient of determination; RMSEE, Root mean square error of estimation; RPD, residual predictive deviation; RMSEP, root mean square error of prediction; Corr, correlation coefficient; IS, integrating sphere; EH, emission head; FD, first derivative; SD, second derivative; MSC, multiplicative scattering correction; SNV, vector normalisation

Stellenbosch University https://scholar.sun.ac.za

Table 8

Model performance for titratable acidity (TA) using different FT-NIR instruments

Parameter	NIR probe	Pre-processing	Spectral range (nm)	Calibration			Validation					
				LV	R^2	RMSEE	R^2	RMSEP	RPD	Bias	Slope	Corr.
TA (%)	IS	None	1064-1333, 1640-2174	14	72.17	0.13	69.75	0.13	1.89	0.04	0.73	0.85
		FD	1064-1333, 1640-2174	9	82.57	0.11	66.90	0.16	1.75	-0.01	0.59	0.83
		SD	1064-1333, 1640-2174	7	71.42	0.12	71.35	0.18	1.87	0.01	0.75	0.85
		MSC	1064-1333, 1640-2174	8	85.58	0.10	73.34	0.14	2.00	-0.03	0.64	0.88
		SNV	1064-1333, 1640-2174	10	67.35	0.13	67.24	0.14	1.75	0.01	0.61	0.83
		FD+MSC	1064-1333, 1640-2174	5	73.59	0.13	62.70	0.16	1.72	-0.05	0.57	0.83
		FD+SNV	1064-1333, 1640-2174	6	73.33	0.13	55.54	0.17	1.61	-0.06	0.62	0.78
	EH	None	1064-1333, 1640-1836	15	73.45	0.12	73.16	0.15	2.08	-0.05	0.76	0.88
		FD	1064-1333, 1640-1836	7	71.53	0.12	64.83	0.13	1.69	-0.00	0.73	0.81
		SD	1064-1333, 1640-1836	7	77.67	0.11	76.78	0.13	2.12	-0.02	0.71	0.89
		MSC	1064-1333, 1640-1836	9	70.43	0.13	70.66	0.14	1.87	0.02	0.74	0.84
		SNV	1064-1333, 1640-1836	15	75.91	0.11	71.63	0.14	1.92	-0.03	0.68	0.85
		FD+MSC	1064-1333, 1640-1836	13	71.00	0.12	68.54	0.15	1.78	-0.00	0.69	0.82
		FD+SNV	1064-1333, 1640-1836	13	75.02	0.11	73.55	0.15	2.00	0.00	0.71	0.86

LV, latent variables; R^2, coefficient of determination; RMSEE, Root mean square error of estimation; RPD, residual predictive deviation; RMSEP, root mean square error of prediction; Corr, correlation coefficient; IS, integrating sphere; EH, emission head; FD, first derivative; SD, second derivative; MSC, multiplicative scattering correction; SNV, vector normalisation; TA, titratable acidity

Stellenbosch University https://scholar.sun.ac.za

Table 9

Model performance for TSS:TA ratio using different FT-NIR instruments

Parameter	NIR probe	Pre-processing	Spectral range (nm)	Calibration			Validation					
				LV	R^2	RMSEE	R^2	RMSEP	RPD	Bias	Slope	Corr.
TSS:TA ratio	IS	None	1064-1333, 1640-2174	10	86.46	0.62	63.20	1.23	1.65	-0.01	0.71	0.80
		FD	1064-1333, 1640-2174	10	86.50	0.64	53.80	1.17	1.47	-0.06	0.70	0.75
		SD	1064-1333, 1640-2174	7	89.10	0.57	49.28	1.32	1.41	0.05	0.51	0.70
		MSC	1064-1333, 1640-2174	11	97.32	0.30	66.25	1.16	1.73	-0.12	0.64	0.81
		SNV	1064-1333, 1640-2174	17	99.54	0.12	86.28	0.74	2.72	0.10	0.81	0.93
		FD+MSC	1064-1333, 1640-2174	15	92.16	0.51	59.05	1.29	1.58	0.19	0.62	0.78
		FD+SNV	1064-1333, 1640-2174	14	94.07	0.43	53.48	1.31	1.48	0.16	0.62	0.74
	EH	None	1064-1333, 1640-1836	12	68.42	0.72	61.63	0.83	1.44	0.02	0.73	0.75
		FD	1064-1333, 1640-1836	9	64.49	0.75	52.02	0.83	1.45	0.04	0.73	0.75
		SD	1064-1333, 1640-1836	6	64.71	0.73	54.36	0.82	1.50	0.05	0.74	0.77
		MSC	1064-1333, 1640-1836	10	62.45	0.73	60.06	0.78	1.65	-0.22	0.58	0.80
		SNV	1064-1333, 1640-1836	12	65.10	0.71	52.13	0.81	1.50	-0.09	0.56	0.73
		FD+MSC	1064-1333, 1640-1836	11	70.91	0.65	52.17	0.81	1.47	0.14	0.78	0.77
		FD+SNV	1064-1333, 1640-1836	10	59.43	0.77	46.49	0.88	1.37	-0.06	0.71	0.73

LV, latent variables; R^2, coefficient of determination; RMSEE, Root mean square error of estimation; RPD, residual predictive deviation; RMSEP, root mean square error of prediction; Corr, correlation coefficient; IS, integrating sphere; EH, emission head; FD, first derivative; SD, second derivative; MSC, multiplicative scattering correction; SNV, vector normalisation; TSS:TA ratio, total soluble solids: titratable acidity ratio

Stellenbosch University https://scholar.sun.ac.za

Table 10

Model performance for BrimA using different FT-NIR instruments

Parameter	NIR probe	Pre-processing	Spectral range (nm)	Calibration			Validation					
				LV	R^2	RMSEE	R^2	RMSEP	RPD	Bias	Slope	Corr.
BrimA	IS	None	1064-1836, 2174-2260	13	95.29	0.17	65.15	0.48	1.70	0.05	0.64	0.81
		FD	1064-1836, 2174-2260	6	80.52	0.33	68.89	0.47	1.86	0.13	0.66	0.85
		SD	1064-1836, 2174-2260	5	80.87	0.34	64.24	0.50	1.79	0.18	0.60	0.84
		MSC	1064-1836, 2174-2260	11	95.23	0.17	66.56	0.47	1.74	0.06	0.63	0.82
		SNV	1064-1836, 2174-2260	6	95.16	0.18	65.03	0.48	1.70	0.05	0.64	0.81
		FD+MSC	1064-1836, 2174-2260	5	74.17	0.40	58.21	0.56	1.55	0.03	0.60	0.76
		FD+SNV	1064-1836, 2174-2260	6	76.13	0.38	57.11	0.54	1.54	0.08	0.57	0.76
	EH	None	1064-1640, 1836-2355	15	76.38	0.34	75.20	0.42	2.02	0.05	0.71	0.87
		FD	1064-1640, 1836-2355	12	77.03	0.33	76.06	0.41	2.07	0.07	0.73	0.88
		SD	1064-1640, 1836-2355	8	80.81	0.31	76.16	0.39	2.08	0.06	0.79	0.88
		MSC	1064-1640, 1836-2355	14	75.11	0.35	74.37	0.43	2.01	0.08	0.71	0.87
		SNV	1064-1640, 1836-2355	15	75.27	0.35	74.09	0.43	2.02	0.10	0.69	0.87
		FD+MSC	1064-1640, 1836-2355	12	74.17	0.35	72.61	0.44	1.94	0.08	0.66	0.86
		FD+SNV	1064-1640, 1836-2355	12	73.64	0.36	73.22	0.44	1.99	-0.10	0.69	0.87

LV, latent variables; R^2, coefficient of determination; RMSEE, Root mean square error of estimation; RPD, residual predictive deviation; RMSEP, root mean square error of prediction; Corr, correlation coefficient; IS, integrating sphere; EH, emission head; FD, first derivative; SD, second derivative; MSC, multiplicative scattering correction; SNV, vector normalisation

Stellenbosch University https://scholar.sun.ac.za

Table 11

Model performance for total phenolics using different FT-NIR instruments

Parameter	NIR probe	Pre-processing	Spectral range (nm)	Calibration			Validation					
				LV	R^2	RMSEE	R^2	RMSEP	RPD	Bias	Slope	Corr.
Total phenolics (g/L)	IS	None	1064-1640, 1836-2355	10	88.09	0.07	77.12	0.15	2.09	0.64	0.67	0.89
		FD	1064-1640, 1836-2355	9	87.77	0.08	74.27	0.16	1.97	-0.78	0.70	0.86
		SD	1064-1640, 1836-2355	5	83.66	0.09	63.10	0.19	1.65	0.17	0.58	0.80
		MSC	1064-1640, 1836-2355	7	88.57	0.08	76.49	0.15	2.07	-0.77	0.75	0.88
		SNV	1064-1640, 1836-2355	7	76.00	0.11	69.43	0.18	1.81	1.37	0.63	0.84
		FD+MSC	1064-1640, 1836-2355	5	75.73	0.11	66.51	0.18	1.73	-0.89	0.75	0.82
		FD+SNV	1064-1640, 1836-2355	5	71.81	0.12	70.61	0.17	1.85	1.09	0.61	0.85
	EH	None	1064-1640, 1836-2355	15	86.56	0.10	85.62	0.12	2.64	-0.80	0.81	0.93
		FD	1064-1640, 1836-2355	13	88.16	0.09	87.97	0.11	2.91	-0.57	0.80	0.94
		SD	1064-1640, 1836-2355	8	86.86	0.09	83.49	0.13	2.49	-1.77	0.83	0.92
		MSC	1064-1640, 1836-2355	13	86.71	0.10	82.82	0.13	2.41	0.48	0.84	0.91
		SNV	1064-1640, 1836-2355	15	86.73	0.01	83.34	0.13	2.45	-0.67	0.80	0.94
		FD+MSC	1064-1640, 1836-2355	8	84.94	0.11	81.04	0.12	2.30	-0.75	0.82	0.90
		FD+SNV	1064-1640, 1836-2355	12	86.71	0.10	81.55	0.14	2.35	1.23	0.79	0.90

LV, latent variables; R^2, coefficient of determination; RMSEE, Root mean square error of estimation; RPD, residual predictive deviation; RMSEP, root mean square error of prediction; Corr, correlation coefficient; IS, integrating sphere; EH, emission head; FD, first derivative; SD, second derivative; MSC, multiplicative scattering correction; SNV, vector normalisation

Stellenbosch University https://scholar.sun.ac.za

Table 12

Model performance for total anthocyanin using different FT-NIR instruments

Parameter	NIR probe	Pre-processing	Spectral range (nm)	Calibration			Validation					
				LV	R^2	RMSEE	R^2	RMSEP	RPD	Bias	Slope	Corr.
Total anthocyanin (g/L)	IS	None	1064-1836, 2174-2355	18	99.46	0.01	60.97	0.09	1.60	0.12	0.62	0.78
		FD	1064-1836, 2174-2355	11	90.72	0.04	52.69	0.11	1.46	-0.91	0.57	0.72
		SD	1064-1836, 2174-2355	5	85.35	0.05	7.50	0.13	1.05	-1.64	0.33	0.45
		MSC	1064-1836, 2174-2355	13	98.51	0.02	51.20	0.11	1.43	0.11	0.46	0.72
		SNV	1064-1836, 2174-2355	17	99.45	0.01	62.59	0.09	1.64	-0.68	0.62	0.79
		FD+MSC	1064-1836, 2174-2355	6	72.36	0.08	30.08	0.13	1.21	1.76	0.35	0.56
		FD+SNV	1064-1836, 2174-2355	10	89.75	0.05	44.03	0.11	1.34	1.07	0.54	0.68
	EH	None	1064-1836, 2174-2355	16	71.85	0.07	53.21	0.08	1.47	-0.68	0.65	0.74
		FD	1064-1836, 2174-2355	9	49.23	0.09	49.38	0.09	1.41	-0.49	0.44	0.71
		SD	1064-1836, 2174-2355	7	60.24	0.07	49.17	0.09	1.40	0.27	0.58	0.71
		MSC	1064-1836, 2174-2355	14	65.61	0.07	52.04	0.09	1.44	-0.17	0.66	0.81
		SNV	1064-1836, 2174-2355	16	73.18	0.07	59.92	0.08	1.59	0.93	0.70	0.79
		FD+MSC	1064-1836, 2174-2355	12	64.14	0.07	40.22	0.10	1.29	-0.25	0.57	0.66
		FD+SNV	1064-1836, 2174-2355	13	66.73	0.07	46.34	0.09	1.47	0.67	0.55	0.69

LV, latent variables; R^2, coefficient of determination; RMSEE, Root mean square error of estimation; RPD, residual predictive deviation; RMSEP, root mean square error of prediction; Corr, correlation coefficient; IS, integrating sphere; EH, emission head; FD, first derivative; SD, second derivative; MSC, multiplicative scattering correction; SNV, vector normalisation

Stellenbosch University https://scholar.sun.ac.za

Table 13

Model performance for Vitamin C using different FT-NIR instruments

Parameter	NIR probe	Pre-processing	Spectral range (nm)	Calibration			Validation					
				LV	R^2	RMSEE	R^2	RMSEP	RPD	Bias	Slope	Corr.
Vitamin C (g/L)	IS	None	1333-1640, 1836-2175	9	74.11	0.08	72.19	0.08	1.99	-1.77	0.76	0.86
		FD	1333-1640, 1836-2175	6	69.53	0.09	62.23	0.11	1.70	-2.99	0.75	0.82
		SD	1333-1640, 1836-2175	3	44.64	0.11	37.60	0.11	1.27	0.92	0.43	0.62
		MSC	1333-1640, 1836-2175	6	73.79	0.08	61.11	0.10	1.60	-0.36	0.71	0.79
		SNV	1333-1640, 1836-2175	7	67.75	0.09	64.47	0.10	1.68	0.88	0.66	0.80
		FD+MSC	1333-1640, 1836-2175	6	68.26	0.08	62.74	0.09	1.64	0.44	0.70	0.80
		FD+SNV	1333-1640, 1836-2175	5	67.50	0.09	62.12	0.11	1.63	0.99	0.64	0.79
	EH	None	1064-1333, 1640-732	15	71.09	0.09	61.34	0.12	1.62	-1.46	0.63	0.79
		FD	1064-1333, 1640-732	12	72.74	0.08	65.79	0.12	1.71	0.01	0.63	0.81
		SD	1064-1333, 1640-732	11	85.48	0.06	76.16	0.09	2.06	-0.90	0.74	0.87
		MSC	1064-1333, 1640-732	15	86.84	0.06	74.71	0.10	1.99	-0.32	0.66	0.87
		SNV	1064-1333, 1640-732	15	73.69	0.08	62.31	0.12	1.64	-1.11	0.58	0.79
		FD+MSC	1064-1333, 1640-732	13	77.59	0.07	73.41	0.10	1.95	-0.82	0.65	0.87
		FD+SNV	1064-1333, 1640-732	15	81.41	0.07	78.47	0.09	2.16	0.55	0.74	0.89

LV, latent variables; R^2, coefficient of determination; RMSEE, Root mean square error of estimation; RPD, residual predictive deviation; RMSEP, root mean square error of prediction; Corr, correlation coefficient; IS, integrating sphere; EH, emission head; FD, first derivative; SD, second derivative; MSC, multiplicative scattering correction; SNV, vector normalisation

Stellenbosch University https://scholar.sun.ac.za

Fig. 1. Illustration of the two different spectrophotometers a) direct contact measurement using integrating sphere of the Multi-Purpose Analyser and b) contactless measurement using the emission head of the Matrix-F

Stellenbosch University https://scholar.sun.ac.za

APPENDIX CHAPTER 5

Table 1

Model performance for total soluble solids using different FT-NIR instruments

Parameter	NIR probe	Pre-processing	Wavelength range (nm)	Calibration			Validation					
				LV	R^2	RMSEE	R^2	RMSEP	RPD	Bias	Slope	Corr.
TSS (%)	IS	None	1064-1333	6	85.75	0.23	79.07	0.31	2.19	-0.024	0.66	0.85
		FD	1064-1333	5	88.38	0.21	61.07	0.36	1.61	-0.006	0.69	0.90
		SD	1064-1333	5	91.09	0.23	53.54	0.44	1.47	-0.003	0.70	0.75
		MSC	1064-1333	4	76.10	0.30	62.56	0.40	1.64	-0.028	0.59	0.79
		SNV	1064-1333	4	75.28	0.30	65.65	0.40	1.72	-0.060	0.60	0.82
		FD+MSC	1064-1333	5	90.88	0.18	56.69	0.43	1.46	-0.040	0.62	0.76
		FD+SNV	1064-1333	4	84.94	0.23	54.05	0.46	1.51	0.090	0.54	0.75
	EH	None	1064-1333, 1587-1724	9	69.48	0.37	56.08	0.50	1.56	0.13	0.56	0.77
		FD	1064-1333, 1587-1724	8	82.71	0.29	75.50	0.38	2.06	0.077	0.72	0.88
		SD	1064-1333, 1587-1724	6	83.71	0.26	62.24	0.34	1.67	0.080	0.64	0.80
		MSC	1064-1333, 1587-1724	6	80.25	0.30	72.19	0.39	1.91	0.038	0.71	0.85
		SNV	1064-1333, 1587-1724	10	88.31	0.24	78.50	0.40	2.26	0.11	0.78	0.90
		FD+MSC	1064-1333, 1587-1724	7	87.55	0.24	84.64	0.30	2.65	0.079	0.79	0.93
		FD+SNV	1064-1333, 1587-1724	9	89.59	0.22	84.37	0.31	2.62	0.078	0.83	0.92

LV, latent variables; R^2, coefficient of determination; RMSEE, Root mean square error of estimation; RPD, residual predictive deviation; RMSEP, root mean square error of prediction; Corr, correlation coefficient; IS, integrating sphere; EH, emission head; FD, first derivative; SD, second derivative; MSC, multiplicative scattering correction; SNV, vector normalisation; TSS, total soluble solids

Stellenbosch University https://scholar.sun.ac.za

Table 2

Model performance for pH using different FT-NIR instruments

Parameter	NIR probe	Pre-processing	Wavelength range (nm)	Calibration			Validation					
				LV	R^2	RMSEE	R^2	RMSEP	RPD	Bias	Slope	Corr.
pH	IS	None	1064-1640	7	83.49	0.12	80.59	0.09	2.32	0.018	0.95	0.91
		FD	1064-1640	2	65.17	0.17	46.30	0.14	1.37	0.010	0.63	0.71
		SD	1064-1640	2	62.04	0.18	45.08	0.15	1.37	0.025	0.77	0.74
		MSC	1064-1640	5	79.84	0.13	70.52	0.11	1.84	-0.002	0.86	0.85
		SNV	1064-1640	6	82.00	0.12	73.95	0.10	1.96	0.004	1.05	0.90
		FD+MSC	1064-1640	3	72.24	0.15	47.32	0.14	1.38	-0.087	0.66	0.72
		FD+SNV	1064-1640	3	73.05	0.15	50.30	0.14	1.43	0.021	0.70	0.74
	EH	None	1064-2100	10	94.35	0.08	57.90	0.16	1.65	-0.056	0.82	0.82
		FD	1064-2100	7	82.62	0.15	34.38	0.19	1.30	-0.059	0.65	0.69
		SD	1064-2100	4	86.66	0.13	55.33	0.16	1.53	-0.037	0.65	0.76
		MSC	1064-2100	10	95.19	0.08	64.83	0.14	1.82	-0.054	0.75	0.84
		SNV	1064-2100	9	95.93	0.076	72.12	0.12	2.00	-0.040	0.85	0.87
		FD+MSC	1064-2100	6	85.18	0.14	80.30	0.10	2.40	-0.036	0.81	0.91
		FD+SNV	1064-2100	6	85.77	0.13	77.55	0.11	2.22	-0.034	0.83	0.89

LV, latent variables; R^2, coefficient of determination; RMSEE, Root mean square error of estimation; RPD, residual predictive deviation; RMSEP, root mean square error of prediction; Corr, correlation coefficient; IS, integrating sphere; EH, emission head; FD, first derivative; SD, second derivative; MSC, multiplicative scattering correction; SNV, vector normalisation

Stellenbosch University https://scholar.sun.ac.za

Table 3

Model performance for titratable acidity using different FT-NIR instruments

Parameter	NIR probe	Pre-processing	Wavelength range (nm)	Calibration			Validation					
				LV	R^2	RMSEE	R^2	RMSEP	RPD	Bias	Slope	Corr.
TA (%)	IS	None	1064-1585, 2100-2353	5	80.44	0.10	79.96	0.13	2.29	0.013	0.82	0.90
		FD	1064-1585, 2100-2353	7	78.94	0.11	61.80	0.17	1.63	0.022	0.51	0.81
		SD	1064-1585, 2100-2353	5	80.12	0.09	38.12	0.15	1.29	-0.003	0.33	0.59
		MSC	1064-1585, 2100-2353	6	86.92	0.09	74.24	0.14	2.08	0.045	0.77	0.88
		SNV	1064-1585, 2100-2353	4	77.21	0.11	70.32	0.15	1.91	0.043	0.68	0.85
		FD+MSC	1064-1585, 2100-2353	6	77.90	0.10	38.24	0.18	1.29	0.033	0.39	0.64
		FD+SNV	1064-1585, 2100-2353	6	71.87	0.11	47.15	0.16	1.38	0.017	0.50	0.69
	EH	None	1064-1333, 1740-1835	10	82.08	0.09	48.98	0.13	1.40	0.004	0.77	0.75
		FD	1064-1333, 1740-1835	10	82.26	0.11	58.49	0.16	1.55	-0.008	0.75	0.79
		SD	1064-1333, 1740-1835	6	84.07	0.09	36.71	0.15	1.27	-0.023	0.53	0.64
		MSC	1064-1333, 1740-1835	6	73.51	0.10	50.23	0.13	1.42	-0.001	0.65	0.73
		SNV	1064-1333, 1740-1835	10	63.29	0.16	56.37	0.20	1.52	-0.002	0.64	0.76
		FD+MSC	1064-1333, 1740-1835	8	85.59	0.10	81.75	0.10	2.34	0.000	0.76	0.91
		FD+SNV	1064-1333, 1740-1835	10	89.62	0.08	66.30	0.14	1.76	0.030	0.71	0.83

LV, latent variables; R^2, coefficient of determination; RMSEE, Root mean square error of estimation; RPD, residual predictive deviation; RMSEP, root mean square error of prediction; Corr, correlation coefficient; IS, integrating sphere; EH, emission head; FD, first derivative; SD, second derivative; MSC, multiplicative scattering correction; SNV, vector normalisation; TA, titratable acidity

Stellenbosch University https://scholar.sun.ac.za

Table 4

Model performance for TSS:TA using different FT-NIR instruments

Parameter	NIR probe	Pre-processing	Wavelength range (nm)	Calibration			Validation					
				LV	R^2	RMSEE	R^2	RMSEP	RPD	Bias	Slope	Corr.
TSS:TA	IS	None	1064-2355	7	82.20	0.87	77.83	1.03	2.13	0.083	0.86	0.89
		FD	1064-2355	9	91.65	0.56	58.57	1.36	1.56	-0.091	0.57	0.77
		SD	1064-2355	2	45.96	1.25	26.00	1.54	1.17	-0.10	0.26	0.51
		MSC	1064-2355	6	76.02	0.95	77.46	1.07	2.11	-0.026	0.74	0.88
		SNV	1064-2355	6	76.81	0.94	76.57	1.10	2.07	-0.051	0.73	0.88
		FD+MSC	1064-2355	5	67.79	1.09	39.57	1.48	1.29	0.046	0.48	0.64
		FD+SNV	1064-2355	14	98.59	0.24	44.02	1.47	1.35	-0.23	0.60	0.69
	EH	None	1064-1333, 1740-1835	10	71.10	1.06	54.52	1.44	1.50	0.20	0.49	0.75
		FD	1064-1333, 1740-1835	8	66.25	1.13	62.62	1.31	1.64	0.059	0.53	0.81
		SD	1064-1333, 1740-1835	3	53.27	1.29	33.61	1.64	1.23	0.017	0.28	0.59
		MSC	1064-1333, 1740-1835	8	79.36	0.89	70.37	1.16	1.84	0.013	0.61	0.85
		SNV	1064-1333, 1740-1835	11	84.16	0.79	62.59	1.31	1.64	-0.069	0.54	0.80
		FD+MSC	1064-1333, 1740-1835	7	75.67	0.96	73.62	1.10	1.95	-0.008	0.62	0.87
		FD+SNV	1064-1333, 1740-1835	9	80.60	0.86	72.05	1.13	1.89	0.027	0.63	0.86

LV, latent variables; R^2, coefficient of determination; RMSEE, Root mean square error of estimation; RPD, residual predictive deviation; RMSEP, root mean square error of prediction; Corr, correlation coefficient; IS, integrating sphere; EH, emission head; FD, first derivative; SD, second derivative; MSC, multiplicative scattering correction; SNV, vector normalisation; TSS:TA, total soluble solids to titratable acidity ratio

Stellenbosch University https://scholar.sun.ac.za

Table 5

Model performance for BrimA using different FT-NIR instruments

Parameter	NIR probe	Pre-processing	Wavelength range (nm)	Calibration			Validation					
				LV	R^2	RMSEE	R^2	RMSEP	RPD	Bias	Slope	Corr.
BrimA	IS	None	1064-1586, 1725-2355	7	77.61	0.42	78.68	0.45	2.17	0.023	0.71	0.89
		FD	1064-1586, 1725-2355	7	86.76	0.33	49.37	0.67	1.45	-0.17	0.56	0.73
		SD	1064-1586, 1725-2355	8	95.63	0.23	39.84	0.73	1.29	0.017	0.57	0.66
		MSC	1064-1586, 1725-2355	5	72.56	0.47	69.58	0.55	1.83	0.078	0.77	0.84
		SNV	1064-1586, 1725-2355	6	75.37	0.45	75.03	0.49	2.01	0.042	0.69	0.87
		FD+MSC	1064-1586, 1725-2355	4	71.70	0.57	52.33	0.77	1.45	0.041	0.56	0.73
		FD+SNV	1064-1586, 1725-2355	7	80.75	0.46	40.86	0.75	1.30	-0.006	0.56	0.66
	EH	None	1064-1333, 1640-1835	8	71.53	0.58	67.51	0.59	1.79	0.12	0.67	0.83
		FD	1064-1333, 1640-1835	6	67.95	0.61	65.28	0.61	1.80	0.21	0.67	0.83
		SD	1064-1333, 1640-1835	3	44.94	0.78	34.29	0.80	1.26	0.17	0.34	0.61
		MSC	1064-1333, 1640-1835	7	71.29	0.58	70.51	0.56	1.84	0.32	0.67	0.84
		SNV	1064-1333, 1640-1835	11	86.35	0.32	67.17	0.55	1.75	-0.015	0.61	0.82
		FD+MSC	1064-1333, 1640-1835	7	83.43	0.36	78.79	0.43	2.22	0.020	0.73	0.89
		FD+SNV	1064-1333, 1640-1835	11	83.49	0.34	69.84	0.52	1.83	0.053	0.69	0.84

LV, latent variables; R^2, coefficient of determination; RMSEE, Root mean square error of estimation; RPD, residual predictive deviation; RMSEP, root mean square error of prediction; Corr, correlation coefficient; IS, integrating sphere; EH, emission head; FD, first derivative; SD, second derivative; MSC, multiplicative scattering correction; SNV, vector normalisation

Stellenbosch University https://scholar.sun.ac.za

Table 6

Model performance for firmness using different FT-NIR instruments

Parameter	NIR probe	Pre-processing	Wavelength range (nm)	Calibration			Validation					
				LV	R^2	RMSEE	R^2	RMSEP	RPD	Bias	Slope	Corr.
Firmness (N)	IS	None	1064-2355	3	68.40	6.05	61.47	6.71	1.62	-0.79	0.59	0.79
		FD	1064-2355	5	75.81	5.06	57.84	7.35	1.55	-0.88	0.59	0.75
		SD	1064-2355	7	95.41	3.50	53.76	11.10	1.48	-1.18	0.64	0.75
		MSC	1064-2355	7	96.42	2.56	56.34	10.00	1.52	-0.78	0.47	0.78
		SNV	1064-2355	6	69.71	8.27	60.19	8.68	1.59	0.44	0.63	0.78
		FD+MSC	1064-2355	8	93.02	4.32	58.36	11.20	1.55	-0.077	0.62	0.77
		FD+SNV	1064-2355	4	55.55	9.92	49.98	8.59	1.51	-3.03	0.58	0.75
	EH	None	1064-1333, 1640-1835	9	62.39	8.78	59.72	8.05	1.58	0.40	0.70	0.78
		FD	1064-1333, 1640-1835	5	64.83	8.11	55.85	8.45	1.50	0.16	0.66	0.76
		SD	1064-1333, 1640-1835	2	55.79	8.88	43.69	9.22	1.33	-0.23	0.46	0.66
		MSC	1064-1333, 1640-1835	5	59.24	9.93	58.45	7.97	1.55	-0.005	0.66	0.77
		SNV	1064-1333, 1640-1835	7	61.55	8.77	61.15	7.70	1.60	0.07	0.75	0.80
		FD+MSC	1064-1333, 1640-1835	3	62.27	8.06	60.34	7.62	1.60	-0.90	0.64	0.78
		FD+SNV	1064-1333, 1640-1835	4	63.37	7.55	54.27	8.15	1.48	0.22	0.58	0.74

LV, latent variables; R^2, coefficient of determination; RMSEE, Root mean square error of estimation; RPD, residual predictive deviation; RMSEP, root mean square error of prediction; Corr, correlation coefficient; IS, integrating sphere; EH, emission head; FD, first derivative; SD, second derivative; MSC, multiplicative scattering correction; SNV, vector normalisation

Stellenbosch University https://scholar.sun.ac.za

Table 7

Model performance for a* value using different FT-NIR instruments

Parameter	NIR probe	Pre-processing	Wavelength range (nm)	Calibration			Validation					
				LV	R^2	RMSEE	R^2	RMSEP	RPD	Bias	Slope	Corr.
a*	IS	None	1064-1183, 1640-1732	4	70.74	1.73	70.66	1.67	1.85	-0.15	0.76	0.84
		FD	1064-1183, 1640-1732	4	73.54	1.69	70.83	1.67	1.86	-0.16	0.72	0.84
		SD	1064-1183, 1640-1732	9	87.43	1.17	67.61	1.77	1.76	0.058	0.68	0.82
		MSC	1064-1183, 1640-1732	4	75.14	1.60	63.43	1.56	1.65	-0.004	0.63	0.80
		SNV	1064-1183, 1640-1732	2	69.90	1.81	66.12	1.84	1.77	-0.44	0.92	0.85
		FD+MSC	1064-1183, 1640-1732	2	59.38	2.01	56.42	1.51	1.54	-0.25	0.75	0.78
		FD+SNV	1064-1183, 1640-1732	2	74.53	1.64	69.85	1.74	1.89	-0.47	0.79	0.85
	EH	None	1064-1360	7	67.71	2.31	62.36	1.92	1.67	0.42	0.69	0.80
		FD	1064-1360	5	59.56	2.56	55.11	2.0	1.54	0.48	0.61	0.76
		SD	1064-1360	6	73.82	2.07	59.53	2.08	1.69	0.77	0.61	0.81
		MSC	1064-1360	5	64.27	2.40	61.63	1.98	1.65	-0.38	0.64	0.79
		SNV	1064-1360	5	64.44	2.40	62.88	1.91	1.68	0.39	0.64	0.80
		FD+MSC	1064-1360	4	57.03	2.62	50.71	2.09	1.52	0.74	0.72	0.77
		FD+SNV	1064-1360	4	57.21	2.62	49.40	2.23	1.48	0.71	0.65	0.75

LV, latent variables; R^2, coefficient of determination; RMSEE, Root mean square error of estimation; RPD, residual predictive deviation; RMSEP, root mean square error of prediction; Corr, correlation coefficient; IS, integrating sphere; EH, emission head; FD, first derivative; SD, second derivative; MSC, multiplicative scattering correction; SNV, vector normalisation

Stellenbosch University https://scholar.sun.ac.za

Table 8

Model performance for Chroma using different FT-NIR instruments

Parameter	NIR probe	Pre-processing	Wavelength range (nm)	Calibration			Validation					
				LV	R^2	RMSEE	R^2	RMSEP	RPD	Bias	Slope	Corr.
Chroma	IS	None	1064-1333, 2000-2174	4	78.37	2.24	67.96	2.31	1.79	0.37	0.65	0.83
		FD	1064-1333, 2000-2174	4	78.24	2.20	68.51	2.39	1.82	0.46	0.68	0.84
		SD	1064-1333, 2000-2174	5	87.89	2.16	55.66	2.90	1.51	0.24	0.64	0.75
		MSC	1064-1333, 2000-2174	2	60.21	2.93	60.18	2.65	1.59	-0.24	0.60	0.78
		SNV	1064-1333, 2000-2174	4	74.46	2.39	56.42	2.81	1.53	0.35	0.59	0.76
		FD+MSC	1064-1333, 2000-2174	2	68.03	2.63	54.90	2.82	1.51	-0.43	0.78	0.78
		FD+SNV	1064-1333, 2000-2174	2	73.36	2.40	63.85	2.53	1.67	0.19	0.67	0.80
	EH	None	1064-1333, 1465-1725	8	65.08	3.41	60.12	2.81	1.73	1.14	0.58	0.82
		FD	1064-1333, 1465-1725	7	71.94	3.07	63.12	2.68	1.78	1.01	0.60	0.84
		SD	1064-1333, 1465-1725	4	66.41	3.89	47.47	3.05	1.43	0.79	0.61	0.72
		MSC	1064-1333, 1465-1725	4	87.61	2.70	68.44	2.83	1.78	0.015	0.63	0.83
		SNV	1064-1333, 1465-1725	7	64.17	4.08	54.15	2.89	1.51	0.59	0.72	0.76
		FD+MSC	1064-1333, 1465-1725	6	69.70	3.74	65.56	2.50	1.72	0.32	0.74	0.82
		FD+SNV	1064-1333, 1465-1725	5	59.31	4.31	57.96	2.77	1.55	0.27	0.59	0.76

LV, latent variables; R^2, coefficient of determination; RMSEE, Root mean square error of estimation; RPD, residual predictive deviation; RMSEP, root mean square error of prediction; Corr, correlation coefficient; IS, integrating sphere; EH, emission head; FD, first derivative; SD, second derivative; MSC, multiplicative scattering correction; SNV, vector normalisation

Stellenbosch University https://scholar.sun.ac.za

Table 9

Model performance for Hue angle using different FT-NIR instruments

Parameter	NIR probe	Pre-processing	Wavelength range (nm)	Calibration			Validation					
				LV	R^2	RMSEE	R^2	RMSEP	RPD	Bias	Slope	Corr.
Hue	IS	None	1064-1333, 2000-2174	5	78.91	5.77	70.60	4.99	1.92	-1.37	0.78	0.86
		FD	1064-1333, 2000-2174	7	88.39	4.33	57.54	6.0	1.57	-1.31	0.76	0.79
		SD	1064-1333, 2000-2174	5	90.42	3.68	63.56	4.62	1.66	0.32	0.69	0.80
		MSC	1064-1333, 2000-2174	7	85.92	4.50	70.69	4.23	1.96	-1.40	0.89	0.87
		SNV	1064-1333, 2000-2174	4	78.33	5.82	69.72	5.09	1.85	-0.95	0.80	0.85
		FD+MSC	1064-1333, 2000-2174	5	89.06	3.48	50.54	5.37	1.42	-0.30	0.57	0.72
		FD+SNV	1064-1333, 2000-2174	6	94.58	2.40	37.80	5.31	1.52	-2.92	0.85	0.80
	EH	None	1064-1333, 1465-1584	10	78.22	5.78	73.64	3.79	2.04	-1.11	0.81	0.87
		FD	1064-1333, 1465-1584	7	82.43	4.86	69.78	3.81	2.02	1.66	0.77	0.87
		SD	1064-1333, 1465-1584	7	95.28	2.60	66.42	4.53	1.84	-1.58	0.87	0.86
		MSC	1064-1333, 1465-1584	9	88.59	4.07	70.69	4.19	1.88	0.73	0.87	0.86
		SNV	1064-1333, 1465-1584	8	77.08	5.87	68.62	4.14	1.87	-1.24	0.83	0.85
		FD+MSC	1064-1333, 1465-1584	6	84.09	4.60	71.77	3.71	2.01	-1.30	0.80	0.87
		FD+SNV	1064-1333, 1465-1584	7	80.39	5.40	49.23	5.23	1.40	0.16	0.80	0.76

LV, latent variables; R^2, coefficient of determination; RMSEE, Root mean square error of estimation; RPD, residual predictive deviation; RMSEP, root mean square error of prediction; Corr, correlation coefficient; IS, integrating sphere; EH, emission head; FD, first derivative; SD, second derivative; MSC, multiplicative scattering correction; SNV, vector normalisation

Stellenbosch University https://scholar.sun.ac.za

Table 10
Model performance for total phenolics using different FT-NIR instruments

Parameter	NIR probe	Pre-processing	Wavelength range (nm)	Calibration			Validation					
				LV	R^2	RMSEE	R^2	RMSEP	RPD	Bias	Slope	Corr.
Total phenolics (g/L)	IS	None	1064-1333	7	76.82	0.14	72.41	0.12	1.97	3.01	0.76	0.86
		FD	1064-1333	5	75.33	0.15	40.39	0.18	1.34	4.33	0.61	0.69
		SD	1064-1333	7	96.71	0.06	53.28	0.19	1.47	-1.30	0.70	0.75
		MSC	1064-1333	5	69.94	0.16	69.54	0.13	1.84	2.06	0.73	0.84
		SNV	1064-1333	5	69.97	0.16	69.49	0.13	1.83	2.02	0.73	0.84
		FD+MSC	1064-1333	7	86.33	0.11	50.08	0.16	1.51	5.74	0.78	0.78
		FD+SNV	1064-1333	4	69.24	0.16	57.01	0.15	1.55	-2.48	0.64	0.77
	EH	None	1064-1333	9	73.30	0.15	67.31	0.16	1.75	-0.76	0.65	0.82
		FD	1064-1333	9	77.22	0.13	72.64	0.14	1.99	-3.94	0.62	0.88
		SD	1064-1333	5	73.30	0.14	65.15	0.12	1.70	0.50	0.63	0.81
		MSC	1064-1333	9	86.48	0.11	82.61	0.11	2.47	0.25	0.82	0.91
		SNV	1064-1333	9	86.41	0.10	79.42	0.12	2.20	-0.23	0.72	0.90
		FD+MSC	1064-1333	8	77.76	0.13	72.86	0.15	1.93	-1.36	0.62	0.87
		FD+SNV	1064-1333	6	68.75	0.16	43.94	0.20	1.39	5.97	0.69	0.83

LV, latent variables; R^2, coefficient of determination; RMSEE, Root mean square error of estimation; RPD, residual predictive deviation; RMSEP, root mean square error of prediction; Corr, correlation coefficient; IS, integrating sphere; EH, emission head; FD, first derivative; SD, second derivative; MSC, multiplicative scattering correction; SNV, vector normalisation

Stellenbosch University https://scholar.sun.ac.za

Table 11

Model performance for total anthocyanin using different FT-NIR instruments

Parameter	NIR probe	Pre-processing	Wavelength range (nm)	Calibration			Validation					
				LV	R^2	RMSEE	R^2	RMSEP	RPD	Bias	Slope	Corr.
Total anthocyanin (g/L)	IS	None	1064-1333, 1640-1835	7	68.81	0.13	68.77	0.14	1.79	-0.08	0.74	0.83
		FD	1064-1333, 1640-1835	7	84.19	0.10	51.29	0.17	1.43	-0.79	0.59	0.72
		SD	1064-1333, 1640-1835	7	95.85	0.05	54.62	0.16	1.54	-4.18	0.65	0.76
		MSC	1064-1333, 1640-1835	7	92.97	0.07	61.44	0.16	1.61	0.04	0.68	0.79
		SNV	1064-1333, 1640-1835	6	77.96	0.11	60.69	0.15	1.60	-0.79	0.64	0.78
		FD+MSC	1064-1333, 1640-1835	7	83.27	0.13	51.13	0.16	1.43	0.40	0.59	0.72
		FD+SNV	1064-1333, 1640-1835	5	74.55	0.11	42.22	0.14	1.32	0.43	0.63	0.69
	EH	None	1064-1333, 1640-1835	9	72.78	0.15	67.05	0.13	1.74	-0.02	0.79	0.83
		FD	1064-1333, 1640-1835	7	69.27	0.15	51.39	0.16	1.49	-0.41	0.57	0.74
		SD	1064-1333, 1640-1835	7	92.00	0.07	49.91	0.13	1.41	-0.59	0.56	0.71
		MSC	1064-1333, 1640-1835	7	68.52	0.15	63.70	0.13	1.66	-0.25	0.68	0.80
		SNV	1064-1333, 1640-1835	9	80.79	0.13	59.38	0.14	1.57	0.74	0.70	0.78
		FD+MSC	1064-1333, 1640-1835	6	70.50	0.16	68.79	0.13	1.79	-0.35	0.70	0.83
		FD+SNV	1064-1333, 1640-1835	6	70.23	0.16	68.00	0.13	1.77	0.80	0.68	0.83

LV, latent variables; R^2, coefficient of determination; RMSEE, Root mean square error of estimation; RPD, residual predictive deviation; RMSEP, root mean square error of prediction; Corr, correlation coefficient; IS, integrating sphere; EH, emission head; FD, first derivative; SD, second derivative; MSC, multiplicative scattering correction; SNV, vector normalisation

Stellenbosch University https://scholar.sun.ac.za

Table 12

Model performance for Vitamin C using different FT-NIR instruments

Parameter	NIR probe	Pre-processing	Wavelength range (nm)	Calibration			Validation					
				LV	R^2	RMSEE	R^2	RMSEP	RPD	Bias	Slope	Corr.
Vitamin C (g/L)	IS	None	1064-1333, 1640-2100	7	85.40	0.08	61.24	0.09	1.64	-1.82	0.60	0.79
		FD	1064-1333, 1640-2100	7	90.98	0.07	51.99	0.09	1.61	-3.80	0.86	0.82
		SD	1064-1333, 1640-2100	7	96.15	0.04	41.38	0.09	1.50	-4.62	0.64	0.75
		MSC	1064-1333, 1640-2100	5	85.99	0.08	44.88	0.10	1.42	-3.37	0.53	0.71
		SNV	1064-1333, 1640-2100	6	83.23	0.09	57.76	0.09	1.55	-1.16	0.59	0.76
		FD+MSC	1064-1333, 1640-2100	5	87.67	0.08	51.42	0.10	1.52	-3.35	0.58	0.75
		FD+SNV	1064-1333, 1640-2100	5	85.58	0.08	52.00	0.10	1.49	-2.55	0.62	0.75
	EH	None	1064-1333	10	84.46	0.11	72.79	0.08	1.96	1.53	0.86	0.87
		FD	1064-1333	6	71.35	0.15	60.99	0.09	1.62	-1.39	0.73	0.80
		SD	1064-1333	4	84.86	0.10	62.20	0.09	1.63	-0.44	0.74	0.80
		MSC	1064-1333	8	82.80	0.11	78.14	0.07	2.17	1.07	0.83	0.89
		SNV	1064-1333	8	84.26	0.11	78.01	0.07	2.17	1.36	0.82	0.89
		FD+MSC	1064-1333	6	78.73	0.10	63.61	0.08	1.66	-0.14	0.82	0.82
		FD+SNV	1064-1333	5	69.18	0.15	55.79	0.10	1.53	-1.79	0.70	0.77

LV, latent variables; R^2, coefficient of determination; RMSEE, Root mean square error of estimation; RPD, residual predictive deviation; RMSEP, root mean square error of prediction; Corr, correlation coefficient; IS, integrating sphere; EH, emission head; FD, first derivative; SD, second derivative; MSC, multiplicative scattering correction; SNV, vector normalisation

Stellenbosch University https://scholar.sun.ac.za

APPENDIX Chapter 6

Table 1
Passing-Bablok regression results for comparison of three FT-IR spectrometers to predict titratable acidity. A joint test on slope and intercept values of the regression lines, at a 95% confidence level.

Alpha predicted vs MPA predicted

PASSING-BABLOK REGRESSION FIT:

	EST	SE	LCI	UCI
Intercept	0.5983763	NA	-0.4233112	1.536611
Slope	0.9464361	NA	0.8561271	1.037671

Alpha predicted vs WineScan predicted

PASSING-BABLOK REGRESSION FIT:

	EST	SE	LCI	UCI
Intercept	0.8609520	NA	-0.2846694	1.678364
Slope	0.9285009	NA	0.8490120	1.023040

MPA predicted vs WineScan predicted

PASSING-BABLOK REGRESSION FIT:

	EST	SE	LCI	UCI
Intercept	-0.2885847	NA	-1.1277086	0.680865
Slope	1.0258241	NA	0.9432677	1.104467

Stellenbosch University https://scholar.sun.ac.za

Table 2
Passing-Bablok regression results for comparison of three FT-IR spectrometers to predict TSS:TA ratio. A joint test on slope and intercept values of the regression lines, at a 95% confidence level

Alpha predicted vs MPA predicted

PASSING-BABLOK REGRESSION FIT:

	EST	SE	LCI	UCI
Intercept	-0.1777647	NA	-0.3477895	-0.0002752027
Slope	1.1652009	NA	1.0351630	1.3034229171

Alpha predicted vs WineScan predicted

PASSING-BABLOK REGRESSION FIT:

	EST	SE	LCI	UCI
Intercept	-0.1154883	NA	-0.2722297	0.05408305
Slope	1.1031027	NA	0.9833815	1.22398664

MPA predicted vs WineScan predicted

PASSING-BABLOK REGRESSION FIT:

	EST	SE	LCI	UCI
Intercept	0.09443581	NA	-0.05025826	0.2125003
Slope	0.93120501	NA	0.83640715	1.0459340

Stellenbosch University https://scholar.sun.ac.za

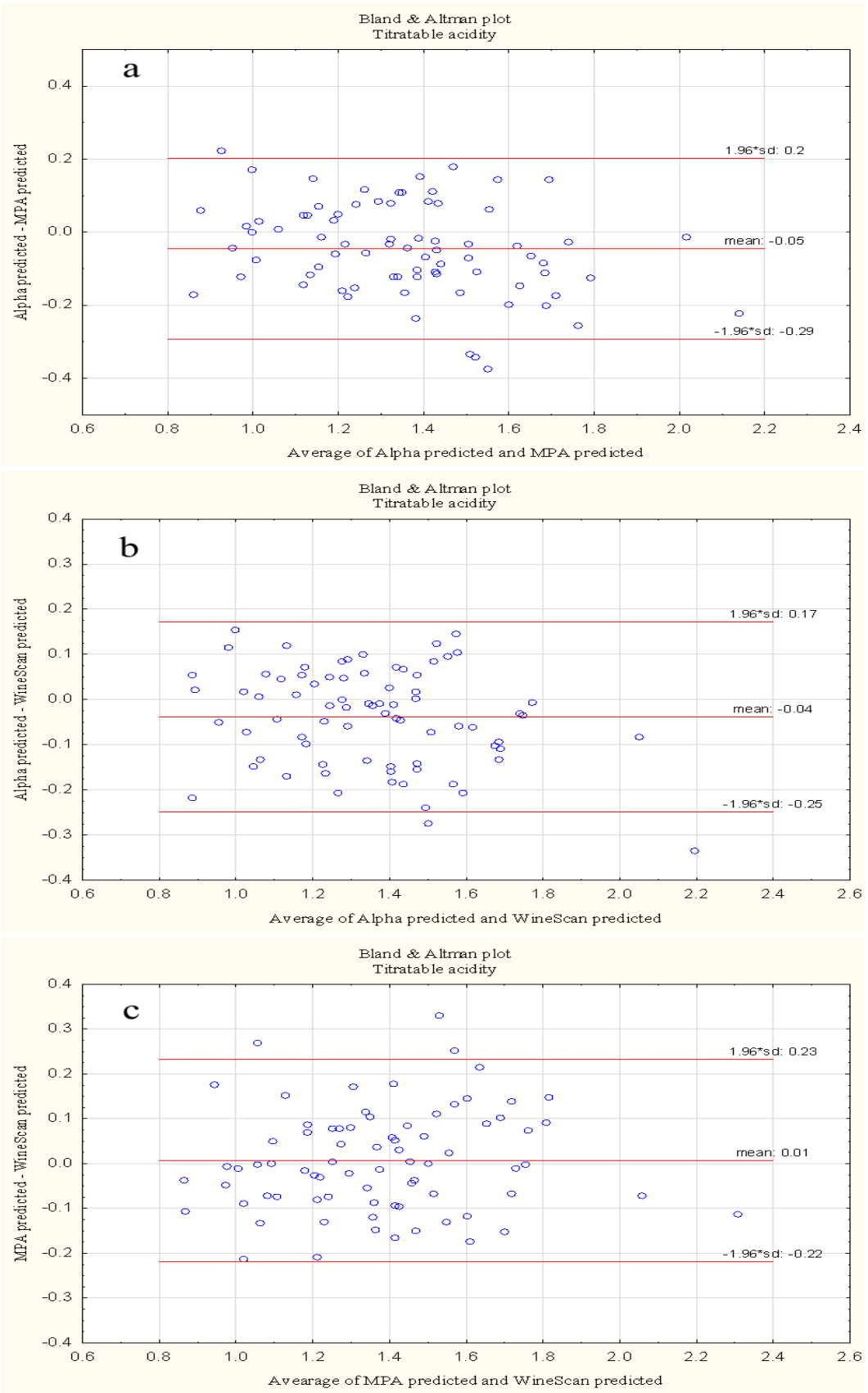

Fig. 1. Bland and Altman plot for TA data with the representation of the limits of agreement (a) Alpha vs MPA (b) Alpha vs WineScan and (c) MPA vs WineScan

Stellenbosch University https://scholar.sun.ac.za

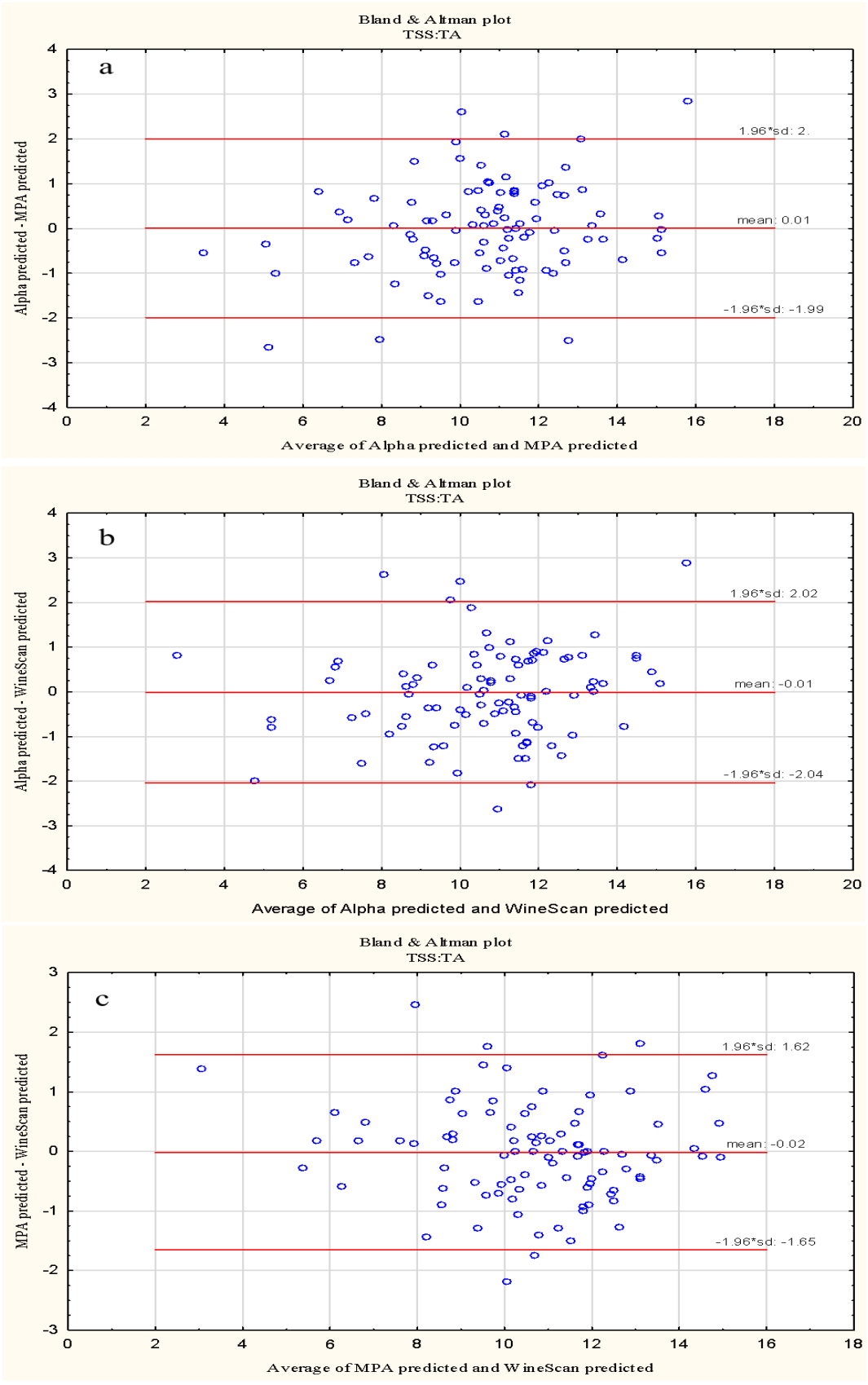

Fig. 2. Bland and Altman plot for TSS:TA ratio data with the representation of the limits of agreement (a) Alpha vs MPA (b) Alpha vs WineScan and (c) MPA vs WineScan

Stellenbosch University https://scholar.sun.ac.za

APPENDIX CHAPTER 8

Table 1
OPLS-DA model for two classes (healthy and infected) with overall performance statistics

Component	R^2X	R^2X(cum)	Eigenvalue	R^2	R^2(cum)	Q^2	Q^2(cum)	R^2Y	R^2Y(cum)	Significance
Model		0.885			0.916		0.879		1	
Predictive		0.455			0.916		0.879		1	
P1	0.455	0.455	111	0.916	0.916	0.879	0.879	1	1	R 1
Orthogonal in X		0.43								
O1	0.246	0.246	60							R 1
O2	0.0699	0.316	17							R 1
O3	0.0564	0.372	13.8							R 1
O4	0.0313	0.403	7.63							R 1
O5	0.0265	0.43	6.46							R 1

R^2X: amount of variation in X that is correlated to Y; R^2X (cum): predicted and orthogonal variation in X that is explained by the model; Eigenvalue: The number of X variables times R^2X; R^2: explained variation of the whole model or individual variables; Q^2 (cum): goodness of prediction, calculated by full cross validation; R^2Y: fraction of Y variation modelled by Y in the component, using the Y model; Significance: CV insignificant (NS) or significant according to rule R_z

Stellenbosch University https://scholar.sun.ac.za

Table 2

OPLS-DA model for three classes, healthy (class 1), moderate scald (class 2), severe scald (class 3) with overall performance statistics

Component	R^2X	R^2X(cum)	Eigenvalue	R^2	R^2(cum)	Q^2	Q^2(cum)	R^2Y	R^2Y(cum)	Significance
Model		0,884			0.766		0.725		1	
Predictive		0.544			0.766		0.725		1	
P1	0.483	0.483	231	0.412	0.412	0.396	0.396	0.469	0.469	R 1
P2	0.0605	0.544	29	0.354	0.766	0.329	0.725	0.531	1	R 1
Orthogonal in X		0.34								
O1	0.135	0.135	64.8							R 1
O2	0.079	0.214	37.8							R 1
O3	0.0535	0.268	25.6							R 1
O4	0.0388	0.307	18.6							R 1
O5	0.0337	0.34	16.1							R 1

R^2X: amount of variation in X that is correlated to Y; R^2X (cum): predicted and orthogonal variation in X that is explained by the model; Eigenvalue: The number of X variables times R^2X; R^2: explained variation of the whole model or individual variables; Q^2 (cum): goodness of prediction, calculated by full cross validation; R^2Y: fraction of Y variation modelled by Y in the component, using the Y model; Significance: CV insignificant (NS) or significant according to rule R_z